Alma Mater Studiorum – Università di Bologna

DOTTORATO DI RICERCA IN

Ingegneria Energetica, Nucleare e del Controllo Ambientale

Ciclo   XXVII

Settore Concorsuale di afferenza: **09/C2**

Settore Scientifico disciplinare: **ING-IND/18**

TITOLO TESI

Severe Accident Simulation in Small Modular Reactor

Presentata da: **Mirco Di Giuli**

Coordinatore Dottorato   **Tutor**

Prof. Vincenzo Parenti Castelli   **Prof. Marco Sumini**

                                                                              Co-Tutor

                                                                              Dr. Didier Volà (IRSN)

Esame finale anno 2015

Aknowledgement

Abstract

Since the Three Mile Island Unit 2 (TMI-2), accident in 1979 which led to the meltdown of about one half of the reactor core and to limited releases of radioactive materials to the environment, an important international effort has been made on severe accident research. The present work aims to investigate the behaviour of the Small Modular Reactor during severe accident conditions. In order to perform these analyses, a SMR has been studied for the European reference severe accident analysis code ASTEC, developed by IRSN and GRS. The thesis consists of six parts. In the first part we will be dealt with the concept of the nuclear safety and its evolution in the last thirty years, moreover will be briefly introduced the two different analysis approaches: probabilistic and deterministic and will be explained the difference between mechanistic and parametric computers codes: computational tools normally used to carried out the deterministic analysis. The second part will be focused on the ASTEC code, the integral code used in this work; will be described the code modular structure, and explained the function of every module. The third part will be devoted to the different type of small modular reactor, currently available on the market. For each one will be presented the characteristics and the design solutions adopted. In the fourth part of the thesis will be described in detail the IRIS Small Modular Reactor; the reference reactor chosen to develop the ASTEC input deck. This input-deck was developed in the framework of a research collaboration with the IRSN development team. The IRIS SMR as well as the advanced nuclear water reactors rely on containment behaviour in realization of some of their passive safety functions. Thus, to simulate correctly the main phenomena involved during an accident scenario, the coupling between primary circuit and containment has to be reproduced accurately. This is the reason why in the fifth part will be described systematically the creation of the ASTEC IRIS input deck: the nodalization scheme adopted, the solution used to simulate the passive safety systems and the strong interaction reactor vessel containment. In the sixth part of the thesis, the ASTEC SMR model will be tested against the RELAP-GOTHIC coupled code model, with respect to a Design Basis Accident, to

evaluate the capability of ASTEC code on reproducing correctly the behaviour of the nuclear system. Once the model has been validated, a severe accident scenario will be simulated and the obtained results along with the nuclear system response will be analysed in the last part of the thesis.

Contents

List of Figures

List of Tables

Nomenclature

ADS	Automatic Depressurization System
A.L.A.R.A.	As Low As Reasonably Achievable
AOO	Anticipated Operational Occurrence
AP1000/600	Advanced Passive Plant1000/600
ASTEC	Accident Source Term Evaluation Code
BAF	Bottom of Active Fuel
BDBA	Beyond Design Basis Accident
B&W	Babcock & Wilcox
BWR	Boiling Water Reactor
CEA	Commissariat à l'énergie atomique et aux énergies alternatives
CES	Containment Enclosure Structure
CFD	Computational Fluid-Dynamics
CMT	Core Makeup Tank
CPA	Containment Part of ASTEC
CRDM	Control Rod Drive Mechanism
CS	Containment Structure
CV	Containment Vessel
DBA	Design Basis Accident
DCH	Direct Containment Heating
DEG	Double Ended Guillotine
DHRS	Decay Heat Removal System
DOE	Department Of Energy
DVI	Direct Vessel Injection
EBS	Emergency Boration System
EBT	Emergency Boration Tank
ECCS	Emergency Core Cooling System
EFPD	Effective Full Power Days
EHRS	Emergency Heat Removal System
FA	Fuel Assembly
FER	University of Zagreb
FP	Fission Product
GOTHIC	Generation Of Thermal-Hydraulic Information for Containments
GRS	Gesellschaftfür Anlagen und Reaktorsicherheit mbH
HHCP	High High Containment Pressure
HLC	High water Level Cavity
HM	Heavy metal
HX	Heat Exchanger
IAEA	International Atomic Energy Agency
I.N.S.A.G	International Nuclear Safety Advisory Group
INEL	Idaho National Engineering Laboratory
IOTSG	Integral Once-Through Steam Generator
iPWR	Integral Pressurized Water Reactor
IRIS	International Reactor Innovative and Secure

IRSN	Institut de Radioprotection et de Sûreté Nucléaire
IRV	Integral Reactor Vessel
JEFF	Joint Evaluated Fission and Fusion
LDPC	Low Differential Pressure Containment
LGMS	Long Term Gravity Makeup System
LLLG	Low Level LGMS
LOCA	Loss Of Coolant Accident
LPL	Low Pressurizer Water Level
LPP	Low Pressurizer Pressure
LM	LOCA Mitigation signal
LSP	Lower Support Plate
LTL	Low Tank water Level
LWR	Light Water Reactor
LU	Lower Upper
MCCI	Melting Core Concrete Interaction
MSR	Moisture Separator Reheater
NPP	Nuclear Power Plant
NRC	Nuclear Regulatory Commission
NSSS	Nuclear Steam Supply System
OCP	Outside Containment Pool
PC	Personal Computer
PCC	Passive Containment Cooling
P.I.E.	Postulated Initiating Event
PORV	Power-Operated Relief Valves
P.S.A	Probabilistic Safety Assessment and Analysis
PSS	Pressure Suppression System
PWR	Pressurized Water Reactor
QT	Quench Tank
RCS	Reactor Coolant System
RELAP	Reactor Excursion and Leak Analysis Program
RPS	Reactor Protection System
RRV	Reactor Recirculation Valves
RVV	Reactor Vent Valve
RWST	Refueling Water Storage Tank
SA	Severe Accident
SBO	Station Black Out
SM	Structural Material
SMR	Small Modular Reactor
SPES	Simulatore Per Esperienze di Sicurezza
SIET	Società Informazioni Esperienze Termoidrauliche
TAF	Top of Active Fuel
UHS	Ultimate Heat Sink System

CHAPTER 1

NUCLEAR SAFETY

1.1   Introduction

The objectives of nuclear safety consist in ensuring the siting and the plant conditions need to comply with adequate principles, such as, for example, the internationally accepted health, safety and radioprotection principles. In particular, the plant at the chosen site shall guarantee that the health of the population and of the workers does not suffer adverse radiation consequences more severe than the established limits and that such effects be the lowest reasonably obtainable (the ALARA – As Low As Reasonably Achievable – Principle) in all operational conditions and in case of accidents. These objectives are frequently subdivided into a General Objective, a Radiation Protection Objective and a Technical Objective, in the International Atomic Energy Agency (IAEA) criteria [1].

The General Nuclear Safety Objective is to protect individuals, society and the environment from harm by establishing and maintaining effective defences against radiological hazards in nuclear installations.

The Radiation Protection Objective is to ensure that in all operational states radiation exposure within the installation or due to any planned release of radioactive material from the installation is kept below prescribed limits and as low as reasonably achievable, and to ensure mitigation of the radiological consequences of any accidents.

The Technical Safety Objective is to take all reasonably practicable measures to prevent accidents in nuclear installations and to mitigate their consequences should they occur; to ensure with a high level of confidence that, for all possible accidents taken into account in the design of the installation, including those of very low probability. The target for existing power plants consistent with the

Technical Safety Objective has been defined by the INSAG (International Nuclear Safety Advisory Group, advisor to the IAEA Director General) as a likelihood of occurrence of severe core damage that is below about 10^{-4} events per plant operating year. Implementation of all safety principles at future plants should lead to the achievement of an improved goal of not more than about 10^{-5} such events per plant operating year. Severe accident management and mitigation measures should reduce the probability of large offsite releases requiring short-term off-site response by a factor of at least 10. It has to be observed that these principles, while indicating the need for strict control of radiation sources, do not preclude the external release of limited amounts of radioactive products nor the limited exposure of people to radiation. Similarly, the objectives require to decrease the likelihood and the severity of accidents, but they recognize that some accidents can happen. Measures have to be taken for the mitigation of their consequences. Such measures include on-site accident management systems (procedures, equipment, operators) and off-site intervention measures. The greater the potential hazard of a release, the lower must be its likelihood.

1.2   The safety in the nuclear power plants

The safety of nuclear power plants (NPPs) is based on the defence in depth concept. This concept, as applied to all safety activities, whether organizational, behavioural or design related. It ensures that they are subject to overlapping system provisions, so that if a failure were to occur, it would be detected and compensated, for or corrected by appropriate measures. Application of the concept of defence in depth in the design of a plant provides a series of 5 levels of defence (inherent features, equipment and procedures) aimed at preventing accidents and ensuring appropriate protection in the event that prevention fails. Every level has its own scope to cover [2]:

- The aim of the first level of defence is to prevent deviations from normal operation, and to prevent system failures. This leads to the requirement that the plant has to be conservatively designed, constructed, maintained and operated in accordance with appropriate quality levels and engineering practices, such as the application of redundancy, independence and diversity. To meet this objective, careful attention is paid to the selection of appropriate design codes and materials, and to the control of fabrication of components and of plant construction. Design options that can contribute to reducing the potential for internal hazards, to reducing the consequences of a given postulated initiating event (PIE), that is, an event identified during design as capable of leading to anticipated operational occurrences or

accident conditions [3], or to reducing the likely release source term following an accident sequence contribute at this level of defence.

- The aim of the second level of defence is to detect and intercept deviations from normal operational states in order to prevent anticipated operational occurrences from escalating to accident conditions. This is in recognition of the fact that some PIEs are likely to occur over the service lifetime of a nuclear power plant, despite the care taken to prevent them. This level necessitates the provision of specific systems as determined in the safety analysis and the definition of operating procedures to prevent or minimize damage from such PIEs.

- For the third level of defence, it is assumed that, although very unlikely, the escalation of certain anticipated operational occurrences or PIEs may not be arrested by a preceding level and a more serious event may develop. These unlikely events are anticipated in the design basis for the plant, and inherent safety features, fail-safe design, additional equipment and procedures are provided to control their consequences and to achieve stable and acceptable plant states following such events. This leads to the requirement that engineered safety features be provided that are capable of leading the plant first to a controlled state, and subsequently to a safe shutdown state, and maintaining at least one barrier for the confinement of radioactive material.

- The aim of the fourth level of defence is to address severe accidents in which the design basis may be exceeded and to ensure that radioactive releases are kept as low as practicable. The most important objective of this level is the protection of the confinement function. This may be achieved by complementary measures and procedures to prevent accident progression, and by mitigation of the consequences of selected severe accidents, in addition to accident management procedures. The protection provided by the confinement may be demonstrated using best estimate methods.

- The fifth and final level of defence is aimed at mitigation of the radiological consequences of potential releases of radioactive materials that may result from accident conditions. This requires the provision of an adequately equipped emergency control centre, and plans for the on-site and off-site emergency response.

A relevant aspect of the implementation of defence in depth is the provision in the design of a series of "protective barriers". The concept of the "protective barriers" (Figure 1-1) involves placing a series of strong, leak-tight physical barriers between the radioactive materials and the environment to contain radioactivity in all circumstances consequences of failures. The barriers for a

commercial water-cooled reactor can be subdivided in :

- first barrier: the fuel, inside which most of the radioactive products are already trapped, is enclosed within a metal cladding;

- second barrier: the reactor coolant system is enclosed within a pressurized metal envelope that includes the reactor vessel which houses the core containing the fuel rods;

- third barrier: the reactor coolant system is itself enclosed in a thick walled concrete containment building.

Maintaining the integrity and leak tightness of just one of these barriers is sufficient to contain radioactive fission products

Figure 1-1: Physical Barriers for an AP1000 reactor

1.3   Safety Analysis

The safety analyses are analytical evaluations of physical phenomena occurring at nuclear power plants. It made for the purpose of demonstrating that safety requirements, for all postulated initiating events that could occur over a broad range of operational states, including different levels of availability of the safety systems, are such as to satisfy the requirement for ensuring the integrity of barriers against the release of radioactive material and various other acceptance criteria are met. The acceptance criteria are used to judge the acceptability of the results of safety analysis. The range and conditions of applicability of each specific criterion have to be clearly specified. The two complementary methods used to carry out the safety analysis are deterministic safety analysis and probabilistic safety assessment and analysis (PSA).These two methods are used jointly in evaluating the safety of an NPP.

1.3.1   Probabilistic Safety Assessment and Analysis (PSA)

The objectives of PSA are to determine all significant contributing factors to the radiation risks arising from a facility or activity, and to evaluate the extent, to which the overall design, is well balanced and meets the probabilistic safety criteria where these have been defined [4]. PSA provides a methodological approach to identifying accident sequences that can follow from a broad range of initiating events and it includes a systematic and realistic determination of accident frequencies and consequences. In international practice, three levels of PSA are generally recognized:

- In Level 1 PSA, the design and operation of the plant are analysed in order to identify the sequences of events that can lead to core damage and the core damage frequency is estimated. Level 1 PSA provides insights into the strengths and weaknesses of the safety related systems and procedures in place or envisaged as preventing core damage. The results of the Level 1 PSA should be used to identify weaknesses in the design or operation of the plant. Weaknesses can be identified by considering the contributions to the risk from groups of initiating events, the importance measures of the safety systems and the contributions of human error to the overall risk. Where the results of the PSA indicate that changes could be made to the design or operation of the plant to reduce risk, the changes should be incorporated where reasonably achievable, taking the relative costs and benefits of any modifications into account.

- In Level 2 PSA, the chronological progression of core damage sequences identified in Level 1 PSA is evaluated, including a quantitative assessment of phenomena arising from severe damage to reactor fuel. Level 2 PSA identifies ways in which

5

associated releases of radioactive material from fuel can result in releases to the environment. It also estimates the frequency, magnitude and other relevant characteristics of the release of radioactive material to the environment. This analysis provides additional insights into the relative importance of accident prevention and mitigation measures and the physical barriers to the release of radioactive material to the environment (e.g. a containment building). The results of the Level 2 PSA should be used to determine if sufficient provision has been made to prevent or mitigate the effects of postulated core damage sequences. In Level 2 PSA, it should be considered whether the containment is adequately robust and whether the protection systems such as hydrogen mixing and recombining systems, containment sprays and containment venting systems provide an adequate level of protection to prevent a large release of radioactive material to the environment. Furthermore, containment bypassing events such as a loss of coolant accident in interfacing systems should be addressed. In addition, Level 2 PSA should be used to identify and optimize accident management measures that could be carried out to mitigate the effects of the damaged core. This could include determining additional measures, for example, measures that could be taken to introduce water into the reactor containment.

- In Level 3 PSA, public health and other societal consequences are estimated, such as the contamination of land or food from the accident sequences that lead to a release of radioactivity to the environment.

Level 1 PSA, Level 2 PSA and Level 3 PSA are sequential analyses, where the results of each assessment usually serve as a basis for the PSA at the next level. Level 1 PSA provides insights into design weaknesses and into ways of preventing accidents leading to core damage, which might be the precursor of accidents leading to major releases of radioactive material with potential consequences for human health and the environment. Level 2 PSA provides additional insights into the relative importance of accident sequences leading to core damage in terms of the severity of the releases of radioactive material they might cause, and insights into weaknesses in measures for the mitigation and management of severe accidents and ways of improving them. Finally, Level 3 PSA provides insights into the relative importance of accident prevention and mitigation measures, expressed in terms of adverse consequences for the health of both plant workers and the public, and the contamination of land, air, water and foodstuffs. In addition, Level 3 PSA provides insights into the relative effectiveness of aspects of accident management relating to emergency preparedness and response. The results of Level 2 PSA and Level 3 PSA should be provided to civil authorities as a technical input for

off-site emergency planning.

1.3.2 Deterministic safety analysis

Deterministic safety analyses for a nuclear power plant predict the response to postulated initiating events [5]. A specific set of rules and acceptance criteria is applied. Typically, these should focus on neutronic, thermal-hydraulic, radiological, thermo-mechanical and structural aspects, which are often analysed with different computational tools. The computations are usually carried out for predetermined operating modes and operational states, and the events include anticipated transients, postulated accidents, selected beyond design basis accidents and severe accidents with core degradation. The results of computations are spatial and time dependences of various physical variables (e.g. neutron flux; thermal power of the reactor; pressure, temperature, flow rate and velocity of the primary coolant; stresses in structural materials; physical and chemical compositions; concentrations of radionuclides) or, in the case of an assessment of radiological consequences, radiation doses to workers or the public. Deterministic safety analyses for design purposes should be characterized by their conservative assumptions and bounding analysis. This is achieved by an iterative process in the design phase, when the limiting case(s) in terms of the minimum margin to the acceptance criteria is (are) determined for each group of postulated initiating events and sequences. To determine the limiting case for a given transient or set of transients, the consequential failures that are caused by the initiating event (internal or external) should be taken into account. A limited number of coincident independent failures (including operator error) should also be addressed. However, the frequency of occurrence will decrease significantly, as each coincident independent failure is taken into account. Only those combinations of transients whose frequency remains within the design basis should be analysed. The time span of any scenario that is analysed should extend up to the moment when the plant reaches a safe and stable end state. What is meant by a safe and stable end state should be defined. In some cases, it is assumed that a safe and stable end state is achieved when the core is covered and long-term heat removal from the core is achieved, and the core is subcritical by a given margin. There are two different methodologies for the deterministic analysis the conservative approach and the best-estimate approach. The conservative hypotheses were introduced in the early days of safety analysis to address the uncertainties that prevailed in the 1970s. A conservative approach usually means that any parameter that has to be specified for the analysis should be allocated a value that will have an unfavourable effect in relation to specific acceptance criteria. The concept of conservative methods was introduced in the early days of safety analysis to take into account the uncertainties

due to the limited capability of modelling and the limited knowledge of physical phenomena, and to simplify the analysis. In these kind of analyses, both the assumed plant conditions and the physical models used are set conservatively. The reasoning is that such an approach would demonstrate that the calculated safety parameters are within the acceptance criteria and would ensure that no other transient of that category would exceed the acceptance criteria. For the purpose of conservative calculations, the initial and boundary conditions should be set to values that will lead to conservative results for those safety parameters that are to be compared with the acceptance criteria. One set of conservative values for initial and boundary conditions does not necessarily lead to conservative results for every safety parameter. Therefore, the appropriate conservatism should be selected for each initial and boundary condition, depending on the specific transient and the associated acceptance criterion. The use of a conservative methodology may be so conservative that important safety issues may be masked. For example, the assumption of a high core power level may lead to high levels of steam–water mixture in the core in the case of a postulated small break loss of coolant accident. Consequently, the calculated peak cladding temperature may not be conservative. As another example, the assumption that reduced interfacial shear between water and steam may lead to higher cladding temperatures in the upper core region is conservative. However, this conservative assumption will lead to an optimistic estimate for the refilling/reflooding time, as it will appear that more water remains in the primary cooling system than is actually the case. The extensive experimental research in the 1980s and 1990s has resulted in a considerable increase of knowledge, and the development of computer codes has improved the ability to achieve calculated results from simulations that correspond more accurately to experimental results. Nowadays, it may be preferable to use a best estimate approach together with an evaluation of the uncertainties to compare the results of calculations with acceptance criteria. This type of analysis is referred to as a best estimate plus uncertainties approach. A best estimate approach provides a more realistic information about the physical behaviour of the reactor, identifies the most relevant safety issues and provides information about the existing margins between the results of calculations and the acceptance criteria. A best estimate approach may be used for accident scenarios in which the margin to the acceptance criterion is not very large. For scenarios with large margins to the acceptance criteria, it is more practical to use a conservative analysis in which detailed evaluation of the uncertainties is not performed. For a best estimate analysis, a best estimate code or other tools that realistically describe the behaviour of physical processes in a component or system should be used. This requires sufficient data to be able to ensure that all-important phenomena have been taken into account in the modelling or that their effects are bounded.

Chapter 1. Nuclear Safety

Establishing that all-important phenomena have been taken into account in the modelling or that their effects are bounded should be part of the validation programme. Because the results of best estimate codes are not designed to bound experimental data, best estimate codes are not intended to provide conservative results. Uncertainties in the results due to unavoidable approximations in the modelling should therefore be quantified using experimental results. The trend in several Countries is to use best estimate plus uncertainty analysis, not to be confused with the probabilistic method.

1.4 Relation of Deterministic Safety Analysis to PSA

A major part of the process of designing and licensing a nuclear power plant is the safety analysis. Reference [6] states that both deterministic methods and probabilistic methods are required to be applied. The objectives are to identify issues that are relevant to safety and to demonstrate that the plant is capable of meeting any authorized limits on the release of radioactive material and on the potential exposure to radiation for each plant state. Thus a deterministic safety analysis alone does not demonstrate the overall safety of the plant, and it should be complemented by a probabilistic safety analysis. While deterministic analyses may be used to verify that acceptance criteria are met, probabilistic safety analyses may be used to determine the probability of damage for each barrier. Probabilistic safety analysis may thus be a suitable tool for evaluation of the risk that arises from low frequency sequences that lead to barrier damage, whereas a deterministic analysis is adequate for events of higher frequency for which the acceptance criteria are set in terms of the damage allowed. To verify that defence in depth is adequate, certain very low frequency design basis accidents, such as large break loss of coolant accidents or rod expulsion with or without the safety systems intervention can be assumed as the initiating event. Thus, deterministic analysis and probabilistic analysis provide a comprehensive view of the overall safety of the plant for the entire range of the frequency–consequence spectrum. Deterministic safety analyses have an important part to play in the performance of a probabilistic safety analysis because they provide information on whether the accident scenario will result in the failure of a fission product barrier. It should be used to identify challenges to the integrity of the physical barriers, to determine the failure mode of a barrier when challenged and to determine whether an accident scenario may challenge several barriers. Best estimate codes and data, should be used to be consistent with the objectives of probabilistic safety analysis, which include providing realistic results. It should be recognized that the results of the supporting analyses are usually bounded by the

results of conservative deterministic analyses. Furthermore, a probabilistic safety analysis fault tree is a powerful tool that can be used to confirm assumptions that are commonly made in the deterministic calculation about the availability of systems; for example, to determine the potential for common cause failures or the minimum system requirements, to identify important single failures and to determine the adequacy of technical specifications.

1.5 NPP operational states and accident conditions

The entire range of conditions for which an NPP is designed according to established design criteria, including all the national regulatory requirements, and for which damage to the fuel and release of radioactive material are kept within authorized limits, form the design basis of an NPP. Within the design basis, a number of unintended events are considered, including operating errors and equipment failures, whose consequences or potential consequences are not negligible in terms of safety. According to the probability of its occurrence and potential consequences, an event may be classified as an Anticipated Operational Occurrence (AOO) (10^{-2} per reactor year) or a Design Basis Accident (DBA) ($>=10^{-5}$ per reactor year). An AOO is an operational process deviating from normal operation, which is expected to occur at least once during the operating lifetime of a facility but which, in view of appropriate design provisions, does not cause any significant damage to items important to safety or lead to accident conditions. For DBA means accident conditions against which a facility is designed according to established design criteria, and for which the damage to the fuel and the release of radioactive material are kept within authorized limits. An accident occurring outside the NPP design basis is called a Beyond Design Basis Accident (BDBA) ($>10^{-5}$ per reactor year). Such an accident may or may not involve degradation of the reactor core (leading to significant core damage). An accident involving core degradation (typically with core melting) is also called a Severe Accident (SA). According to the IAEA Safety Requirements, on the Safety of Nuclear Power Plants; the severe accidents are also to be considered in the design and operation of NPPs. Some regulatory bodies prescribe that these accidents have to be taken into consideration in the plant design. The entire range conditions of a NPP according to Nuclear Safety Standard Code are illustrated in (Figure 1-2). As already highlighted above, the deterministic safety analysis predicts the response of an NPP in specific predetermined operational states to postulated initiating events. This type of safety analysis applies a specific set of rules and specific acceptance criteria. Probabilistic safety analysis (PSA) combines the likelihood of an initiating event, potential scenarios in the development of the event and its consequences into an estimation of core damage frequency, source term or overall risk arising from operation of the

NPP. The number of event sequences can be very large. The method applied to realize a safety analyses for different type of conditions could be different. In fact, the DBA analysis and BDBA analysis are based on different approaches. DBA is based on a deterministic approach, where proof is given that the plant is safe in a comprehensive set of accident sequences defined on the basis of conceivable initiating events, conservative assumptions and the single failure criterion.

Operational states		Accident conditions			
		Within design basis accidents		Beyond design basis accidents	
Normal operation	Anticipated operational occurrences	a	Design basis accidents	b	Severe accidents
					Accident management
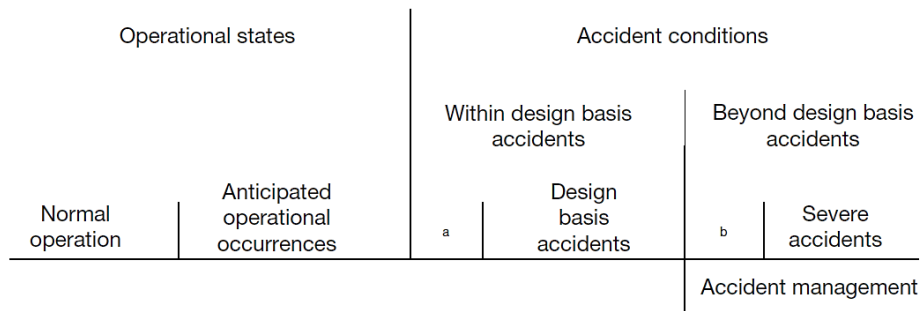
Figure 1-2: NPP conditions according to Nuclear Safety Standard Code

Acceptance criteria in the form of limits on physical parameters are defined that should be met in all accident sequences. In general, there are different acceptance criteria for different types of sequences. The conservative approach is used for all the input parameters. Another approach to DBA analyses is the use of best estimate analyses, involving no conservatism in the initial and boundary conditions, but with an uncertainty evaluation of the analysis. The BDBA is to a large extent based on the probabilistic approach, with the aim of demonstrating that the total risk to the environment and the public due to the plant operation is acceptably small. The acceptance of BDBA is based on the acceptance of the plant risk function that combines probability and radiological consequences. Generally, the selection of a limited number of sequences to be analysed in detail by a complex severe accident code is based on the results of PSA Level 1. The severe accident analysis methodology does not use conservative assumptions, the reason being that determining which assumption is conservative cannot be done in advance. In addition, a conservative assumption related to a particular phenomenon may not be conservative to another severe accident phenomenon. Therefore, BDBA analyses rely on best estimate data. However, this does not exclude the performance of bounding analyses for a particular analysis application.

1.6   Computer codes

Computer codes used for BDBA are often classified into mechanistic codes and parametric ones [7]. Mechanistic codes are

characterized by best estimate phenomenological models to enable, as far as possible, an accurate simulation of the behaviour of an NPP in the case of a severe accident. Parametric codes include a combination of phenomenological and user defined parametric models to simulate the integral behaviour of the whole plant (reactor coolant system, containment, fission product behaviour). In the recent years, the rapid increase of computer performance increasingly enables the replacement of parametric models by mechanistically based ones in the parametric codes. Therefore, the distinction between parametric and mechanistic codes became questionable. It became apparent that a classification based on requirements for different applications would be more appropriate. From the point of view of real application, existing severe accident codes can be classified into three classes: fast running integral codes, detailed codes and special (dedicated) codes.

- Integral codes: These codes should be characterized by a well balanced combination of detailed and simplified models for the simulation of the relevant phenomena within an NPP in the case of a severe accident. 'Fast running' may have different meanings but it should be close to real time (on workstations or personal computers), and the analyses of typical scenarios should not last longer than 12 hours. These codes are primarily not designed to perform best estimate simulations; the objective is rather to allow the user to bound important processes or phenomena by numerous user-defined parameters. Integral codes are usually used to support PSA Level 2 analyses and for the development and validation of accident management programmes. Their models are less mechanistically based but more of parametric character, i.e. model parameters allow the user to investigate the consequences of uncertainties on key results. These kinds of codes may also have been used for the design and validation of severe accident prevention and mitigation systems; however, to obtain realistic results, a deep knowledge of the involved physical phenomena as well as user experience in performing severe accident analysis is required. Benchmark exercises with mechanistic codes may support the justification. Simplification of the models aims to reduce computation time. Some examples of fast running integral codes are MELCOR [8], MAAP [9] and ASTEC [10].
- Detailed codes: The detailed codes use a different approach in comparison with the integral codes. The strategy for detailed codes is to model as far as possible all relevant phenomena in detail by mechanistic models. Basic requirements for detailed codes are that the modelling uncertainties are comparable with (i.e. not higher than) the uncertainties in the experimental data used to validate the

code and that user defined parameters are only necessary for phenomena which are not well understood due to insufficient experimental data (including scaling problems). Using detailed codes, best estimate analysis can be performed; however, uncertainties also exist and must be consequently quantified. Since, as a principle, they should not have user options, existing uncertainties in the simulation of the different phenomena must be specified to enable the definition of the uncertainties of the key results. The main disadvantage of the detailed code is due to the high demand on computation time; mechanistically based codes typically simulate only either the reactor coolant system or the containment. The acceptable computation time depends on the scope of the application but it normally does not exceed 10 times the real time on workstations or personal computers. Another limitation can be deduced from the requirement that computation time should not be a dominant part of the overall project timescale: analysis of a particular scenario should not last longer than one week. Anyway, the high demand on computer time is decreasing continuously, thanks to the rapidly increasing performance of computers. ATHLET-CD [11], SCDAP/RELAP5 [12], ICARE/CATHARE [13-15], COCOSYS, GOTHIC [16], CONTAIN [17], are examples of detailed codes. In addition, ASTEC and MELCOR can be considered detailed codes, if the calculation is based on extensive nodalization and detailed model options

- Dedicated codes: These codes dealing with single phenomena have become important in context with the requirements of the regulatory authorities to take into account severe accidents in the design of new NPPs and to reduce uncertainties of risk-relevant phenomena (more reliable likelihoods for the branches in an accident progression event tree). Depending on their task, they may be simple and consequently fast running, or very complex with the drawback of large calculation time. Typical issues for which special codes are required include: Lower head melt retention, Hydrogen distribution, Recriticality, etc.

Reference Chapter 1

[1] Petrangeli, G., "*Nuclear Safety*", Book Elsevier ISBN 13: 978-0-7506-6723-4, 2006 pag. 1.

[2] INTERNATIONAL ATOMIC ENERGY AGENCY,IAEA Safety of Nuclear Power Plants: Design, IAEA Safety Standards Series No. NS-R-1, IAEA, Vienna (2000).

[3] INTERNATIONAL ATOMIC ENERGY AGENCY, IAEA Safety Glossary: Terminology used in Nuclear Safety and Radiation Protection 2007 edition, IAEA, Vienna (2007).

[4] INTERNATIONAL ATOMIC ENERGY AGENCY, IAEA Safety Standard for protecting people and environment: Development and application of Level 1 Probabilistic Safety Assessment for Nuclear power plant, IAEA Safety Standards Series No. SSG-3, Vienna (2010).

[5] INTERNATIONAL ATOMIC ENERGY AGENCY, IAEA Safety Standard for protecting people and environment: Deterministic Safety Analysis for Nuclear Power Plants, IAEA Safety Standards Series No. SSG-2, Vienna (2010).

[6] INTERNATIONAL ATOMIC ENERGY AGENCY, IAEA, International atomic energy agency, use and development of coupled computer codes for the analysis of accidents at nuclear power plants. Proceedings of a technical meeting held in Vienna (2003).

[7] INTERNATIONAL ATOMIC ENERGY AGENCY Approaches to the Safety of Future Nuclear Power Plants, IAEA-TECDOC-905, IAEA, Vienna (1996).

[8] http://www.nrc.gov/reading-rm/doc-collections/nuregs/contract/cr6119/

[9] http://www.epri.com/abstracts/Pages/ProductAbstract.aspx?ProductId=000000003002003113

[10] https://www-astec.irsn.fr/

[11] Trambauer K., Bals C., et al., ATHLET-CD mod 2.2 cycle A-User's Manual Gesellschaftfür Anlagen und Reaktorsicherheit mbH (GRS), 2009

[12] SCDAP/RELAP5 Development Team "SCDAP/RELAP5/ MOD 3.2 code Manual " Vol. 1-5, NUREG/CR-6150, INEL-96/ 0422, U.S Nuclear Regulatory Commission (July 1998)

[13] CATHARE 2 V2.5_1: User's Manual, SSTH/LDAS/EM/2005-035, G. Lavialle, 2006.

[14] CATHARE2 V2.5_1: User Guidelines, DER/SSTH/LDAS/EM/05-034, G. Lavialle, 2006.

[15] P. Chatelard, F. Fichot, et al., ICARE2V3mod2 User's Manual, IRSN DRS/SEMAR 2003/54, Institut de Radioprotection et de Sûreté Nucléaire (2003)

[16] GOTHIC Containment Analysis Package: Technical Manual,NAI 8907-06 Rev16, 2005.

[17] fas.org/sgp/othergov/doe/lanl/lib-www/sand/971735.pdf

CHAPTER **2**

THE ASTEC INTEGRAL CODE

2.1 Introduction

The ASTEC code (Accident Source Term Evaluation Code), jointly developed since several years by the French Institut de Radiopro-tection et de Sûreté Nucléaire (IRSN) and the German Gesellschaftfür Anlagen und Reaktorsicherheit mbH (GRS), aims at simulating an entire severe accident (SA) sequence in a nuclear water-cooled reactor from the initiating event through the release of radioactive elements out of the containment. The main ASTEC applications are therefore source term determination studies, Probabilistic Safety Assessment level 2 (PSA2) studies including the determination of uncertainties, accident management studies and physical analyses of experiments to improve the understanding of the phenomenology [1]. In particular, the V2.0 version used in this work, includes advanced core degradation models (issued from the IRSN ICARE2 mechanistic code) and the ASTEC applicability has been extended to Gen. III reactor designs, so that the V2.0 allows to simulate the EPR reactor or to launch investigations about the mitigation strategy relying on the In-Vessel melt Retention concept (IVR). Besides these, two key evolutions, other physical models have also been improved (e.g. first account for gas chemistry kinetics in the Reactor Cooling System (RCS) or new modelling of hydrogen combustion in the containment) and ASTEC V2 is now coupled to the SUNSET IRSN statistical tool to make easier the uncertainty and sensitivity analyses.

2.2 The ASTEC code structure

The ASTEC scope of application covers most of the physical phenomena involved in SA, except steam explosion and mechanical response of the containment. For the latter phenomena, the code can yield initial and boundary conditions for a specific analysis using

Chapter 2. The ASTEC Integral code

detailed codes such as, respectively, Computational Fluid-Dynamics (CFD) and Finite Element codes. For the hydrogen risk in containment, ASTEC provides a global evaluation of the risk; nevertheless, such evaluation needs to be consolidated by CFD approach. The ASTEC code structure is modular, each of its modules simulating a reactor zone or a set of physical phenomena (Figure 2-1). Two different running modes are possible in ASTEC V2.0:

- Stand-alone mode for running each ASTEC module independently, which is useful for module validation and calculation of separate-effect tests;
- Coupled mode where all (or a subset of) the ASTEC modules are run sequentially within a macro-time step. This mode allows explicit feedback between modules.

A specific tool SIGAL-ODESSA was specifically developed by IRSN in Fortran for managing the database associated to any transient calculation. The ASTEC modules communicate with each other through a "dynamic" memory (Figure 2-1) and data are exchanged between the ASTEC modules at macro-time steps through this dynamic database, i.e. evolving throughout the calculation and mirroring at each time the state of the reactor.
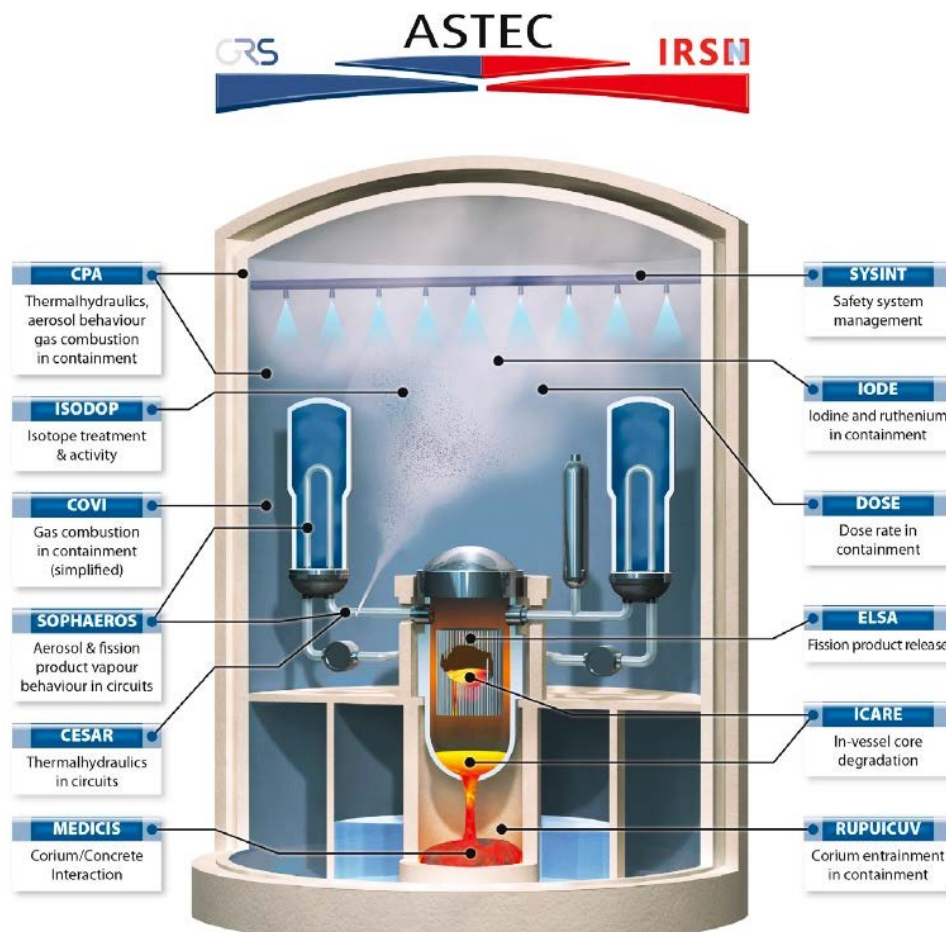
Figure 2-1: Structure of the ASTEC code with its modules and related phenomena

The ASTEC V2 programming language is mainly Fortran (today mainly Fortran 95 with progressive evolution towards Fortran2003). The code size is about 450,000 lines, distributed in more than 2000 routines and the ASTEC V2.0 computer targets are personal computers (PCs) with both Linux and Windows operating systems [2].

2.3   The ASTEC modules

2.3.1   The CESAR module

The CESAR ASTEC module simulates the thermal-hydraulics [3] in the primary circuit, secondary circuit and in the reactor vessel (with a simplified core modelling) up to the beginning of core degradation phase, i.e. roughly up to the start of core uncovering, and in any case before the start of Zr cladding oxidation process by steam interaction. After the onset of the core degradation phase, the CESAR module computes only the thermal-hydraulics in primary and secondary circuit as well as in the vessel upper plenum. The ICARE module performs the thermal-hydraulics in the reactor vessel during core degradation. The CESAR thermal-hydraulics modelling is based on a 1-D 2-fluid 5-equation approach. Up to 5 non-condensable gases (Hydrogen, Helium, Nitrogen, Argon, Oxygen) are available. As a result 5+N differential equations and 1 algebraic equation are solved:

- 2+N mass differential balance equations, one for the vapour phase, N for the non-condensable gases and one for the liquid phase,
- 2 energy differential balance equations, one for the gas mixture phase and one for the liquid phase,
- 1 mixture (liquid and gas phases) differential momentum balance equation,
- 1 algebraic equation which models the interfacial drag between the liquid phase and the gas phase. The interfacial drag is a complex model which has been assessed on a large number of experimental data.

Most of the CESAR physical constitutive laws are issued from the correlations, which are included in the French best-estimate thermal-hydraulics CATHARE2 code. In particular, the critical break flow rate is based on the Gros D'Aillon correlation whereas the heat transfer coefficient between the structure and the fluid is based on a boiling (Nukiyama) curve. Different heat transfer processes are modelled: forced convection to liquid, nucleate boiling, critical heat flux, transition boiling, film boiling, forced convection to vapour and radiative heat transfer. Moreover a droplet projection model is implemented which enables CESAR to simulate the reflooding of intact or slightly degraded cores (i.e. still in rod-like geometries). The primary pump description is done through a 0-D approach. The

numerical method follows the finite volume technique. The space is discretized using a staggered grid with the use of the donor cell principle. The time integration is performed using a Newton's method and a fully implicit scheme is used. The Jacobian matrix inversion is based on a highly optimized Lower Upper (LU) algorithm, which makes CESAR a fast running module.

2.3.2   The ICARE module

The ICARE module [4] deals with the in-vessel degradation phenomena (both early and late degradation phases). The ICARE module performs the thermal-hydraulics in the RPV (core, core by-pass, lower plenum and downcomer) during core degradation. The core degradation process is characterized by the high complexity of phenomena to be considered and geometry to be accurately presented, with a permanent appearance and disappearance of a large number of components in each control volume by e.g. melting, failure, relocation, and chemical reactions. This demands a dynamic management of these components. Besides, the geometry of a degraded core is very complex and heterogeneous. Therefore, as illustrated on Figure 2-2, ICARE allows simulating the early phase of core degradation with fuel rod heat-up, ballooning and burst, exothermic clad oxidation, control rods behaviour, fuel rod embrittlement.
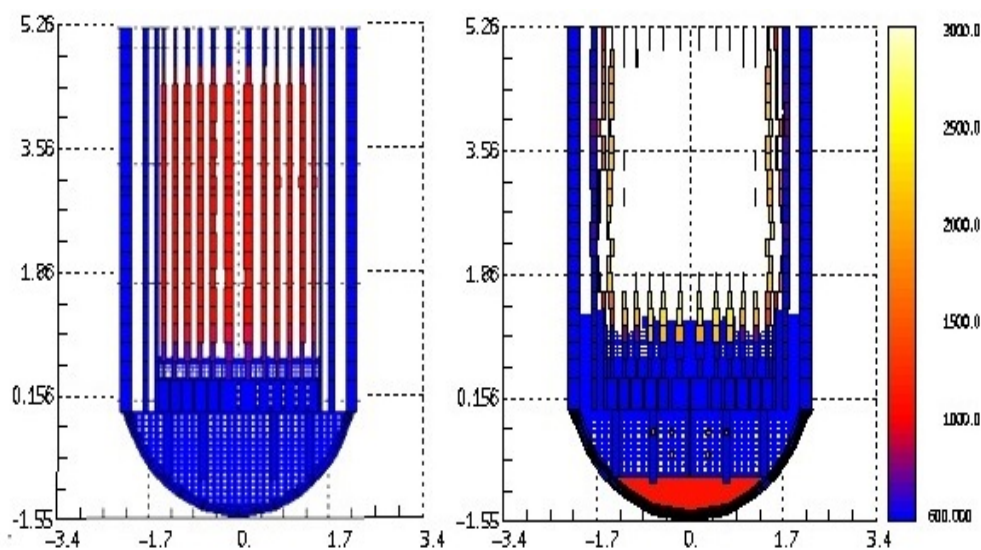
Figure 2-2: Core degradation simulation with ICARE

During the late phase of core degradation, ICARE can simulate the melting, molten mixture candling and relocation, with corium accumulation within the core channels and formation of blockages, corium slump into the lower head and corium behaviour in the lower head until vessel failure. The main ICARE models in ASTEC V2.0 are:

Chapter 2. The ASTEC Integral code

- Thermal-hydraulics: simplified modelling based on 0D liquid water components below (r–z) gas flows, i.e. quasi static swollen level of water in a multi-channel configuration (no equation of motion for the liquid phase, simply assuming pressure equilibrium at the channel inlet), and, in the core region above, 2D gaseous phase composed of steam and non-condensable gases; in addition, a special channel made of one single mesh models the lower head region (Figure 2-3);
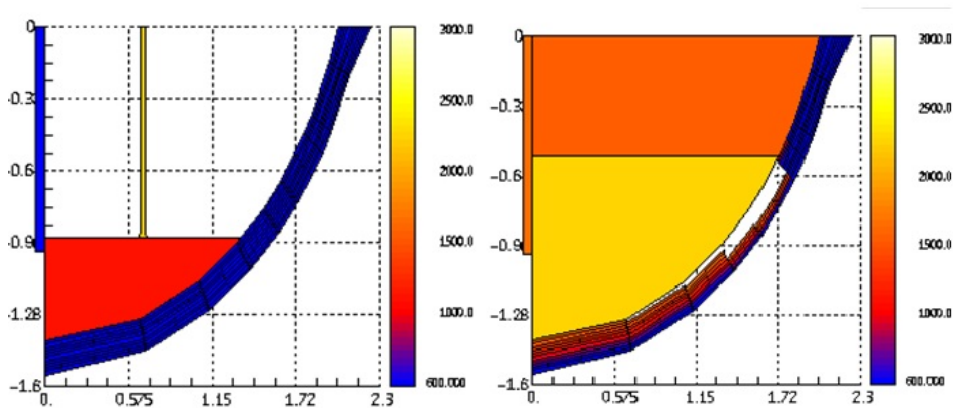
Figure 2-3 : ICARE one volume lower head model

- Heat transfer: axial and radial conduction between two walls, gap exchanges between rod and clad, convection between fluid and wall as well as radiation. For the latter, a general in-core heat transfer model (based on an equivalent radiative conductivity approach) allows to deal with radiative exchanges in a reactor core whatever the degradation level is (intact rods, moderately degraded rods, severely damaged core, large cavities), thus managing in a continuous way the heat transfers all along the evolution of the core geometry degradation. In addition, radiation from the lower core structures to the residual water in lower plenum is also modelled, which favours vaporization of water;

- Power: either nuclear power generated by fission products (FPs) or generated in a given material, or electric power generated in some out-of-pile experiments;

- Rod mechanics: ballooning, creep and burst of Zircaloy fuel rod claddings (including both Zry-4 and Zr1%Nb alloys), creep of control rod stainless steel claddings, loss of integrity of fuel rods(using user-criteria);

- Chemistry: oxidation of Zr by steam (including correlations for both Zry-4 and Zr1%Nb alloys), oxidation of stainless steel by steam, dissolution of UO_2 by solid and liquid Zr, dissolution of Zr by liquid Silver–Indium–Cadmium alloy, dissolution of Zr by solid steel, oxidation and degradation of B_4C control rods,

20

oxidation/dissolution of relocating and relocated U–O–Zr magmas, oxidation of solid debris particles

- Vessel lower head rupture: melt-through or mechanical failure (either instantaneous plastic rupture or creep rupture) accounting for the corium and water loading on the lower head wall and also for the possible vessel wall partial melting based on different approaches considering e.g. different lower head geometries; user-criteria such as temperature, degradation rate, stress can also be defined;

The flexible description of geometry of vessel lower head allows simulating any type of shape such as hemispherical one for PWRs and ellipsoidal one for most of VVERs. Indeed, two alternative models are available for the vessel lower head mechanical failure: a general one (LOHEY model) valid for both hemispherical and elliptical shapes and a more sophisticated one, valid (OEUF model) only for hemispherical shape which peculiarity is to assume the final shape to look like an "egg" shell. As concerns numeric, the oxidation reactions obey an implicit scheme in order to manage the calculation of hydrogen production while reducing computing time. Moreover, as already noticed, there is a special coupling at the core boundaries between the CESAR and ICARE modules.

2.3.3   The ELSA module

The ELSA module aims at simulating the release of Fission Product (FP) and structural material (SM) from the degraded core. ELSA is tightly coupled with the ICARE module. The modelling allows describing the release from fuel rods and control rods, followed by the release from debris beds. The modelling is based on a semi-empirical approach and the physical phenomena taken into account are the main limiting phenomena, which govern the release. For intact fuel rods and debris beds, the FP release is described according to the degree of fission product volatility. Three categories are distinguished with the following characteristics [5]:

- Release of volatiles (such as I or Cs including noble gases) is described by species intra-granular diffusion through UO_2 fuel grains, taking account of fuel oxidation (UO_2 þx) and of a grain-size distribution. The Te, Se and Sb can be partially trapped in the cladding depending on the temperature and on the degree of cladding oxidation. At fuel melting point, all the remaining species located in the liquid part of the fuel are supposed to be instantaneously released.
- Release of semi-volatiles (Ba, Ru, Sr, La, Eu, Ce, Mo) is described by evaporation and mass transfer processes.
- Release of low-volatiles (such as U or Pd) is described by fuel volatilization treated as the vaporization of UO_3.

Concerning the SM, release of Ag, In, Cd, Sn, Fe, Ni and Cr is taken into account in ELSA as follows:

- Ag, In and Cd (AIC) are released from degraded control rods. The same approach as for semi-volatile species is used, that is evaporation and mass transfer processes.
- Fe, Ni and Cr are supposed to be released during the candling of steel materials, using the same approach as for the release of Ag, In and Cd. Tin (Sn) is supposed to be released as a proportion of the rate of ZrO_2 formation. All mentioned SM can also be released from the corium molten pool.

2.3.4   The SOPHAEROS module

The SOPHAEROS module simulates transport of FP vapours and aerosols in the RCS, composed of a 1D series of control volumes, through gas flow to the containment, accounting for the chemical reactions in the vapour phase. Using five states (suspended vapours, suspended aerosols, vapour condensed on walls, deposited aerosols, sorbed vapours), SOPHAEROS uses either a mechanistic or a semi-empirical approach to model the main vapour-phase and aerosol phenomena [6]. The module, calculates the gaseous-species masses in thermodynamic chemical equilibrium in each control volume from the masses of the elements, the temperature and the volume. The chemical equilibrium is assumed to be reached instantaneously within the gaseous phase and chemical reactions are neglected in condensed phases, i.e. aerosols or deposits. The energy involved in chemical reactions is neglected and the carrier gas mass does not change even if some of it participates in chemical reactions. These assumptions are approximations imposed by the fact that this module does not calculate thermal-hydraulic conditions. Concerning the aerosol phenomena the module describes:

- Agglomeration: gravitational, Brownian diffusion, turbulent diffusion;
- Deposition mechanisms: Brownian diffusion, turbulent diffusion, eddy impaction, sedimentation, thermophoresis, diffusion-phoresis, impaction in bends. Deposit of aerosols in a flow contraction (either abrupt one with a 90∘angle or conical) can be simulated;
- Remobilization of deposits: revaporisation and mechanical resuspension;
- Dedicated pool-scrubbing model to deal for example with the retention of aerosols in the secondary side of flooded steam generators in case of SGTR scenario.

By default, the RCS axial nodalization (set of volumes connected by junctions) used by SOPHAEROS is fitted on the CESAR one.

2.3.5 The CPA module

The CPA module simulates thermal-hydraulics (including hydrogen combustion) and aerosol behaviour in the containment [7]. It consists of two main sub-modules, namely THY (for thermal-hydraulics) and AFP (for aerosols and FPs). The discretisation through a "lumped-parameter" approach (0D zones connected by junctions and surrounded by walls) simulates simple or multi-compartment containments (tunnels, pit, dome) with possible leakages to the environment or to normal buildings, with specified openings to the environment. Either several real compartments can be combined to become one CPA zone or large compartments can be divided into several zones to cover flow peculiarities more conditions. Peculiarities more realistically, e.g. steam or hydrogen plumes. Using the sources of steam, hydrogen, FP gases and aerosols from RCS or from corium in the cavity during Molten Core Concrete Interaction MCCI provided by other modules of ASTEC, CPA calculates gas distribution, temperature field, pressure build-up, hydrogen combustion and FP and aerosol distribution and deposition.

2.3.6 The SYSINT module

The SYSINT module allows the user to simulate the management of engineered safety features, such as, for instance, safety injection systems, pressurizer spray and heaters, management.

2.3.7 The RUPUICUV module

The RUPUICUV module simulates the Direct Containment Heating (DCH), which may potentially develop after vessel lower head rupture occurrence under relatively high pressure. The corium is discharged at high temperature driven by primary pressure into the cavity (involving vessel blow-down and cavity pressurization), where some part of the ejected corium may be potentially oxidized and entrained into the containment, thus contributing to the containment heat-up and additional hydrogen production. The simple CORIUM parametric module simulates the behaviour of corium droplets transported by hot gases into the containment atmosphere and sump, heat transfer between corium and gas being modelled in each containment zone.

2.3.8 The MEDICIS module

The MEDICIS module [8] simulates Molten-Core–Concrete Interaction (MCCI) using a lumped-parameter 0D approach with averaged corium layers. Corium remaining in the cavity interacts with concrete walls and both bottom and lateral interfaces. This module assumes either a well-mixed oxide/metal pool configuration or a possible pool stratification into separate oxide and metal layers, with in both cases the possibility to account for a detailed description of the upper crust. It describes concrete ablation (Figure 2-4), corium

oxidation and release of non-condensable gases (H_2, CO, CO_2) into the containment.
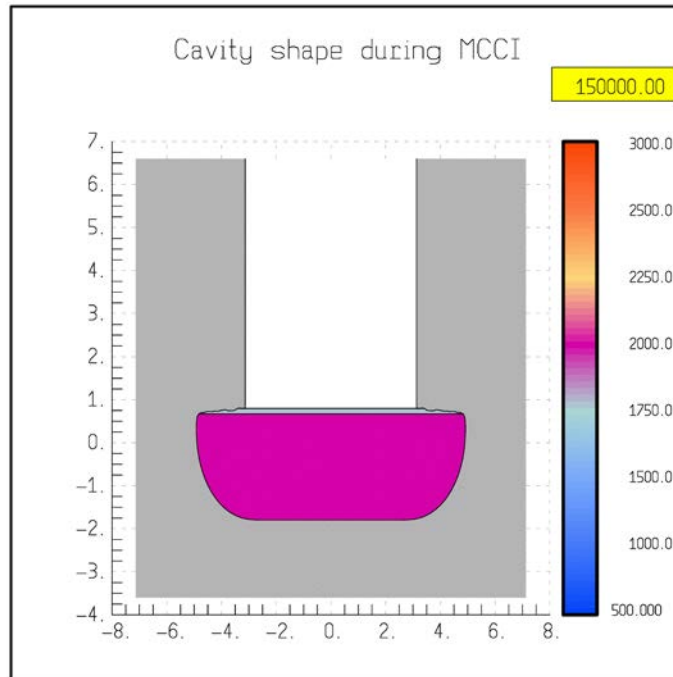
Figure 2-4: Cavity ablation simulation with MEDICIS

2.3.9   The IODE module

The IODE module simulates iodine and ruthenium behaviour inside the containment, except the transport through compartments of the associated species, which is computed by the CPA module (i.e. as for transport, the IODE module is directly using the junction flow rates given by the CPA containment module). The module is validated using, for example, experiments conducted under the auspices of SARNET [9].

2.3.10   The DOSE module

The DOSE module, which was designed for use in most of the IODE gas phase chemical reactions, was specifically implemented in ASTEC V2 to answer IRSN PSA2 requirements. This module allows evaluating the dose rate in bulk gas phase for each zone of the containment, as well as the inner wall dose rate, knowing that the, dose rates include and radiation contributions relative to each isotope. Anyway, it has however to be underlined that, up to now, this module was only validated by comparison with dedicated IRSN codes.

2.3.11   The ISODOP module

The ISODOP module simulates decay of FP and actinide isotopes in different zones of the reactor and of the containment. It starts the calculation using an initial isotope inventory generated by a

dedicated code (for instance the CEA code PEPIN) and allows estimating decay heat and activity in the core, in the RCS, in the containment and in the environment. The ISODOP module was based on the DOP database from CEA containing the description of 720 isotopes while the JEFF (Joint Evaluated Fission and Fusion) database dealing with ~3800 isotopes is now also available in the subsequent V2.0 revisions as an alternative to the original CEA database.

2.4 Use and Coupling modules of ASTEC code

To simulate an accident scenario with ASTEC code, a stationary input deck for CESAR has to be built, to establish the initial conditions of the transient. This stationary transient has to run for a time chosen by the user, in order to verify that the calculated conditions were steady and the actual initial conditions of the simulation were achieved. The restart file generated by this run has been used as initial condition for the transient simulation. When the transient of a severe accident starts, during the entire front-end phase, the CESAR module alone, calculates the thermal-hydraulics in the whole RCS, i.e. including the vessel (lower plenum, core, bypass, downcomer and upper plenum). An automatic switch to ICARE for simulation of in-vessel core degradation phenomena is then applied, depending on specific criteria e.g. void fraction in primary circuit loop, void in the upper plenum, void fraction at the top of the core, steam temperature at the top of the core, and non-isolated accumulators mass fraction. This switch becomes effective around time of start of core uncovery, and in any case before the start of Zry cladding oxidation by steam. After the switch, CESAR calculates only thermal-hydraulics in the loops and the vessel upper plenum, while in addition to the degradation phenomena ICARE calculates thermal-hydraulics in the remaining part of the vessel (core, bypass, lower plenum and downcomer) all along the degradation phase. During the degradation phase (i.e. after the switch), a specific prediction-correction numerical coupling approach is used between CESAR and ICARE. At each macro time-step, first the RCS thermal-hydraulics is predicted by ICARE using as inputs the CESAR outputs from the previous macro time-step. Then CESAR computes the two-phase thermal-hydraulics in the circuits using source and sink terms supplied by ICARE at the vessel junctions and it finally evaluates the possible waterfall back into the vessel at the end of the macro time-step. Both numerical schemes are therefore disconnected and each module is running at its own time-step. Meeting points occur at the end of an intermediate macro time-step. This macro time-step management had been differentiated from the other modules in order to gain CPU time.

Chapter 2. The ASTEC Integral code

Reference chapter 2

[1] P. Chatelard, N. Reinke, Overview of the integral code ASTEC V2.0, Report ASTEC-V2 DPAM/SEMCA-2009-149.

[2] P. Chatelard, N. Reinke, et al., "*ASTEC V2 severe accident integral code main features, current V2.0modelling status, perspectives*", Progress in Nuclear Energy 70 (2014) pg. 20-28

[3] N. Tregoures, G. Bandini, L. Foucher, J. Fleurot, P. Meloni, "*Validation of CESAR Thermal-hydraulic Module of ASTEC V1.2 Code on BETHSY Experiments*", Journal of Power and Energy Systems, Vol. 2, No. 1, 2008, pp 386-395

[4] Chatelard, P., Fleurot, F., Marchand, O., Drai, P., 2006. ICONE-14 conference, July17–20, Miami, FL, USA. Assessment of ICARE/CATHARE V1 severe accident code.

[5] Brillant, G., Marchetto, C., Plumecocq, W., 2013b. "*Fission product release from nuclear fuel II. Validation of ASTEC/ELSA on small and large scale experiments*". Annals of Nuclear Energy 61, 96–101.

[6] Cousin, F., Dieschbourg, K., Jacq, F., 2008. "*New capabilities of simulating fission product transport in circuits with ASTEC/SOPHAEROS v1.3*". Nuclear Engineering andDesign 238, 2430–2438.

[7] Kljenak, I., Dapper, M., Dienstbier, J., Herranz, L.E., Koch, M.K., Fontanet, J., 2010. "*Thermal-hydraulic and aerosol containment phenomena modelling in ASTEC severe accident computer code*". Nuclear Engineering and Design 240,656–667.

[8] Cranga, M., Fabianelli, R., Jacq, F., Barrachin, M., Duval, F., 2005. The MEDICIS code, a versatile tool for MCCI modelling. In: ICAPP'05, May 15–19, Seoul, Korea.

[9] Haste, T., Clément, B., et al., "*Main outcomes of fission product behavior in the Phébus FPT3 test*". In: 4th European Review Meeting on Severe Accident Research (ERMSAR-2010) Bologna Italy, 11-12 May

CHAPTER 3

SMALL MODULAR REACTORS

3.1   Definition of Small Modular Reactors

The continued development of economic and environmentally friendly nuclear power plants (NPPs) can play a fundamental role in the improvement of living standards worldwide. As the life of existing NPPs is extended and new plants are designed and built, public perceptions of the safety of these plants will continue to have an important impact on the future of these plants. In many cases, one of the most critical factors in public perception is the potential for the occurrence of severe accidents. Because of more than two decades of research in the field of severe accidents in NPPs, it has become increasingly clear how the consequences of such accidents can be reduced or even eliminated through the use of improved training, through the development of more realistic accident management strategies and, ultimately, through the development of more advanced reactor designs. This is the reason why, in the recent years, the Small Modular Reactors (SMRs) have been attracting considerable attention around the world. The same U.S. Department of Energy (DOE) affirmed that the next big thing in nuclear energy would be a small thing: the SMR. The IAEA defines a "Small" reactor as one having electrical output less than 300MWe and a "Medium" reactor as one having output between 300 and 700MWe. More often, the two are combined into the commonly termed "Small and Medium-sized Reactors" or the same "Small Modular Reactors" representing those with an electrical output less than 700 MWe [1]. The minimum rating assures that, the reactor delivers power suitable for the practical industrial application of interest. The maximum rating constrains these designs to power levels at which the expected advantages of serial production and incremental deployment as well as the match to electric grid siting opportunities

Chapter 3. Small Modular Reactor

and constraints can be realized. The term "Modular" refers to the unit assembly of the Nuclear Steam Supply System (NSSS) which, when coupled to a power conversion system or process heat supply system, delivers the desired energy product. The unit assembly can be assembled from one or several sub-modules. The desired power plant can then be created from one or several modules as necessary to deliver the desired power rating. Currently, there are more than 45 SMR designs under development for different application issues [2]. These SMRs could be broadly classified into three major groups according to their designs. The first group of SMRs is based on the design concepts of proven and widely utilized light water reactors, namely Pressurized Water Reactors (PWRs). This kind of reactors is considered, the most mature, having the lowest technical risk and will be treated in this chapter. The second group consists of gas-cooled SMRs. The third group includes the SMRs designed from advanced and innovative concepts, using non-LWR coolants such as liquid metal, helium or liquid salt, which may offer added functionality and affordability. Incorporation of inherent and passive safety design features has become a 'trademark' of most of these SMR concepts including several evolutionary designs and nearly all innovative concepts. Hereafter will be described the main characteristics and some model of the SMR belonging to the first group; given that, this kind of SMR are already in a state of advanced development.

3.2   Main Characteristics of the SMRs

The current pressurized water SMR designs, mainly rooted from two origins, the marine-based power reactors, such as the mPower derived from the Otto Hahn marine reactor and the land based electricity generation reactor, such as WSMR from the AP1000 reactor [3]. The design objectives of SMR are smaller power grade, smaller configuration size, smaller generation cost, and smaller operation risk. Consequently, the SMR designs absorb the advantages of the existing marine-based and land-based reactors, meeting the design objectives through progressive or significant innovation. In the SMR designs, the defence in depth strategy is used as in larger reactor designs to protect the public and environment from accidental releases of radiation. The main goal is to prevent or eliminate as many accident initiators and accident consequences as possible. Certain common measures of SMR lead themselves to safety are the relatively smaller core sizes enabling integral coolant system layouts, the larger reactor surface-to-volume ratios, and the lower core power densities. The intended outcome is greater plant simplicity with high safety levels and possibly reduced emergency response requirements. Most of this kind of reactors adopts an Integral Pressurized Water Reactor designs (iPWR), in

Chapter 3. Small Modular Reactor

which most of the primary system components are contained within a single vessel. The integral design reduces the number and size of penetrations and welding links through the reactor pressure vessel, eliminating the high-consequence accident scenario of a large pipe-break Loss Of Coolant Accident (LOCA). In a PWR the maximum size pipe penetrating the reactor vessel is on average 5-7 cm in diameter, while in a large PWR pipes that connect the reactor vessel to the external steam generator vessels are 80-90 cm diameter. The SMRs focus them safety functions on proper cooling of reactor core in case of accidents through this following approach [4]:

• The adoption of an increased relative coolant inventory.

An enlarged vessel yields a larger inventory of water per unit of power than in the loop type plant, which increases the relative thermal inertia within the reactor vessel (Figure 3-1). This result in a reduction in the rate at which the system temperature increases during a loss of forced flow transient, providing the operators with more time to respond to an upset condition.

Figure 3-1: IRIS and AP1000 vessel comparison (Rhinoceros 5)

- An increased relative heat transfer area.

A simple calculation could reveal that relative surface area of the iPWR vessel per unit power is increased. Roughly speaking, if a diameter of a SMR reactor core is 1/n of a large reactor, then the relative surface area of reactor vessel per unit power could be at least n times of a large reactor.

- An increased passive cooling capability.

The vessel height-to diameter ratio of a SMR is 2-3 times larger than that of a large reactor since more equipment are incorporated vertically inside the vessel. This increases gravity-driven natural convection circulation capability.

Concerning the prevention of radiation release, SMRs have following measures:

- Smaller radionuclide inventory.

The radionuclide inventory in a reactor core is roughly proportional to power level. In addition to the intrinsically smaller radionuclide inventory of an SMR, some SMR designs add additional barriers to fission-product release to achieve a dramatically smaller accident source term.

- Under-ground construction.

The smaller plant footprint of an SMR makes it more economically viable to construct the primary reactor system fully below ground level, which significantly hardens it against external impacts such as aircraft or natural disasters. As an example, the WSMR design has a containment vessel volume that is more than 23 times smaller than the Westinghouse AP-1000 containment. Below-grade construction of the reactor and containment vessels also provides the potential for additional seismic resistance and helps reduce the number of paths for fission-product release in the event of an accident.

3.3 Main design features of the SMRs

Currently, four integral pressurized water SMRs are under development in the USA: Babcock & Wilcox's mPower, NuScale, SMR-160 and the Westinghouse SMR. The mPower design consists of two 180 MWe modules and its design certification application is expected to be submitted to the US Nuclear Regulatory Commission (NRC) in the short term. NuScale Power envisages a nuclear power plant made up of twelve modules producing more than 45 MWe and has a target commercial operation in 2023 for the first plant that is to be built in Idaho. The design certification application of NuScale to the NRC is expected in the second half of 2016. The Westinghouse SMR is a conceptual design with an electrical output of 225 MWe, incorporating passive safety systems and proven components of the AP1000. The SMR-160 design generates power of 160 MWe adopting passive safety features and its conceptual design is to be completed in 2015. In academic domain, the Politecnico di Milano (POLIMI) in Italy and universities in Croatia and

Japan performs one of the research and development activities on SMRs, that are continuing the development of the International Reactor Innovative and Secure (IRIS), previously lead by the Westinghouse consortium. IRIS is an integral PWR design with an electrical capacity of 335 MWe.

3.3.1 The mPower reactor

Babcock & Wilcox (B&W) unveiled the mPower reactor in June 2009 [5]. The reactor had a planned capacity of 125 MWe when originally announced, and the reactor's rated capacity was raised to 530 MWt of thermal power and 180 MWe of electrical power after its pre-application design certification interaction to the U.S. Nuclear Regulatory Commission (NRC) [6]. The mPower reactor is a direct descendent of the B&W maritime reactor program, which was used in the nuclear powered merchant ship Otto Hahn that had been successfully launched in 1964 [7]. Key features of the Otto Hahn reactor design are incorporated in the B&W mPower reactor design, which includes the placement of NSSS components within a single pressure vessel. The control rod drives do not penetrate the integral reactor vessel (IRV), but are instead wholly enclosed within the IRV Figure 3-2. The pressurizer is at the top of reactor vessel. The integral once-through steam generator (IOTSGs) surround the central riser, below the pressurizer. These IOTSGs are an advanced derivative of the steam generators used in older B&W designs. The mPower is designed to produce superheated steam and does not require steam separators and dryers prior to admitting steam into the high-pressure turbine. The reactor coolant pumps are located in the downcomer annulus, just below the steam generator. The core is located at the bottom of the reactor vessel. The B&W mPower has a "conventional core and standard fuel" (< 20 t) enriched to about 3.5÷5 %, with burnable poisons, to give a four/five-year operating cycle between refuelling, 60-year service life is envisaged, as sufficient used fuel storage would be built on site for this. The safety feature profits from the integral design of the reactor vessel. As it contains the entire primary coolant loop within the reactor pressure vessel with automatic primary loop depressurization, the integral reactor vessel does not have large cold or hot leg piping thus the potential of large break loss of coolant accidents is eliminated. As no electrically driven pumps are required, heat removal can be used in the event that these systems are exhausted by flooding the containment and establishing natural circulation. Passive safety concept is adequately utilized since the heat power is much smaller and the relative cooling ability could be enhanced. There are water supplies located above and within the containment that can cool the vessel with gravity driven-cooling if secondary cooling is lost. The Figure 3-3 shows the safety systems adopted by the mPower reactor.

Chapter 3. Small Modular Reactor

1) Pressurizer,
2) Steam generators
3) feed water inlet
3) steam outlet
4) Pumps
5) CRDMs
6) Upper internals
7) Reactor core
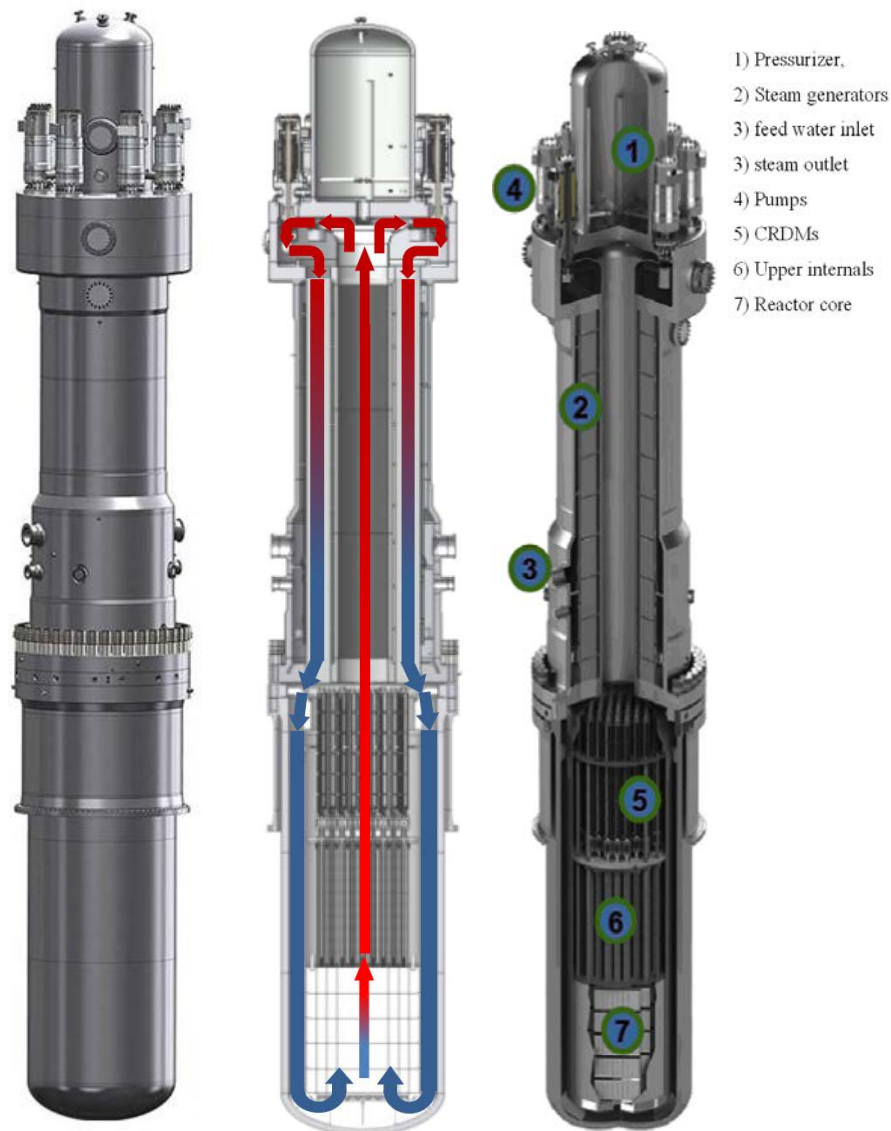
Figure 3-2: mPower Integral Reactor Vessel (IRV)

The inherent safety features of the reactor design include:

- a low core linear heat rate which reduces fuel and cladding temperatures during accidents;
- a large reactor coolant system volume which allows more time for safety system responses in the event of an accident;
- small penetrations at high elevations, increasing the amount of coolant available to mitigate a small break loss of coolant accident (LOCA).

The emergency core cooling system is connected with the reactor coolant inventory purification system and removes heat from the reactor core after anticipated transients in a passive manner, while also passively reducing containment pressure and temperature. The plant is designed without taking any safety credit for standby diesel

generators, and a design objective is no core uncovery occurs during any credible design basis accident. As statement before the large pipe break LOCA is not possible, because the primary components are located inside the pressure vessel and the maximum diameter of the connected piping is less than 7.6 cm [2]. The mPower SMR has decay heat removal systems that consist of a passive heat exchanger connected with the atmosphere (as the ultimate heat sink), an auxiliary steam condenser on the secondary system, water injection or cavity flooding using the reactor water storage tank, and passive containment cooling.
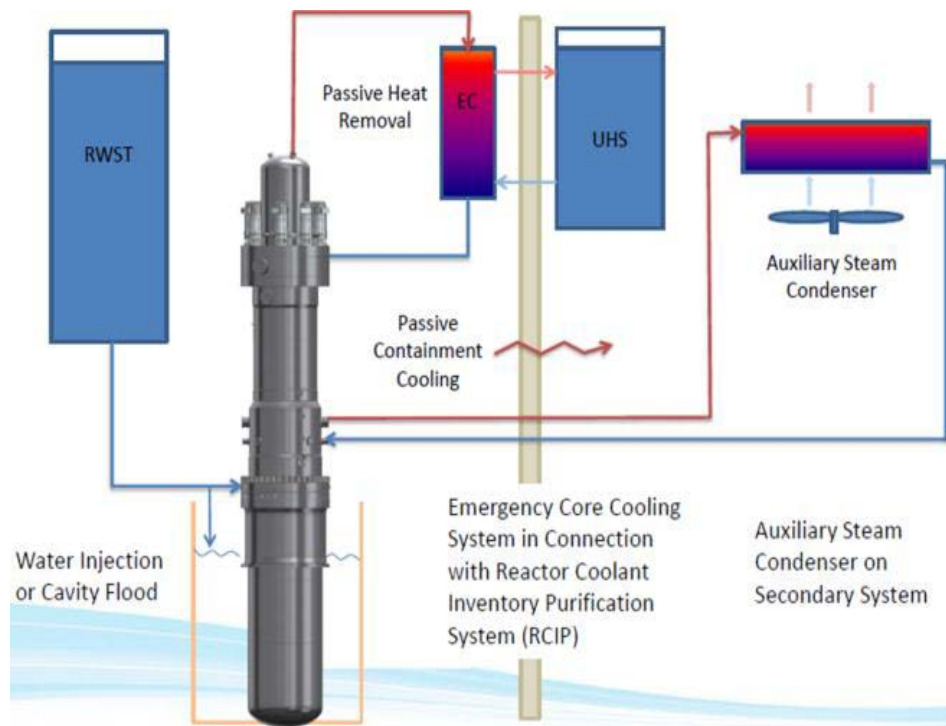
Figure 3-3 : mPower reactor safety systems

The philosophy implemented in B&W mPower for coping with an accident does not rely on the plant-containment coupling. Figure 3-4 shows a layout of a two-unit site and a cutaway view of the containment building, which is a low-leakage, reinforced concrete, steel-lined seismic category-I structure. The containment building and other critical structures are located below ground level. Normal access is via two personnel hatches, and a removable equipment hatch on the top of the building provides access for large component replacement. The other buildings are situated below grade level, except for the reactor service building, which is located partially below grade level, and the turbine building, which is located above the ground level.

Chapter 3. Small Modular Reactor

Figure 3-4: Two-Unit plant layout Figure and Containment building

3.3.2   The NuScale reator

The NuScale SMR plant is an innovative design that builds on 50 years of worldwide experience with the commercial application of pressurized, light-water-cooled reactor (LWR) technology.
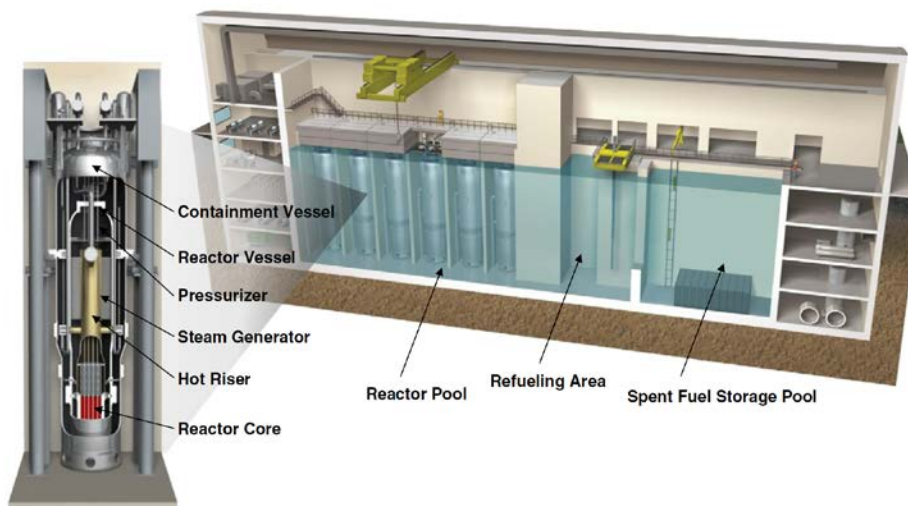
Figure 3-5 : NuScale power module (L) and cutaway of 12-modules plant (R).

The design incorporates several features that reduce complexity, improve safety and enhance operability. From the outset, the top-level design goals for the NuScale plant have been to achieve a high level of safety and asset protection while providing an affordable approach to nuclear power that gives the plant owner the maximum flexibility in construction, operation and application of the plant. The

fundamental building block of the NuScale plant is the NuScale power module. The power module consists of a small 160 MW$_t$ reactor core housed with other primary system components in an integral reactor pressure vessel and surrounded by a steel containment vessel, which is immersed in a large pool of water. Several power modules – as many as 12 modules – are co-located in the same pool. Models of a single power module and a multi-modules plant are shown in Figure 3-5. The reactor vessel is approximately 20 m tall and 2.7 m in diameter. The integral vessel contains the nuclear core consisting of 37 fuel assemblies and 16 control rod clusters. The fuel assemblies are shorter than traditional pressurized water reactor (PWR) fuel assemblies but use the same 17x17 pin array geometry, same materials, and same fuel type. Above the core is a central hot riser tube, a helical coil steam generator surrounding the hot riser tube, and a pressurizer. The helical coil steam generator consists of two independent sets of tube bundles with separate feedwater inlet and steam outlet lines. A set of pressurizer heaters and sprays is located in the upper head of the vessel to provide pressure control. Primary reactor coolant is circulated upward through the reactor core and the heated water is transported upward through the hot riser tube. The coolant flow is turned downward at the pressurizer plate and flows over the shell side of the steam generator, where it is cooled by conduction of heat to the secondary coolant and continues to flow downward until its direction is again reversed at the lower reactor vessel head and turned upward back into the core. The coolant circulation is maintained entirely by natural buoyancy forces of the lower density heated water exiting the reactor core and the higher density cooled water exiting the steam generator [8]. On the secondary side, feedwater is pumped into the tubes where it boils to generate superheated steam, which is circulated to a dedicated turbine–generator system. Low-pressure steam exiting the turbine is condensed and recirculated to the feedwater system. The entire nuclear steam supply system is enclosed in a steel containment that is 24.6 m tall and 4.6 m in diameter. The small volume, high design pressure containment vessel is a unique feature of the NuScale design and contributes significantly to the large safety margins and overall resilience of the plant design. The reactor building is a Seismic Category 1 reinforced concrete structure designed to withstand the effects of aircraft impact, environmental conditions, natural phenomena, postulated design basis accidents, and design basis threats and houses all the systems and components required for plant operation and shutdown. Portions of the reactor building are located above and below grade, The NuScale Power Modules, reactor pool, and the spent fuel pool are located at or below nominal plant grade level, while the hoisting and handling equipment is

Chapter 3. Small Modular Reactor

located above grade. The surface of the reactor pool water is located at approximately ground level. At a 12-module facility, the NuScale Power Modules are installed in a vertical position and are arranged into two rows of 6 modules along the reactor pool walls. Concrete walls separate the modules in individual reactor bays. An extra reactor bay is located adjacent to the units for either module maintenance or storage of a possible spare module. A central channel is provided between the rows of modules to allow for moving of the modules between the reactor pool and the connected refueling pool. Pipes interfacing with the NuScale Power Module (i.e., feed water piping, steam piping, the chemical and volume control system, containment evacuation system, instrumentation, and power connections) are located above the water level. Pipefittings are provided in this area to permit manual connection and disconnection during module installation, refueling outages, and during replacement or removal of modules. The reactor pool consists of a large, below-grade concrete pool with a stainless steel liner that provides stable cooling for the NuScale Power Modules for an unlimited period of time following any actuation of the Emergency Core Cooling System (ECCS). Furthermore, this unique design of the NuScale containment vessel and its immersion in the ultimate heat sink allows the ECCS to be simplified considerably compared to other reactor designs. The ECCS consists of just two independent Reactor Vent Valves (RVVs) and two independent Reactor Recirculation Valves (RRVs) and the Decay Heat Removal System (DHRS). The ECCS provides a means of long-term decay heat removal in the event of a LOCA. The ECCS removes heat and limits containment pressure by steam condensation on the inside surface of the cold containment vessel. It also allows heat conduction through the containment vessel walls to the water in the reactor pool. The DHRS provides secondary side reactor cooling for non-Loss of Coolant Accident (LOCA) events when normal feed water is not available (Figure 3-6). The system is a closed loop, two-phase natural circulation cooling system. Redundant trains of decay heat removal equipment are provided, one attached to each steam generator loop. Each train is capable of removing 100 % of the decay heat load to cool the reactor coolant system [8]. Each train has a passive condenser submerged in the reactor pool. The condensers are maintained with sufficient water inventory for stable operation. Long-term cooling of the reactor core is established via recirculation of steam condensate back into the reactor pressure vessel via the RRVs. Following a LOCA or other condition resulting in an actuation of the ECCS, heat removal through the containment vessel rapidly reduces heat removal through the containment vessel rapidly reduces the containment pressure and temperature and maintains them at acceptably low levels for extended periods of

Chapter 3. Small Modular Reactor

time. Steam is condensed on the inside surface of the containment vessel, which is passively cooled by conduction and convection of heat to the reactor pool water.
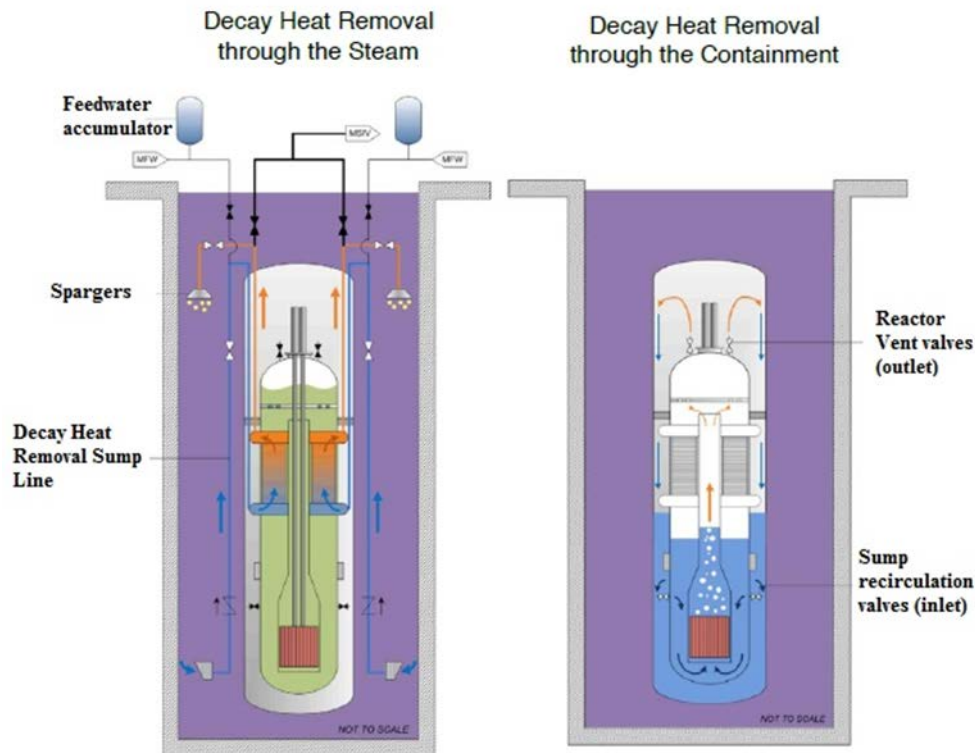
Figure 3-6: DHRS through the steam and DHRS through the containment

In the event of a complete station blackout (SBO), as experienced at the Fukushima Daiichi plants, heat is removed from the reactor modules by fail-safe actuation of the ECCS and allowing the reactor building pool to heat up and boil. Water inventory in the reactor pool is sufficiently large to cool all of the reactors and prevent fuel damage for at least 30 days without any source of power, operator action, or makeup water. After 30 days, water boil-off and passive air cooling of the containment vessel provide adequate cooling for an unlimited period of time. The stages of passive removal of the reactor decay heat for a long-term cool-down of the reactor module is illustrated in Figure 3-7. The key to ensuring the transition from water cooling to air cooling is the very small decay heat and the large containment surface area. After reactor shutdown, the power has decayed to 10 MW_t and after one day, the power has decayed down to 1.1 MWt. After 30 days, the decay heat being generated per module is less than 400 kW equivalent to about 250 hair dryers. This extremely robust safety feature is a direct consequence of the unique design of the compact containment vessel, the assured supply of long-term cooling afforded by the reactor pool, and the relatively low power output of each module.
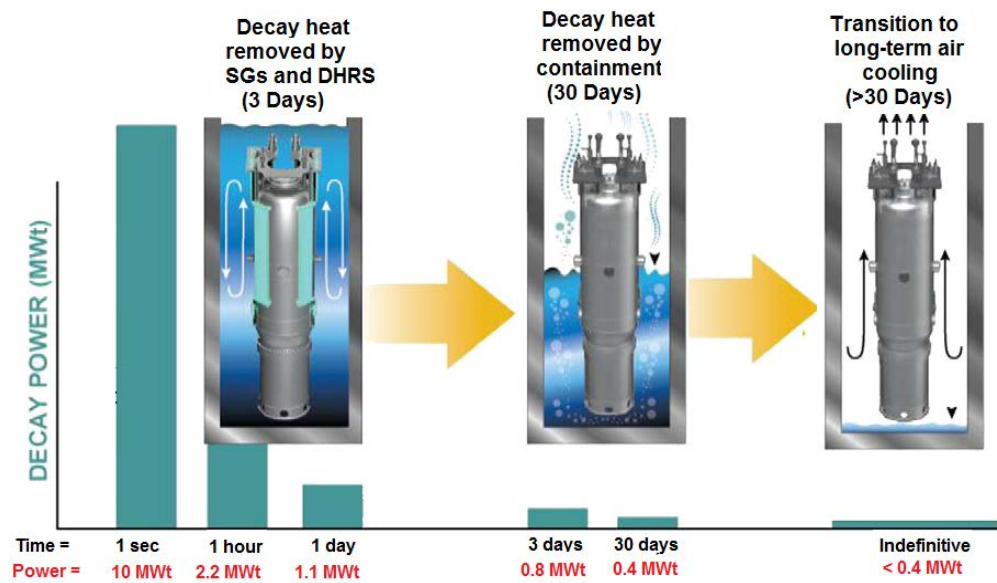
Figure 3-7: NuScale power module heat removal during a prolonged SBO event

3.3.3 The SMR 160 reactor

The SMR-160 conceptual design has been developed by Holtec International as an advanced PWR-type, small modular reactor, producing power of 525 MW$_{th}$ or 160 MW$_e$ adopting passive safety features. Simplification in the design is achieved by using fewer valves, pumps, heat exchangers, instrumentation, and control loops than conventional plants, simplifying operator actions during all plant modes, including diagnosing and managing off-normal and accident conditions. The SMR-160 uses fuel very similar to existing commercial LWR product lines, includes no reactor coolant pumps and utilizes a large vertical steam generator. The SMR-160 uses natural circulation for all power and accident modes and states. The reactor coolant system (RCS) continues to circulate by thermo-siphon action during accident scenarios [9]. The RCS is comprised of the reactor pressure vessel (RPV) and a steam generator (SG) in an offset configuration with an integrated pressurizer flanged to the top of the steam generator. The RPV and the SG are connected by a single connection (Figure 3-8), which houses both the hot leg and the cold leg. The hot leg is the inner pipe and the cold leg is the annular region of this single connection. Unique among integrated PWRs, the offset configuration allows easy access to the core without moving the RPV or SG during refuelling. The SG has a superheating feature, which eliminates the need for a Moisture Separator Reheater (MSR) and trains of feedwater heaters while not compromising the thermodynamic efficiency of the plant [2]. The secondary side has only one feedwater heater simplifying plant operations and maintenance. The RPV is located in a free standing

steel containment vessel called the Containment Structure (CS), supported within a reinforced concrete reactor building called the Containment Enclosure Structure (CES) which also provides missile protection. The annular region between the CS and the CES also called the Coolant Reservoir (CR) is filled with water and serves as the Ultimate Heat Sink (UHS) for SMR-160. The control rod drive mechanism (CRDM) based on existing technology is located outside the reactor coolant system on the RPV top head.
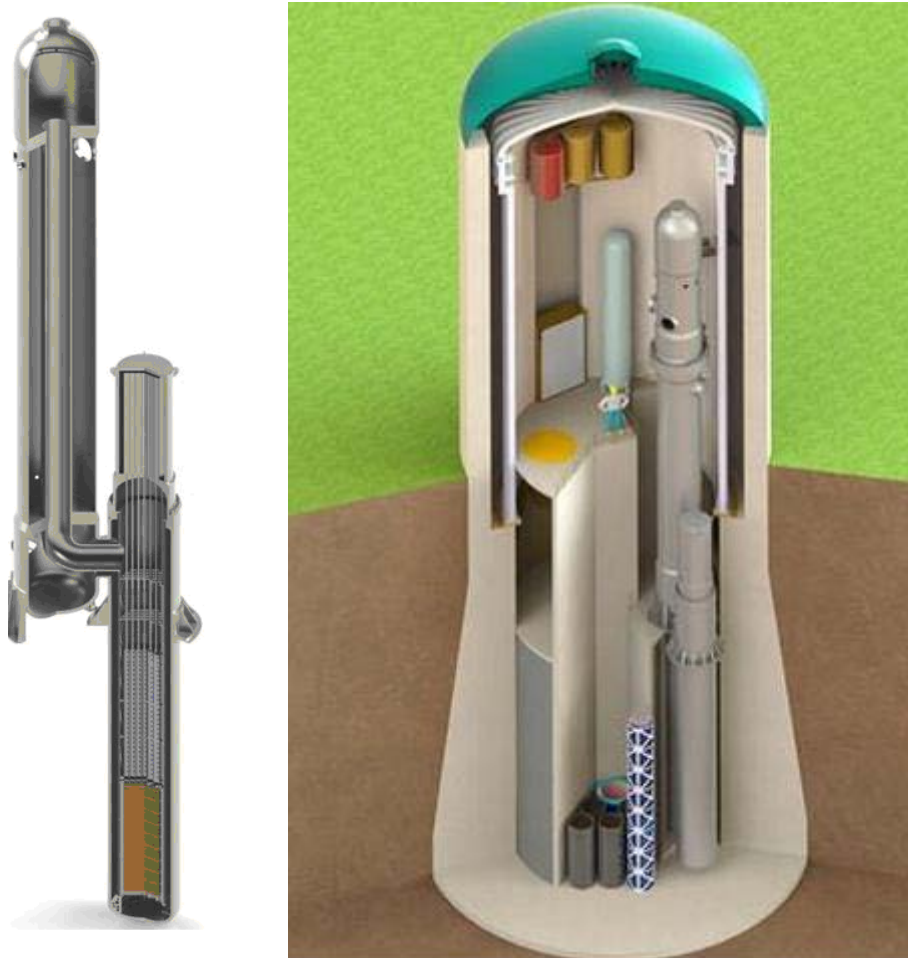
Figure 3-8: SMR-160 Reactor pressure Vessel RPV and Containment Structure (CS) and Containment enclosure structure (CES)

The pressurizer uses heaters and cold-water injection nozzles to perform the same functions of a typical pressurizer. Integrating the pressurizer with the steam generator eliminates the typical primary cold- and hot-legs along with their supporting structures normally connecting the primary external loop of a PWR to an external pressurizer and reactor coolant pumps. All of the electrical connections required to run the CRDMs and the pressurizer's heaters are external resulting in a highly simplified design. All of the

electrical connections required to run the CRDMs and the pressurizer's heaters are external the resulting design is highly simplified. The underground containment vessel part of the SMR-160 design houses the RPV and sections of the unitized integral steam generator unit, and the above ground part houses the top sections of the integral steam generator and pressurizer unit.

3.3.4   The SMR Westinghouse

The Westinghouse SMR is a modular pressurized water reactor with an integral configuration that improves on the concepts of simplicity and advanced passive safety demonstrated in the AP1000 plant.
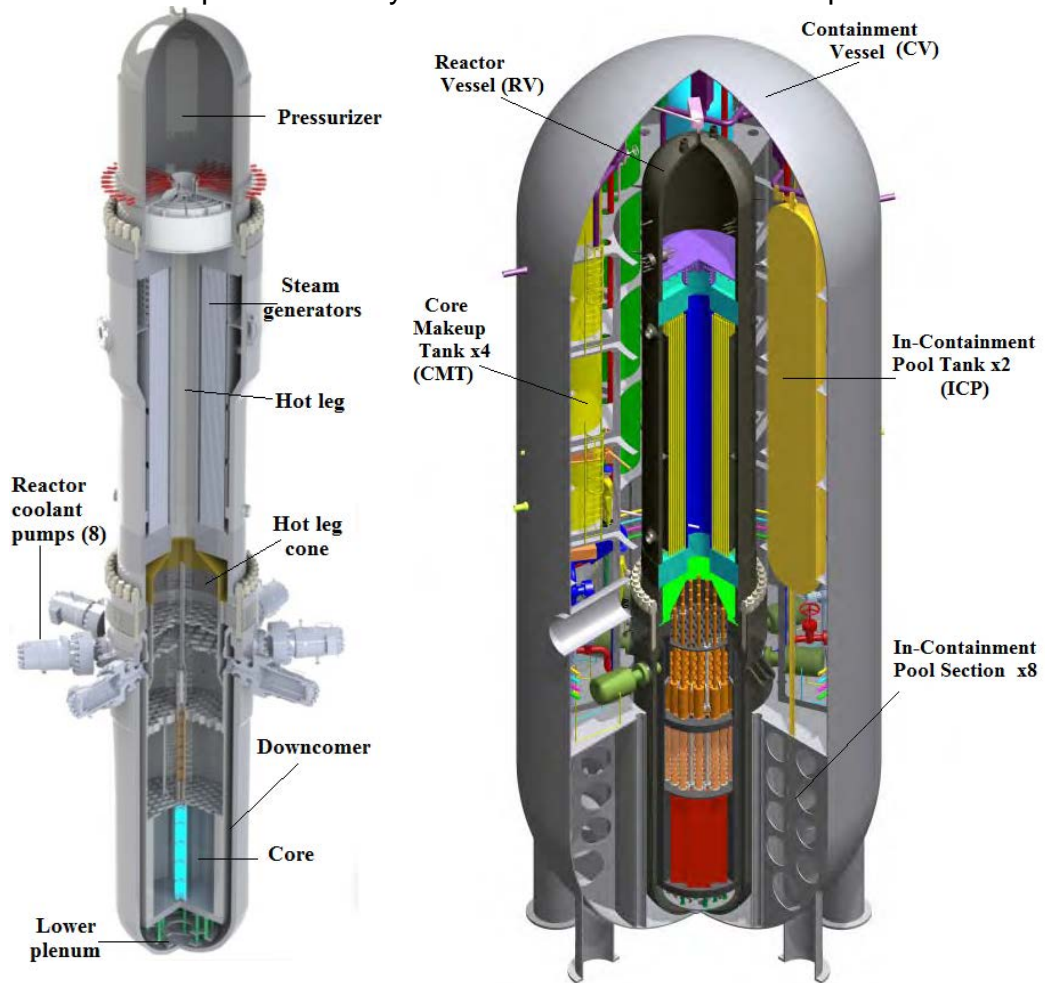
Figure 3-9 : Westinghouse SMR Vessel (RV) and Containment Vessel (CV)

The plant conceptual design was completed in 2011 and the preliminary design is currently underway. The plant is not reliant on AC power or other support systems to perform its safety functions. The seven day minimum coping time following loss of offsite power is a fundamental advancement over the three day coping time of the best, currently licensed plants. The integral reactor design

eliminates large loop piping and potential large break LOCA, and significantly reduces the flow area of postulated small break LOCAs. The below grade locations of the reactor vessel, containment vessel, and spent fuel pool provide protection against external threats and natural phenomena hazards. The small size and low power density of the reactor limits the potential consequences of an accident relative to a large plant. The plant is designed to be "stand-alone" with no shared systems, eliminating susceptibility to failures that cascade from one unit to another in a multi-unit station. The result is a plant capable of withstanding natural phenomena hazards and beyond-design-basis accident scenarios, including long-term SBO. The fully modular constructed Westinghouse SMR containment vessel has a height of 28.5 m and an outer diameter of 9.75 m. The reactor vessel has a height of 28 m and an outer diameter of 3.7 m. The core is based on the licensed Westinghouse robust fuel assembly (RFA) design, and uses 89 standard 17 x 17 fuel assemblies, the same of AP1000 reactor, but with an 2.4 m active fuel height, and Optimized ZIRLO cladding for corrosion resistance. A metallic radial reflector is used to achieve better neutron economy in the core while reducing enrichment requirements to less than the existing statutory limit of 5.0 wt% ^{235}U. Approximately 40% of the core is replaced every two years, resulting in an efficient and economical operating cycle of 700 Effective Full Power Days (EFPD) that coincides with existing regulatory surveillance intervals [10]. Further based on the AP1000 plant design, the reactor vessel internals are modified for the smaller core and to provide support for the internal control rod drive mechanisms. Eight proven, horizontally mounted axial-flow pumps provide the driving head for the reactor coolant system while eliminating the need for pump seal injection. The recirculating, once-through, straight tube steam generator design, achieves a compact physical envelope with an innovative approach to steam separation. Finally, the pressurizer is integrated into the reactor vessel head to eliminate the need for a separate component. The power station delivers a thermal output of 800 MWth and an electric output of greater than 225 MWe. Three diverse decay heat removal methods are provided in the Westinghouse SMR (Figure 3-8). The first method of decay heat removal uses gravity feed from the steam drum through the steam generator for approximately 80 minutes of natural circulation cooling. In this scenario, steam is released to the atmosphere through two redundant power-operated relief valves (PORV). The second decay heat removal method can be achieved by cooling the RCS with a passive decay heat removal heat exchanger, one of which is located in each of four core makeup tanks (CMT). Heat from the CMTs is then rejected to four heat exchangers located in two Ultimate Heat Sink System (UHS) tanks. The UHS tanks are sized to provide a

Chapter 3. Small Modular Reactor

minimum of seven days of decay heat removal, with additional options to replenish lost inventory and cool the plant indefinitely. A third diverse method of decay heat removal capability is available by cooling the RCS with diverse bleed and feed methods. This method includes a two-stage automatic depressurization system (ADS) that vents the RCS to the containment through Direct Vessel Injection (DVI) pathways, water injection from the four CMTs and in-containment pool (ICP) tank paths, and gravity-feed boric acid tank water makeup to the DVI paths. The steam vented from the RCS to the containment is cooled and condensed by the containment shell. The containment shell is cooled by the water, in the outside containment pool (OCP), which surrounds the containment. When the OCP water eventually boils, makeup water is provided by gravity from each of the two redundant UHS tanks that maintain the OCP full of water. The water condensed on the containment shell flows back into the RCS through two sump injection flow paths.
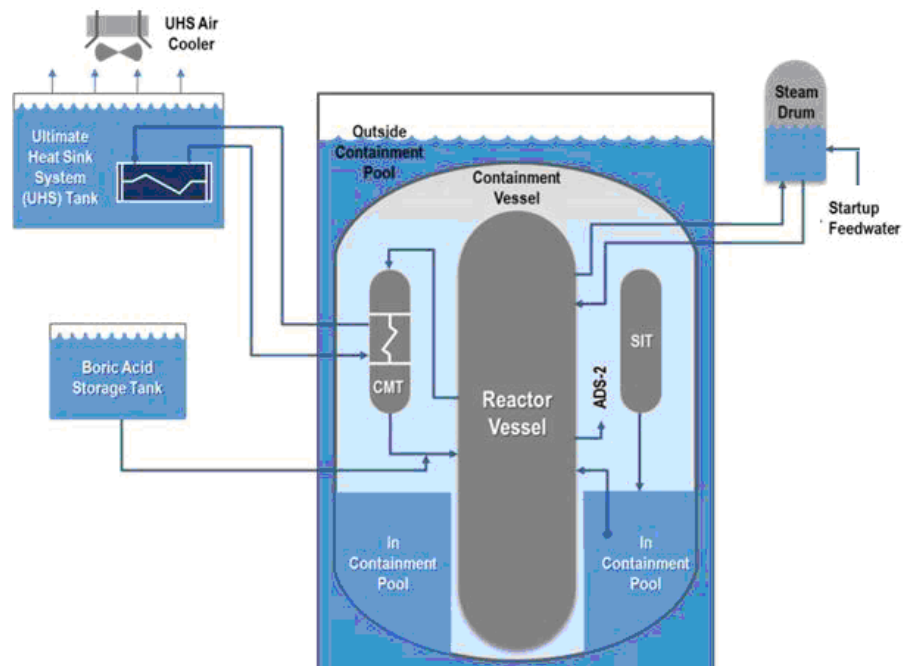
Figure 3-10: Westinghouse SMR safety Systems

Chapter 3. Small Modular Reactor

References chapter 3

[1] International Atomic Energy Agency, "*Innovative Small and Medium Sized Design features, safety approaches and R&D trends*", Final report of a technical meeting held in Vienna, 7-11 June 2004, IAEA-TECDOC-1451, Vienna (2005).

[2] International Atomic Energy Agency, "*Advances in Small Modular Reactor Technology Development*", A Supplement to IAEA Advanced Reactors Information System (ARIS), September 2014, Vienna.

[3] Zhitao Liu, Jihong Fan "*Technology readiness assessment of Small Modular Reactor (SMR) designs*", Progress in Nuclear Energy 70 (2014) pg. 20-28

[4] Nuclear Engineering International, 11 June 2009. Babcock & Wilcox Unveils Its New Modular Reactor. http://www.neimagazine.com/story.asp?storyCode=2053239.

[5] US.NRC, July 10, 2012. B&W mPower_ Project Overview. http://www.nrc.gov/reactors/advanced/mpower.html.

[6] J. Simpson, "*Nuclear Power from Underseas to Outer Space*", American Nuclear Society, (December 1994).

[7] D.T. Ingersoll, Z.J. Houghton, R. Bromm et al, 2012. "*NuScale small modular reactor for Co-generation of electricity and water*", Desalination 340 (2014) 84–93.

[8] 2014 NuScale Power, LLC, http://www.nuscalepower.com/reactormodules.aspx

[9] 2014 SMR a Holtec international Company, http://www.smrllc.com/safety.html

[10] Nuclear Engineering International, 24 October 2013 , http://www.neimagazine.com/features/featurefueling-the-westinghouse-smr/

[11] Conway, L.E., et al., "IRIS Plant Description Document," WCAP-16062-NP (NonProprietary), Westinghouse, March 21, 2003.

[12] Hone, M., et al., "AP1000 Core Reference Report" WCAP-17524-NP (Non Proprietary), Westinghouse, Revision 0, March 2012.

CHAPTER 4

THE IRIS REACTOR

4.1 Introduction

This chapter is devoted to the description of the IRIS reactor, the nuclear system selected to develop the ASTEC SMR model. The IRIS reactor has been developed for about ten years by an international consortium led by Westinghouse Electric Co, reaching an advanced design status. The IRIS consortium included a number of US and international companies, universities and national laboratories and organizations. The contribution of the universities to the IRIS program was very important. Innovative design solutions have been proposed and developed by the universities, and IRIS was perhaps the first and only commercial reactor project where academia and industry was in a partnership equally co-responsible for the design. The leading principle imposed on the IRIS design was that safety is based on eliminating as many systems as possible, using a few simple passive systems rather than a multitude of complex active systems. Although firmly based on the proven LWR technology, the IRIS project has developed many engineering and project innovations. In some cases, IRIS has developed and introduced novel solutions; in other, it has advanced a known feature to a new level [1]. The IRIS concept reactor can be classified as a pressurized medium size, modular reactor, with a thermal power of 1000 MW_t. Its main technical characteristic that distinguish it from the current commercial nuclear plant are that, every primary system component is integrated in the vessel and the containment is designed to be thermodynamically coupled with the integrated primary system during accident conditions. The IRIS reactor rendering figures has been realized using the program Rhinoceros 5.

4.2   SPES3-IRIS integral facility

The licensing process required by the U.S. Nuclear Regulatory Commission (NRC) foresees a series of experimental tests on properly built facilities suitable to verify the behaviour of the new plant and its safety system capabilities to cope with postulated accidents. This is the reason why, an integral test facility, denominated SPES3-IRIS, has been designed to study this kind of phenomena that take place during a LOCA. The SPES3-IRIS facility is an integral simulator of the IRIS reactor under construction at SIET laboratories in Piacenza (Italy), suitable to test the plant response to postulated DBAs and to provide experimental data for code validation and IRIS plant safety analyses.
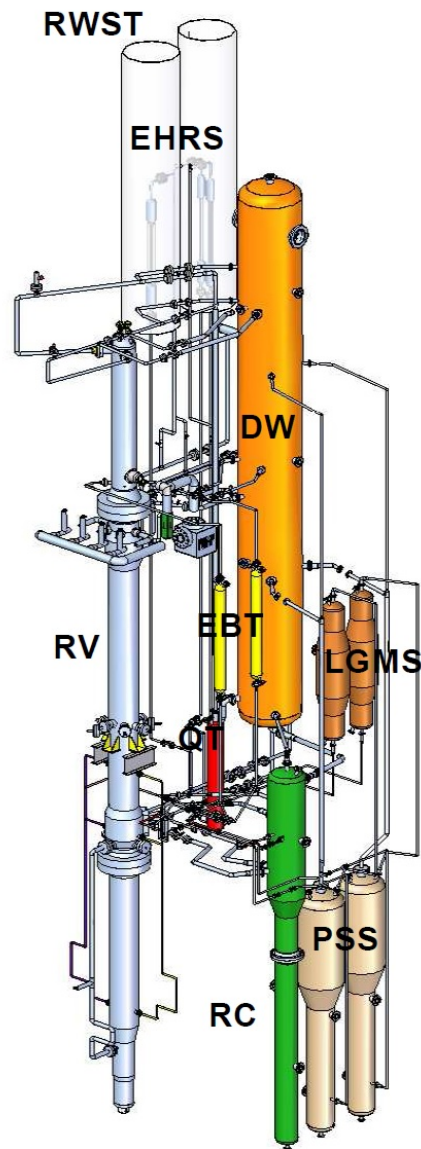

Figure 4-1: SPES3-IRIS facility layout

The facility reproducing with 1:100 volume scale and 1:1 height scale (Figure 4-1), the IRIS reactor [2], and in particular:

- the primary circuit including the reactor pressure vessel with power channel and fuel box, lower riser, upper riser, pressurizer, upper downcomer, steam generators (SG), riser-to-downcomer connection check valves, lower downcomer, lower plenum, circulation pump;
- the secondary circuit up to the Main Isolation Valves, including SG, Feedwater lines and Steam Lines;
- the safety system including the Emergency Boration Tanks (EBT), the Emergency Heat Removal System Heat Exchangers (EHRS-HX) located in the Refuelling Water Storage Tank (RWST) and the Automatic Depressurization System (ADS);
- the containment system including the Dry Well, the Quench Tank (QT), the Pressure Suppression System (PSS), the Reactor cavity and DVI room, the Long Term Gravity Make-up System (LGMS), and the DVI lines.

A nodalization of SPES3 has been developed at SIET, for the RELAP5 thermal-hydraulic code to simulate the facility and compare the results with the IRIS simulations performed by the University of Zagreb (FER), making use of the RELAP5 and GHOTIC coupled codes: the former for the primary and secondary systems, the latter for the containment system. A design-simulation feedback process has led, step by step, to understand and reduce the differences between the SPES3 and IRIS behaviour up to obtain a nodalization suitable to simulate all the tests foreseen in the test matrix, in compliance with IRIS performances. In particular, the DVI SBLOCA (Direct Vessel Injection Small Break Loss of Coolant Accident), which provides the database for the Fractional Scaling Analysis (FSA), has been carefully analyzed. Such analysis, provided a quantitative evaluation of the discrepancies of the most important thermal-hydraulic parameters of the transient evolution, and confirmed that SPES3 simulates IRIS adequately [3].

4.3 The IRIS reactor

4.3.1 IRIS general description

The IRIS design still relies on the proven technology provided by 40 years of operating PWR experience, and on the established use of passive safety features pioneered by Westinghouse in the NRC certified AP1000 plant design [4]. Like the AP1000 designs, the IRIS safety features, once actuated, rely on natural driving forces such as gravity and natural circulation flow for their continued function. These safety systems do not use active components (such as pumps, fans or diesel generators) and are designed to function without safety-grade support systems (such as AC power, component cooling water, service water, or HVAC). Because of the safety by design approach, the number and complexity of the safety

systems and required operator actions are further minimized in IRIS. The net result is a design with significantly reduced complexity and improved operability, and extensive plant simplifications to enhance construction. All the main primary system components are located inside the reactor pressure vessel. In Figure 4-2 is shown the IRIS integral vessel and the primary coolant flow path. Water flows upwards through the core and upward through the riser region (defined by the extended core barrel). At the top of the riser, the coolant is directed into the upper annular plenum where the suction of the reactor coolant pumps is located. Eight pumps are employed, and the flow of each pump is directed downward through its associated helical coil steam generator module. The flow path continues down through the annular downcomer region outside the core to the lower plenum and then back to the core completing the primary coolant flow path.
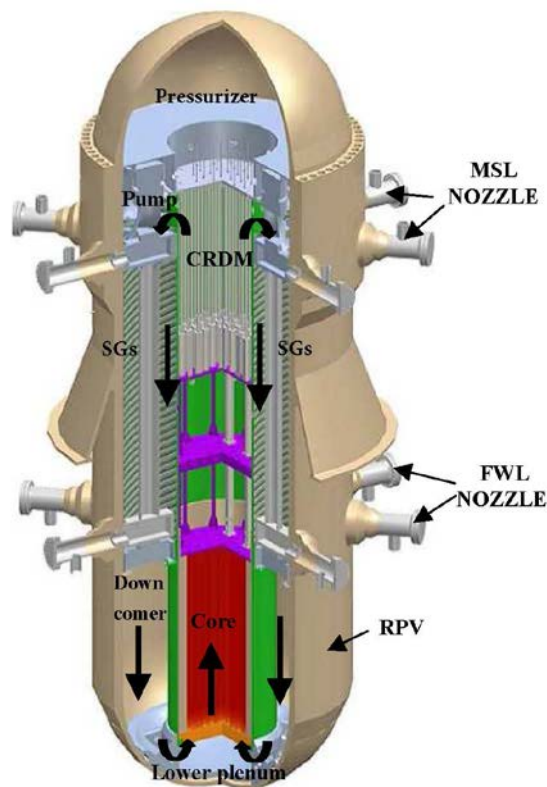
Figure 4-2: IRIS Integral vessel

The integral reactor vessel configuration allows the use of a small, high design pressure, spherical steel containment resulting in a high level of safety and economic attractiveness. The IRIS containment vessel (CV) (Figure 4-3) is a spherical steel structure, 25 m in diameter, designed to sustain high pressure in transient, with two steam suppression pools that combines the best characteristics of PWR and BWR containments. The size reduction, combined with the spherical geometry, results in a capability of sustaining a design pressure of 13E5 Pa.
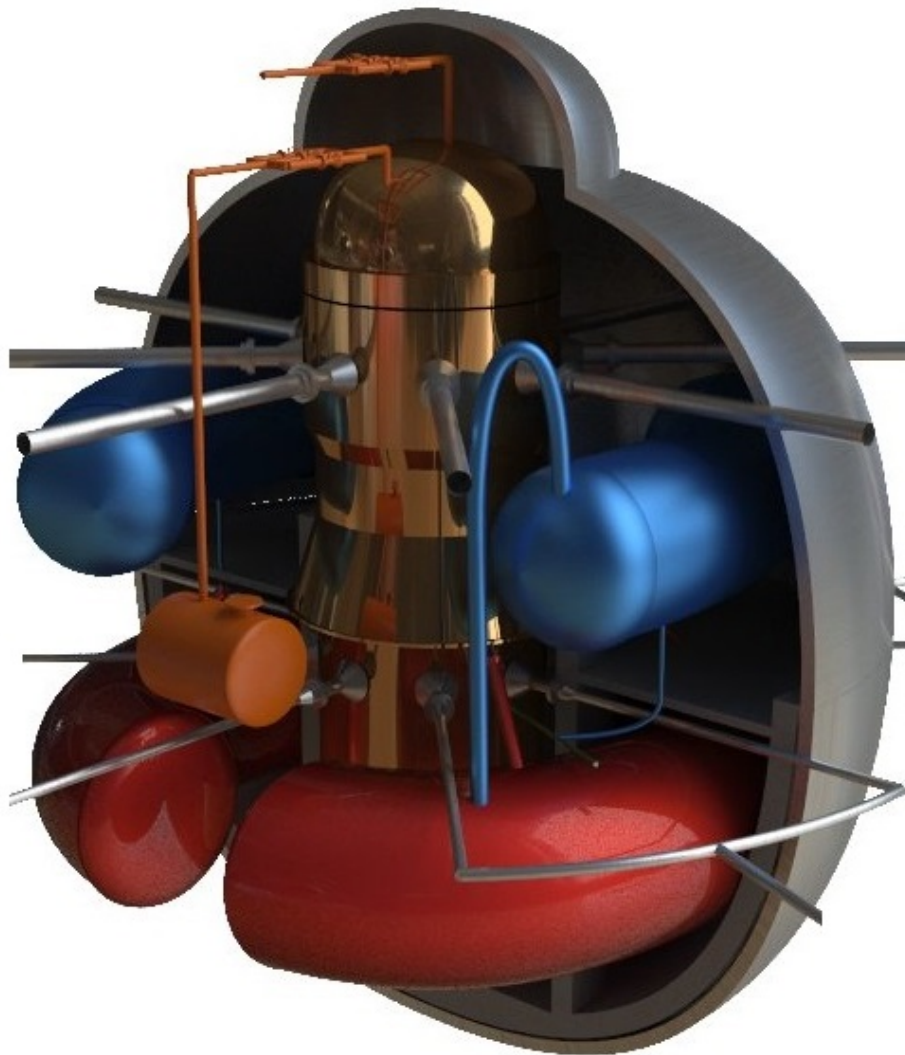
Figure 4-3: IRIS containment (Rhinoceros 5)

The IRIS core and fuel characteristics are approximately the same of those of a conventional Westinghouse PWR design. However, several features have been modified to enhance performance as compared to conventional plants, while retaining existing technology. The FA consists of 264 fuel rods in a 17x17 square array. Low-power density is achieved by employing a core configuration consisting of 89 FAs with a 4,267 mm active fuel height, and a nominal thermal power of 1,000 MWt. The average linear power density is reduced by about 46% as compared to AP1000 (9.974/18.76 kW/m) [6-7]. The IRIS FA design is similar to the Westinghouse 17x17 XL Robust FA design used by AP1000 [5], but can operate over a three to four years long fuel cycle. To longer the fuel cycle, the fission gas plenum volume in the upper and lower part of the fuel rod was increased, rising the FA height of 41 cm. This technical solution is due to allow achieving higher fuel burnup in the future. Anyway, given the integral vessel layout, where the

vessel height is mostly determined, by the steam generators, this plenum increase is possible with no corresponding increase in vessel height. In order to take advantage of the extended IRIS fuel cycle and to improve the overall plant availability, an optimized maintenance approach for all major components is being developed, which will also extend the interval between maintenance shutdowns to as long as 48 months.

4.3.2 IRIS design approach

The IRIS design provides for multiple levels of defense for accident mitigation (defense-in-depth), resulting in extremely low core damage probabilities while minimizing the occurrences of containment flooding, pressurization and heat-up situations. The first line of defense in the defense in depth approach is to eliminate initiators that could convincibly lead to core damage. In IRIS, this concept is implemented through the "safety by design" approach, which can be simply described as "design the plant in such a way to eliminate the accidents from occurring, rather than coping with their consequences". If it is not possible to eliminate the accidents altogether, then the design should be such to inherently reduce their consequences and/or decrease their probability of occurring [8]. The key difference from previous practice is that the integral reactor design is intrinsically conducive to eliminating accidents, to a degree impossible in conventional loop-type reactors. The elimination of the large LOCAs, since no large primary penetrations of the reactor vessel or large loop piping exist, is only the most easily visible of the safety potential characteristics of integral reactors. Many others are possible, but they must be carefully exploited through an appropriate design that is kept focused on selecting design characteristics that are most amenable to eliminate accident-initiating events. Defense-in-depth is built into the IRIS design, where the design goal is to always maintain the core covered with water and avoid fuel damage, with a multitude of individual plant features capable of providing some degree of defense of plant safety. After the safety by design, five additional aspects of the IRIS design contribute to defense in-depth:

Stable Operation. In normal operation, the most fundamental level of defense-in-depth ensures that the plant can be operated stably and reliably. This is achieved by the selection of materials, by quality assurance during design and construction, by well-trained operators, and by an advanced control system and plant design that provide substantial margins for plant operation before approaching safety limits.

Physical Plant Boundaries. One of the most recognizable aspects of defense-in-depth is the protection of public safety through the physical plant boundaries. The fuel cladding, the reactor pressure boundary, and the containment pressure boundary directly prevent releases of radiation. For the fuel cladding boundary, the reactor

Chapter 4. The IRIS reactor

protection system is designed to actuate a reactor trip whenever necessary to prevent exceeding the fuel design limits. The core design, together with defense-in-depth process and decay heat removal systems, provides this capability under expected conditions of normal operation, with appropriate margin for uncertainties and anticipated transient situations. The reactor coolant pressure boundary is designed with complete overpressure protection and appropriate materials to provide and maintain the boundary during all modes of plant operation. The containment vessel, in conjunction with the defense-in-depth heat removal systems, is designed so that: its design pressure is not exceeded following postulated DBAs; a large margin to the design basis pressure is maintained during postulated design basis accidents to minimize leakage probability; and, containment failure does not occur even under severe accident conditions.

Non-safety Systems. The next design level of defense-in-depth is the availability of certain non-safety systems for reducing the potential for events leading to core damage. For more probable events, these defense-in-depth, non-safety systems automatically actuate to provide a first level of defense to reduce the likelihood of unnecessary actuation and operation of the safety-related systems. These non-safety-related systems establish and maintain safe shutdown conditions for the plant following design basis events, provided that at least one of the non-safety related AC power sources is available. In addition, to minimize core damage probability, diverse, non-safety systems are provided to back up the main functions of the passive safety related systems. These systems are being defined on the basis of PSA considerations so to minimize the core damage and the radioactivity release probabilities. This diversity exists, for example, in the residual heat removal function. The emergency heat removal system (EHRS) is the passive safety-related feature for removing decay heat during a transient. In case of multiple failures in the EHRS, defense-in-depth is provided by a simple, non-safety, passive containment cooling system and by the gravity driven injection from the pressure suppression system tanks and automatic depressurization (passive feed and bleed) functions. The introduction of these diverse features in the design is made amenable by the intrinsic characteristics of the integral layout, as exploited in the safety by design approach.

Containing Core Damage. The IRIS is designed so that the reactor cavity floods following any severe accident event that may have the potential for core uncovery and melting. The objective of this cavity flooding action is to prevent reactor vessel failure and subsequent relocation of molten core debris into the containment. Retention of the debris in the vessel significantly reduces the uncertainty in the assessment of containment failure and radioactive release to the environment due to ex-vessel severe accident phenomena. Again, it must be emphasized that IRIS is designed to avoid core uncovery and consequently melting, under all accident conditions. The

capability of in vessel core retention is an added feature.

4.3.3   Safety systems and features

The use of passive safety systems provides improvements in plant simplification, safety, reliability, and investment protection over conventional plant designs. The IRIS follows the AP1000 approach and uses passive safety systems to improve the safety of the plant and to satisfy safety criteria of regulatory authorities. The passive safety systems require no operator actions to mitigate design basis accidents. Once actuated, these systems rely only natural forces such as gravity and natural circulation for continued operation. No pumps, fans, diesels, chillers, or other active machinery are used. A few simple valves align and automatically actuate the passive safety systems. To provide high reliability, these valves are designed to actuate to their safeguards positions upon loss of power or upon receipt of a safeguards actuation signal. However, they are also supported by multiple, reliable power sources to avoid unnecessary actuations. The IRIS passive systems design, takes full advantage of the safety by design approach. Thus, the consequent elimination of some postulated design basis events (large LOCAs) and the inherent mitigation of several other (steam generator tube rupture, steam line break, locked rotor) through the definition of a safety strategy that is specifically tailored to respond to those remaining accident initiators, that are the more important contributors to core damage frequencies. This design approach allows the licensing safety criteria to be satisfied with a greatly simplified plant design. The passive safety systems provide a major enhancement in plant safety and investment protection as compared with conventional plants. They establish and maintain core cooling and containment integrity indefinitely, with no operator or AC power support requirements. The passive systems are designed to meet the single-failure criteria, and the PSAs are used to verify their reliability [8]. The IRIS passive safety systems are even simpler than previous passive safety designs since they contain significantly fewer components, reducing the required tests, inspections, and maintenance, require no active support systems, and their readiness is easily monitored.

4.3.4   Passive core and containment cooling

The IRIS passive systems configuration is presented in and includes [9]:

- Two compact (12.8 m^3) full-system pressure emergency boration tanks (EBTs) which deliver emergency borated water through the Direct Vessel Injection (DVI) lines for transient events. By their operation these tanks also provide a limited gravity feed makeup water (at high pressure) to the primary system;
- An Automatic Depressurization System (ADS) from the

pressurizer steam space, which assists the EHRS in depressurizing the reactor vessel when/if the reactor vessel coolant inventory drops below a specific setpoint. This ADS has two stage and consist of two set composed by three parallel 4 inches lines ADS stage-1, and three parallel 6 inches lines ADS stage-2. The ADS stage-1 line discharges into the quench tank through a sparger, while the ADS stage-2 line discharges directly into the drywell. This ADS function ensures that the reactor vessel and containment pressures are equalized in a timely manner limiting the loss of coolant and thus preventing core uncovery following postulated LOCAs (Figure 4-4);
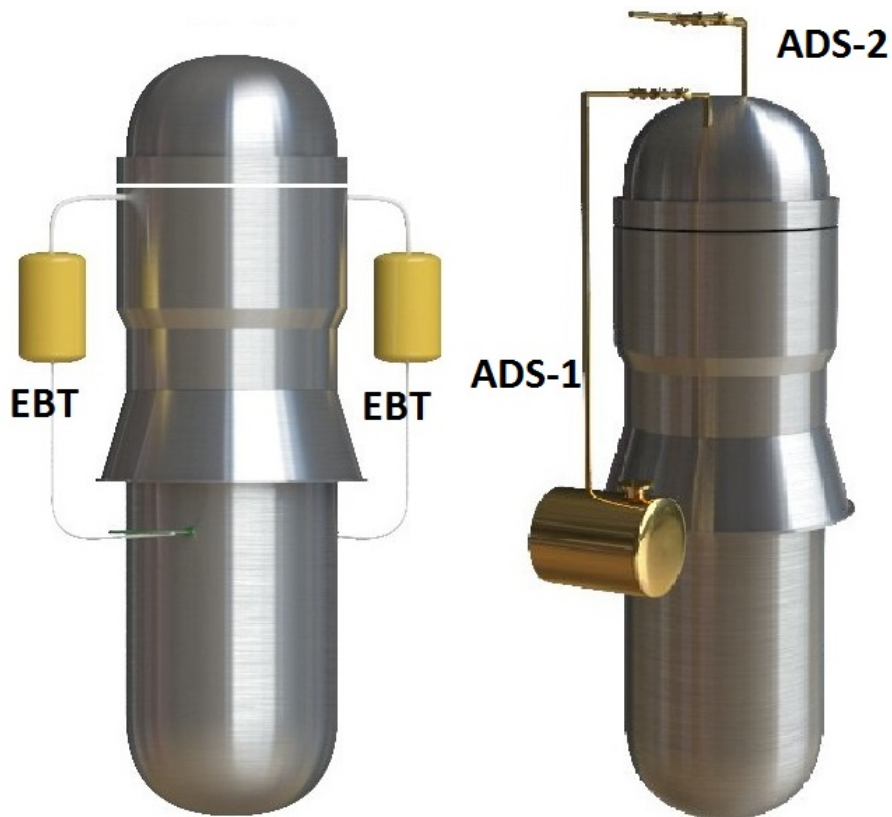
Figure 4-4: EBT and ADS system (Rhinoceros 5)

- Two Long Term Makeup Gravity Tanks (LGMS) which provide an elevated source of water that is available for gravity injection into the reactor vessel through the DVI lines in the event of a loss of coolant accident (LOCA);
- A containment Pressure Suppression System (PSS) which consists of 2 suppression pools. Each suppression pool is connected to the containment atmosphere through a vent pipe, connected to a submerged sparger to condense steam released in the containment following a LOCA or steam/feed line break accident. The suppression system limits the peak containment pressure following a blowdown event to less than the containment design pressure. The suppression system water

tanks are connected to LGMS tanks, pressurizing the system (Figure 4-5).
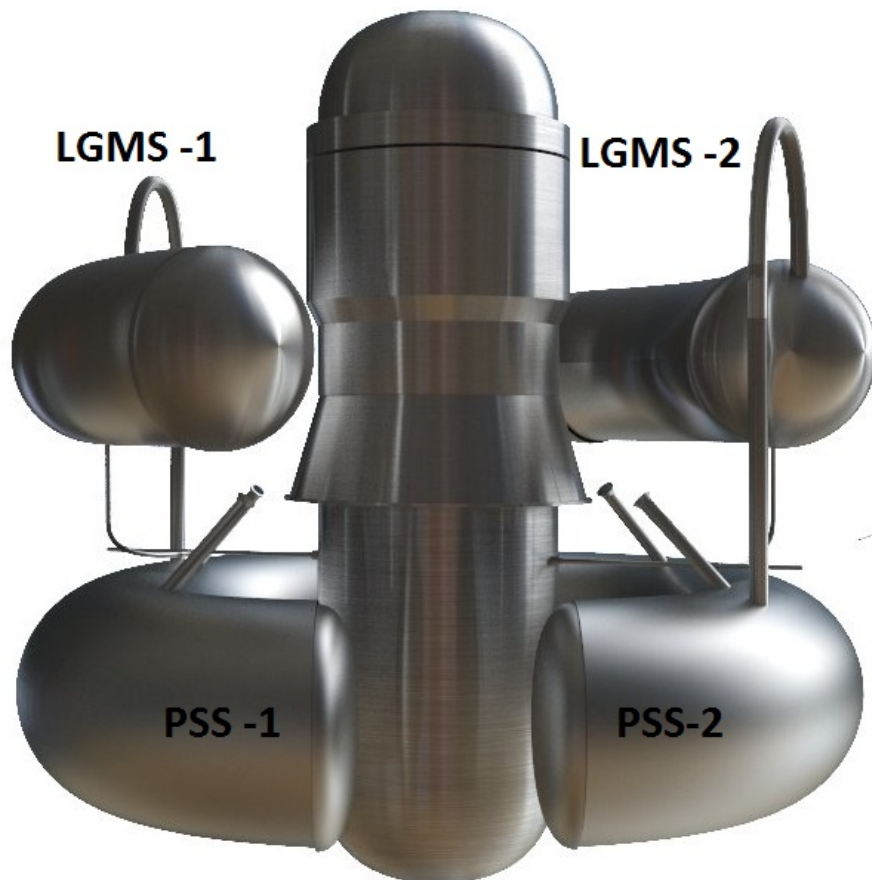
Figure 4-5: LGMS and PSS system (Rhinoceros 5)

- A passive emergency heat removal system (EHRS) made of four independent trains; each includes a vertical heat exchanger located in the Refueling Water Storage Tank (RWST) located outside the containment structure that is connected to a separate SG feed/steam line, which includes 2 SGs. The RWST provides the heat sink for the EHRS heat exchangers. The EHRS is sized so that a single train can provide decay heat removal in the case of a loss of secondary system heat removal capability. The EHRS operates by natural circulation removing heat from the primary system through the steam generators heat transfer surface, condensing the steam produced in the EHRS heat exchanger, and transferring the heat to the RWST, and returning the condensate back to the SGs. The EHRS provides the main post-LOCA depressurization (depressurization without loss of mass) and coolant makeup function for IRIS because it condenses the steam produced by the core directly inside the reactor vessel minimizing the break flow, while transferring the decay heat to the environment, thus performing the functions of both core cooling and containment depressurization (Figure 4-6);
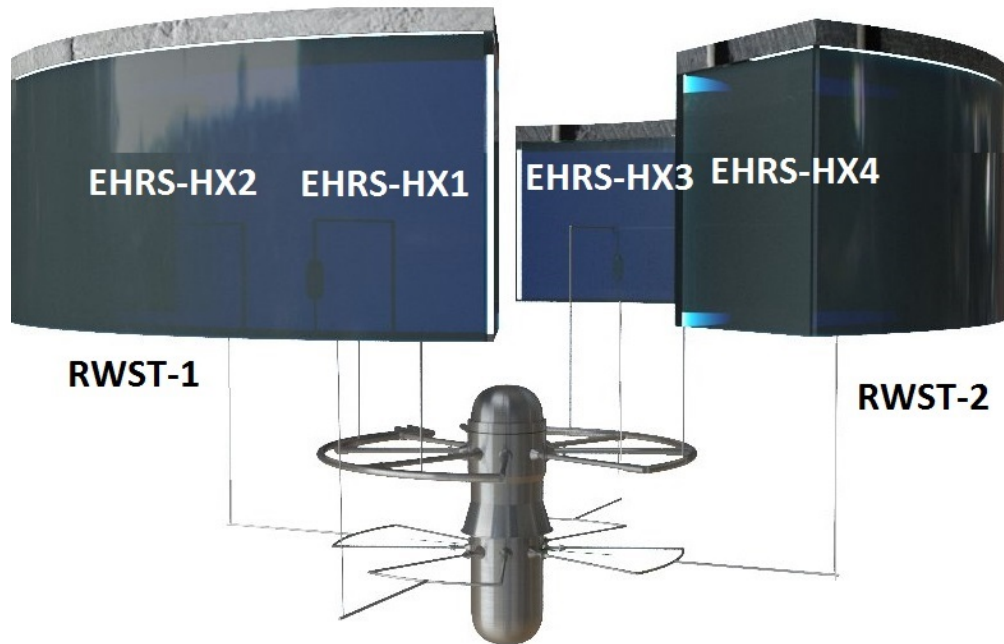
Figure 4-6: EHRS and RWST system (Rhinoceros 5)

- A specially constructed lower containment volume that collects the liquid break flow as well as any condensate from the containment in a cavity where the reactor vessel is located. During a LOCA, the cavity floods above the core level, creating a gravity head of water sufficient to provide coolant makeup to the reactor vessel through the DVI lines (Figure 4-7).

Figure 4-7: Reactor cavity (Rhinoceros 5)

- Eight internal by-pass valves connecting the riser line with the eight SGs to ensure natural circulation in accident condition

Thus, the IRIS passive systems provides the same safety functions as the active systems in current reactors and as the AP1000 passive systems. The safety strategy of IRIS provides a diverse means of core shutdown by makeup of borated water from the EBT and core cooling and heat removal to the environment through the EHRS in the event that normally available active systems are not available. In the event of a significant loss of primary-side water inventory. The primary line of defence for IRIS is represented by the large coolant inventory in the reactor vessel, and the fact that in IRIS depressurization is attained with very limited loss of mass, thus maintaining a sufficient inventory in the primary system and guaranteeing that the core will remain covered for all postulated LOCAs. The IRIS strategy relies on "maintaining" coolant inventory, rather than "injecting" makeup water. This strategy is sufficient to ensure that the core remains covered with water for an extended period (days and possibly weeks) [10]. Of course, when the reactor vessel is depressurized to near containment pressure, gravity flow from the LGMS and then from the cavity will maintain the coolant inventory for an unlimited period. However, this function would not be strictly necessary for any reasonable recovery period since the core decay heat is removed directly by condensing steam inside the pressure vessel, thus preventing any primary water from leaving the pressure vessel

4.3.5 Severe accidents (Beyond design basis accidents)

The IRIS is designed to provide in-vessel retention (IVR) of core debris by depressurizing and cooling the outside of the reactor vessel following severe accidents. With the reactor vessel intact and debris retained in the lower head, phenomena that may occur as a result of core debris being relocated to the reactor cavity are prevented. The IRIS has reactor vessel insulation that promotes in-vessel retention and surface treatment that promotes wettability of the external surface. The design features of the containment ensure flooding of the vessel cavity region during accidents and submerging the reactor vessel lower head in water. Liquid effluent released through the break during a LOCA event is directed to the reactor cavity. The IRIS design also includes a provision for draining part of the PSS water tanks water, into the reactor cavity. The IRIS design also includes a second means of containment cooling should cooling via the EHRS be defeated. In this event, direct cooling of the containment outer surface is provided and containment pressurization is limited to less than its design pressure. This cooling plus multiple means of providing gravity driven makeup to the core provides a diverse means of preventing core damage and ensuring containment integrity and heat removal to the environment [11].

Chapter 4. The IRIS reactor

Reference chapter 4

[1]   Petrovich, B., Ricotti, M., "*Pioneering role of IRIS in the resurgence of small modular reactors*" Nuclear Technology, vol. 178 May 2012 pg 126-152

[2]   M. D. Carelli, et al,, et al, "Spes-3 experimental facility design for iris reactor integral testing*",* Proc. of ENC 2007, Bruxelles 16-20 September 2003.

[3]   M. D. Carelli, et al, "The SPES3 experimental facility design for IRIS Reactor simulation", Science and Technology of Nuclear Installations, Volume 2009, 12 pages (2009).

[4]   http://www.nrc.gov/reactors/newreactors/designcert/ap1000.html

[5]   Hone, M., et al., "AP1000 Core Reference Report" WCAP-17524-NP (Non Proprietary), Westinghouse, Revision 0, March 2012

[6]   Westinghouse, Westinghouse AP1000 Design Control Document Rev.19, Chapter 4, Section 4.3, (2011) pp (4.3) 44 – 46

[7]   Westinghouse Electric Company LLC., *"IRIS Plant Description Document,"* WCAP-16062-NP (Non Proprietary), March 21, 2003

[8]   T.K.Larson, *et al.*, "*IRIS small break loca phenomena identification and ranking table (PIRT)*" Nucl. Eng. Design, 237, pp. 618-626 (2007).

[9]   M. D. Carelli, et al,, et al, "IRIS (International Reactor Innovative and Secure) Design Overview and Deployment Prospects*",* Proc. of NENE 2005, Bled 5-8 September 2005.

[10]   M.D. Carelli et al., "The Design and Safety Features of the IRIS Reactor," Nucl. Eng. Design, 230, pp. 151-167 (2004).

[11]   Conway, L.E., et al., "IRIS Plant Description Document," WCAP-16062-NP (Non Proprietary), Westinghouse March 21, 2003.

CHAPTER 5

SMR ASTEC MODEL

5.1 Introduction

In this chapter will be illustrated, the modelling of the IRIS reactor developed with ASTEC code v2.0r2p2. The SPES3-IRIS facility data, appropriately scaled for reproducing the IRIS real dimension, [1-6] along with the IRIS plant description document [7-9] was used to produce the meshing scheme of primary loop, secondary loop passive core cooling system and containment for the ASTEC code. Concerning the core modelling, it has been used, the same fuel assemblies adopted by the AP1000 reactor [10-11]. The meshing scheme of the modelled system was established using the ASTEC code guidelines given in the code user's manual. This requires knowledge in depth of both the capabilities of the code and the specifics of the system modelled. Development of the nodalization scheme is typically an essential part of the preparation of the input data, since in most codes the quantification of the nodes plays an important part in the modelling of certain phenomena or specific effects in the system. However, refined nodalization does not always produce more precise analysis results. The adequacy of the nodalization needs to be confirmed by spatial convergence studies or on the basis of previous experience. The IRIS ASTEC input-deck consists of 17808 lines, with the addition of the file for the decay heat description (time dependence, FP's transmutation processes). In the case of the IRIS reactor, the main difficulties encountered have been the simulation of the IRIS strategy to mitigate LOCA consequences. Because the IRIS strategy is based on "maintaining water inventory" rather than on the principle of safety injection [4]. This new safety approach poses significant issues for computational and analysis methods since the IRIS vessel and containment are strongly

coupled, and the system response is based on the interaction between the two. Thus, to simulate correctly the main phenomena involved during an accident scenario, the coupling between primary circuit and containment had to be accurate. Three ASTEC modules have been used to model the IRIS reactor, ICARE for in-vessel phenomena, CESAR for the thermal-hydraulic of the primary and secondary circuit and CPA for the thermal-hydraulic in the containment.

5.2   ICARE model

The core and the vessel was modelled by ICARE module. The main characteristics of the IRIS vessel that, differentiate it from a commercial PWR are the larger volume of the downcomer and the lower plenum whilst, the internals and the FAs are similar to those adopted by the standard reactors (Figure 5-1).
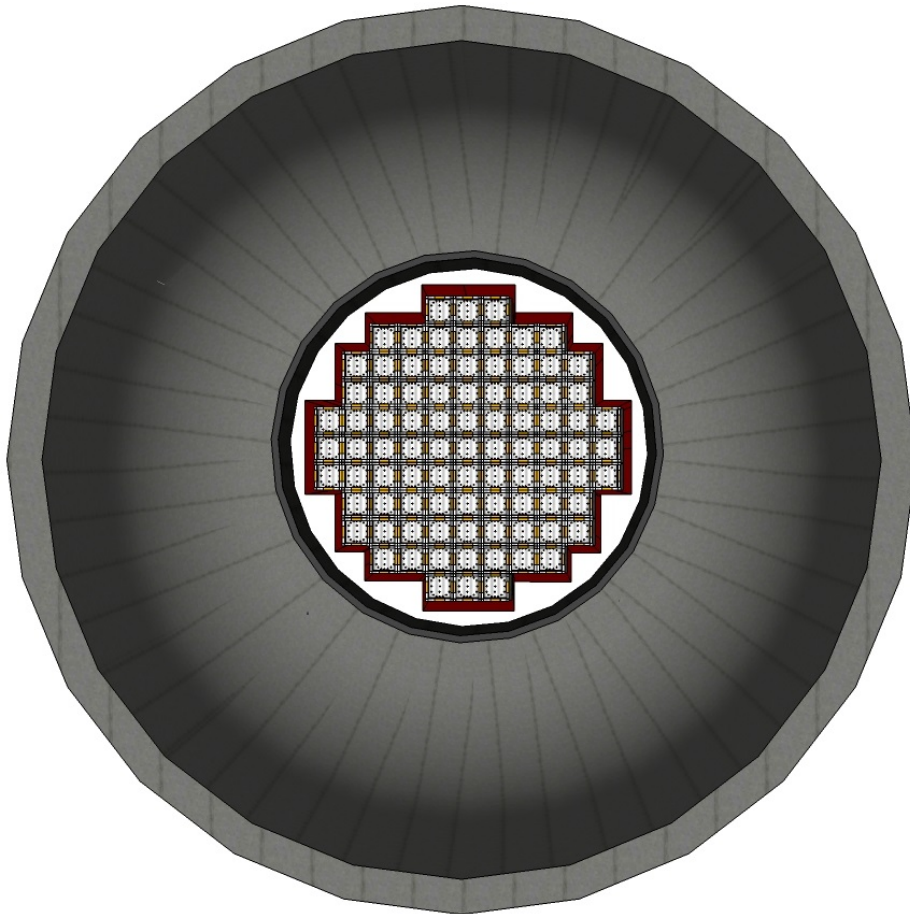
Figure 5-1 : IRIS core configuration and vessel

The radial discretization used to simulate the IRIS vessel with ICARE module, subdivides the core active zone in five concentric rings, a sixth ring for the reflector, a seventh and eighth ring for the barrel and for the downcomer region. Between the ring sixth and seventh is included the bypass area. In the core region (ring 1 to ring 5), two kinds of representative rods are modelled in each ring,

one fuel rod and one instrumentation tube, (the control rods was not modelled); two nozzle (bottom and top), and also the lower support plate. Each modelled element was associated to a "weight", i.e. to a fixed number of identical rods, nozzles or part of lower support plate. For instance, the "ring 1" is composed of "NF1 fuel rods" which are identical to the representative fuel rod in this ring, and of "NN1 nozzles" which are identical to the representative nozzles (bottom and top).

5.2.1 Core discretization scheme

The IRIS core parameters are reported in Table 5-1 [7]

Table 5-1: IRIS Core data

IRIS Core design	
Power plant output (MWe)	335
Core thermal output (MWt)	1000
Fuel assemblies	89
Equivalent core diameter (m)	2.413
Active core height (m)	4.267
Heat transfer surface (m²)	2992
Thermal heat flux peak factor Fq	2.6
Average core power density (Vol)	51.26 kW/l
Fuel inventory [tons U]	48.5
Fuel inventory [tons UO_2]	55021
Zircaloy clad weight (kg)	12077
Number CR blocks	37
CR per control assemblies	24
Adsorber material 1	Ag-In-Cd (black)
Adsorber material 2	Ag-In-Cd steel (gray)

In Figure 5-2, are shown the radial rings meshes adopted for the model. The scheme chosen aims to reproduce in the better way the cylindrical geometry, requested by ICARE.
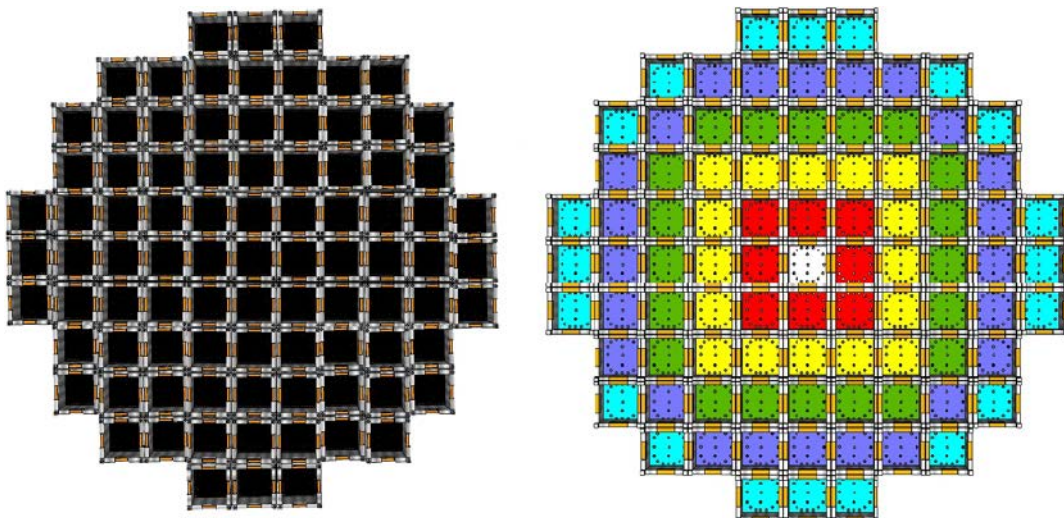

Figure 5-2: Core Radial rings scheme

Chapter 5. SMR ASTEC model

Table 5-2 shows in detail the geometrical parameter and the number of fuel pin, guide tube and instrumentation tube for each ring.

Table 5-2: Number of fuel pin, guide tube, instrumentation tube for each ring

Core radial ring	Eq. diam. [m]	Section [m²]	n° FAs	n° Fuel pin	n° Guide tube	n° Instr. tube
1°Ring (red)	0.76	0.457	9	2376	225	225
2° Ring (yellow)	1.27	1.270	16	4224	400	400
3° Ring (violet)	1.70	2.286	20	5280	500	500
4° Ring (green)	2.11	3.506	24	6336	600	600
5° Ring (blue)	2.41	4.573	20	5280	500	500

Being the IRIS Fuel Assembly (FA) design similar to the Westinghouse 17x17 XL Robust Fuel Assembly design. The ICARE FAs model was developed using the data of AP1000 FAs, except for the greater cladding length, due to the increase in volume of the gas plenum (upper and lower). In Table 5-3 are illustrated the Fas data.

Table 5-3: IRIS Fuel Assemblies data

IRIS Fuel assemblies	
Rod Array	Square Lattice 17x17
Rod per assembly	264
Rod pitch (cm)	1.26
Overall transverse dimensions (cm)	21.4 x 21.4
Tot. FA lenght (cm)	520.7
Tot. Active height (cm)	426.7
Fuel weight, as UO_2 (kg)	611
Zircaloy clad weight (kg)	136
Number of grids per assembly	15
Top and bottom - (Ni-Cr-Fe Alloy 718)	2
Intermediate - ZIRLO	8
Intermediate flow mixing (IFM) - ZIRLO	4
Protective - (Ni-Cr-Fe Alloy 718)	1
Number of guide tube per FA - ZIRLO	24
Diameter of guide thimbles (cm)	0.442 ID x 0.482 OD
Fuel rods per FAs	264
Outside diameter (cm)	0.95
Diameter gap (cm)	0.0165
Clad thickness (cm)	0.057
Clad material	ZIRLO
Fuel pellets	
Material	*UO2 sintered*
Density (% of theoretical)	95.5
Diameter (cm)	0.3225
Length (cm)	0.387

Chapter 5. SMR ASTEC model

In the ICARE, input deck, the cylindrical structures, as the cladding, the fuel, etc. are called "macro-component", and are defined independently from the space meshing. They are characterised by a geometry (internal and external diameter, axial extension) and an axially dependent chemical composition. In Table 5.4 are illustrated the parameters used to model the fuel cladding. As it is possible to see the thickness of the clad, varies at different elevation.

Table 5-4: Fuel cladding geometrical parameters

Clad level [m]	ID_{clad} [mm]	OD_{clad} [mm]	Thick clad [mm]
5.0549	0	0.95	0.94996
5.0465+eps	0	0.95	0.94996
5.0465	0.8357	0.95	0.1143
UPPER PLENUM			0.1143
			0.1143
			0.1143
			0.1143
4.6738+eps	0.8357	0.95	0.05715
4.6738	0.8357	0.95	0.05715
FUEL ZONE			0.05715
			0.05715
			0.05715
			0.05715
			0.05715
			0.05715
			0.05715
0.4066+eps	0.8357	0.95	0.05715
0.4066	0.7214	0.95	0.1143
LOWER PLENUM			0.1143
			0.1143
			0.1143
0.0838+eps	0.7214	0.95	0.1143
0.0838	0	0.95	0.94996
0.0635	0	0.95	0.94996

Diagram labels (left figure): SEAL WELD, TOP END PLUG, GIRTH WELD, 8.4 mm, PLENUM SPRING, UPPER PLENUM, 372.7 mm, UO₂ PELLETS, 4267.2 mm, ZIRCONIUM ALLOY CLAD, PELLET STACK BASE (LOWER PLENUM), STANDOFF TUBE (LOWER PLENUM), 322.6 mm, GIRTH WELD, BOTTOM END PLUG, 20.3 mm, INTERNAL GRIP CONNECTION

In the same way for the fuel, for the grids, the top and bottom nozzle, it is necessary to provide the initial and final elevation and the internal

and external equivalent diameter, (when necessary). The Figure 5-3 illustrates the modelization of the nozzles as a hollow cylinder. The weight of this macro-component is equal to the number of the FAs, one on the bottom and one on the top (Figure 5-3).
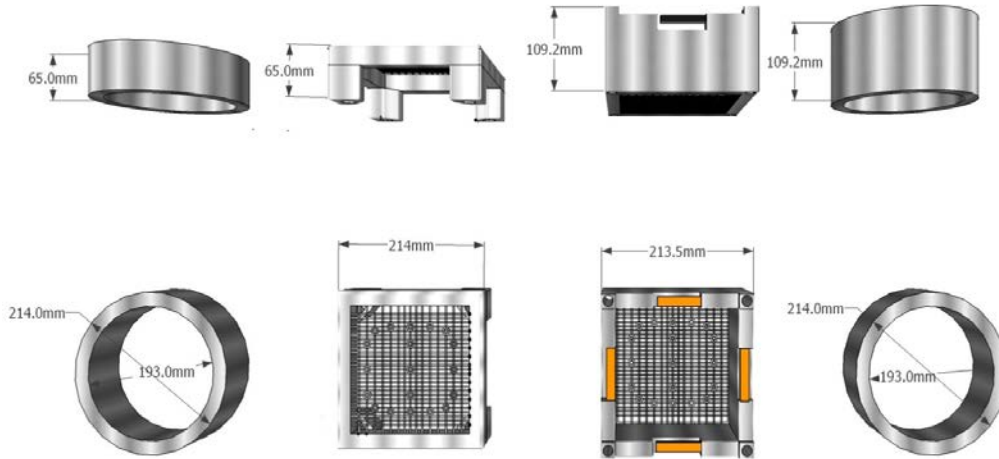

Figure 5-3: Bottom and top nozzle modelling

5.2.2   Internals

The ICARE model takes into account all the internals of the vessel. The lower support plate was simulated always using cylindrical elements (Figure 5-4).
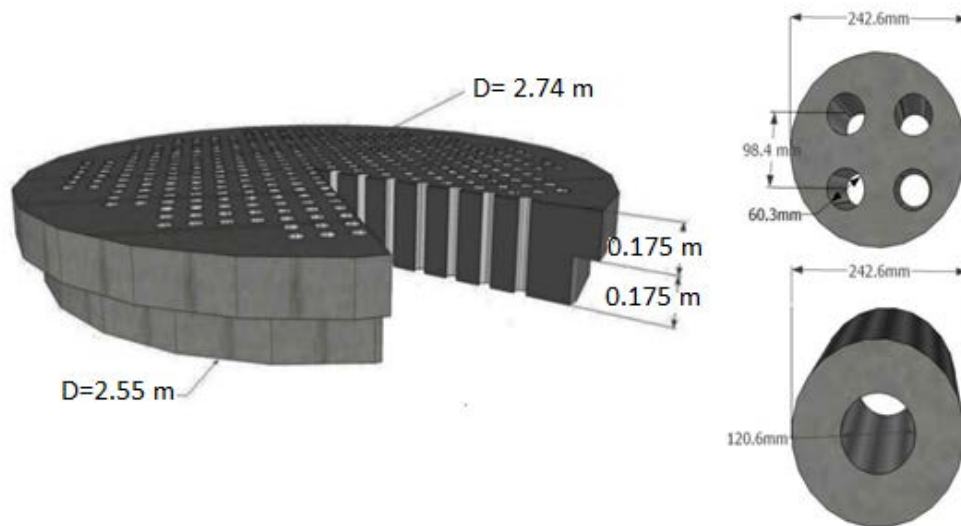

Figure 5-4: IRIS lower support plate and equivalent hollow cylindrical elements

The perforated surface of the plate has been subdivided in five rings (Figure 5-5 and Table 5-5). Actually, with this approach, the lower support plate total mass is not reproduced correctly. In order to fix this discrepancy the more external ring of the plate, that one without the holes, it was considered as, the bottom part of the reflector. In this

manner, the mass of the reflector has been increased of the missed mass of the lower support plate. In every lower support plate radial ring, the number of the cylindrical elements is the same of the FAs ones.
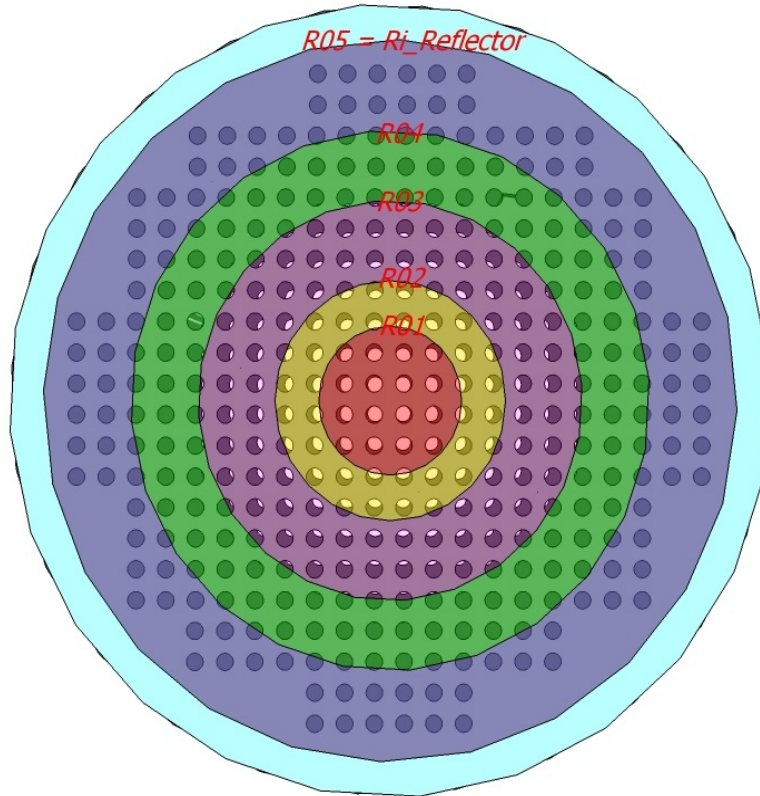

Figure 5-5: Radial meshing Lower support plate

Table 5-5: Parameters lower support plate rings

Cylindrical elements	n° elements	Holes Surface [m²]	No_Holes surf. [m²]	Total surface. [m²]	H_s /Tot_s. [%]
1 element		0.01142	0.0348	0.04624	0.247
1° Ring	9	0.10280	0.3133	0.41615	0.247
2° Ring	16	0.18276	0.5570	0.73983	0.247
3° Ring	20	0.22846	0.6963	0.92479	0.247
4° Ring	24	0.27415	0.835	1.10975	0.247
5° Ring	20	0.22846	0.6963	0.92479	0.247
TOTAL	89	1.01665	3.0986	4.11533	0.247

A heavy reflector and a cylindrical barrel surround the IRIS core. The reflector has been modeled as one equivalent hollow cylinder. The model conserve the total mass, and as just stated before its lower part include the external part of the lower support plate as illustrated in Figure 5-6 along with the original IRIS reflector. The

Chapter 5. SMR ASTEC model

Figure 5-7 shows a z-view of the IRIS reflector and the model. The Table 5.6 shows the reflector geometrical parameters for both.
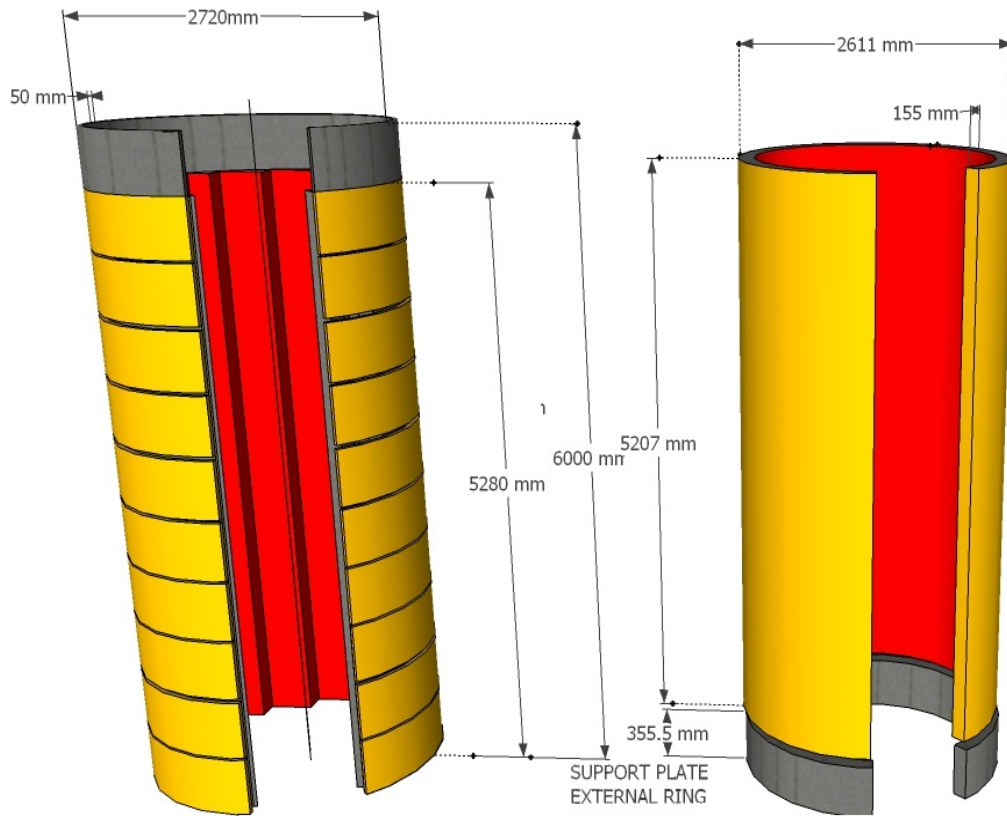

Figure 5-6: IRIS reflector and ICARE model reflector (cutaway view)
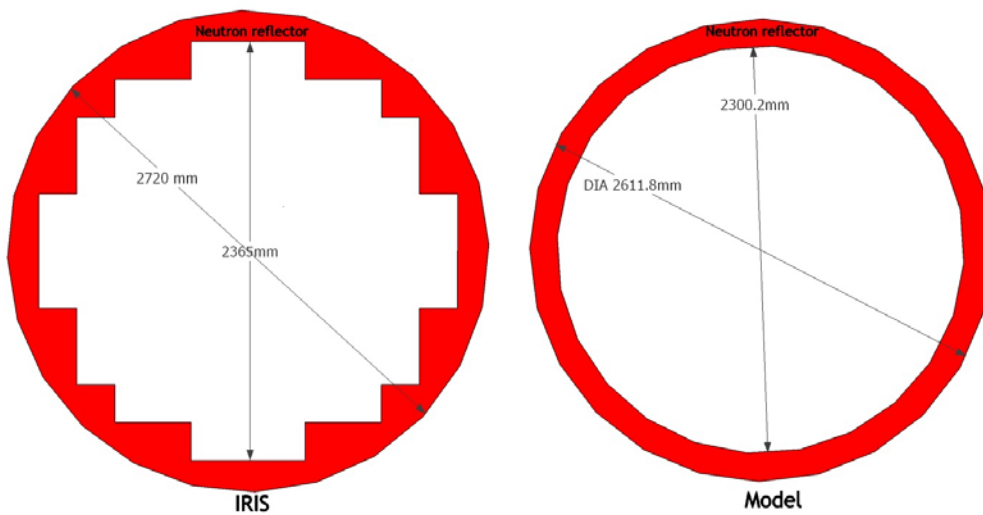

Figure 5-7: IRIS reflector and ICARE model reflector (z view)

Chapter 5. SMR ASTEC model

Table 5-6: IRIS reflector and ICARE model reflector parameters

Reflector	IRIS	ICARE
active height [m]	5.26	5.56
total height [m]	6	5.56
material	316L SS	316L SS
outer diameter [m]	2.72	2.62
inner diameter [m]	2.365	2.3
total mass (ton)	50000	50000+(2745)

The total height of the IRIS barrel is 16 m, only the part that housed the core, it is taken into for the ICARE model. Thus, the total height of the ICARE barrel model is equal to the total length of the FA plus the height of the lower plate support. The remainder part was taken into account as wall structure in the CESAR input deck. The Table 5-7 reports the IRIS barrel and ICARE barrel model data.
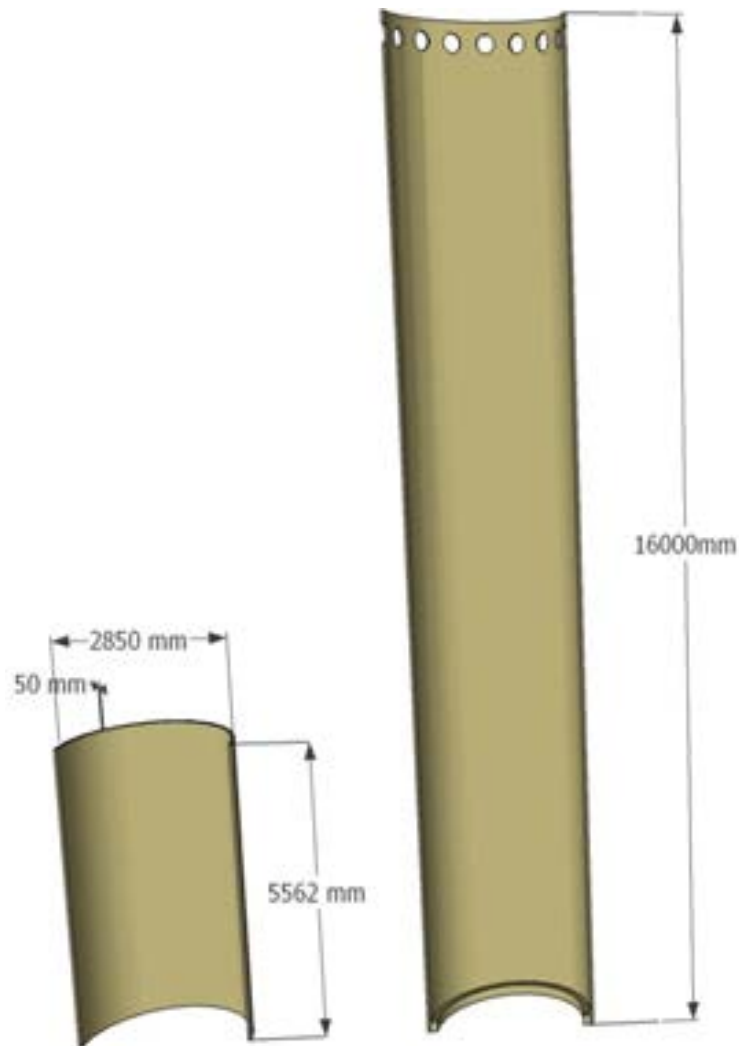

Figure 5-8: ICARE barrel model and Iris barrel

Chapter 5. SMR ASTEC model

Table 5-7: IRIS barrel and ICARE model barrel parameters

BARREL	IRIS	ICARE
total height [m]	16	5.56
material	316L SS	316L SS
outer diameter [m]	2.85	2.85
inner diameter [m]	2.75	2.75
total mass (ton)	54890	19075

Using this nodalization approach for the reflector and the barrel, these two concentric cylinders produce a space between them. This space in the model simulated the by-pass area. The by-pass area generated has a width of 0.178 m. As shown in Figure 5-9.
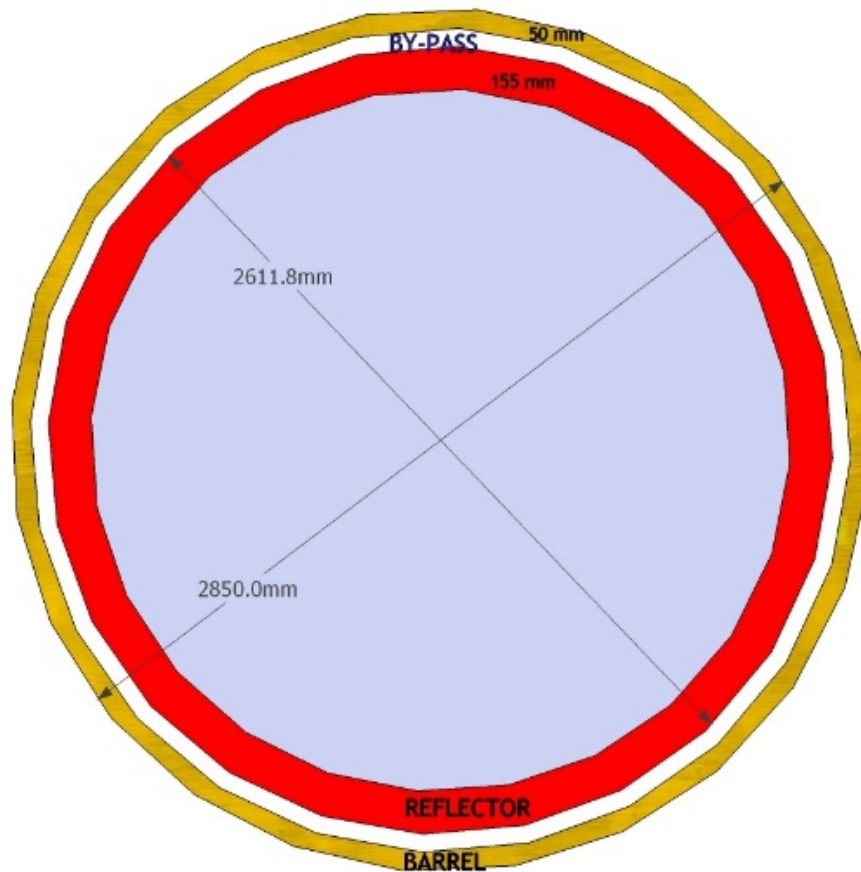

Figure 5-9: By pass area gerated by the nodalization

The by-pass area along with the reflector are included inside the sixth ring of the ICARE model. The last ring of the ICARE model contains the barrel, the downcomer area, and the vessel. In Table 5-8 are displayed the main parameters of the IRIS vessel [7].

Chapter 5. SMR ASTEC model

Table 5-8: IRIS vessel main parameters

IRIS Core design	
Reactor vessel I.D., [m]	6.223
Reactor vessel O.D.,[m]	6.783
Nominal base metal thickness [m]	0.28
Reactor vessel lenght,[m]	22.214
Dowcomer annulus width, [m]	1.68
Reactor vessel design temperature, [K]	626.46
Vessel material	Carbon steel SA 508, Gr.3,Cl.2
Cladding material (inner vessel surfaces)	Stainless Steel

The values of the vessel parameters, which can possible to find in the literature can vary of some cm, respect those used in this model. The total radial meshing of the IRIS core is illustrated in Figure 5-10, while in the Table 5-9 are reported the radi of the seven radial rings.
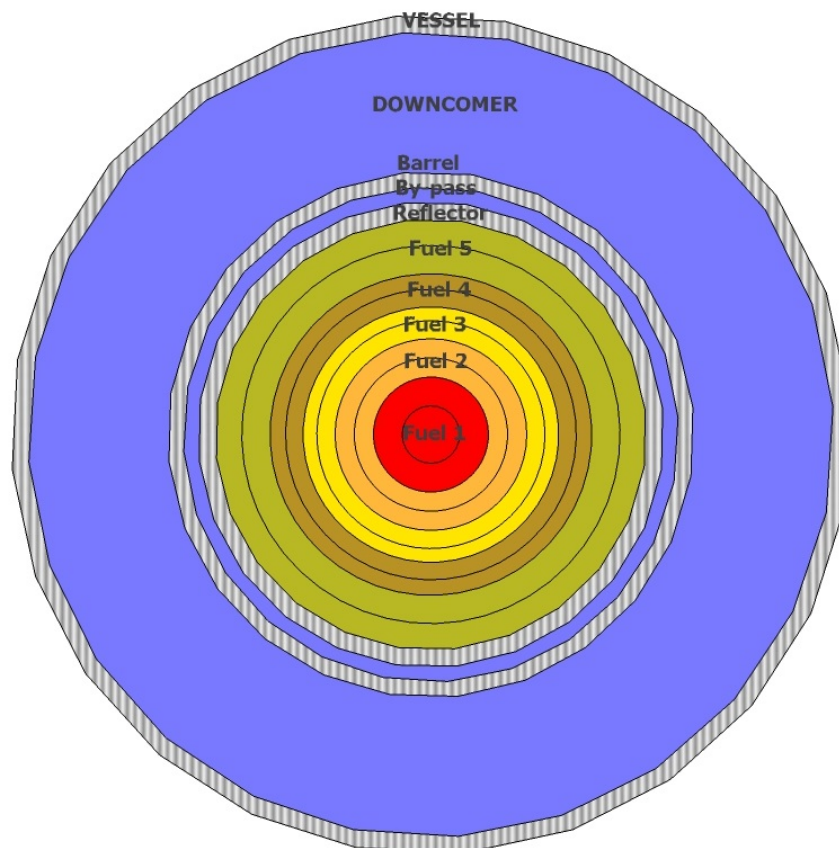

Figure 5-10: ICARE model radial meshing

Chapter 5. SMR ASTEC model
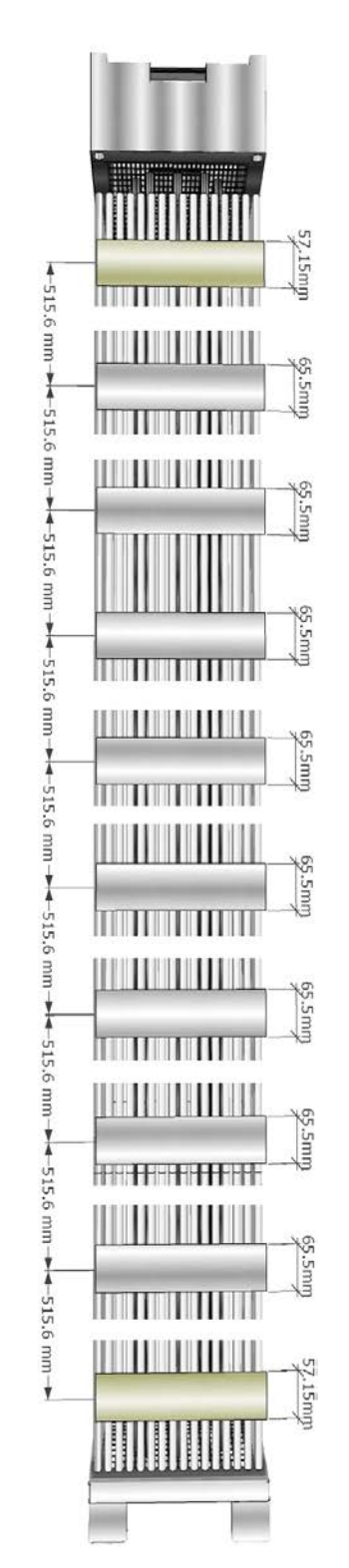
Table 5-9: Radial rings data

RADIAL CORE MESH	[m]	ICARE MESH GENERATED		CHANNEL	[m]
0° Radial mesh R00	0	0			
		1° ring		channel 1	0.1907
1° Radial mesh R01	0.3815	0.3815			
		2° ring		channel 2	0.5087
2° Radial mesh R02	0.6359	0.6359			
		3° ring		channel 3	0.7445
3° Radial mesh R03	0.8531	0.8531			
		4° ring		channel 4	0.9548
4° Radial mesh R04	1.0564	1.0564			
		5° ring	Radius in Reflector 1.15095	channel 5	1.1315
	1.2065	1.206			
		REFLECTOR			
5° Radius out Reflector	1.355	1.3567			
		6°ring	Radius out Barrel 1.375	By-pass	1.3658
		1.3817		By_pass vol.	0.9470
		BARREL		D_h by-pass	0.0183
6° Radius out Barrel	1.425	1.4321			
		7° ring	Radius in Vessel 3.1115	Downcomer	2.38325
		3.1266		Downcomer vol.[m^3]	133.686
7° Radial mesh R07	3.3915				

Terminated the radial nodalization; it was chosen the axial meshing. The core meshing must be fine enough to have a sufficient resolution of temperature. In ICARE the intersection between the axial and radial space grids on one hand and all the macro-components on the other hand, leads to divide each macro-component in several parts called components. The only constrain of ICARE is that, one mesh cannot contain more than one grid component. Thus given than in the model are represented 10 grids, it was paid attention to produce a homogenous meshing able to satisfy this imposition. The resulting scheme obtained, subdivide the IRIS core model in 22 axial mesh, of 26 cm each one. The axial meshing is schematically illustrated in the Table 5-10 with the relative elevation. Using this nodalization scheme, the mesh's total

Chapter 5. SMR ASTEC model

number of the ICARE core model is 148.

Table 5-10: Schematic axial meshing of the ICARE model

Height [m]	Level [m]	Grid n°	Levels [m]
	5.207		
0.26035			
	4.94665	Upper height	4.900175
0.26035		grid10(inconel)	4.8716
	4.6863	Lower height	4.843025
0.26035			
	4.42595	Upper height	4.38875
0.26035		grid9(ZIRLO)	4.356
	4.1656	Lower height	4.32325
0.26035			
	3.90525	Upper height	3.87315
0.26035		grid8(ZIRLO)	3.8404
	3.6449	Lower height	3.80765
0.26035			
	3.38455	Upper height	3.35745
0.26035		grid7(ZIRLO)	3.3247
	3.1242	Lower height	3.29195
0.26035			
	2.86385	Upper height	2.84185
0.26035		grid6(ZIRLO)	2.8091
	2.6035	Lower height	2.77635
0.26035			
	2.34315	Upper height	2.32625
0.26035		grid5(ZIRLO)	2.2935
	2.0828	Lower height	2.26075
0.26035			
	1.82245	Upper height	1.81065
0.26035		grid4(ZIRLO)	1.7779
	1.5621	Lower height	1.74515
0.26035			
	1.30175	Upper height	1.29505
0.26035		grid3(ZIRLO)	1.2623
	1.0414	Lower height	1.22955
0.26035			
	0.78105	Upper height	0.77945
0.26035		grid2(ZIRLO)	0.7467
	0.5207	Lower height	0.71395
0.26035			
	0.26035	Upper height	0.25965
0		grid1(inconel)	0.231075
	0	Lower height	0.2025
0.355			
	-0.355	Lower support plate	

5.2.3   Lower head and vessel

The ICARE module simulates the lower head using only one volume. The position of lower support plate in the IRIS reactor is inside the lower plenum. The ICARE module can not place the Lower Support Plate (LSP) inside the lower plenum, the LSP can be placed only inside the cylindrical part of the vessel. Thus, there are only two solution to approach this problem. The Figure 5-11 shows the actual IRIS lower vessel and the two vessel configurations.

Figure 5-11: IRIS lower part vessel and the two lower part vessel models

Chapter 5. SMR ASTEC model

The first one is to reproduce the exact geometry of the lower head, but placed the LSP in the cylindrical part of the vessel. The second one is to place the LSP at the actual IRIS elevation, but in this case, the shape of the lower head does not match the real shape of the IRIS reactor one. In the first case, the volume of the vessel undergoes a substantial increase. Table 5-11 shows the different parameters between the two vessel configurations and the actual IRIS vessel.

Table 5-11: Vessel parameters

GEOMETRICAL DATA	IRIS	MODEL 1	MODEL 2
Low. Plenum height [m]	3.105	3.105	1.27
Cylindrical part Vessel height [m]	3.727	5.562	5.562
Total height [m]	6.832	8.667	6.832
Vessel ID [m]	6.223	6.223	6.223
Cylindrical part Vessel Vol. [m³]	113.357	169.168	169.168
Lower plenum volume [m³]	62.959	62.959	25.751
Total volume [m³]	176.31	232.128	194.920
Δ volume [m³]	0	55.811	18.6039
Surf. lower plenum [m²]	60.830	60.830	39.057

As just stated the model 1 reproduces the correct shape and volume of the lower head but placing the LSP at the beginning of the cylindrical part of the vessel, the total volume of the ICARE model vessel increases of 55 m³. In case of a severe accident the time of emptying is an important parameter for the exact computation of the core degradation transient. The model 2 reproduces the correct position and height of the lower part of the vessel, but the volume of the lower plenum is decreased of more than 50 %, but in compensation the vessel volume is increased of only 18 m³.

Table 5-12: Lower plenum model 1 meshes

| LOWER HEAD MODEL 1 : EMISPHERICAL FORM			
material		Steel SA533B	
minimum thickness [m] 0.19		maximum thickness [m] 0.28	
Number of radial mesh (mesr.)			10
Number of axial mesh (mesas)			10
axial mesh positions			
degree	level [m]	radius [m]	
0	-0.355	3.115	
9.1	-0.8429	3.0463	
16.8	-1.2505	2.966	
24.7	-1.6439	2.8023	
33.5	-2.0508	2.5722	
42	-2.4138	2.2923	
50.8	-2.7408	1.9474	
59.5	-3.0283	1.5747	
69.5	-3.2407	1.0789	
79.2	-3.3849	0.578	
90	-3.46	0	

Chapter 5. SMR ASTEC model
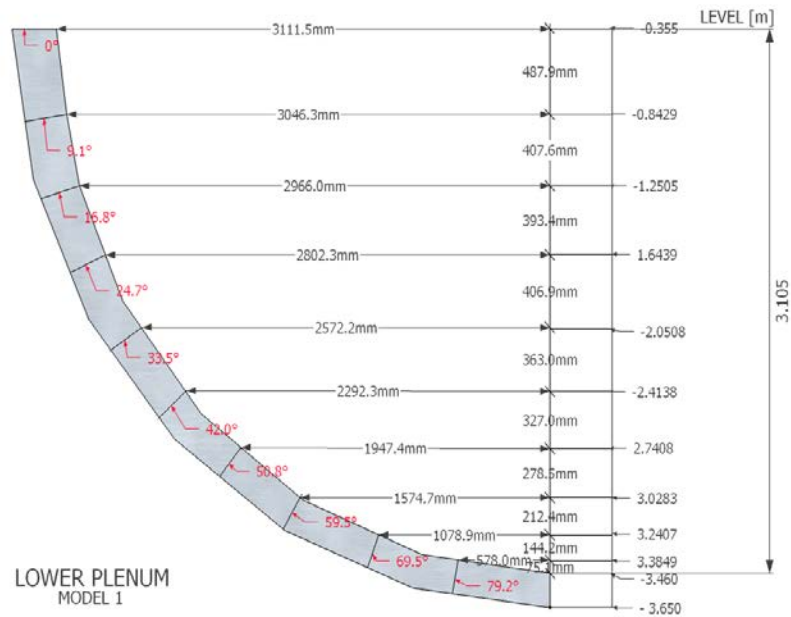
Figure 5-12: Lower head type 1 meshes

In the Table 5-12 and Figure 5-12 are illustrated, the axial meshes of the lower head model 1; the same data are reported for the model 2 in Table 5-13 and Figure 5-13. In both the model was utilized 10 radial meshes. In order to evaluate the effect of the lower plenum shape, a series of ICARE stand-alone computation was done, using different vessel rupture models. The comparison results are reported in Appendix A.

Table 5-13: Lower plenum model 2 meshes

LOWER HEAD MODEL 2		
material	Steel SA533B	
minimum thickness [m] 0.19	maximum thickness [m] 0.28	
Number of radial mesh (mesr.)		10
Number of axial mesh (mesas)		8
axial mesh positions		
degree	level [m]	radius [m]
0	-0.355	3.115
5.7	-0.6315	2.7987
11.5	-0.8605	2.5006
18	-1.0687	2.1944
25.7	-1.2374	1.8351
35.3	-1.3761	1.4421
48.8	-1.5041	1.004
66.2	-1.59	0.5452
90	-1.625	0

Figure 5-13: Lower head type 2 meshes

5.2.4 Decay heat

A fundamental data is the power decay. Decay heat power may be used directly as a heat source inside ASTEC modelling, however such a model does not enable to take into account FP release from the core and transport and retention phenomena inside the upper plenum, containment, primary circuit or environment for which an initial FP inventory should obviously be provided. In the other way, if a FP initial inventory is provided, the ISODOP module of ASTEC computes the decay heat at each time step directly from the inventory. As these phenomena are of high importance for core degradation kinetics and evaluation of the source term, a provisional solution was devised using a scaled French 1300 MWe PWR FP inventory. In the input deck the user has to provide a radial distribution and an axial profile of the decay heat generated from the component fuel, because at the beginning of the transient before the core degradation, the ICARE module relates the decay heat to UO_2 material.

5.2.5 ICARE core degradation parameters

The main In-vessel core degradation parameters and modelling options used in the input-deck of IRIS reactor, to evaluate the core melt progression during early and late degradation phases of the transient are illustrated in Table 5-14. The parameters and model options were mainly selected on the basis of specific code user guidelines and engineering judgment. Different empirical correlations can be used in ASTEC to compute the zircaloy clad oxidation (BEST-FIT, URBANIC-HEIDRICK). The cladding failure criteria are based on oxide layer thickness and clad temperature. These parameters mainly determine the capability of the oxidized cladding to retain the metallic zircaloy and dissolved fuel during the early degradation phase following oxidation runaway and fuel rod

Chapter 5. SMR ASTEC model

temperature escalation above the melting point of clad material. The melting point of pure ceramic material UO_2 is lowered by several hundreds of degrees in the ASTEC calculation, according to the results of severe fuel damage Phébus FP tests [12]. Different corium relocation flow paths into the lower plenum of the vessel are considered in ASTEC thanks to the use of the MAGMA model: laterally through the core bypass after baffle melting and/or through the lower core support plate after fuel rod melting or pool relocation above it. The failure lower head criteria used is the LOHEY model. This model utilizes the mechanical properties of vessel steel, based on experimental results for SA533B1 [13].

Table 5-14: ICARE In-vessel core degradation parameters and modelling

Parameter	ICARE
Zircaloy oxidation kinetics	**1** BEST-FIT correlation: Cathcart-Pawel in the low temperature range and Prater-Courtright in the high temperature range 2 Urbanic-Heidrick correlation
Cladding failure criteria	Tclad > 2300 K and ZrO2 thickness < 0.3 mm; or T > 2500 K
Melting point of UO_2-ZrO_2 ceramic material	2550 K (PHEBUS FP tests)
Molten core relocation into the Lower plenum	Baffle melting (relocation through core by-pass) or melting at core bottom (relocation through core support plate)
Reactor pressure vessel failure	LOHEY model plastic strain intensity > the ultimate failure strain creep deformation limit

5.3 The CESAR model

The part of the integral vessel above the core forms the primary circuit of the IRIS reactor. The eight helical steam generators housed in the zone above the downcomer form the secondary circuit (Figure 5-14). In the IRIS reactor CESAR model, the RWST and EBT passive safety systems, were modelling as control volumes of the primary circuit; while the EHRS were taken into account as control volumes belonging to the secondary circuit. The cavity and the LGMS, which carry out the safety system functions, were modelled as zones of the CPA module.
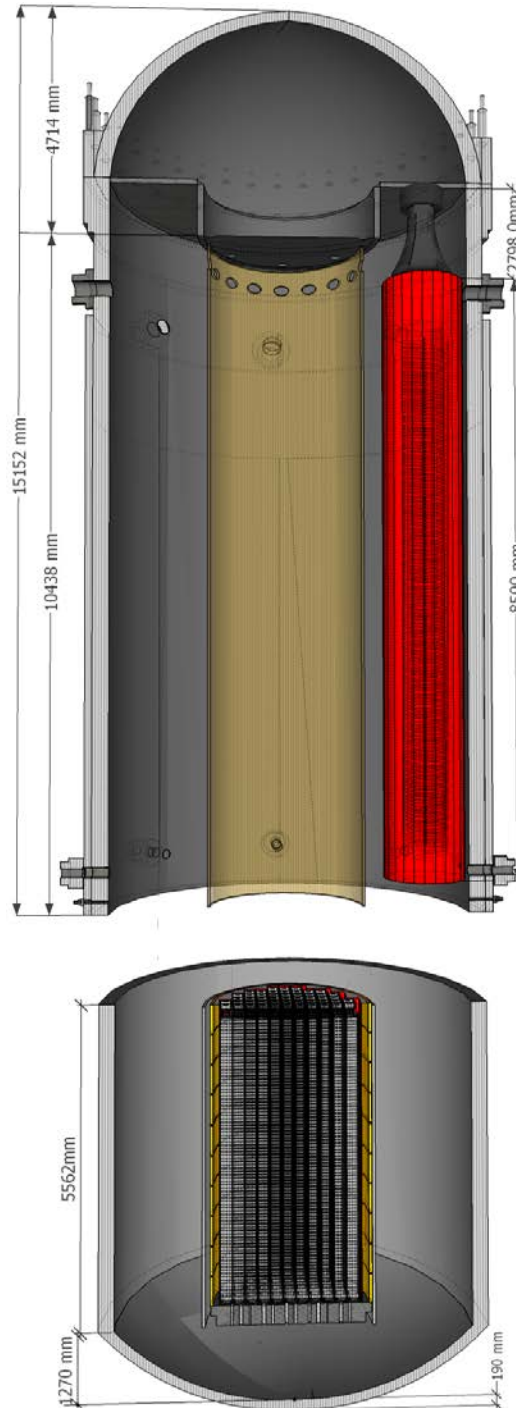
Figure 5-14: ICARE and CESAR domain

Chapter 5. SMR ASTEC model

The IRIS primary circuit consists of two concentric cylinder. The inner cylinder is the rising line, which starts from the top of the core and arrive until the base of the pressurizer, wrapped by the barrel structure. The outer cylinder is a sort of high downcomer, which encloses the inner cylinder for its complete height. As just state before this dowcomer houses the 8 pumps and the 8 SGs which form the secondary circuit.
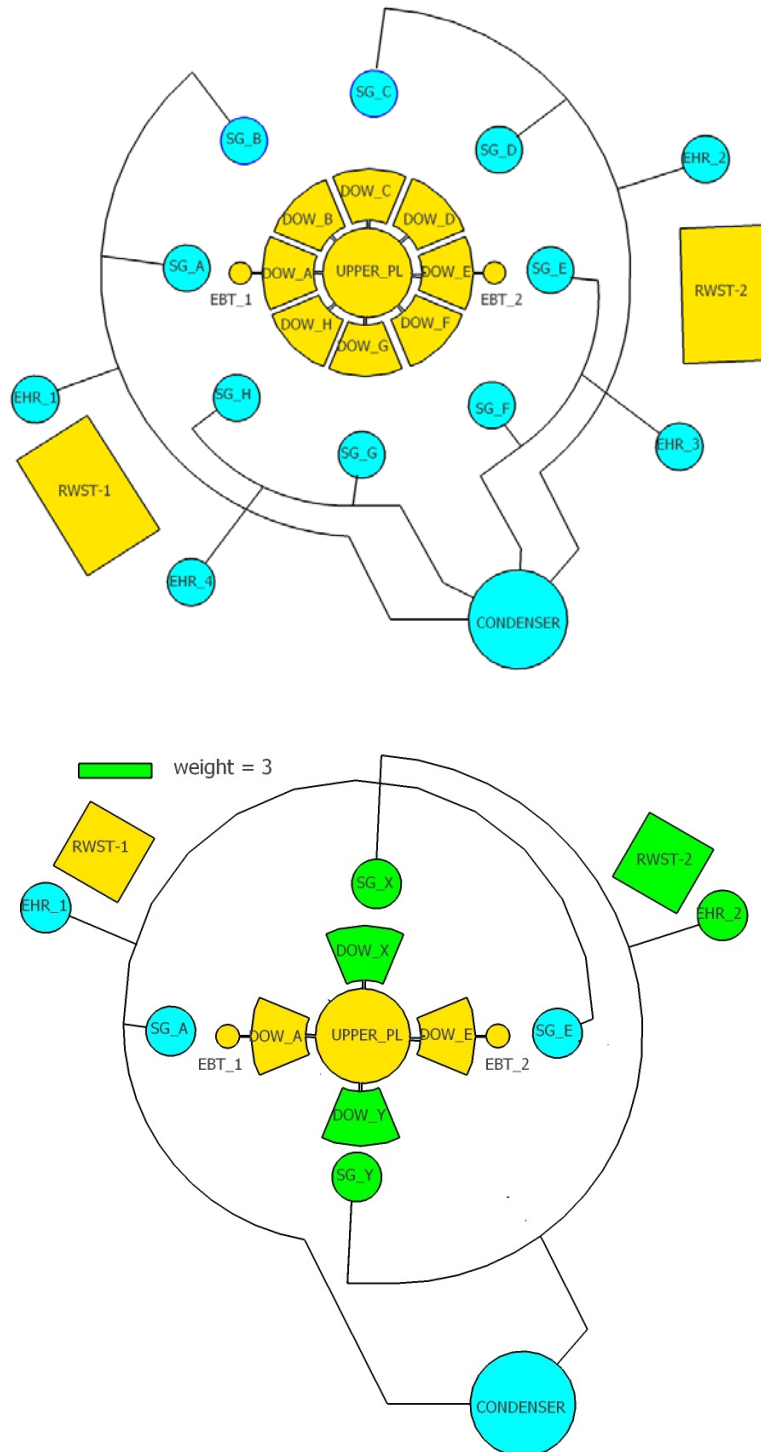
Figure 5-15: IRIS schematic layout of the Primary and secondary circuit

The Figure 5-15 shows the schematic layout of the IRIS reactor and the layout of the CESAR model. The CESAR primary circuit model reproduces the 8 internal loops using a lumping based on a 1-1-3-3 approach that was considered sufficient to take into account different transient and accident sequences. The safety systems, Emergency Boration System (EBS) (2 units) and (1+3 units) Refueling Water Storage Tanks (RWSTs), belong to the primary circuit. The secondary circuit model, reproduces (1+1+3+3) steam generators and the Emergency Heat Removal Systems (1+3). It was used this approach to limit the nodes number and given the symmetry of the system; moreover, this lumped approach does neglect the main thermal-hydraulic phenomena.

5.3.1 Primary circuit nodalization

The primary circuit model is a coarse node representation of the hydraulic system and structures comprising 104 hydraulic control volumes. Most of the control volumes have a linear size in the range of 0.7 to 0.9 m except the pressurizer. The Figure 5-16 illustrates the nodalization of the vessel high part of the primary circuit.
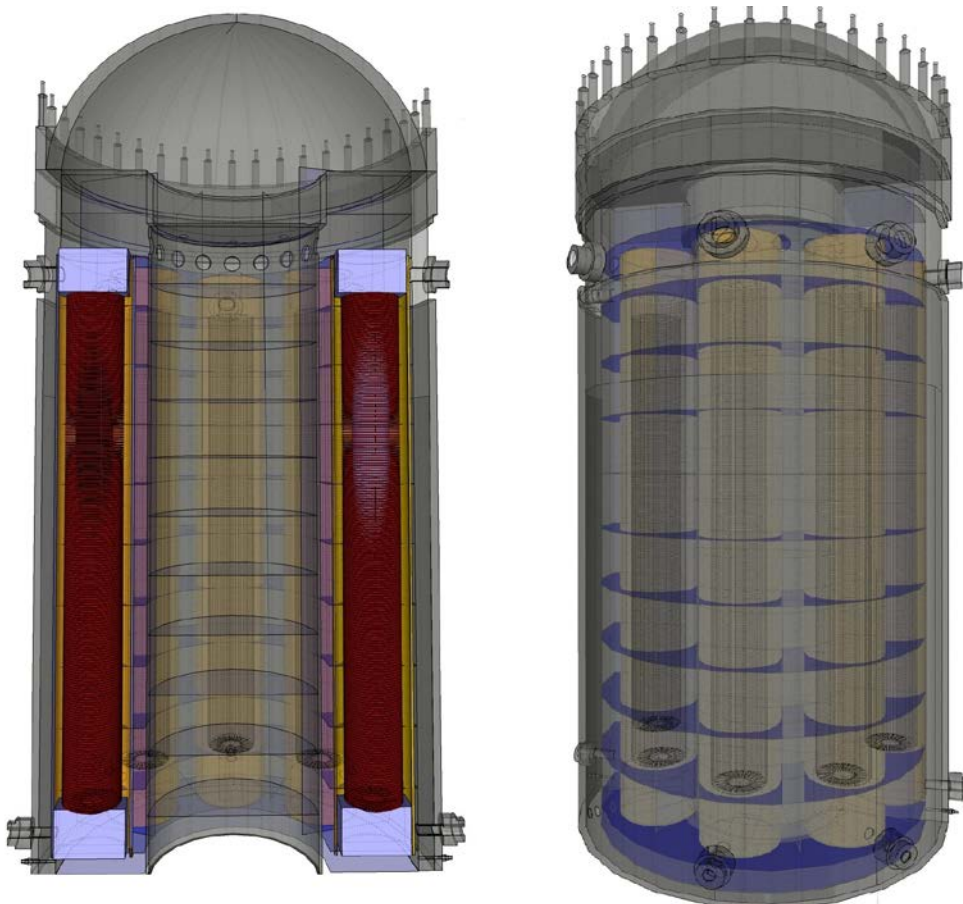

Figure 5-16: Vessel high part nodalization

The rising line has been subdivided in 10 control volumes, while the dowcomer in 13 volumes each one (Figure 5-17). The pressurizer is represented by one only volume, swollen type. All the internal

walls are taken into account. The top control volume of the riser line is connected to all the top downcomer volumes and the pressurizer. Eleven downcomer volumes, share the same wall structures along with the 11 nodes that model the tubes of the SGs in the secondary circuit. The ADS valves were represented using valve system type 'SEBIM' [14], the ADS stage-1 discharging directly inside the Q-tank zone in the CPA model, while the ADS stage-2 directly to the drywell. The two EBTs are modelled with one swollen volume each one, and are double connected to the downcomer in the high part for the pressurization and in the lower part for the water discharging.
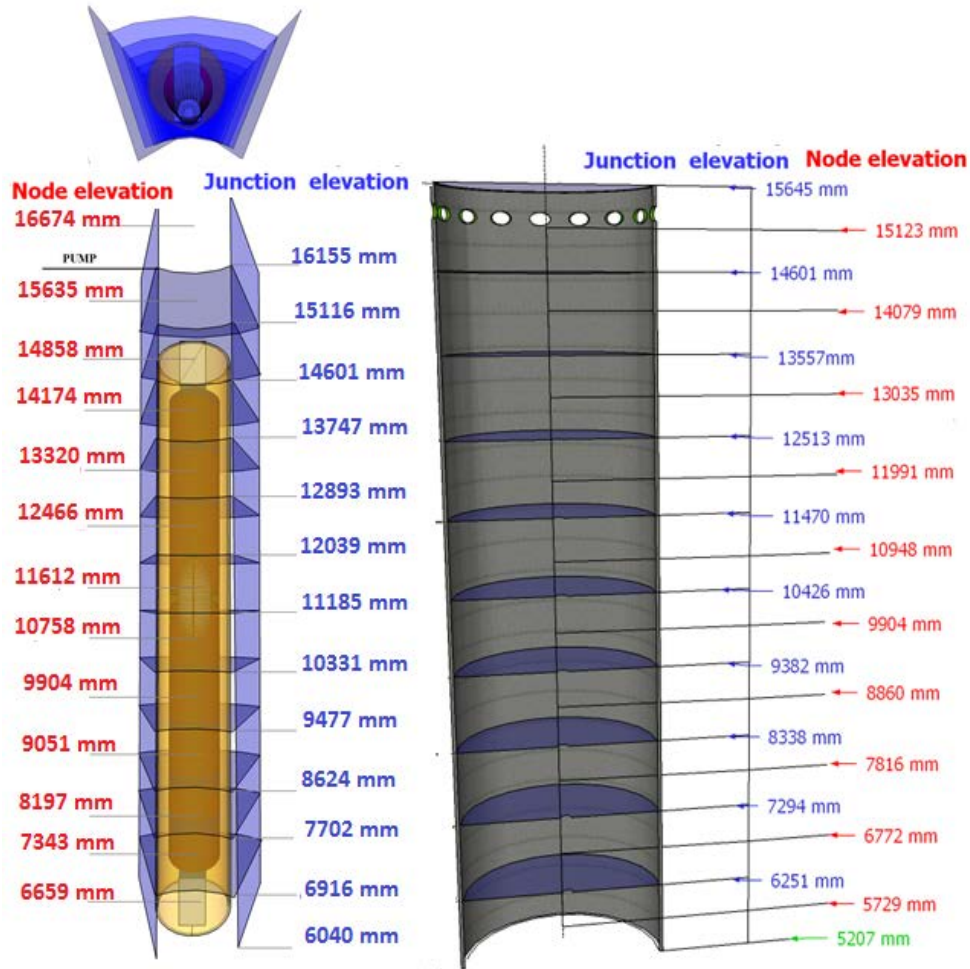
Figure 5-17: Dowcomers and rising line nodalization

The RWST in the model simulates the ultimate heat sink (UHS) of the EHRS systems and is represented by a two-slice approach using 15 control volumes. This kind of approach is because inside the RWST are located the EHRS heat exchanger (HX). The size of the volumes that exchange heat with the EHRS-HX have to be smaller than the volumes do not, in order to taken into account the larger increase of temperature in the zones surrounding the EHRS-HXs. As for the downcomers control volumes in contact with the SGs, even the RWST ones share the same walls with the EHRS-HXs nodes. In

Chapter 5. SMR ASTEC model

Figure 5-18 are illustrated the complete nodalization of the primary (white) and the secondary circuit (blue).
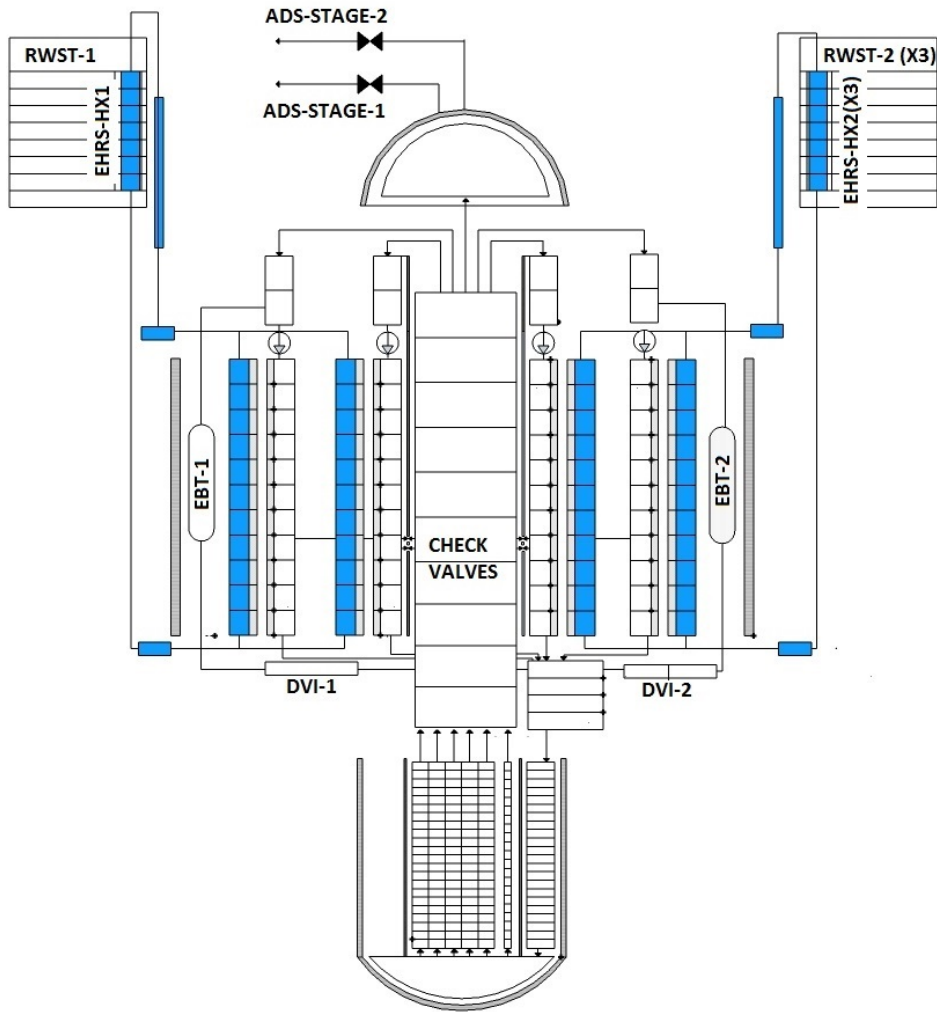

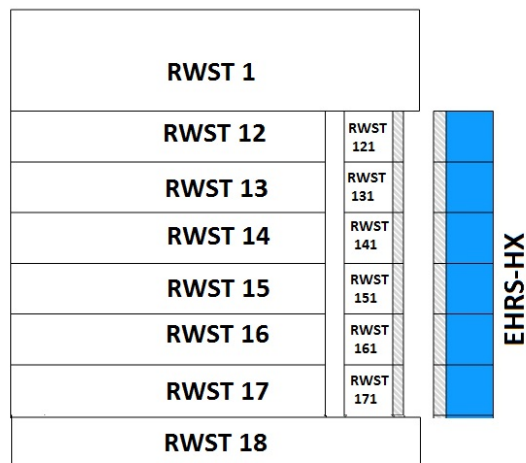Figure 5-18: IRIS primary and secondary circuit nodalization

Figure 5-19: RWST nodalization (two-slice approach)

In the CESAR model are also reproduced the (1+1+3+3) check valves, between the rising line and the downcomer. The aim of this valve is to ensure natural circulation in accident condition. The Reactor Coolant Pumps are modelled using 'DPPOWER' type pump, imposing a coastdown time of 100s after the pumps turn off.

5.3.2 Secondary circuit nodalization

The IRIS secondary circuit is composed by the 8 helical coil SG, represented as 1+1+3+3, 4 EHRS systems simulated as (1+3), the feedwater line, the main steam line and the condenser (Figure 5-20). The condenser is simulated with a big volume, which draws a constant quantity of steam by means of a structure "CONNECTI" from the main steam lines.
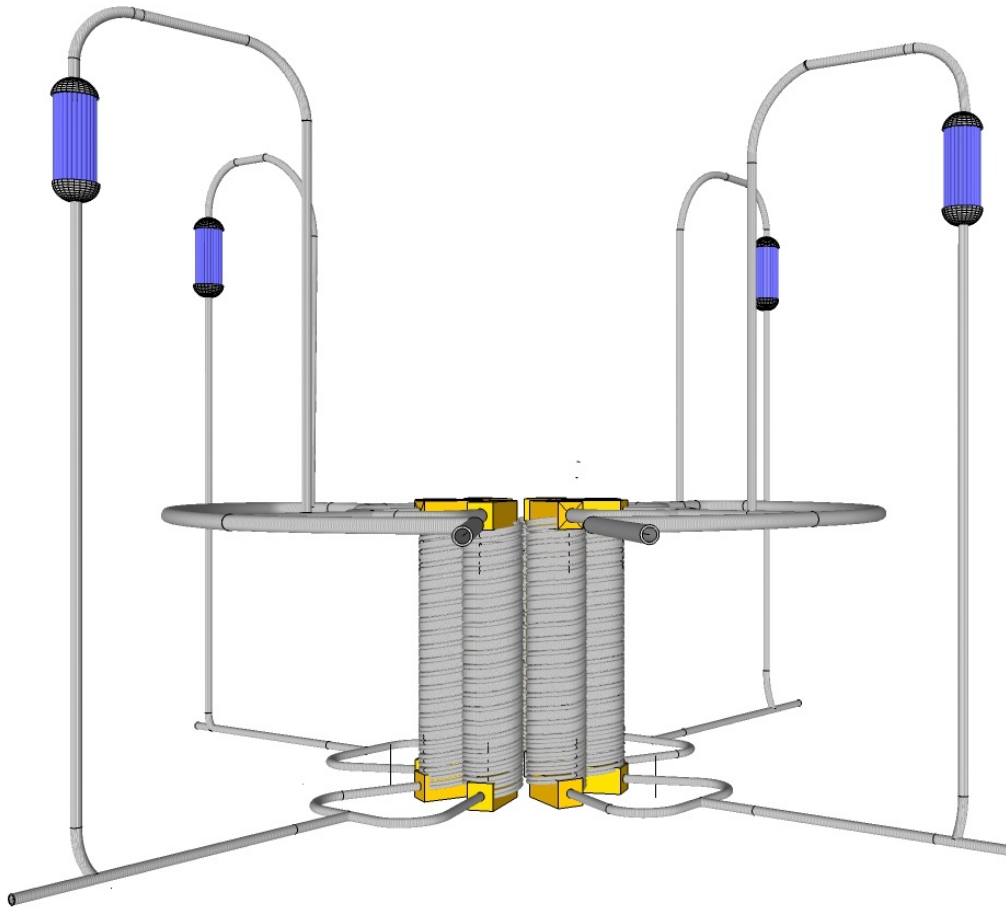

Figure 5-20: IRIS secondary circuit layout simplified

The CESAR module cannot reproduce the helical shape of the tube of the SGs. The SGs are modelled as once through straightforward SGs. In order to reproduce in the better way the thermal-hydraulic characteristics of the helical coil SGs; the SG model conserves the total head losses (primary and secondary side) but the number of tubes was increased of 4.3 times (Figure 5-21), in order to have the same total heat exchange surface, maintaining the same SG height. In the Table 5-15 are reported the IRIS SGs parameters.
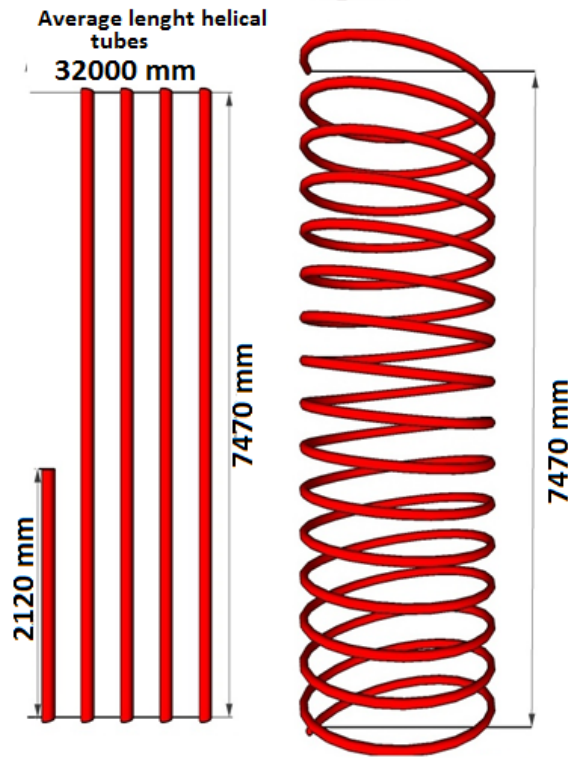
Chapter 5. SMR ASTEC model

Figure 5-21: Number of straight tubes to reproduce an elical shape tube

Table 5-15: IRIS helical coil steam generators parameters

IRIS Steam Generator parameters (1 of 8)	
Rated power [MW]	125
Tube O.D. [mm]	17.46
Tube I.D. [mm]	13.24
N°helical row	21
Tubes N°	656
Tubes Av Lenght [m]	32
SG overall height [m]	8.5
Primary side inlet temperature [°C]	328.4
Primary side outlet temperature [°C]	292
Feedwater temperature	223.9
Steam temperature	317
Primary side pressure [Mpa]	15.5
Steam outlet pressure [Mpa]	5.8
Primary flow rate [kg/s]	589
Secondary flow rate [kg/s]	62.5
Primary side head losses [kPa]	72
Secondary side head losses |kPa]	296
Total heat exchange surface [m²]	1150

Chapter 5. SMR ASTEC model

Table 5-16: IRIS and model SGs parameters

SGs	IRIS	MODEL	Assumption
Type	Helical coil l tubes	Straight tubes	Straight tubes
tube ID [m]	0.01324	0.01324	0.01324
tube OD [m]	0.01746	0.01746	0.01746
thick wall [m]	0.00211	0.00211	0.00211
N° tubes	655	2806	2806
Total Cross section [m²]	0.090179361	0.386325627	0.090179361
L. tube[m]	32	7.47	7.47
Surf. Ex. [m²]	1149.702274	1149.747253	1149.747253

As it is possible to see in the Table 5-16 the total cross section of the SG model has been equalized to IRIS SGs one; in this manner the velocity of the water remains the same. However, it is not possible to reproduce the residence time of the water or steam, inside the SG with this kind of modelization. An EHRS train consists of a heat exchanger, connected to the steam line and the feed line, which rejects the primary side heat to a pool (RWST) through the steam generators. The EHRS is suitable to remove the reactor decay heat in case of accident and secondary loop isolation. Each couple of SGs forms a closed loop with an EHRS-HX. Inside this closed loop, the fluid is in natural circulation, boiling in the SG and condensing in the EHRS-HX tubes. The IRIS EHRS-HX consists of two twin vertical modules of 120 Inconel-600 pipes connected to horizontal cylindrical headers (240 tubes per EHRS-HX) located inside the two RWSTs. In order to reproduce the correct quantity of heat removed by the EHRS, the heat transfer coefficients (HTC), left side (condensation) and right side (boiling) of the EHRS-HX tubes calculated by CESAR, were compared with the literature values, evidencing great differences, both in the condensation and boiling HTC [15]. The EHRS CESAR model tends to underestimate the HTC on the right side (boiling), while overestimates the HTC on the tube side (condensing). Using the CESAR HTC computed values; the EHRS-HX total heat removed predicted, is underestimated on the long term, and overestimated in the first phase of the transient. To fix this discrepancy, it was decided to use the HTC values find in literature for the EHRS-HX walls. The HTC values selected were 8000 W/m²K for the left side (condensing) and 28000 W/m²K for the right side (boiling) (Table 5-17).

Table 5-17: HTC used in the IRIS model

Pressure = 40 Mpa	ASTEC	Literature [16]
HTC boiling side (Pool) W/(m²K)	28000	26000-30000
HTC condensation side (tube) W/(m²K)	8000	8100-11000
HTC global W/(m2K)	3480	3400-3600

Chapter 5. SMR ASTEC model

This is a strong constraint for the model, because for the entire transient the HTC values remain constant, and independent by the thermal-hydraulic of the EHRS loop.

5.4 CPA model

The IRIS containment as stated before, is thermodynamically coupled with the vessel, it has to be considered as a safety system. The layout consists of a spherical steel containment vessel. The containment can be roughly subdivided in seven zone: the Drywell, the cavity, the two Long Term Gravity Makeup System (LGMS), the quench tank (Q-TANK) and the two Pool Suppression System (PSS), as illustrated in Figure 5-22.
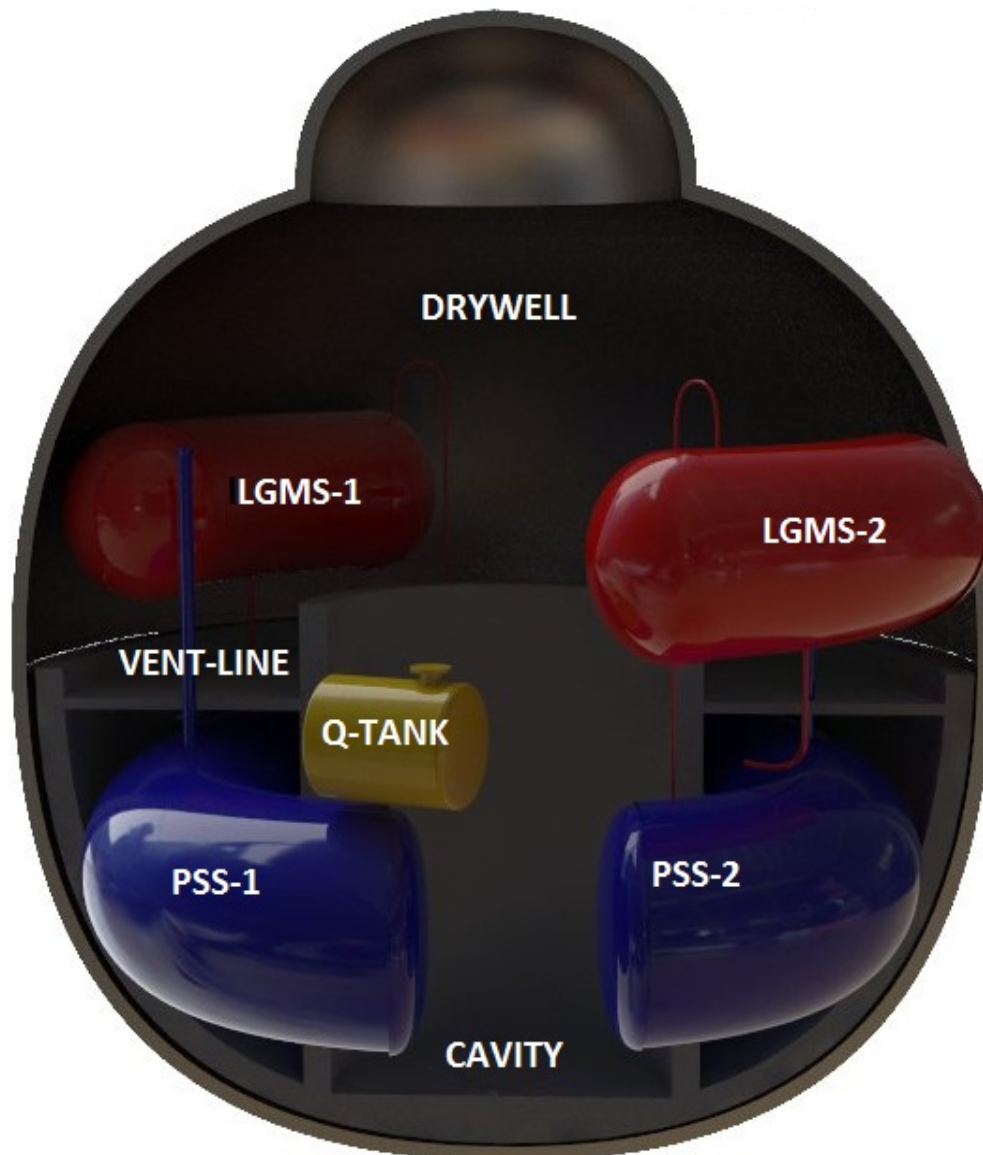
Figure 5-22: IRIS containment simplified layout (Rhinoceros 5)

Chapter 5. SMR ASTEC model

The CPA steam condensation on walls correlation used is based on the Stephan's law [18]. In the DBA model, only the drywell steel wall surfaces, the drywell concrete floor and the cavity walls were taken into account, for the steam condensation. The two suppression pools were reduced in one pool. In order to reproduce the reverse flow between the PSS and the drywell during the accidental transient a virtual connection with a pump was reproduced. Furthermore, in the containment model, used for the severe accident simulation one volume, which belongs to the nuclear building, a tank and a connection have been added. These supplement elements aim to simulates the Passive Containment Cooling System (PCCS). The PCCS is a non-safety grade, ultimate heat sink, for the removal of the core decay heat from the containment that is diverse from EHRS. The PCCS provide the possibility to flooding the entire IRIS containment, by means of fire protection pumps or alternative water supplies. The containment main parameters are illustrated in Table 5-18.

Table 5-18: IRIS containment parameters

IRIS Containment Parameters [17-5]	
Containment diameter/height [m]	25/32
Design pressure	13e5Par
Drywell volume [m³]	3226
Drywell height [m]	11.5
LGMS volume [m³]	150 (x2)/100 water(x2)
PSS volume [m³]	459 (x2)/150 water(x2)
Q-Tank volume [m³]	33.6
Cavity volume [m³]	450
Cavity height [m]	11.75
Containment liner material	Steel
Containment liner thickness [m]	0.0445
Containment liner surface [m²]	1055
Containment floor material	concrete
Containment floor thickness [m]	0.30
Containment floor surface [m²]	256
Initial gas composition	100% N_2
Initial temperature [K]	322.05

The containment nodalization scheme is illustrated in Figure 5-23. The containment has been subdivided in 13 volumes, plus the external environment. Double parallel junctions were realized in horizontal direction in order to simulate counter current flows. The pressure suppression pool was simulated using the "INSERTION INJECTION" model. A reverse line flow has been introduced because; the CPA pool suppression model cannot reproduce the water reverse flow through the vent lines. This fundamental phenomenon cannot be neglected, in order to predict the correct pressure trend inside the containment. In

Chapter 5. SMR ASTEC model

red are marked the connections at the points of hydraulic contact (the break, ADS, and gravity makeup flow paths) between the vessel and the containment. The two connections between the LGMS and the vessel that simulate the injection of water by gravity head and PSS pressurization to the vessel through the DVI line, were reproduced using two pumps. The pump flows are calculated at each time step by means of a special structures "EVENT", which take into account the level of the water inside the LGMS, the head losses, the volumes elevation, and the pressures. Similar connections but with different parameters are also applied to reproduce the water injection from the cavity (when it is full) to the DVI lines. Another structure 'EVENT' was used to take into account the counter pressure at the break. This structure computes the change of pressure at the break due to the water level inside the cavity.
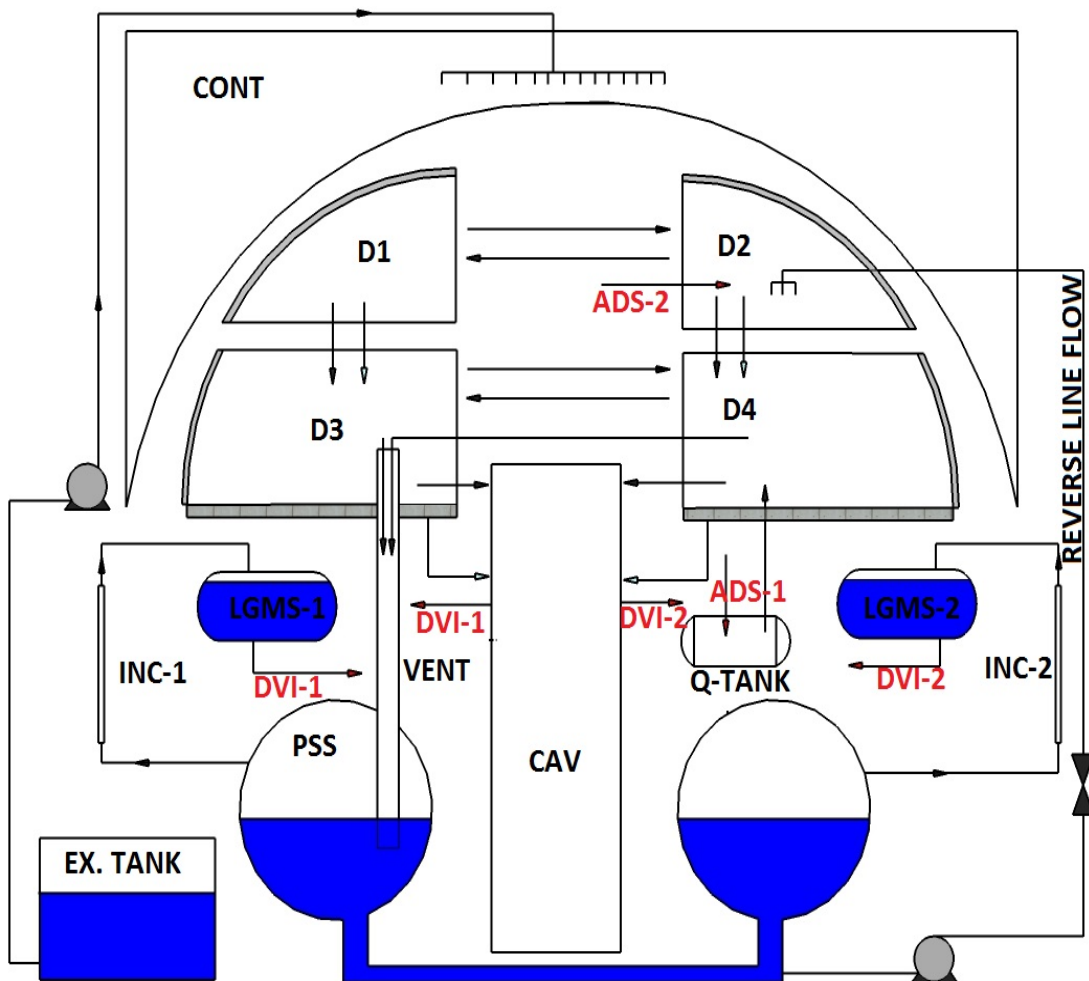
Figure 5-23: CPA IRIS containment model

5.5 Reactor Protection System

The ASTEC model also includes a preliminary version of the basic reactor protection system (RPS). The RPS is managed by means of 132 sensors and 70 structures 'EVENT'. The setpoints and the

Chapter 5. SMR ASTEC model

systems time delay were found in [5], while for the ADS-stage1 system were assumed the data in [9].The main safety system setpoint and time delay utilized are illustrated in Table 5-19.

Table 5-19: Set point and time delay assumed in the accident analyses

Functions	Setpoint safety system	Time delay (s)
Reactor SCRAM	High containment pressure >1.7 E5 Pa HCP signal	0.2
Reactor SCRAM	Low pressurizer pressure < 1.172E5 Pa LPP signal	0.2
Reactor SCRAM	Low pressurizer water level < 0.4 m LPL signal	0.2
CVCS isolation	SCRAM signal	1.0
Turbine isolation	SCRAM signal	5
Feed-water pumps stop	SCRAM signal	5
EHRS train-1 starts	SCRAM signal	19
RCPs stop	Low pressurizer water level < 0.4 m LPL	25
Check valves open	Low pressurizer pressure < 1.172E7 Pa & High containment pressure >1.7E5 Pa LM signal	15
EBT lines open	Low pressurizer pressure < 1.172E7 Pa & High containment pressure >1.7E5 Pa LM signal	15
ADS stage-1 opens	Low pressurizer pressure < 1.172E7 Pa & High containment pressure >1.7E5 Pa LM signal	30
EHRS train-2 starts	Low pressurizer pressure < 1.172E7 Pa & High containment pressure >1.7E5 Pa LM signal	19
LGMS lines open valve	Low differential pressure vessel containment < 5.0E4 Pa LDPC signal	10
Start reverse flow PSS-drywell	PSS pressure > drywell pressure + hydrostatic head vent line HDPP signal	0
Stop reverse flow PSS-drywell	PSS pressure < drywell pressure + hydrostatic head vent line LDPP signal	0
ADS stage-2 opens	LGMS water level < 0.65 m LLLG signal	0
DVI-Cavity valve open	Cavity water level 6.6 m HLC signal	0
Counter pressure connection open	Cavity water level 6.6 m l HLC signal	0
PCC system starts	Containment pressure >1.05E6 Pa HHCP signal	0
PCC system stops	Tank water level < 1.0 m LTL signal	0

Chapter 5. SMR ASTEC model

References chapter 5

[1] R. Ferri, C. Congiu, "*Conceptual design of the SPES3-IRIS facility*", SIET 01 334 RT 07 Rev.1, September 5th, 2008

[2] R. Ferri, C. Congiu, "*SPES3-IRIS facility nodalization for RELAP Mod. 3.3 code and steady state qualification*", SIET 01 423 RT 08 Rev.0, January 30th, 2009

[3] R. Ferri, C. Congiu, "*SPES3-IRIS facility RELAP5 sensitivity analyses of the Lower Break transient for design support*", SIET 01 499 RT 09 Rev.0, June 11th, 2009

[4] R. Ferri, C. Congiu, "*SPES3-IRIS facility RELAP5 base case transient analyses for design support*", SIET 01 489 RT 09 R.

[5] R. Ferri, "*SPES3-IRIS facility RELAP5 sensitivity analyses on the containment system for design review*", SIET 01 526 RT 09 Rev.0, August 31st, 2010

[6] R. Ferri, "*Simulating capabilities of the SPES3 facility*", SIET 01 757 RT 11 Rev.0, August 4th, 2011

[7] Westinghouse Electric Company LLC., *"IRIS Plant Description Document,"* WCAP-16062-NP (Non Proprietary), March 21, 2003

[8] J.M. Collado, "Design of the reactor Pressure Vessel and Internals of the IRIS Integrated Nuclear System" Proceeding of ICAAP 03, Cordoba Spain, May 4-7, 2003

[9] Hone, M., et al., "AP1000 Core Reference Report" WCAP-17524-NP (Non Proprietary), Westinghouse, Revision 0, March 2012

[10] http://www.nrc.gov/reactors/new-reactors/design-cert/ap1000.html

[11] Westinghouse, Westinghouse AP1000 Design Control Document Rev.19, Chapter 4, Section 4.3, (2011) pp 4.3-44 – 4.3-46

[12] De Luze O, Haste T, Barrachin M, Repetto G," *Early phase fuel degradation in Phébus FP: Initiating phenomena of degradation in fuel bundle tests*", Ann. Nucl. Energy in publication, Ann. Nucl. Energy 61, pp. 23-35, 2013.

[13] J.L. Rempe, S.A. Chavez, and G.L. Thinnes. "Light water reactor lower head failure analysis", NUREG/CR-5642, EGG-

2618, Idaho National Engineering Laboratory, Idaho Falls, Idaho, USA, 1993.

[14] G. Guillard, F. Jacq, C. Seropian, W. Plumecocq, ASTEC V1 code SYSINT module Management of events and safety systems interactions Rev. 1, Report ASTEC-V1/DOC/07-21, 2007

[15] R. Ferri, P. Meloni," Approach for a correct simulation of the SPES3-IRIS Emergency Heat Removal System with the RELAP5/MOD3 Code", SIET 01 745 RT 11 Rev.0, May 31st, 2011

[16] M. Ricotti, D. Papini, A. Cammi, D. Grgic: "Modelling of Condensation Phenomena for Passive Safety System and Implementation in the Thermal-Hydraulic" Code.CIRTEN-ENEA Doc. N° XCIRTEN-P9LU-020 - 28/12/2008.

[17] D. Paini, M.E. Ricotti," Follow-up del programma sperimentale SPES3", CERSE-POLIMI RL 1132/2010, Report RdS/2010/65

[18] J. Bestele, et. Al, Containment Thermahydraulics and Aerosol and Fission Product Behaviour, User's Guideline, ASTEC/V0-DOC/00-14, September 2000.

CHAPTER 6

SMR MODEL VALIDATION

6.1 Introduction

The creation of a plant model for computer codes is an interactive procedure, that includes the selection of a nodalization scheme and preparation of the code input deck, and the documentation of these activities as previously done. Depending on the objectives of the analysis, the plant model, or the code input deck, could be accident dependent. Thus, to evaluate the validity of an integral code model, a benchmark with a best-estimate code or a more detailed code, should be compulsory. The purpose of the validation of the input model is to demonstrate that the input model adequately represents the behaviour and the functions of the modelled system. A preliminary assessment has led to the conclusion that in order to develop an appropriate evaluation model for the IRIS reactor, the coupling between the vessel modules (CESAR) and the containment module (CPA) has to be correctly captured. This is the reason why, before conducting, a severe accident analysis, in order to test the SMR ASTEC input deck, a BDBA reference accident was performed. The BDBA scenario simulated was a Direct Vessel Injection (DVI) line double-ended guillotine (DEG) break. The calculated results, was compared with those obtained by the University of Zagreb (FER) in cooperation with Westinghouse using the well-established best-estimate coupled codes RELAP5 and GOTHIC [1]. The comparison of the code simulation results, allowed investigating specific phenomena evidenced by the codes, according to the related modelling approach of components with detailed nodalization and coarse mesh nodalization.

6.2   RELAP code and RCS model

The RELAP5 code has been developed for best-estimate transient simulation of light water reactor coolant system during postulated accidents. The code was developed at the Idaho National Engineering Laboratory (INEL) for the U.S. Nuclear Regulatory Commission (NRC). The code uses include analyses required to support rulemaking, licensing audit calculations, evaluation of accident mitigation strategies, evaluation of operator guidelines, and experiment planning analysis. The RELAP5 code is based on a nonhomogeneous and non-equilibrium model for the two-phase system that is solved by a fast, partially implicit numerical scheme to permit economical calculation of system transients [1]. The RELAP5 IRIS reactor coolant system input-deck, has been developed at the University of Zagreb (FER) in collaboration with Westinghouse and the Polytechnic of Milan [2].The nodalization includes 1845 volumes, and 1940 junction, 1015 heat structures with 8600 mesh points [3]. All the main flow paths are modeled with sufficient detail, with almost all of the minor flow paths. Sliced approach was used in the discretization of the reactor vessel taking into account importance of natural circulation in chosen safety concept. Most of the calculation nodes have linear size in range 0.2 to 0.5 m. The nodalization was prepared so to maintain free volume of the system and elevation differences (due to importance of natural circulation) as well as core and SG heat exchange areas. The IRIS RCS model with RELAP5mod3 is provided in Figure 6-1. The model can be divided in the following main regions:

- Lower downcomer
- Lower plenum,
- Core and bypass region ,
- Riser,
- Pressurizer,
- Upper downcomer and Reactor Coolant Pump Suction Plenum,
- Reactor coolant pumps (RCP),
- Primary side of the Steam Generator (SG) modules,
- Inactive volume around the SG modules and, inactive volume inside the SG module central support column.
- Steam Generator Shroud check-valves.
- Each of the eight RCP/SG modules is explicitly modeled: this detailed nodalization of the coupled RCP and SG modules was selected in order to better address potential asymmetrical effects in the coolant system.
- Two SG modules are connected to each feed/steam line, so that the system features four steam and four feed lines.
- The Secondary Side of the SG
- The secondary system and the balance of plant are only

modeled in detail up to the main feed and steam isolation valves. A simplified turbine and feedwater system is also provided
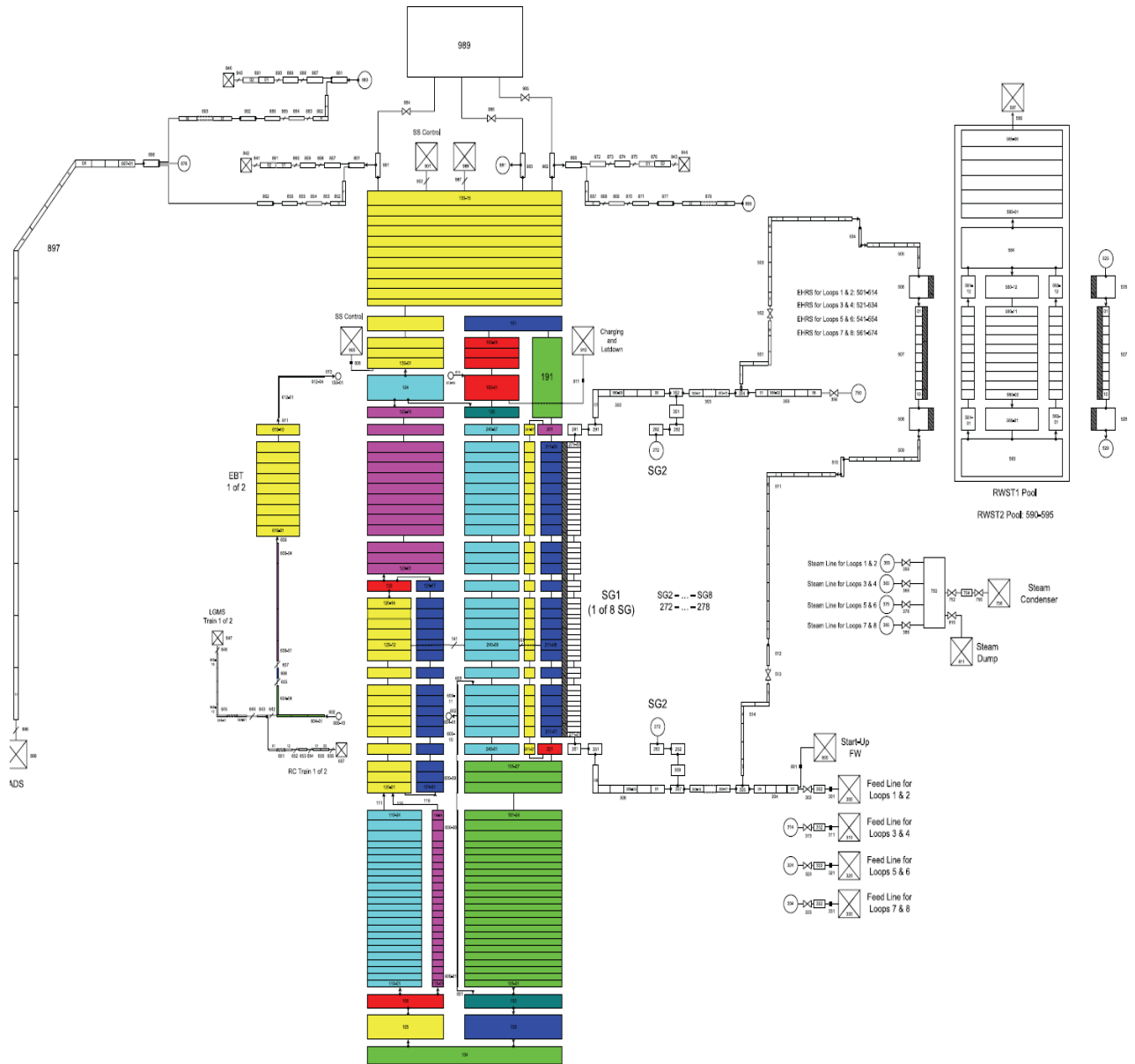

Figure 6-6-1: IRIS primary and secondary circuit nodalization for RELAP5 code

Finally, the Engineered Safeguards Features of the plant are also modelled. Among these, the ones included in the RELAP5 model are the emergency heat removal system (EHRS) and the emergency boration system (EBS). In addition, the refueling water storage tank (RWST) is modeled as the ultimate heat sink for the EHRS heat exchangers. These systems are sufficient for the analysis of all IRIS NON-LOCA transients and accidents. Since the remaining IRIS safety features, (automatic depressurization system, ADS; pressure suppression system; long-term core makeup

system) establish an interaction between the integral reactor coolant system and the containment. The main differences between the RELAP and CESAR RCS model are:

- RELAP model takes into account the two SG non-active zone (inside and outside SG);

- RELAP reproduces the total length of the SG tubes (32 m), and the geometry;

- No lumping approach. Every system is simulated.

- RELAP considers the ADS discharge line, while in the CESAR model, the ADS system is simulated as a break.

6.3 GOTHIC code and containment model

GOTHIC is a CFD-like code that predicts compartment thermal-hydraulic behaviour using conservation of mass, momentum, and energy equations for multiphase (vapour phase, continuous liquid phase, droplet phase) multicomponent (water, air, H_2, noble gases) compressible flow. Phases can be in thermodynamic equilibrium or constitutive relations can be used to predict interaction between phases for non-homogenous non-equilibrium flow. Hydraulic volumes are analysed using 1D, 2D, 3D or lumped approach and can have any number of 1D-heat structures. In addition, models for all engineering devices (pumps, fans, valves, heat exchangers, etc), usually found in NPP containments, are available [4]. The GOTHIC input-deck has been developed at the University of Zagreb (FER) in collaboration with Westinghouse, and reproduces the IRIS containment by means of 85 volumes, 28 junctions, and 57-heat structure (Figure 6-2). The IRIS drywell model developed with GOTHIC code is based on a subdivided volume approach. GOTHIC drywell volume is comprised thus of 64 subvolumes (4 axial levels, provided with a square matrix 4x4 each one). The GOTHIC heat structure modelling are represented by means of a multi-node concept. The heat structures are obtained following a distributed scheme, where the external spanned conductor modelling containment liner is subdivided in more conductors, surrounding the subdivided drywell volume. Boundary related information with side heat transfer could be hence properly accounted, reproducing local effects and distinguishing between how steam condensation is provided at the top of the drywell and on its lateral walls. Natural convection is handled in different ways for vertical and horizontal part of the structures too. Break terms are employed as boundary conditions, linked to drywell volume with the respective flow paths. Break pressure, temperature, flow and liquid fraction (both for reactor vessel side and for DVI side of the break) dependence with time is provided with suitable forcing functions.
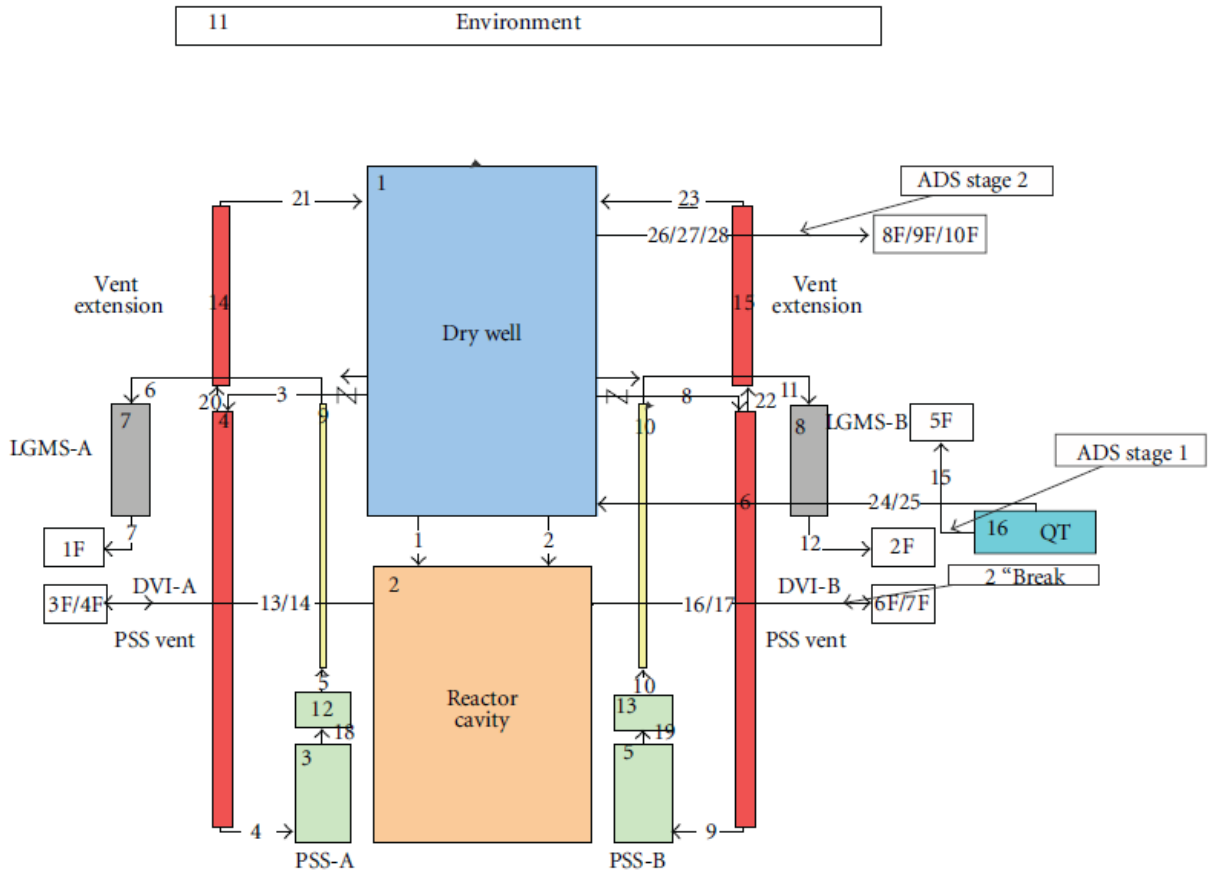
Chapter 6. SMR model validation

Figure 6-2: IRIS containment nodalization for GOTHIC code

6.4 DBA accident analysis

6.4.1 Steady state calculation

Before to simulate the DBA accident scenario a stationary input deck for CESAR was built to establish the initial conditions of the transient. The restart file generated by this run was used as initial condition for the transient simulation. This input deck was constrained by introducing different controllers by means of structures 'REGU' [6] (Controlled Steady State Phase). The task of the structures 'REGU' is to adjust the different parameters in order to fit the computed response with the expected one. In this way, they were set to the desired physical values for PZR level and pressure, SG flow rate, SG steam produced, SG water level, water flow across the core, just to name a few. This stationary transient was run for 30000 s to verify that the calculated conditions were steady and the actual initial conditions of the simulation were achieved. After the desired steady-state conditions were achieved, all the structures 'REGU' were removed to verify the stability of the modelling (Free Steady State Phase). As further, confirm of the parameters steadiness, a "null transient" was performed for another 20000 s. The comparison between the steady-state calculated results

obtained by the ASTEC code and those computed by RELAP5-GOTHIC coupled codes is summarized in Table 6-1. All the selected RELAP code steady state calculated values have been found in [7]. As it can be seen, the calculated values were in good agreement with each other.

Table 6-1: IRIS Steady state predicted result

Parameters	ASTEC	RELAP5/GOTHIC
	TIME(s)	TIME(s)
Pressurizer Pressure (Pa)	1.556E7	1.555E7
Core inlet Temperature (K)	566.15	564.15
Core outlet Temperature (K)	602.14	602.15
Core mass flow/(by pass) (kg/s)	4707/(203)	4517/(213)
Core power (MW)	1000	1000
SG inlet temperature (K)	497.15	497.15
SG outlet temperature (K)	588.2	590.40
SG steam pressure (Pa)	5.86E6	5.80E6
SG collapsed level (m)	1.84	1.95
Feedwater flow (kg/s)	64.22	62.85
RCS water mass	324580	324500
Primary to secondary heat transfer	998.24	1000
EBT A/B water mass (kg)	12795	12400 (x2)
EBT A/B water Temp. (K)	303.05	322.05
RWST A/B water mass (kg)	625000 (x4)	1194200 (x2)
RWST A/B water Temp. (K)	290.05	293.15
RWST A/B water level. (m)	8.6	9.1
PSS A/B water mass (kg)	300000 (x1)	145300(x2)
PSS A/B water Temp. (K)	322.05	322.05
PSS water level (m)	2.06	3.00
LGMS A/B water mass(kg)	100000	9890 (x2)
LGMS A/B water Temp. (K)	322.05	322.05
Containment atm. Temp (K)	322.05	322.05
Environment atm. Temp (K)	308.15	308.15

6.4.2 The DBA scenario

The DBA scenario considered in this analysis is the guillotine rupture of the direct vessel injection (DVI) line Figure 6-3

Chapter 6. SMR model validation
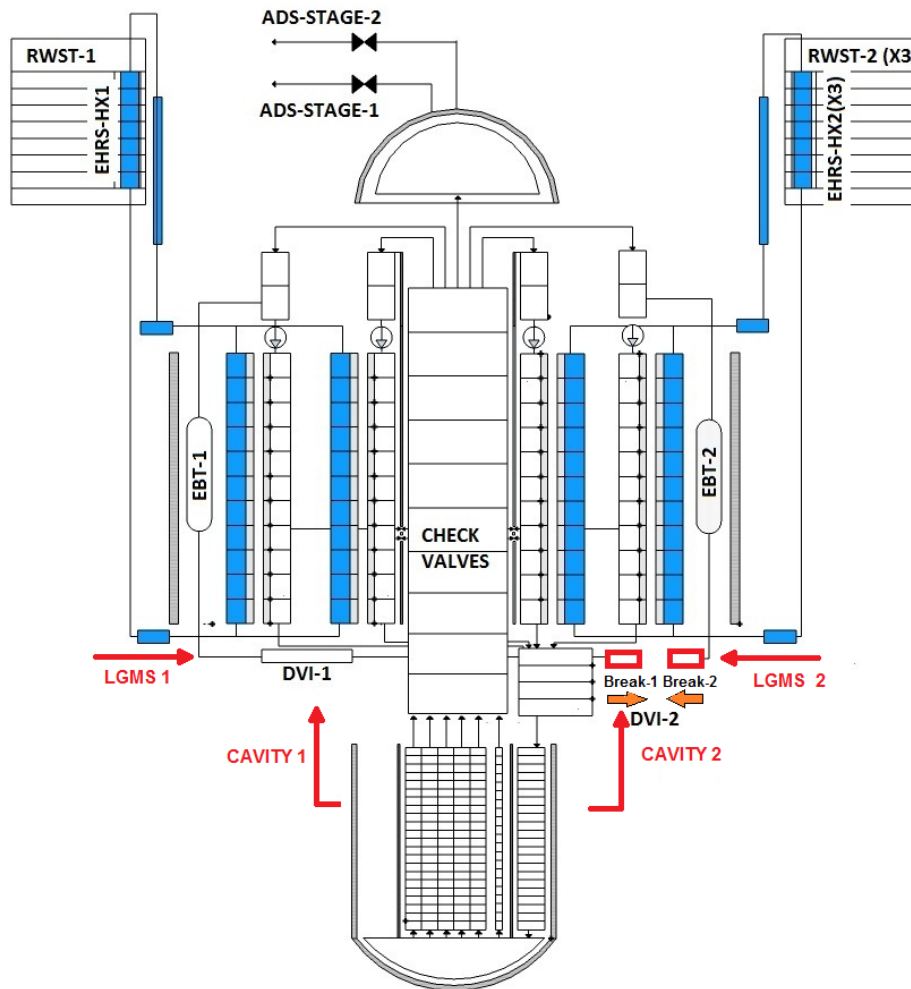
Figure 6-3: DVI DEG LOCA schematic description

Although this is the smaller line connected to the vessel, it requires a particular analysis due to its position nearer to the top of the active core (TAF). The DVI line is connected to the reactor coolant system in the annular region near the bottom of the steam generators. Another important feature of this line is that, it is the discharge line of the LGMS, EBS and reactor cavity (when completely flooded). The double-ended break can be considered conservative from the point of view of liquid level and containment pressurization. A SBLOCA transient for IRIS reactor can be divided in three distinct phases (Figure 6-4). The first one, denominated the blow-down phase is defined as the period during which the reactor coolant system pressure is reduced and the containment pressure increases until the reactor coolant system and containment pressures equalize. The containment pressure in this phase is limited by the PSS and the reduced break flow due to the EHRS heat removal from the vessel. This phase, due to the relatively small dimensions of the break and of the ADS stage-1 lines, can be long for IRIS, in the order of 2000 seconds for the considered case. The

Chapter 6. SMR model validation

blow-down phase is considered concluded when the pressures in the vessel and in the containment are in equilibrium with a containment vessel peak lesser than 10E5 Pa. The break flow stops and the gravity makeup from the LGMS becomes available.
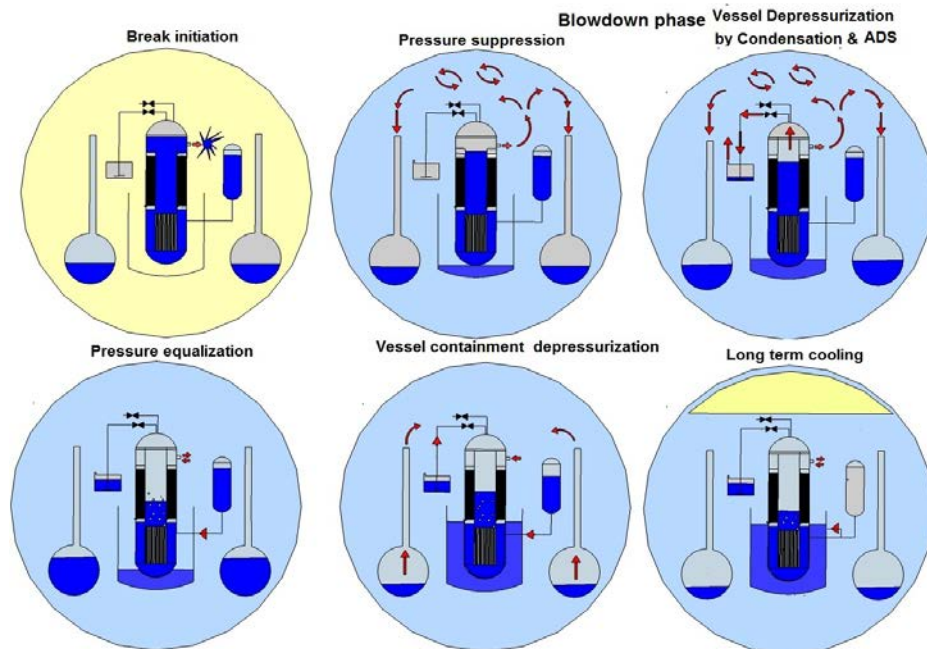
Figure 6-4: Overview of IRIS response to SBLOCA sequence

The blow down phase is followed by a depressurization phase. This phase can be further divided in two portions, before and after the opening of the ADS-stage2 lines. In the first one the pressure in the vessel remains lower than the pressure in the containment and the break flow reverses since heat is removed not from the containment, but directly from inside the vessel. During this phase the drywell pressure is reduced following the steam condensation on the containment walls and by the cool water discharged from the LGMS through the DVI break line. As the drywell pressure is reduced faster than the PSS pressure, a portion of suppression pool water is pushed out through the vent lines and assist in flooding the vessel cavity. After the opening of the ADS stage-2 lines the drywell and reactor vessel pressures are coupled and the coupled system is depressurized by the EHRS. The depressurization phase is followed by the long-term cooling phase, where the containment and vessel pressure is slowly reduced as the core decay heat decreases. During this phase of the accident recovery, gravity makeup from reactor cavity is available as required. Since decay, heat is directly removed from within the vessel and the vessel and containment are thermodynamically coupled, the long-term break

flow does not depend on the core decay heat, but it is in fact limited to only the containment heat loss.

6.4.3 Transient analysis

The transient starts after 30000 s of steady state. Break opening is initiated at t=0 s transient time. The first 86400 s (1 day) of accident are calculated and the main parameters are compared. All times of the events are given with respect to the break time assumed as time 0 s. The comparison of the main event during the DBA DEG transient is illustrated in Table 6-2.

Table 6-2: Main event cronologies

MAIN EVENT	ASTEC	RELAP5/GOTHIC
	TIME(s)	TIME(s)
Double guillotine Break opens on DVI-2 line	0.0	0.0
High Containment pressure signal HCP signal	28.6	30.0
Reactor SCRAM	28.8	30.0
CVCS isolation	30.0	
Secondary system isolation on SCRAM signal	30.0	30.0
EHRS-train1 starts on SCRAM signal	49.7	40.0
Low Pressurizer level signal LPL signal	94.2	130.0
Shroud valves open (HCP + LPL)	105.0	140.0
RCPs stops on LPL signal	119.2	143
Low Pressurizer pressure signal LPP signal	173.3	174.0
EBT line opening On LM signal (HCP + LPP)	188.3	174.0
ADS stage-1 opening On LM signal (HCP + LPP)	191.0	174.0
EHRS-train2 starts On LM signal (HCP + LPP)	193.0	174.0
Low differential pressure vessel containment LDPC signal	1825.0	1585.0
LGMS starts to inject On LDPC signal	1840.0	1585.0
Pressure equalization DW-Vessel	2130.0	1730.0
Reverse flow starts PSS-DW	2310.0	2504.0
HLC signal	4114.0	1585.0
Cavity-DVI valves open On HLC signal	4114.0	open on LDPC signal
LGMS water level signal LLLG signal	16874.0	14110.0
ADS stage-2 opening	16874.0	14120.0
Flow from cavity to vessel	70000.0	65414.0

The breaks, the EBS and the check valves

The break opening at 0 s, causes the vessel depressurization and containment pressurization. The containment pressure reaches the 1.7E5 Pa around 30 s and a SCRAM signal is generated for both the simulation. After the SCRAM signal, the EHRS train-1 starts to work (RELAP-GOTHIC (R-G), 40 s ASTEC 49.7 s).Figure 6-6 illustrates the breaks mass discharge flow. The vessel side break mass flow peaks and trends, are quite similar in ASTEC and R-G in the first 1000 s then, until the containment and vessel pressure equalization (1936 s R-G, 2127 s ASTEC), the mass discharge flow predicted by ASTEC is greater than RELAP one, driven by the high primary side pressure. After 4000 s, ASTEC predicts a negative flow, while the R-G results, swing between negative and positive, and tend to positive values after 7000 s. The reason why of this difference is that, the RCS CESAR model does not reproduce the not active zone inside and around the SGs; this latter is the actual zone in where the break occurs. In the CESAR model, all the downcomer volumes exchanges heat with SGs, affecting the vessel pressure and generating this continuous reverse flow. In the RELAP model the SG not active zone maintain a higher pressure then the active SG zone. Concerning the break mass flow, containment side, it is related to the safety injection of the EBT (174 s R-G, 208.3 ASTEC) actuated by the LLP signal. The EBT2 injection into the broken DVI line is initially about 16 times larger than EBT1 injection into the intact DVI line, due to the presence of the break (Figure 6-7). On the long term, the break containment side is related to the LGMS injection triggers on LDPC signal. Inside the vessel, the natural circulation is guaranteed through the check valves, connecting riser and downcomer at one-third of the SG height (Figure 6-8). The actual configuration of the check valves systems connects the rising line to the SGs internal cylinder, and the recirculation water is not in contact with the SGs tubes. In the ASTEC model, the rising line is directly connected to the downcomer volumes. However, this approximation does not completely explain the difference observed in the first 10000 s.

The ADS stage-1

Figure 6-9 shows the R-G and ASTEC predicted pressurizer pressures. The depressurization rate is similar until the ADS intervention (191 s for ASTEC and 174 s for RELAP), activated by the LM signal, after that the ASTEC code calculates an abruptly pressure decreases between 200 and 400 s, before resuming values higher than RELAP ones. This is due to the modelling of the ADS-stage1 system, which is simulated as a simple break in the pressurizer in the ASTEC model, and it does not reproduce the actual configuration, of the ADS stage-1. The ADS is composed by two three parallel train and a 15 m long discharge line for ADS stage-1. In Figure

Chapter 6. SMR model validation

6-10 and Figure 6-11, are shown the ADS-stage1 release (divided in double train (DT) and single train (ST) for R-G) and cumulative release, respectively. Concerning the ADS-stage-1 release, the calculated results are quite similar until the pressure equalization; when R-G predicts a greater reverse flow, which is not reproduce by ASTEC. Consequently, the ASTEC cumulative release computed is higher than R-G one. This difference is due to the faster vessel depressurization calculated by R-G, after the pressure equalization (at 2130 s for ASTEC and at 1730 s for R-G) (Figure 6-20).

The EHRS and SGs

After the secondary system isolation, the SGs pressure increases due to the heat transfer from the primary side that makes evaporate the water contained in the SG tubes. The secondary side pressures are shown in Figure 6-12. The SG pressure peaks are reached around 57 s for both calculations, then the pressure decreases after some oscillations lasting until water stored in EHRS–HX is poured into the loops and power begins to be removed and the SGs tube level increases (Figure 6-13 and Figure 6-14). The signal of low pressurizer pressure triggers the second train of EHRS and a natural circulation flow establishes. The EHRS loop Filling Ratio defined as the ratio between the total mass in the closed loop and the total mass of cold water that could be stored into the loop is 0.34 in ASTEC and 0.4 in R-G. The Figure 6-15 and Figure 6-16 show the EHRS-HX power removed and the water temperature inside the RWST calculated by the two codes. The curves shows a very similar trend throughout the transient.

The LGMS

The signal of low differential pressure (LDPC) between the vessel and the drywell triggers the LGMS injection into the DVI line. LGMS injection is related both to gravity and to LGMS air space pressurization (through PSS to LGMS balance lines) by non-condensable gas entering the PSS from the drywell. On contrary of the EBS, the predicted LGMS1 and LGMS2 mass discharged flow are similar, for both the codes. The difference between the break and the intact line is not so marked Figure 6-17. The ASTEC code as stated before, calculates the LGMS mass flow using a structure pump, for each LGMS. Therefore, the LDPC signal in the ASTEC model triggers the pumps, for which, the flows are calculated at each time step by means of two structure "EVENT" in order to reproduce the gravity flow. The same approach was utilized to simulate the water injection from the reactor cavity to the DVI intact line.

The containment (Drywell and PSS)

The Figure 6-18 shows the calculated drywell pressure. The increase observed around 200 s is due to the ADS stage-1 intervention. The

containment space drywell and cavity pressurization causes the transfer of a steam-gas mixture from the drywell to the PSS through the vent lines lasting until mass flow exits the ADS-Stage-1. The Figure 6-19 show the non-condensable gas quality inside the drywell and the way steam sweeps away gas from the drywell seems similar between the two codes. A part of the steam released condenses on the drywell walls, transferring power to the drywell structures. The power transfer occurs until a thermal equilibrium is reached on the walls (Figure 6-20). At the peak, the ASTEC calculated power (75 MW) is about 7 times the RELAP-GOTHIC (R-G) power (11.2 MW). During this phase the DW and cavity pressure increases up to reach a peak of 0.957 MPa in ASTEC at 1850 s and 0.936 MPa in R-G at 1405 s. Once, the vessel and drywell pressures equalize (Figure 6-21), the ADS Stage-1 and the break mass flow stop, and the drywell pressure decreases thanks to the LGMS injection into the vessel (intact loop) and into the cavity (broken loop). When the differential pressure between PSS and drywell (Figure 6-22) is sufficient to overcome the hydrostatic head of the PSS vent pipes, a reverse flow starts from the PSS to the DW through the vent lines, lasting between 2310 s and 4050 s for R-G and 2504-4094 s for ASTEC (Figure 6-23). This event, explains the faster DW depressurization, which occurs after 2000 s. These phenomenon is reproduced by ASTEC as a containment spray system in recirculation mode, where the suppression pool is the source of the water. The pump of this system starts to work when the pressure difference greater than the hydrostatic head and stops when is lower. The mass flow was imposed by means of the pump characteristics. Following the PSS injection, the reactor cavity level, initially increased for break and ADS mass flow collection, rapidly increases up to the complete fill-up (Figure 6-24) at 14891 s in R-G and around 30000 s in ASTEC (12 m level from bottom in ASTEC and 11.75 m in RELAP). The ASTEC delay is due to the lower LGMS2 mass flow calculated.). In the R-G model, the PSS and drywell volumes remain separated, from the pressure point of view, as the PSS to drywell vent pipes remain full of water after the PSS injection to drywell is over, and non-condensable gas cannot flow from PSS to drywell and equalize pressure. In the ASTEC model, this event was re-create imposing a high value to the connection flow resistance coefficient in negative direction, between the PSS and the vent line volumes. When the reactor cavity level is above the DVI connection (around 8000 s in ASTEC and 5000 s in R-G) and the containment pressure overcomes the vessel pressure, water can enter the vessel through the cavity to DVI connections. The mass injected from cavity to DVI is shown in Figure 6-25. The injection occurs around 70000 s for ASTEC and for R-G. In the ASTEC simulation taking into account the effect of the cavity water level on the outside pressure at the break, when the cavity water level exceed the DVI line elevation is activated a structure 'EVENT' which calculates the counter pressure at the break at each time step, due to the water gravity head. The reaching of both LGMS low mass signals

actuates the ADS Stage-2 valves, (16874 s for ASTEC and 14120 for R-G), to allow steam circulation between the vessel and the drywell in the upper part of the plant and enhance condensation on the SG tubes in the long term of the transient. The opening of the ADS stage-2 re-equalize the pressure between the containment and the drywell, and the vessel inventory starts to decrease (Figure 6-26) until to reaches the equilibrium and stabilize around 25000 s. After that, the differential pressure between the vessel and containment and the amount of water in one or the other side of the plant drives the broken DVI line mass flow, and the vessel water inventory remains constant.

6.5 Discussion

Most of the main parameters calculated by the ASTEC code has shown a good agreement with those computed by R-G coupled codes from the qualitative and quantitative point of view. The main discrepancies are due to the coarse meshing approach in the ASTEC model. Some points to remark are:

- ASTEC computes a DW walls deposited power 7.5 times greater than R-G one. The reasons of this difference are not clear. The drywell surface and the thickness data, adopted in the simulation are the same used in different scientific works in the literature. The boundary condition are the same for both the codes. The discrepancy should affect the drywell pressure rise, but the calculated ASTEC drywell pressure rise is very similar to R-G one;

- The drywell pressurization and vessel depressurization trend are similar, even if slightly delayed in ASTEC until 3000 s. After the reverse flow stopped, the ASTEC calculated drywell pressure is higher while the vessel pressure is lower than RELAP ones. The drywell pressure discrepancy is probably due to the PSS modelling; indeed the suppression pool zone is simulated as an adiabatic volume without walls to exchange heat and the water expulsion is simulated with a pump system so, the ASTEC code do not reproduce the depressurization following this phenomenon. This kind of approach tends to overestimate the PSS water temperature of about 50 K (Figure 6-27). Thus, the reverse flow is less effectiveness due to the higher temperature of the PSS water pushed out. Furthermore, the high water temperature could be also the cause of the calculated higher peak pressure inside the PSS than in the drywell.

- ASTEC predicts a lower pressure of the vessel than R-G coupled codes after 10000 s. The discrepancy could be due to the temperature at which the EHRS-HX exchange heat. In the ASTEC model, the calculated flow steam quality, enters EHRS-HX is lower than R-G one, because of the different

Chapter 6. SMR model validation

length of the SGs tubes (32 and 7.40 m). Furthermore, having imposed a constant steam condensation heat transfer coefficient, in the EHRS-HX tube side, the model tends to overestimate the water subcooling on EHRS-HX outlet flow, (sensible heat is removed instead of latent heat). This also explain why the ASTEC calculated drywell pressure is lower than R-G one, at the end of the transient given the system characteristics (thermodynamically coupled). Anyway, the final difference is around 5E4Pa, and given the simplification adopted, the result could be considered satisfactory.

Overall, the analysis of the DBA transient by the comparison between the ASTEC code and R-G coupled codes has provided comforting answers. The interaction of the IRIS vessel with the containment following the accident scenario and the behaviour of the passive safety systems are well reproduced by the ASTEC code. This preliminary testing of the model has showed that the discretization approach is acceptable and that the model produces reasonable steady state, and transient results. After this test, the model can be used to simulate a severe accident scenario.

Chapter 6. SMR model validation
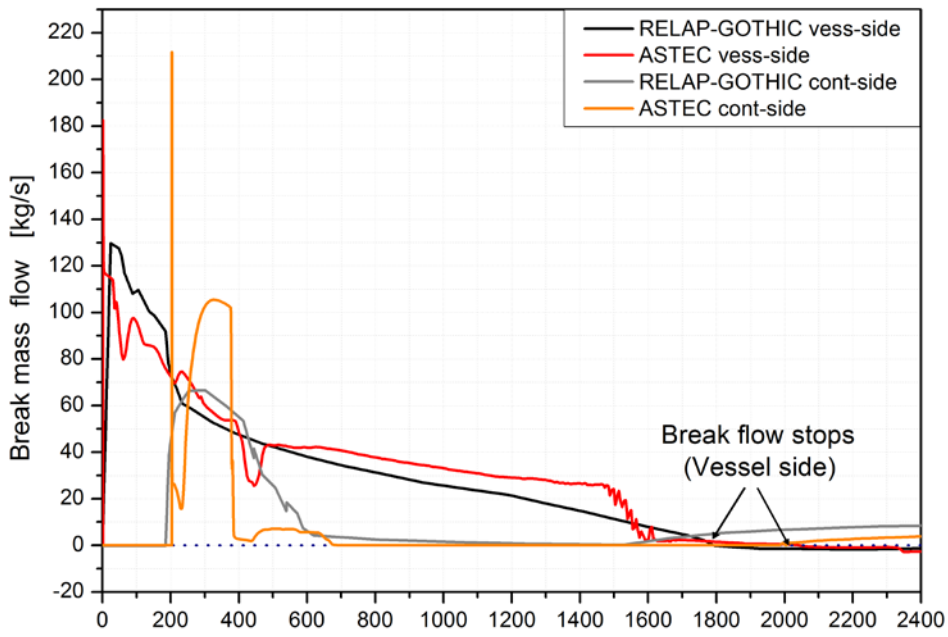
Figure 6-5: Break mass flow containment and vessel side (0-2000 s)
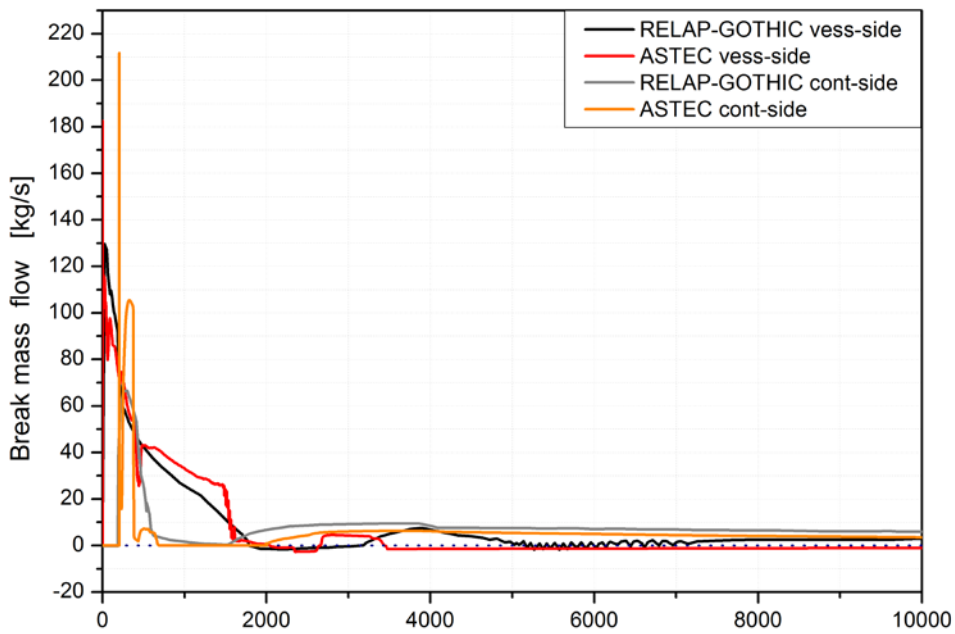
Figure 6-6: Break mass flow vessel side (0-10000 s)

Chapter 6. SMR model validation
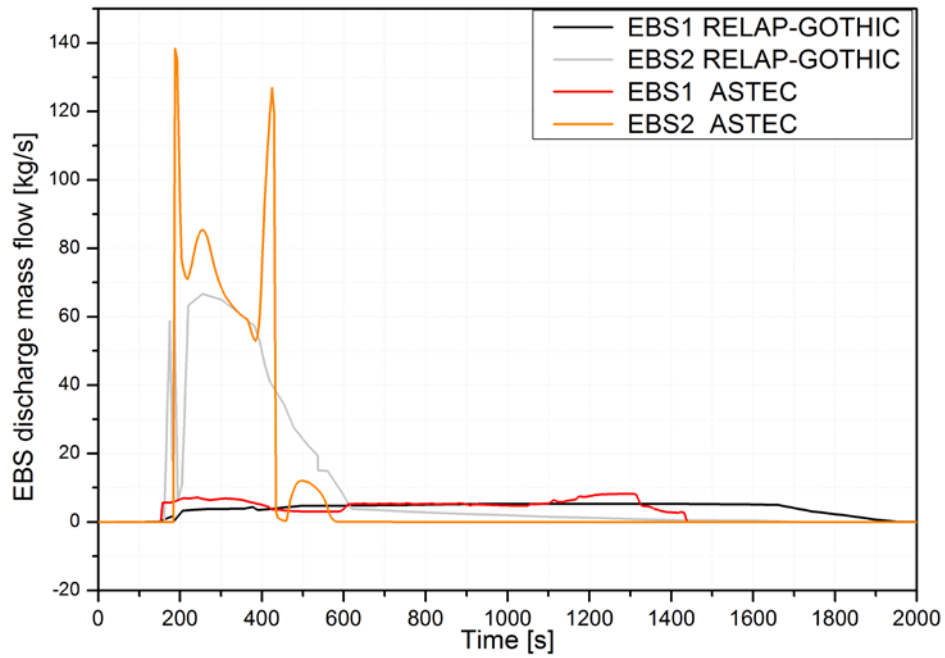
Figure 6-7: EBS discharge mass flow
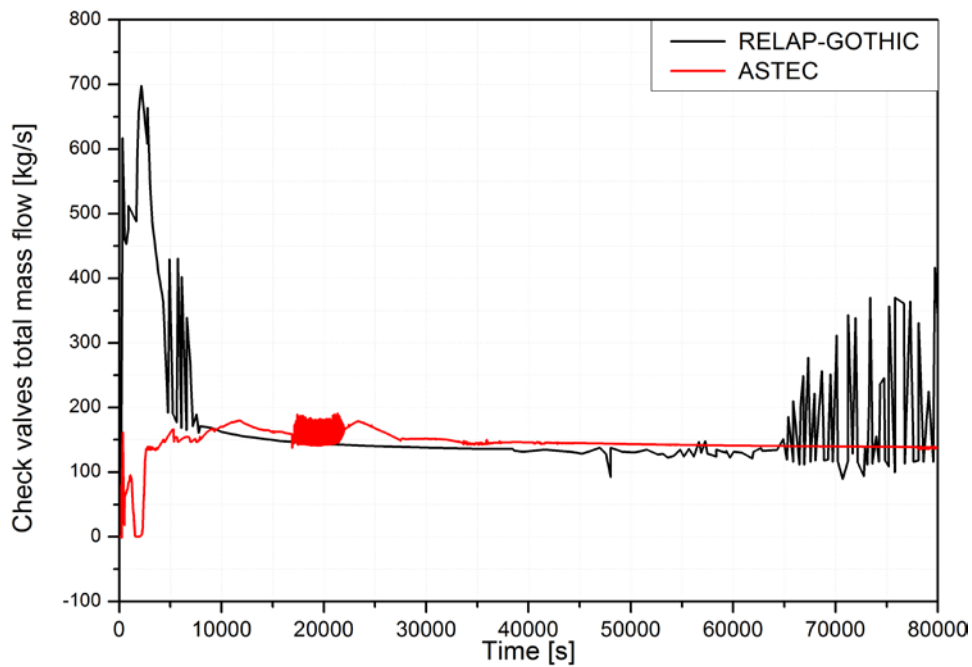
Figure 6-8: Check valves total mass flow

Chapter 6. SMR model validation
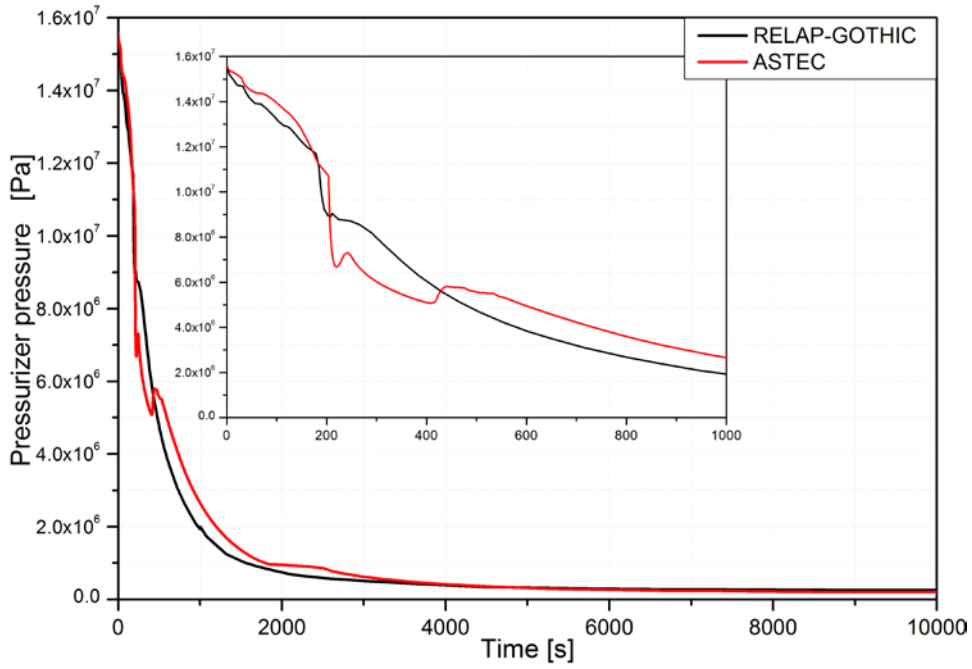
Figure 6-9: Pressurizer pressure
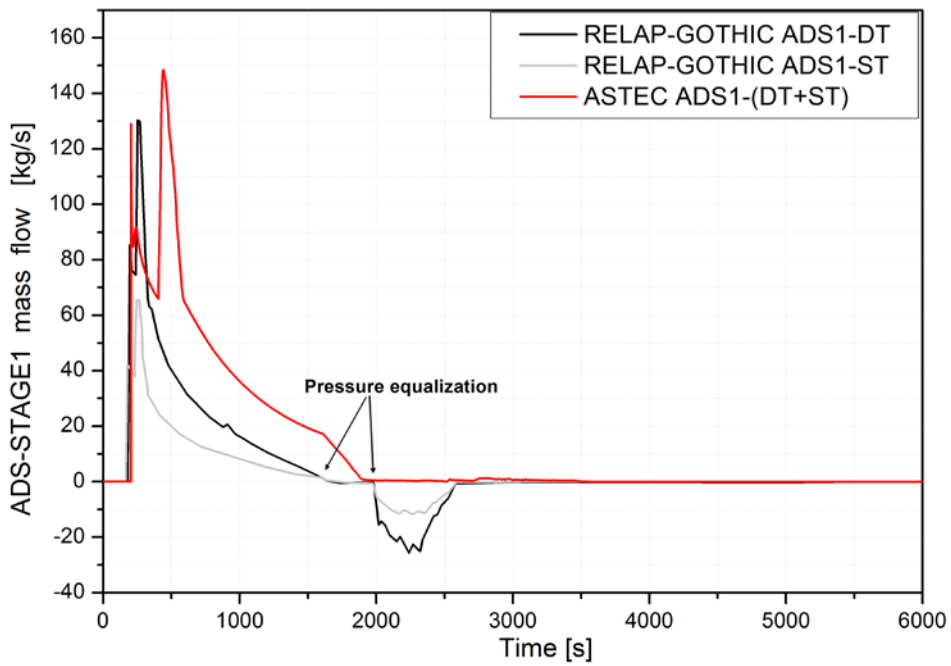
Figure 6-10: ADS-STAGE1 discharge mass flow
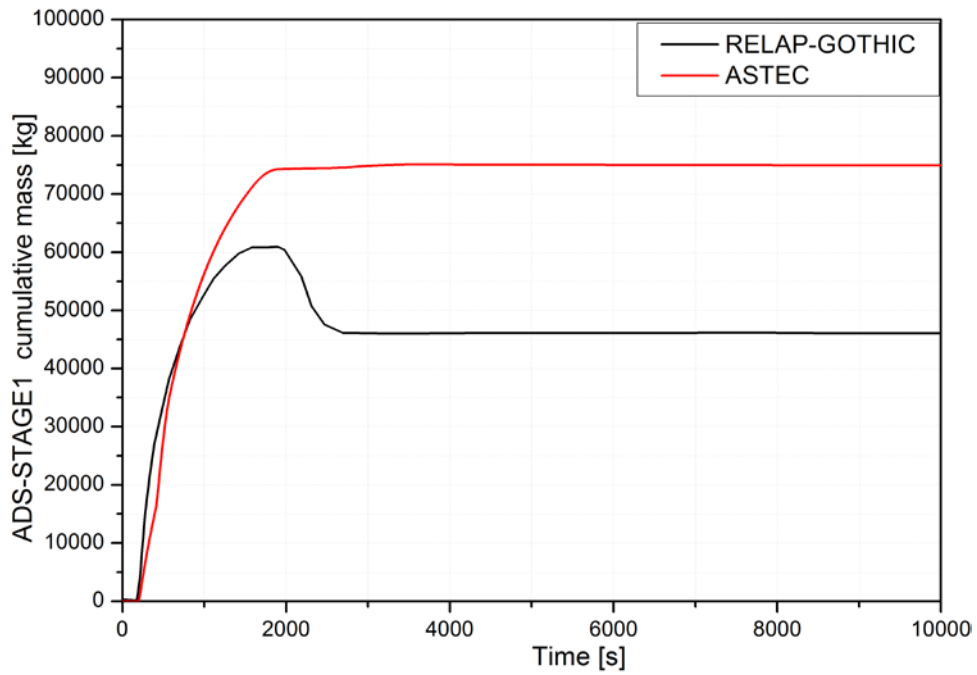
Figure 6-11: ADS-STAGE1 cumulative mass
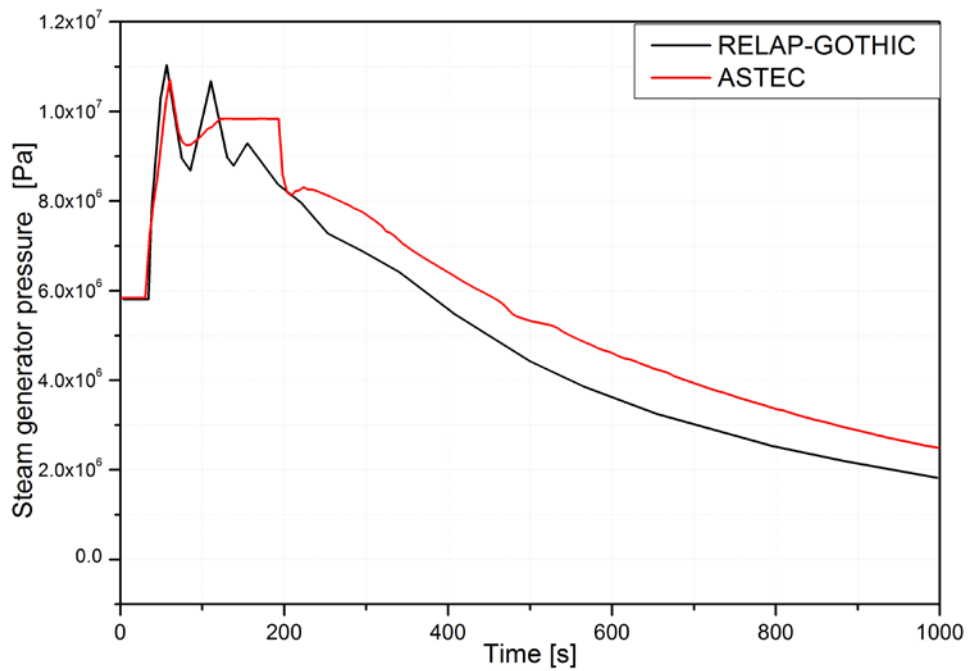
Figure 6-12: Steam generator pressure

Chapter 6. SMR model validation
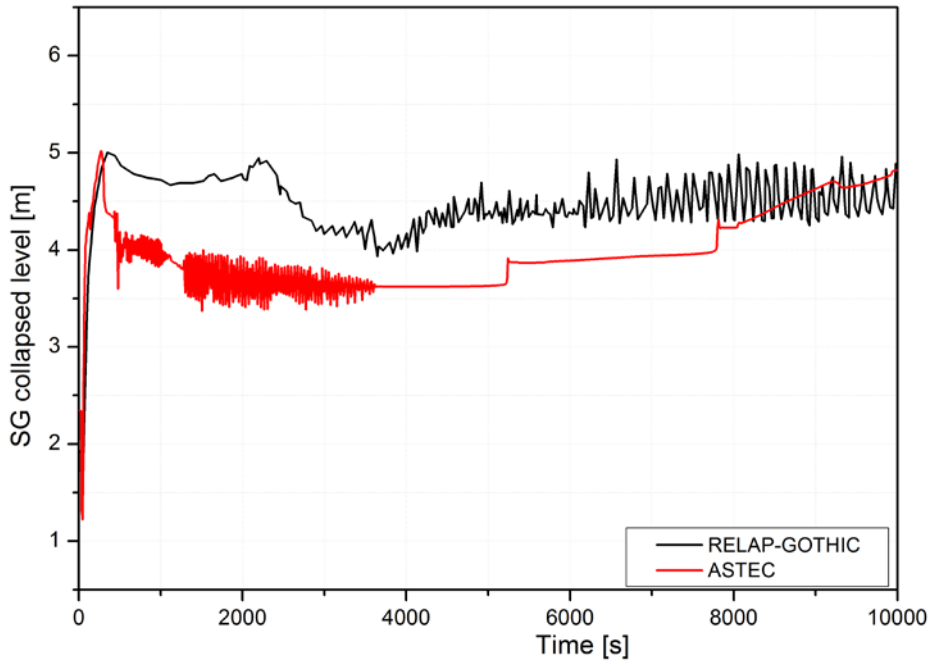
Figure 6-13: Steam generator collapsed level
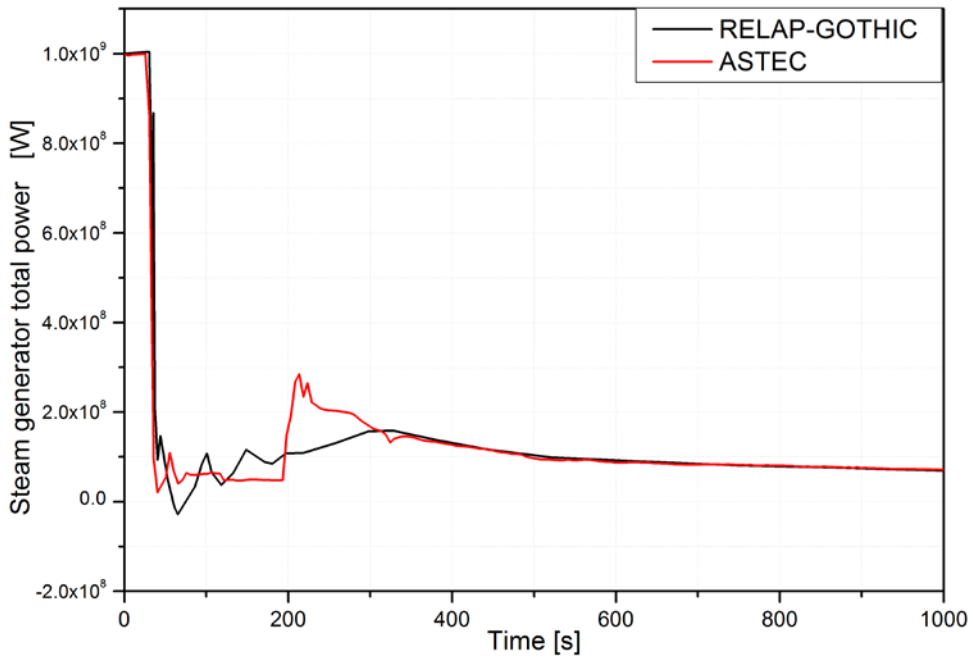
Figure 6-14: Steam generator power

Chapter 6. SMR model validation
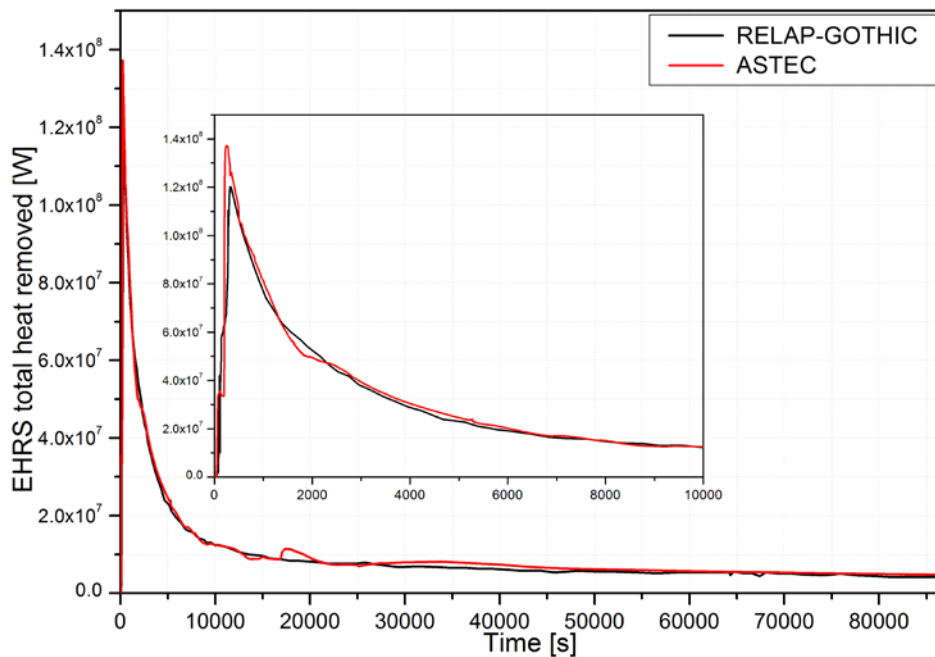
Figure 6-15: EHRS total heat removed
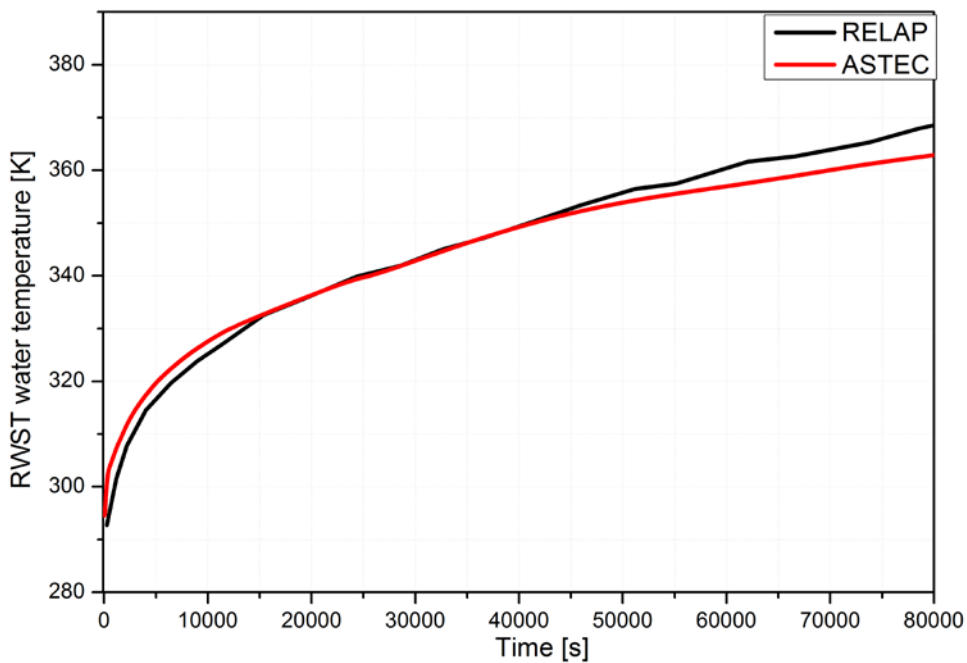
Figure 6-16: RWST water temperature

Figure 6-17: LGMS discharge mass flow
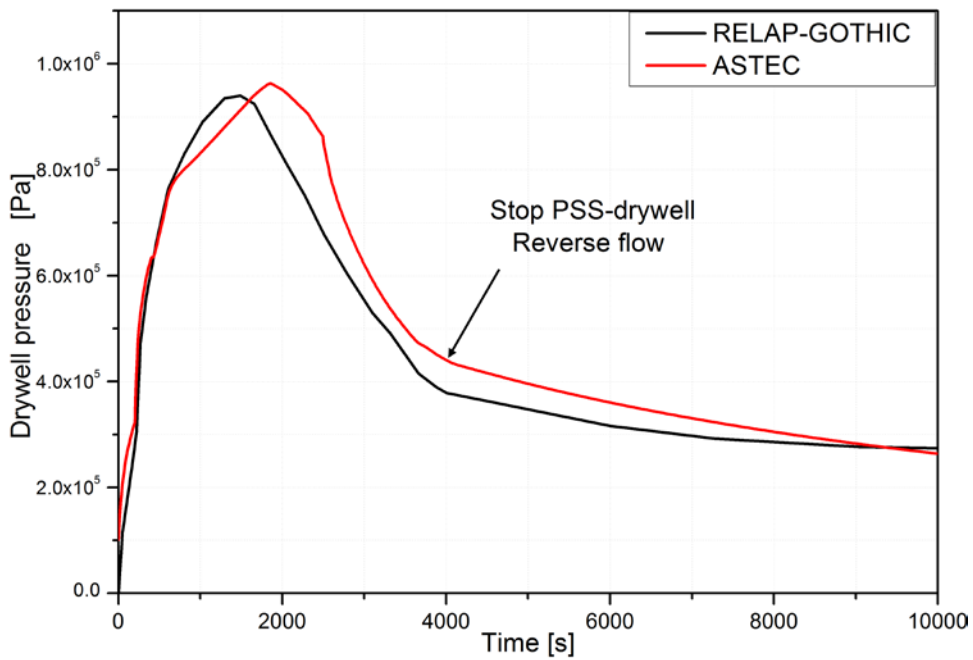
Figure 6-18: Drywell pressure
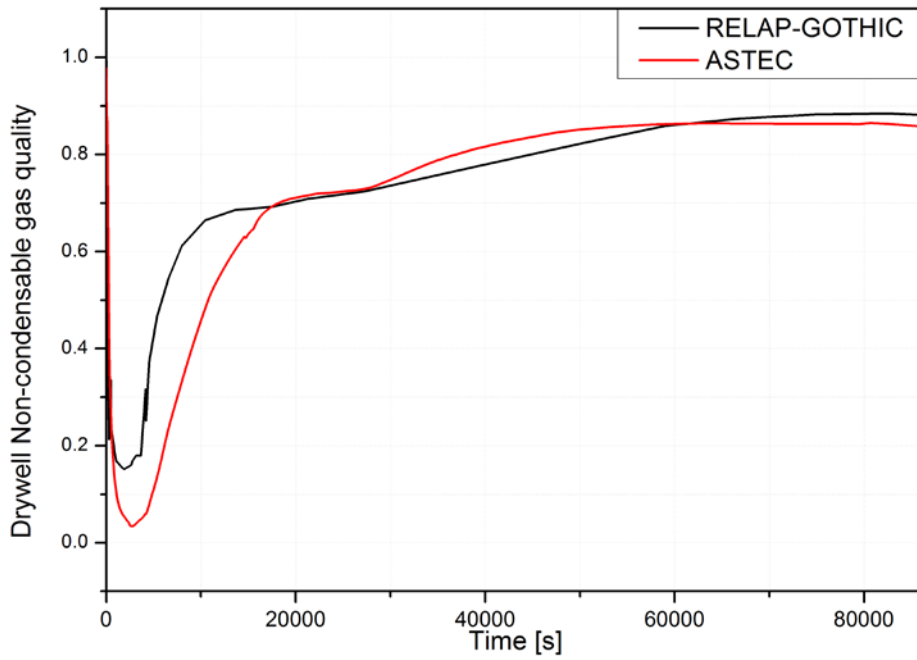
Figure 6-19: Drywell non condensable gas quality
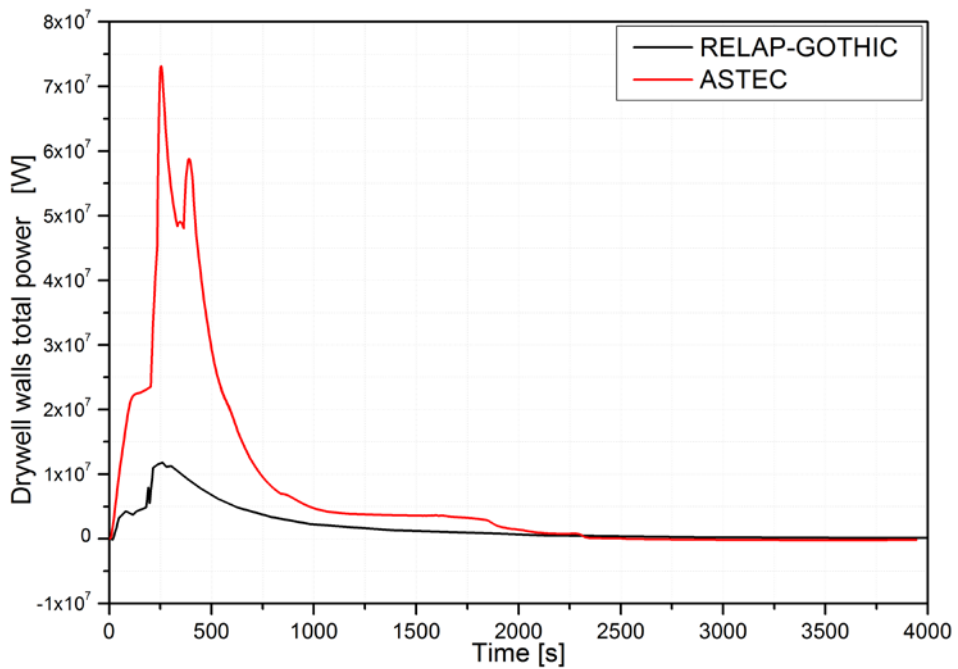
Figure 6-20: Total drywell walls power

Chapter 6. SMR model validation
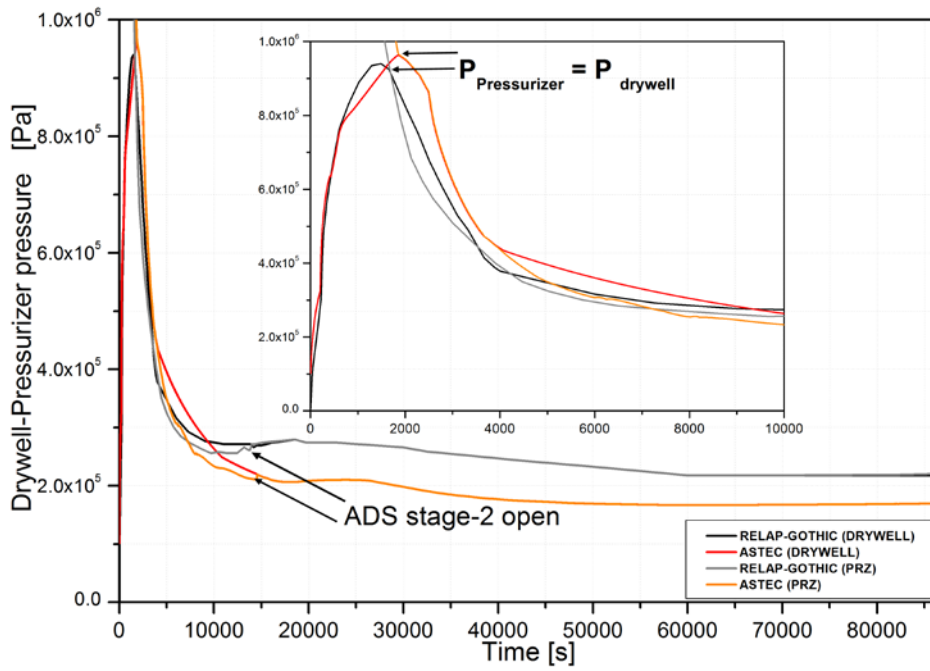
Figure 6-21: Drywell and pressurizer pressure
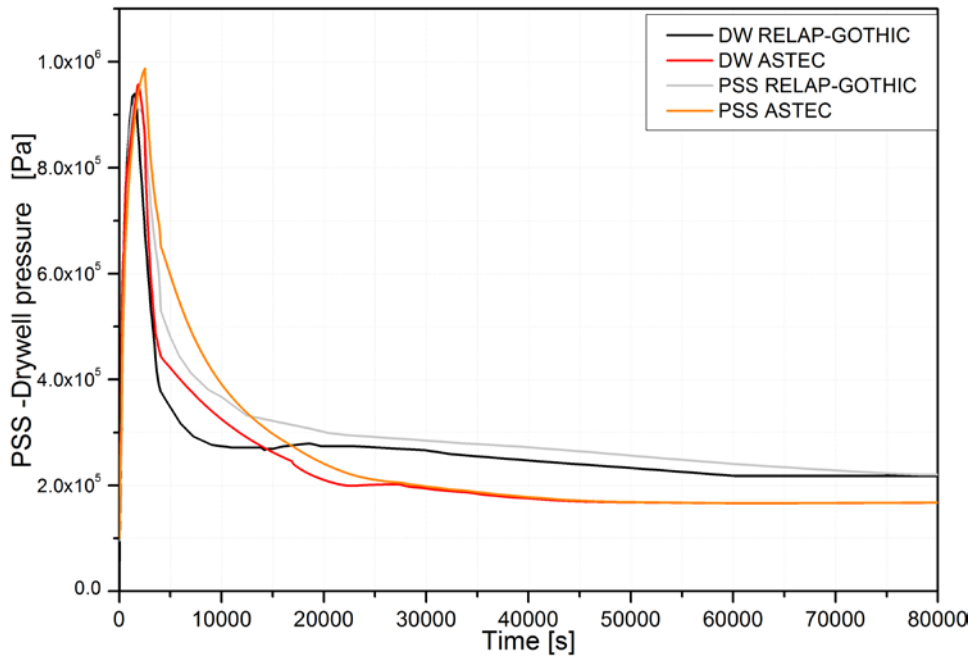
Figure 6-22: PSS-drywell pressure

Chapter 6. SMR model validation
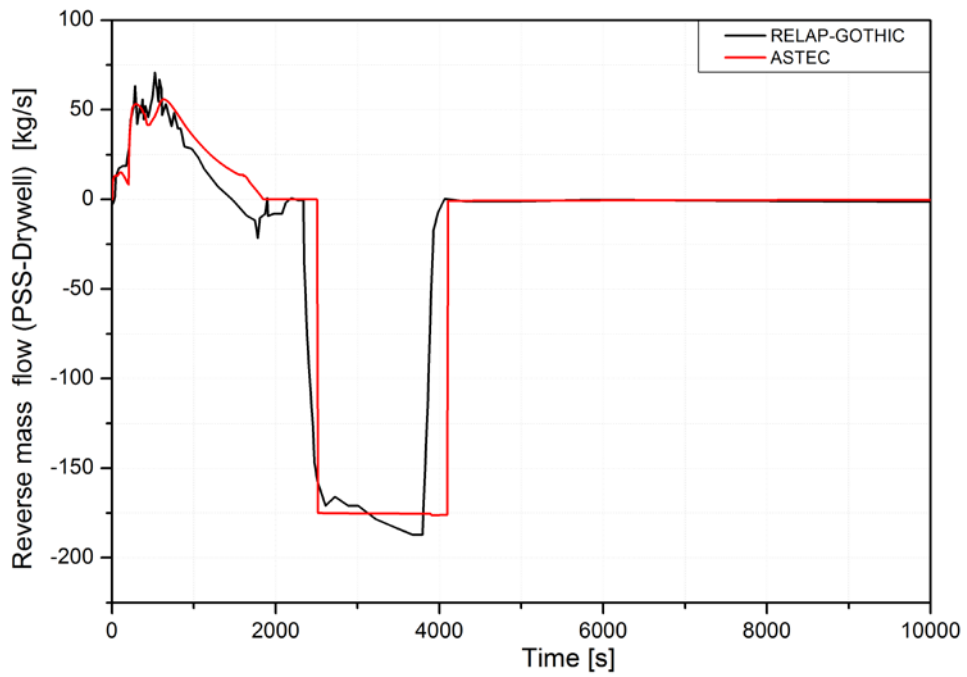
Figure 6-23 PSS-drywell reverse flow
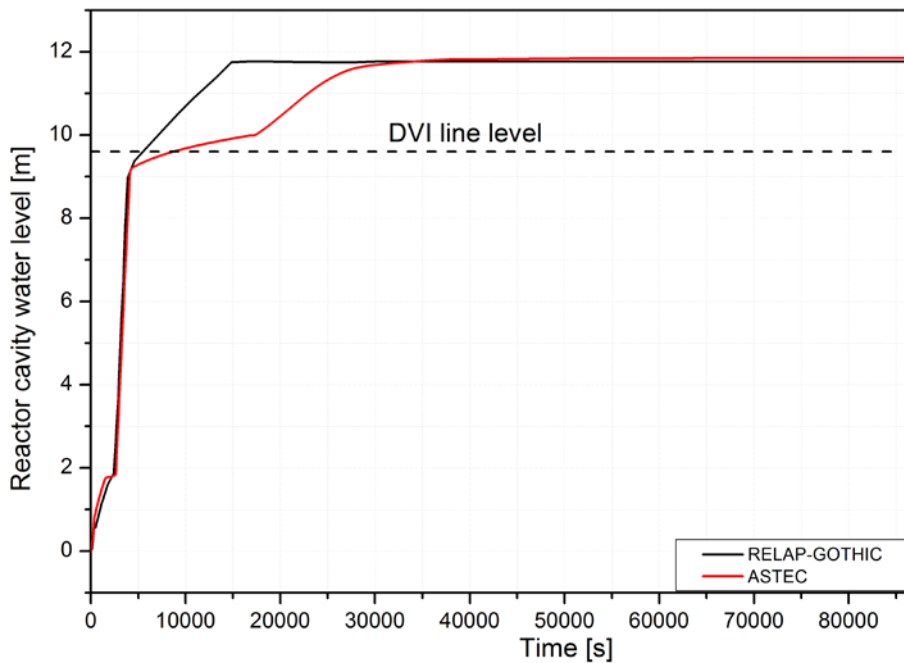
Figure 6-24: Reactor cavity water level

Chapter 6. SMR model validation
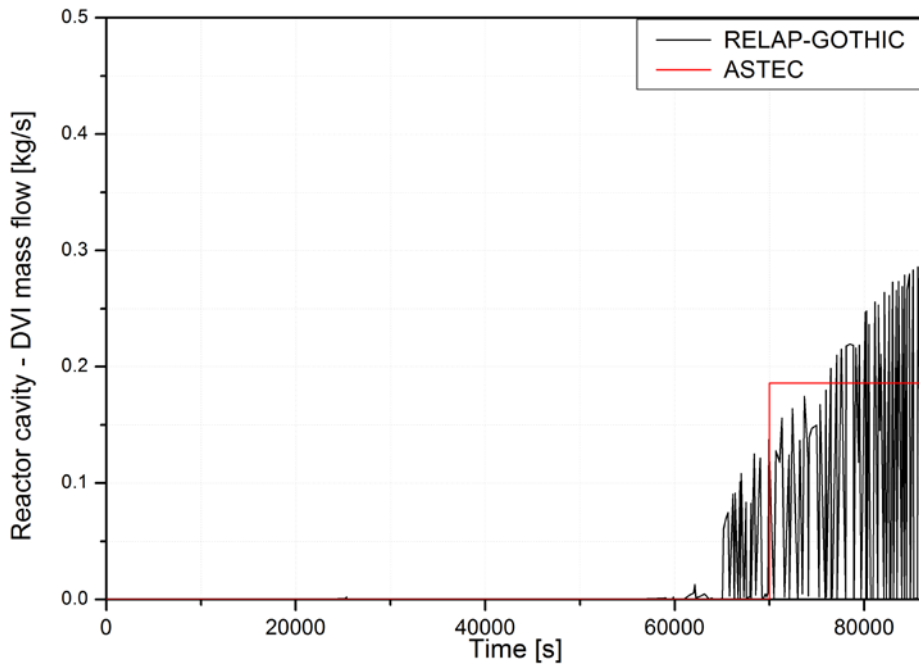
Figure 6-25: Reactor cavity-DVI line mass flow
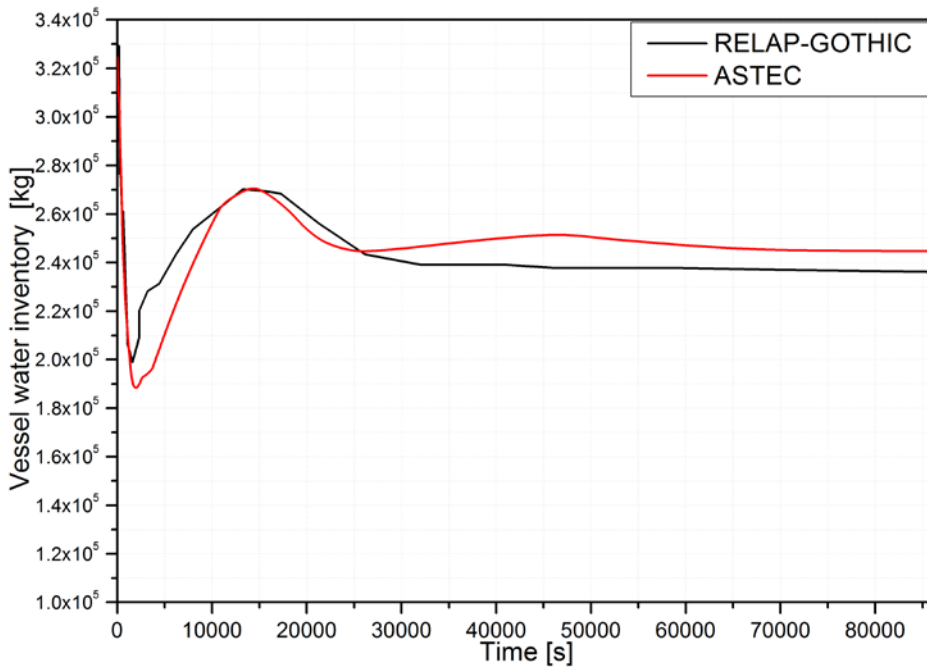
Figure 6-26: RCS water mass inventory

Chapter 6. SMR model validation
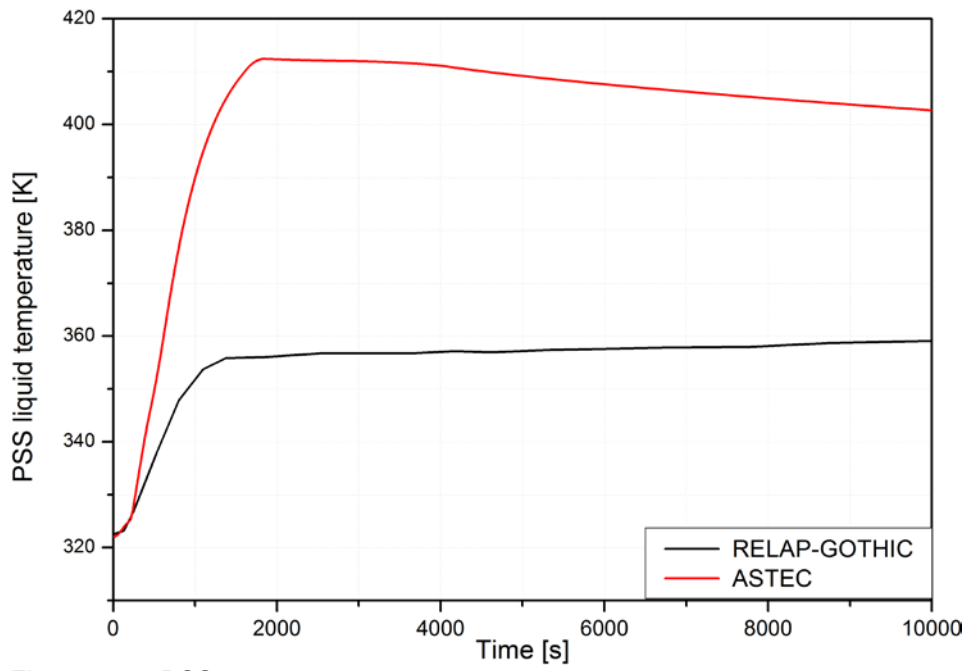
Figure 6-27: PSS water temperature

Chapter 6. SMR model validation

Refereces chapter 6

[1]   RELAP5/MOD3.2. Code Manual, Vol.1-5, NUREG-CR-5535, 1995.

[2]   T. Bajs, D. Grgić, V. Šegon, L. Oriani, L.E. Conway, "*Development of RELAP5 Nodalization For IRIS Non-LOCA Transient Analyses*", Proc. of American Nuclear Society Topical Meeting in Mathematics & Computations (M&C), Gatlinburg, TN, USA, April 6-10, 2003.

[3]   Achilli, A., Davor, G., et al., "*SPES3-IRIS facility RELAP5 sensitivity analyses on the containment system for design review*" Science and Technology of Nuclear Installations, Volume 2012, Article ID 173637, 19 pg.

[4]   GOTHIC Containment Analysis Package: Technical Manual, NAI 8907-06 Rev16, 2005.

[5]   Papini, D., Grgić, D., Cammi, A., Ricotti, M., "Analysis of different containment models for IRIS Small Break LOCA, using GOTHIC and RELAP5 codes", Proc. of NENE 2009, Bled 14-17 September 2009.

[6]   N. Tregoures, A. Moal, ASTEC V1 code : CESAR physical and numerical modelling, Report ASTEC-V2 IRSN/SEMAC-2006-188.

[7]   R. Ferri, "SPES3-IRIS facility RELAP5 sensitivity analyses on the containment system for design review", SIET 01 526 RT 09 Rev.0, August 31st, 2010

[8]   M. Di Giuli, M. Sumini, G. Bandini, "*Pressurized Water Small Modular Reactor (SMR), Design Basis Accident Analysis using the ASTEC code*", Proc. of NENE 2014, Portoroz 8-11 September 2014. *(Best Poster Award)*

CHAPTER 7

ASTEC SEVERE ACCIDENT SIMULATION

7.1 Introduction

A severe accident analysis, as compared to a DBA analysis, requires a fundamental understanding of severe accident phenomena. The user has to select additional modelling parameters because of the large number of physical models required to represent severe accident behaviour. This is particularly true for the use of the integral codes, which rely extensively on user, defined modelling parameters to control the calculations. The input data have to be extended by the severe accident models. The thermal-hydraulic input model can be adapted to the needs of specific severe accident analysis, that is, time-consuming nodalizations can be simplified and the modelling of certain thermal-hydraulic phenomena can be suppressed if they are not necessary for the analysis. The availability of some safety systems may be neglected given that, it is necessary to assume the failure of one or several safety systems for the reactor analysed, in order that a DBA develops to a severe accident, modelling of the failed systems may be unnecessary. The choice of a bounding scenario of a severe accident is plant specific and, therefore, a unique bounding scenario for a particular plant design does not exist. It depends on the purpose of the analysis. The idea is to obtain the most severe response of the system related to a specific criterion. In the case of IRIS reactor, there is not a specific criterion. The aim of this work is to carry out an exploratory study on the behaviour of a SMR plant during a severe accident.

Chapter 7. ASTEC severe accident analysis

7.2   Severe accident scenario

Once, verified the capability of the ASTEC code on reproducing the thermal-hydraulic phenomena occurring during a DBA transient, a severe accident scenario was supposed. As well known, the IRIS integral configuration eliminates the large primary penetration or large loop-piping makes impossible the possibility that, a large break LOCA occurs. In order to have a SA event, it was assumed a multiple failures of the safety systems leading to significant core degradation. The scenario selected, starting with the break of both, the DVI lines thus, the loss of the capability to provide water to the vessel by means of the LGMS and the EBS. All the EHRS unavailable and the PCC as the only device suitable to remove the decay heat. The ADS stage-1 trigger with a 1000 s delay on LM signal. The PCC in the ASTEC model consists of the possibility to flood the containment external surface with water at the temperature of 298 K, to limit the peak pressure into the system; in order to avoid the venting to the outside environment. Given the characteristics of the chosen scenario, the EHRS, the EBS and the RWSTs, have been removed by the ASTEC model. This simplification permits to decrease the calculation time, and carry out this SA analysis without neglecting the main thermal hydraulic phenomena. Moreover, further walls structures were added to the CPA model as the cavity bottom wall and the LGMS walls. These further structures were taken into account because in these SA analysis was activated the SOPHAEROS module. This module predicts the behaviour of the FPs inside the primary and secondary circuit; its output becomes the input of the CPA AFP module, to compute the FP behaviour inside the containment as the deposition and suspension. It was notice in some SA simulation that, the lack of these added heat structures affects the quality of the CPA AFP results. One simulation was run also using the ISODOP module. The ISODOP module can calculate the FP and actinide isotopes masses and activity in core, primary circuit, containment, and environment taking into account the FPs transmutation and energy released.

7.2.1   Severe accident analysis

The simulated SA event foresees the failure of the EHRS train-1 actuation on SCRAM signal and the failure of EHRS-train-2 on LM signal. The ADS stage-1 triggers with a 1000 s delay on the LM signal. The transient starts from the break occurrence and runs for 200000s (2.3 days), when the trend of the main parameters settles on quasi-stationary values. All times of the events are given with respect to the break time assumed as time 0 s. The main events are reported in Table 7-1.

Chapter 7. ASTEC severe accident analysis

Table 7-1: Main events chronologies

MAIN EVENT	ASTEC
	TIME(s)
Double guillotine Break open on DVI-1 and DVI-2 lines	0.0
Scram Signal : High Containment pressure (HCP)	7.8
Reactor SCRAM	8.0
CVCS Isolation	13.0
Turbine isolation	13.0
Feedwater pumps stop	24.3
Low Pressurizer level signal LPL signal(LPL)	20.6
EHRS-train1 fails on SCRAM signal	29.0
Shroud valves open (HCP + LPL)	30.8
RCPs stop	45.6
Low Pressurizer pressurel signal LPP signal (LPP)	45.8
EBT line opening On LM signal (HCP + LPP)	60.8
ADS stage-1 fails On LM signal (HCP + LPP)	73.8
EHRS-train2 fails On LM signal (HCP + LPP)	75.8
ADS stage-1 opening	1100.0
High High containment pressure signal (HHCP)	1150.0
PCCS system starts	1160.0
Water flow (from SP to DW)	1884.1
Low differential pressure vessel containment LDPC signal	2559.0
LGMS starts to inject On LDPC signal	2559.0
Zr oxidation begins	2565.0
Cavity completely flooded (IVR strategy starts)	2941.0
ADS stage-2 opening	4171.0
Pressure equalization DW-Vessel	4220.0
Melting pool formation in the core	4901.0
First material slump into lower plenum	31211.0
First slump of corium with FPs in lower plenum	57531.1
First total core uncovery	100791.0
Massive corium relocation into the lower plenum	101566.2
Transient over	2000000.0

Chapter 7. ASTEC severe accident analysis

The reactor vessel

The double breaks opening at 0 s, causes the vessel depressurization and containment pressurization. The containment pressure reaches the 1.7E5 Pa around 7.8 s and a SCRAM signal is generated. The SCRAM triggers the closure of the main steam valve and the CVCS valves; at 13 s, the vessel is isolated. The EHRS train-1 actuation fails 20 s after the SCRAM signal. The low pressurizer water level signal triggers the primary pumps coastdown and the natural circulation inside the reactor is ensured until the vessel water level is above the check valves connecting riser and downcomer. The pressurizer pressure is illustrated in Figure 7-1. After an abrupt depressurization until 1.0E7 Pa, the vessel pressure stabilizes around this value until 1100 s. This is due to the location and dimension of the breaks and to the characteristics of the SGs. The breaks location is under the water level, and as it is possible to see in Figure 7-2; the ASTEC code predicts that, only water is discharged from the breaks during the first 1000s of the transient. Moreover, the helical coil once through steam generators (OTSGs) do not have a sufficient thermal inertial, which is able to settle the pressure of the primary circuit at the same pressure of the secondary circuit. The IRIS OTSGs water inventory is around 1000 kg, during normal operation. In Figure 7-3 is illustrated the calculated trend of the SGs pressure. The IRIS secondary circuit is designed to withstand the same pressure of the vessel; indeed, after the LOCA the SGs pressure reaches peaks of 1.2E7 Pa, following assumes the same value of the reactor vessel. The ADS stage-I, the system for the fast depressurization of the vessel, failed following the LM signal, starts to work at 1100 s. The ADS stage-1 intervention causes an abruptly reactor vessel pressure decreases, passing from 1.0E7 Pa to 2.0E6 Pa, in 2000 s, whilst the SGs pressure remains constant around 8.0e6 Pa. An interesting result predicted by ASTEC is the reverse flow at the DVI line breaks after 100000s until the end of the transient.

The drywell and the PSS

The drywell pressure (Figure 7-4) increases following the breaks occurrence, when the ADS stage-1 opens the code computes a sudden increase at 1100 s, reaching a peak of 1.26E6 Pa (1884 s) very closed to the containment design pressure fixed to 1.3E6 Pa. The intervention of the PCCS at 1151 s on HHCP signal, along with the water reverse flow from the PSS at 1836 s, due to the differential pressure generated between the two containment zones (Figure 7-5 and Figure 7-6), can reduce quite quickly the drywell pressure. The LDP signal at 2559 s triggers the injection of the LGMS, which provides an additional support to the drywell depressurization, discharging water on the break DVI lines, and flooding the reactor cavity. After that, the drywell pressure tends to settle around 5.0E5

Chapter 7. ASTEC severe accident analysis

Pa. The ASTEC calculated results predict the same value of pressure for the coupled system vessel/drywellt and the same trends throughout the entire transient after the equalization pressure that occurs around 4000 s. The modelling of the PCC system as stated before, consist of the injection of water on the external surface of the DW, the aim of this system is to increase the heat removed by steam condensation on the drywell walls (Figure 7-7). On the long term, the power removed by the drywell walls surfaces thanks to the PCCS is around 3 MW. Once the cavity is completely flooded, in order to simulate the IVR strategies, two structure 'CONNECTI' were activated, which impose new boundary conditions on the lower plenum and on the vessel external surface. These boundary conditions consist of the HTC 10 kW/m^2 K^{-1}, and the actual external temperature 423 K, which corresponds to the reactor cavity water temperature. The external HTC values are set to values known from the literature [1] [2] [3] [4].

Core degradation

The core starts to uncover at 1846 s (Figure 7-8 and Figure 7-9) as a consequence of the breaks, while core heatup starts at 2000 s at the core top, because the core decay power is no more removed. Core level is predicted to reach the bottom of the active fuel after 34000 s since the beginning of the transient and then it shows a lengthy decrease to the lower support plate level, at 100000 s. Because of the slow emptying phase, the core degradation progression is delayed. The Figure 7-10, 7-11, 7-12 and 7-13, illustrate the core degradation chronologies. The ASTEC code predicts the first cladding perforation by grid at 4590 s, and the first melting pool formation in the core at 4900s. The first structural material relocation into the lower head occurs at 31211 s. As it is possible to see in the figures, the core degradation occurs with the lower head full of water, and the reactor cavity zone totally flooded. The corium starts gradually forming above the water level. The ASTEC predicts a continuous melt pool formation (black volumes), which tend to solidify, little by little descending towards the colder zone, close to the water level. This process goes on until 100000 s, when above the water level is formed a corium material mass of 63 t , then the code computes a massive corium material slump into the lower head of 54 t in mass. This material relocation generates an extreme and sudden water vaporization; the produced steam increases the vessel pressure up to 1.8E6 Pa and the containment pressure up to 11E5 Pa (Figure 7-14). The corium material massive relocation seems to be due to a creep failure of the metal structures below the degraded material caused by high mechanical load of the huge mass along with the high temperatures. After that, the ASTEC code calculates only a little corium mass relocation into the lower head, which falls down around 120000 s (Figure 7-15). The very slow core degradation depends on the boundary condition imposed

to the vessel and lower head external surfaces when the cavity is completely flooded. Changing or delaying the actuation of the boundary conditions; the core degradation time decreases. In other simulations varying these two parameters, was observed an earlier and lesser corium material relocation. It was chosen to analyze this sequence because was the transient generating the worst possible accident conditions.

The Oxidation phase

The main oxidation phase takes place (Figure 7-16) between 3200 s and 7600 s since the beginning of the transient. During this phase almost 360 kg of hydrogen are generate, with a maximum rate of about 0.18 kg/s around 5000 s. The cumulative hydrogen mass predicted is 616 kg; this high value is due to the large quantity of water in the lower head and consequently high steam availability in the core during the entire transient. Furthermore, the slow degradation process favours the hydrogen production, because the original core geometry remain intact for a long time. During the main oxidation phase, the power released by means the chemical reactions is about 25 MW versus only 12.5 MW due to the decay heat. The calculated results predict that almost 90 % of the total mass of zirconium reacts with the steam to form ZrO_2 and in minor part in ZrO (Figure 7-18). The hydrogen released from the cladding affects the containment pressure, in Figure 7-19 is shown the partial pressures inside the drywell. As it is possible to see, the H_2 partial pressure is around 3E5 Pa on a total pressure of about 5E5 Pa, this means a H_2 concentration of about 10-11%, due to the small volume of the drywell (3227 m^3). Nevertheless, the drywell nitrogen atmosphere can limit the risk of a hydrogen explosion.

IVR analysis

The combination of low decay power of IRIS reactor in comparison with a standard 1000 MW_e PWR, the large lower plenum that allows reducing the heat flux on the surfaces and the huge thermal inertia of the water sink (500 m^3) make the IRIS IVR management strategies very effectiveness. The IVR modelization depending on the HTC value selected; using a HTC equal to 8000 W/m^2 K rather then 10000 W/m^2 K, the massive core relocation occurs at 83000 s instead of 100000 s (Figure 7-20). The peak pressure calculated is lower, because is minor the corium material mass relocated (33 t and 54 t), and even the final mass collapsed inside lower head is lesser in the IVR 8000 case than in the studied case (Figure 7-21). However, the other parameters show the same trend even if slightly shifted. During the analyzed transient, the lower plenum external surface remains always around the boiling temperature of the water and the peak flux computed is around 80 kW/m^2 (Figure 7-22). It is interesting to note that until the last massive core relocation around

100000 s the code computes negligible values of the heat flux on the lower plenum surface. Notably that, not all the decay heat inside the lower head is removed by means of the IVR strategies; part of the decay heat is exchanged by means of the corium material upper surface, as radiative heat (Figure 7-23). Taking into account that, the critical heat flux (CHF) computed by the empirical formula developed for the AP1000 and AP600 reactor [5], provide values, according to the type and configuration of the lower head surface and reactor cavity includes between 0.8 and 1.2 MW/m^2. It is possible to say that, in this scenario the risk of the lower head failure is very unlikely. This statement is further confirmed by the lower head maximum temperature calculated during the transient, which is 400 K below the steel melting temperature. Indeed the ASTEC code does not predict ablation phenomena on the lower head internal surfaces during the entire transient. If the IVR is not taken into account, the ASTEC code predicts the lower head failure after 83590 s, at the elevation of -1.39 m, in the bottom part of the structure. The Figure 7-23 and Figure 7-24 illustrate the temperature distribution in corium pool inside the lower head at different instants.

Fission product release and transport

The calculated fission product release from the fuel has a strong impact on the transport through the circuit and the source to the containment. In the IRIS reactor SA analysis, given the breaks location on the DVI lines all the fission products are released through the ADS-stage-1 and ADS-stage-2. The ASTEC core initial inventory is illustrated in Table 7-2. Because the period between the onset of core degradation and the collapsed of corium material inside the lower head, is longer, there is ample opportunity for volatile radionuclides to escape the fuel. Indeed, the degrading core materials become hot enough to sustain the continued release of volatile radionuclides, starting around 2700s until 37000 s. The analysis here considers the release from volatile, semi-volatile, and low volatile species (Figure 7-27 and Figure 7-28). The ASTEC code computes the same trend for all volatile fission products and noble gas, with a final cumulative release of about 90 % of the initial inventory. Concerning the semi-volatile as Mo only the 20% of the initial inventory is released as the low volatile Ru. It is possible to note a little anomaly concerning Ba; the code predicts a release of the 90% (very high if compared with the Phébus tests results), with a trend similar to that of the high volatile fission products but shifted of 2000 s. Regarding La, the release computed is around 8 %. In Figure 7-29 to Figure 7-34 are illustrated the total mass of I, Cs, Te, Ru, Ba, Mo released from the reactor core to the vessel, compared with the release from the vessel to the containment, furthermore, for these latter the dot curves also show the radionuclide forms (aerosol, gas/vapor). To underline that the absence of the control rods material in the model affects the form of the FP releases.

Chapter 7. ASTEC severe accident analysis

Indeed, the predicted Cs and I gas/vapour release fraction seems to be very high. The differences between the straight curves represent the FP depositions inside the vessel. Almost the 90% of Iodine, Barium released from the fuel reaches the containment. Caesium, Ruthenium and Tellurium show a different behavior; the deposition inside the vessel is higher, notably for Te;. ASTEC computes that, more of the 75 % of the Te released from the core is deposited on the vessel internal surfaces.

FPs behaviour inside the Containment

In Figure 7-35 and Figure 7-36 are illustrated the behavior of the aerosol released from the vessel to the containment. The CPA AFP module carries out this computation. The CPA AFP module considers all the FPs entering the containment in aerosol form. The aerosol deposition is mainly concentrated in the lower part of the drywell (zones D3 and D4) and especially inside the cavity (zone CAV). The water inside the cavity and on the drywell floor supports the deposition of the aerosol. Concerning the suspended aerosol behavior, the results are more complex to understand. During the oxidation phase the aerosol concentration changes continuously due to the small dimension of the containment, the strong natural circulation and the elevated concentration of aerosol. As it was possible to see, every change occurring inside the vessel reflects immediately on the containment. Therefore, the aerosol depletion rate is slower in comparison with that predicted for a standard PWR containment. From the safety point of view, the aerosol deposition on internal surface can reduce the release of radioactivity, while the high-suspended aerosol mass predicted inside the IRIS containment could make easy a possible radioactive release (for example following a containment venting). In the Figure 7-37 is illustrated the radioactivity distribution inside the plant. The ISODOP module performs this computation. The initial core radioactivity inventory computed is 3.79E20 Bq, in agreement with reference [7] (6.3E6 GBq/kg HM;), while at the end of the transient the predicted radioactivity inside the vessel and the containment are respectively 4.88E19 and 1.25E19 Bq.

Chapter 7. ASTEC severe accident analysis

Table 7-2: ASTEC total initial FP and uranium inventory

ASTEC IRIS total initial FP inventory Burnup = 32000 MWd/tU					
	kg		**kg**		
Ac	0.000	Am	5.699	Se	43.5208
Ba	67.111	Cd	3.662	Tb	0.000
Cm	2.150	Cu	0.000	Tl	244.503
Er	0.007	Ga	0.00	Y	169.165
Ge	0.0246	I	10.1542	Ag	0.000
Kr	17.28	Mo	152.234	Br	67.111
Nd	171.922	Pa	0.00	Cs	2.150
Pm	9.132	Pu	439.255	U	46414.28
Rb	13.6210	Rh	19.274	Zn	0.000
Sb	1.172	Sm	29.7910	As	0.005
Sr	43.520	Tc	37.1862	Ce	130.018
Th	0.0	Tm	0.003	Np	9.132
Xe	244.503	Yb	0.000	Pr	13.621
Zr	169.165	As	0.0055	Re	1.1724
Ac	0.000	Ce	130.018	Ru	111.847
Ag	67.111	Dy	0.1178	Sn	3.144
Br	2.152	Gd	4.0879	Te	22.345
Cs	0.007	In	0.0837	La	171.920
Eu	0.024	Nb	2.096	Ra	0.000
Ho	17.280	Pd	52.525		

7.3 Discussion

One of the worst and more unlikely accident scenario was selected to analyse the IRIS reactor behaviour, in this extreme condition [8]. The ASTEC calculated results confirmed the effectiveness of the IRIS safety design solution adopted. The integral layout, the lack of large primary penetration along with the huge vessel water inventory, can face even this type of scenario, ensuring no radioactive release outside the plant to the environment. The pool suppression without vacuum breakers guarantees the flooding of the cavity in every situation. Moreover, the IVR management strategies in this kind of reactor is able to cool the lower head for long time, given the combination of a great heat transfer surface and a low decay heat. The low decay heat does not depend only on the lesser power than a standard PWR, but also to the reactor vessel water inventory. The integral vessel ensures a long emptying time and in this period the decay heat further decreases. The heat flux on the lower head are ten times less than the critical heat flux calculated for the commercial reactors. The major risk is connected to the corium relocation inside the lower head and the consequently steam explosion. In spite of the small containment can resist to very high pressure, during the corium material relocation, the ASTEC code predicted the generation of a peak pressure following the intense lower head water vaporization which could reach the containment design pressure. This is a complicated situation to manage, because the pressure wave generated could damage seriously the integrity of the containment. Even a containment venting could not be sufficient to engage this event. The predicted duration of the FP release phase of the transient is long because of the slow core degradation (around 35000 s) this allows for more an extensive release of volatile radionuclides. Release fractions after 100000s are very low, because the ASTEC code does not take into account the possible revaporization of radionuclides that were released from fuel during the release phase, but deposited in the vessel surfaces and did not reach containment. Concerning the Hydrogen production, it is commonly agreed that the hydrogen average source rate, typically about 0.2 kg/s for a 1000 MWe PWR, and that this value is sufficiently accurate as long as the core geometry remains intact [6]. The Zr oxidation Urbanic-Heidrick correlation was used in this simulation because it gives better results when compared to integral tests such as Phébus; indeed the ASTEC code predicts a H_2 maximum rate equal to 0.18 kg/s. The cumulative hydrogen produced and released to the containment is 616 kg. This is an issue pointed out by the SA analysis because; it is very unlikely, that the containment can ensure, that no hydrogen release, from the containment to the nuclear building occurs, for

an extended period of time. The risk associated to a H_2 release to the nuclear building is an explosion. The blast could cause extensive damage to the containment. Another important aspect to underline is the predicted behaviour of the aerosol inside the containment. Because, the principal mechanism by which source terms of gaseous and particulate radionuclides to the containment can emerge into the environment is by leakage of the containment atmosphere. The concentrations of radionuclides in the leaking atmosphere of containment depend on both the rates at which radionuclides reach the containment and the rates at which they are removed from the atmosphere.

The simulation results predict an elevated aerosol concentration in the containment atmosphere for long periods; this is probably due to the intense natural circulation inside the containment, given to the limited free volume of this latter. The vessel retention factor calculated the ratio of activity released to the vessel to the activity released to the containment is 3.9. Anyway, in order to improve the reliability of these results, a sensitivity or uncertainty analysis on key parameters (those that are influenced by sensitivities or uncertainties in the plant data, the plant model and the physical models) is compulsory, to show that there is no large increase in risk if one of these parameters is changed within its uncertainty band. Concerning the computational tool, the ASTEC code has shown a good flexibility and capability to simulate almost all the phenomena occurs during the transient. The computational time for this SA scenario was around 12 hours, using a standard notebook.

Chapter 7. ASTEC severe accident analysis
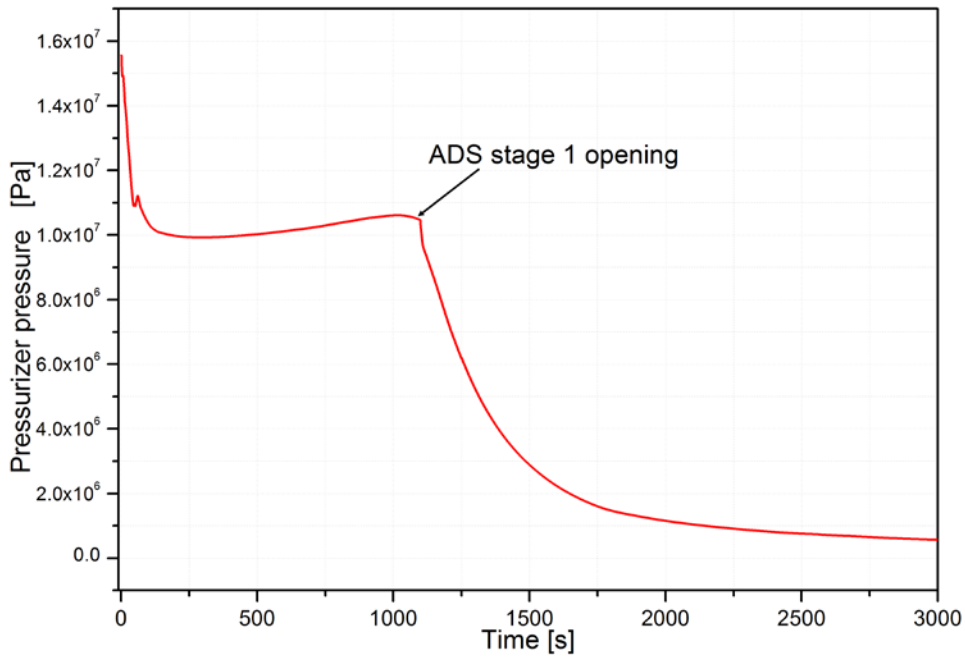
Figure 7-1: Pressurizer pressure
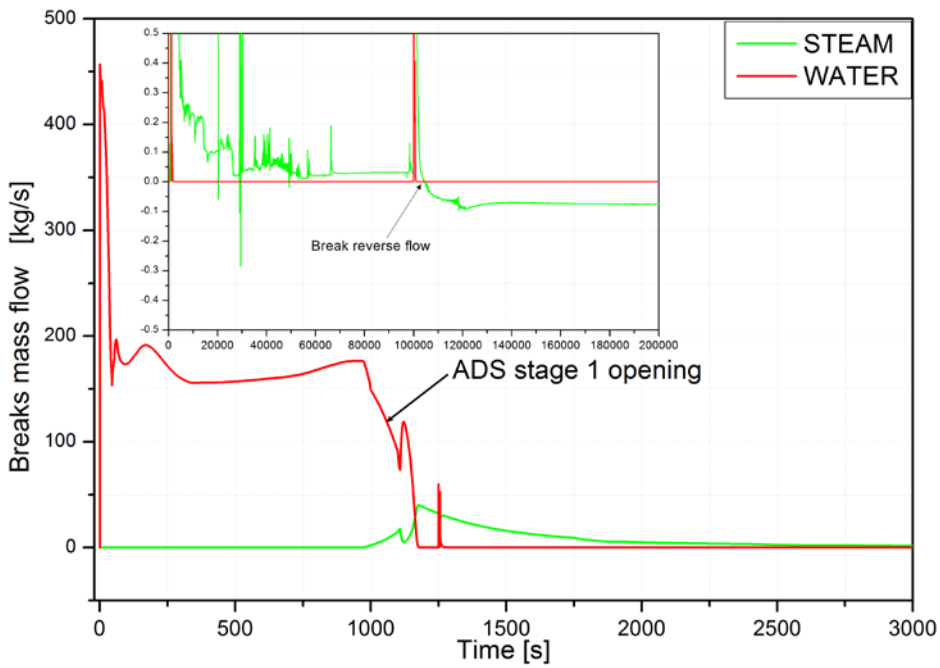
Figure 7-2: Breaks mass flow

Chapter 7. ASTEC severe accident analysis

Figure 7-3: SGs pressure

Figure 7-4: Drywell pressure
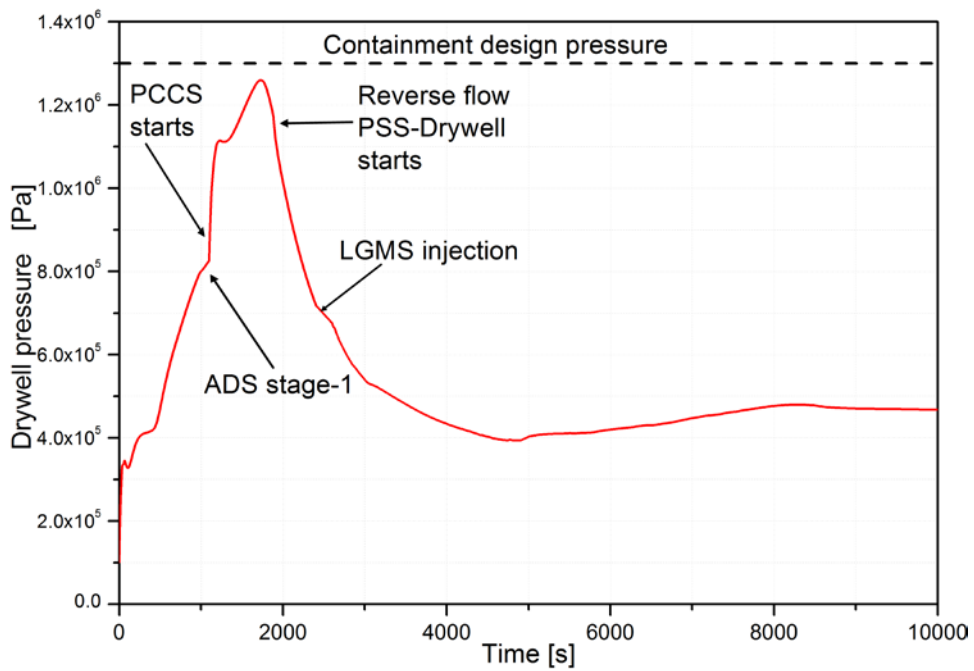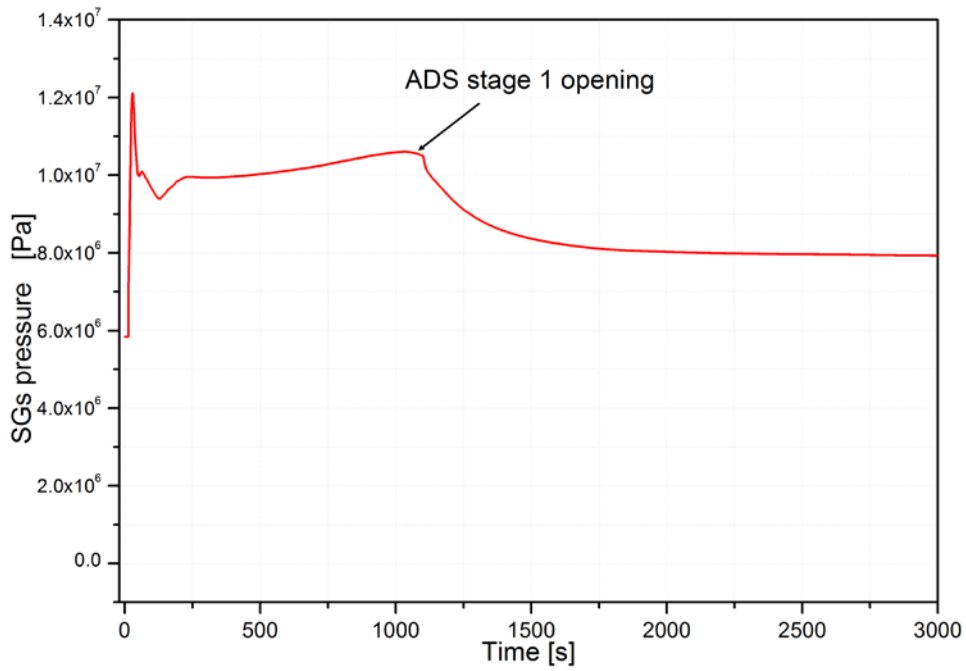
Chapter 7. ASTEC severe accident analysis
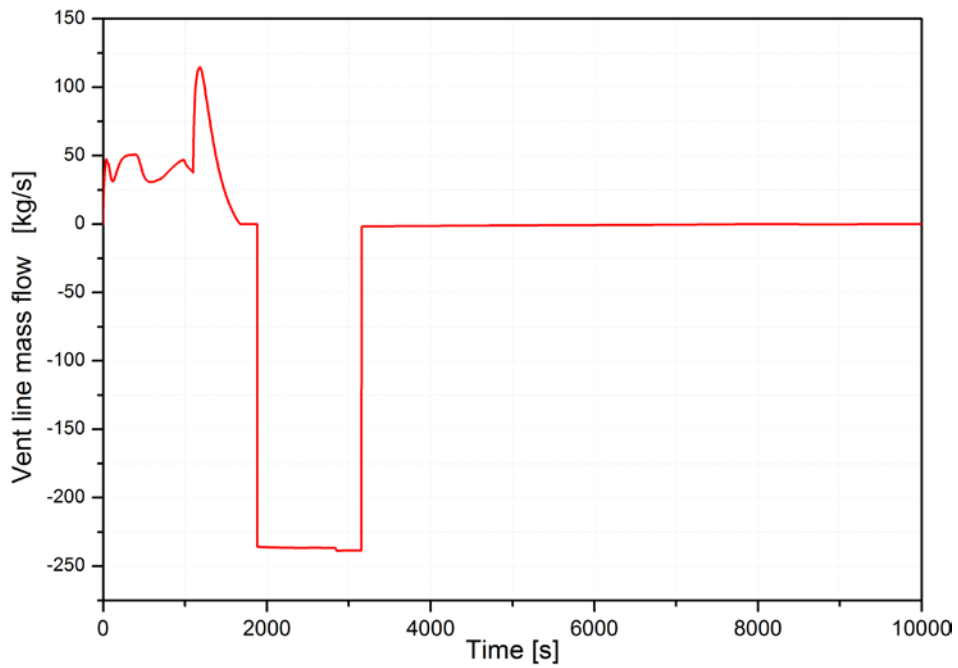
Figure 7-5: PSS-Drywell reverse flow
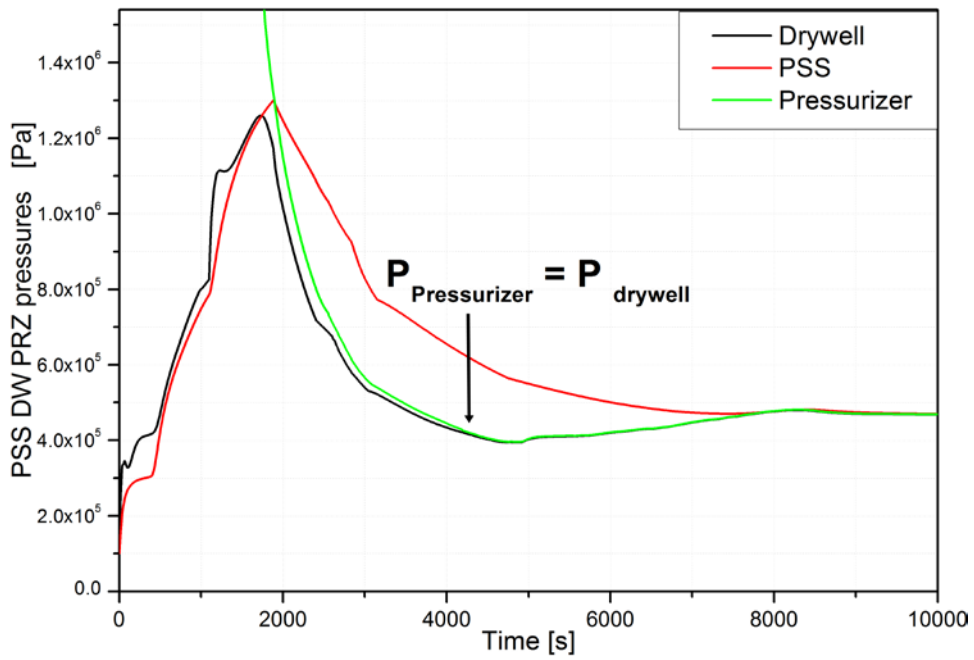
Figure 7-6: "Drywell, PSS, PRZ pressure

Chapter 7. ASTEC severe accident analysis
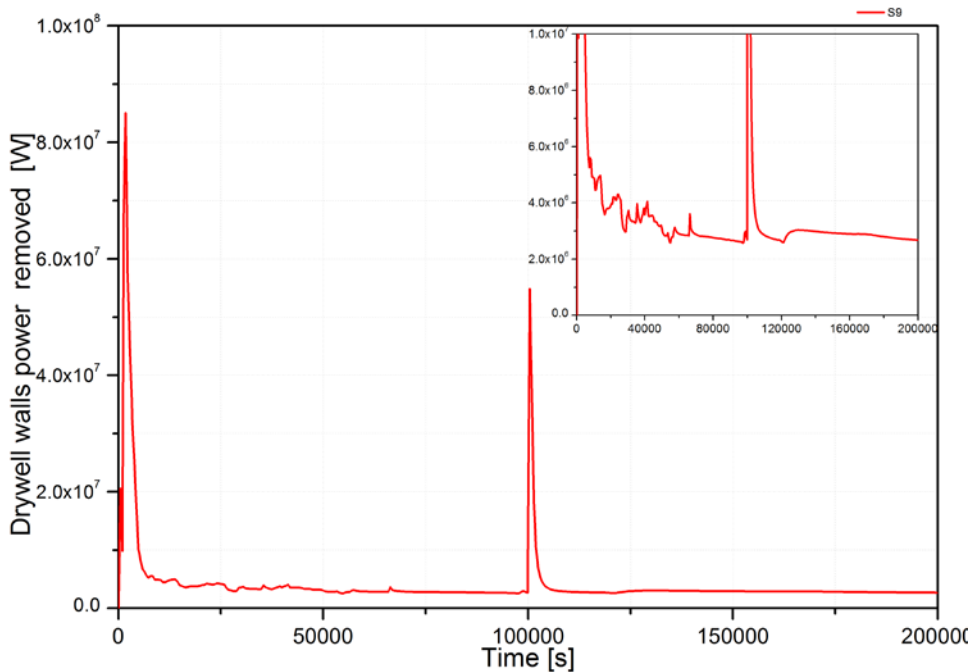
Figure 7-7: Drywell walls power removed
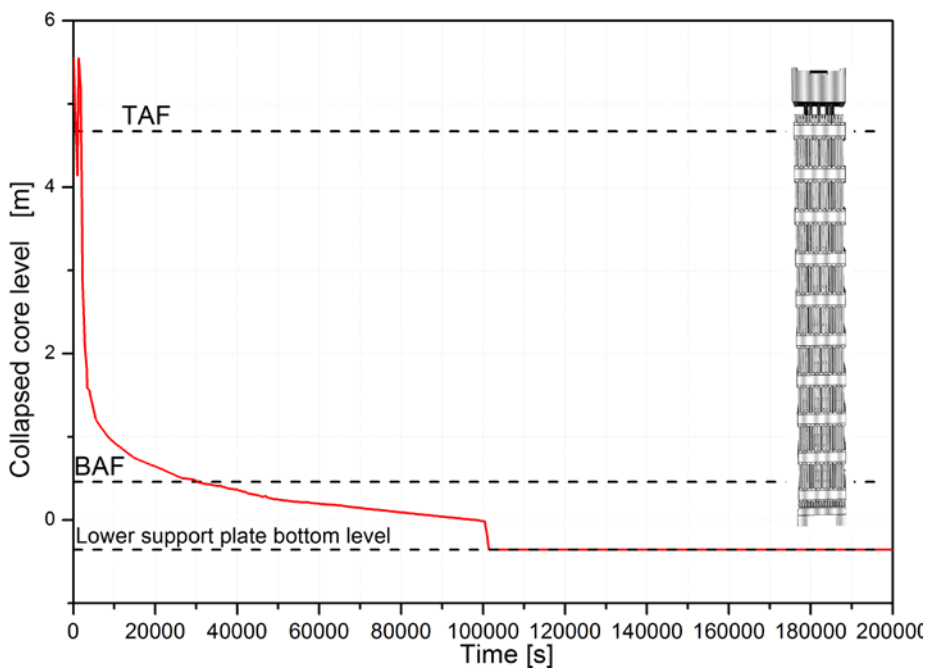
Figure 7-8: Core water level
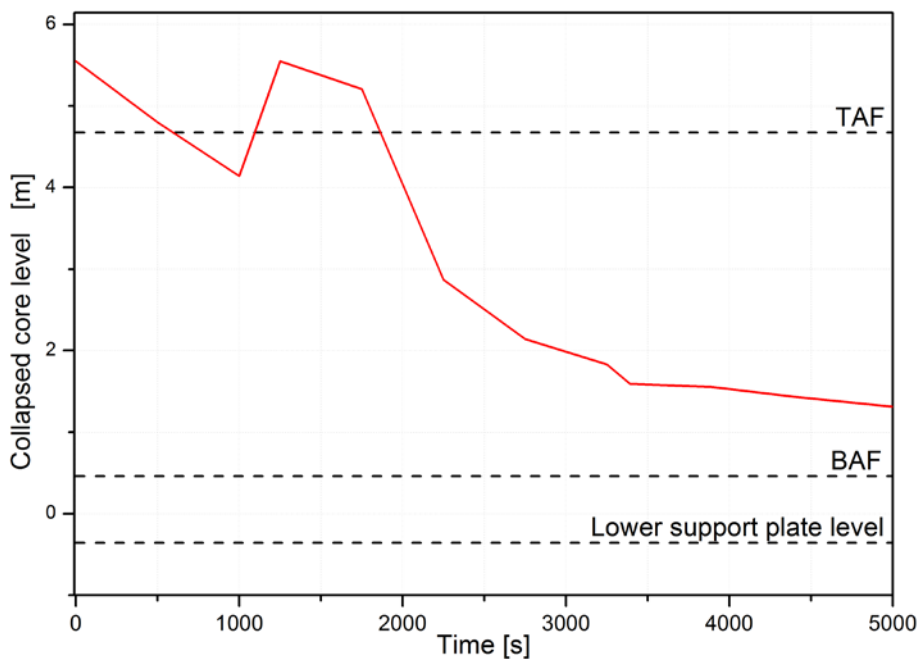
Figure 7-9: Core water level (0-2000s)
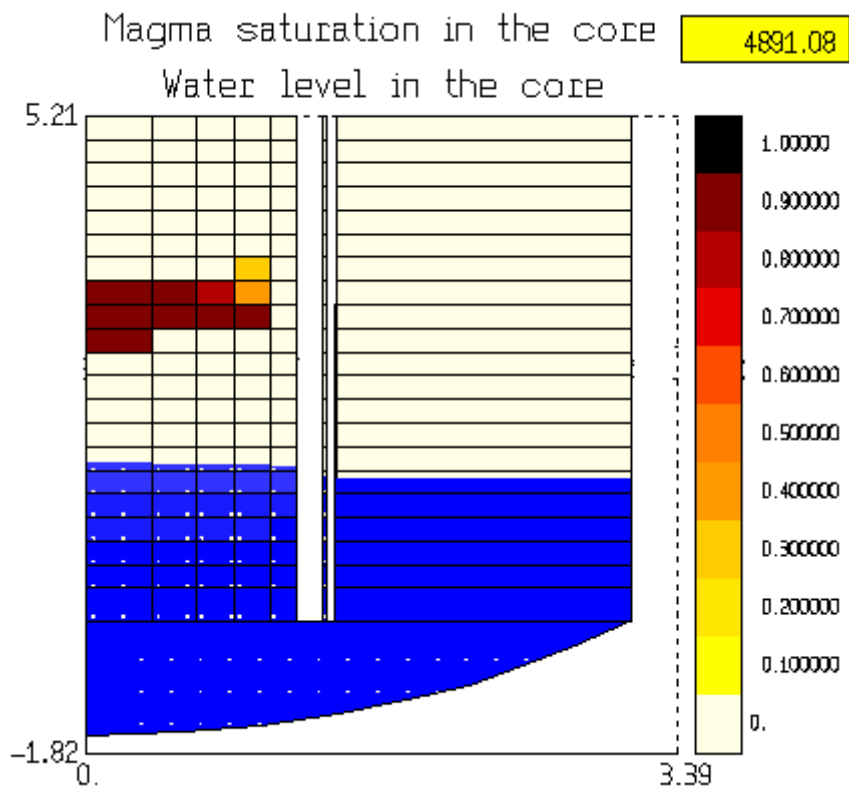
Figure 7-10: First pool formation in the core

Chapter 7. ASTEC severe accident analysis
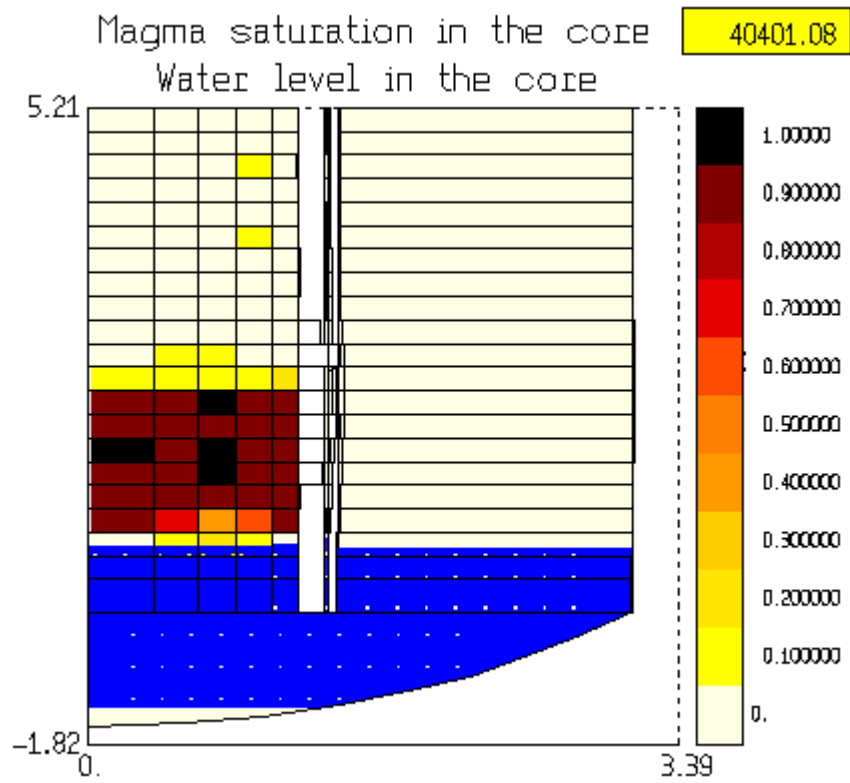
Figure 7-11: First structural material relocation into the lower head
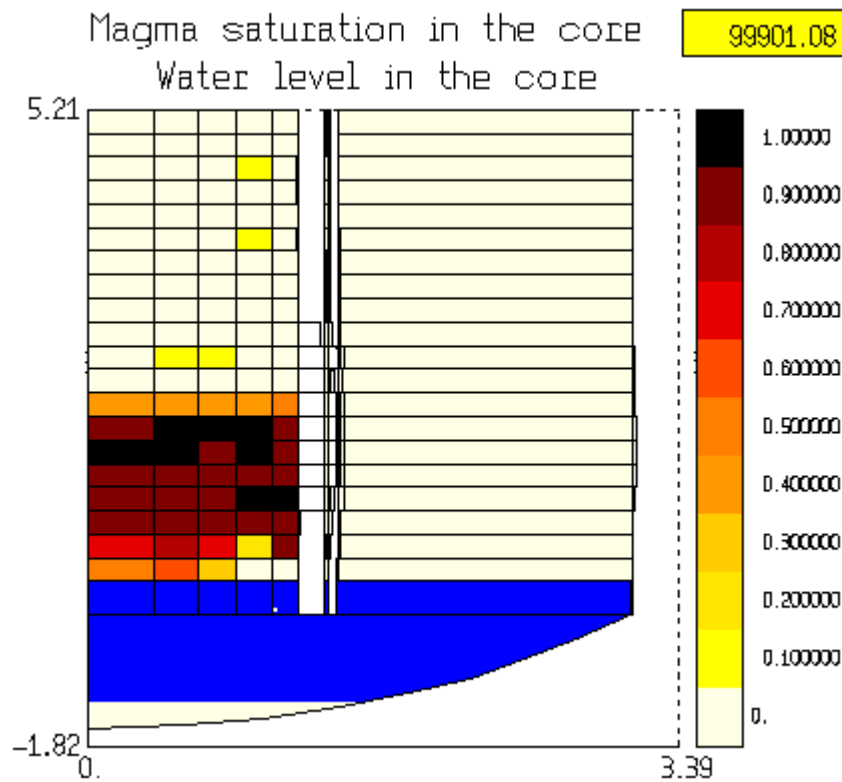
Figure 7-12: Core state before the slump into the lower head

Chapter 7. ASTEC severe accident analysis
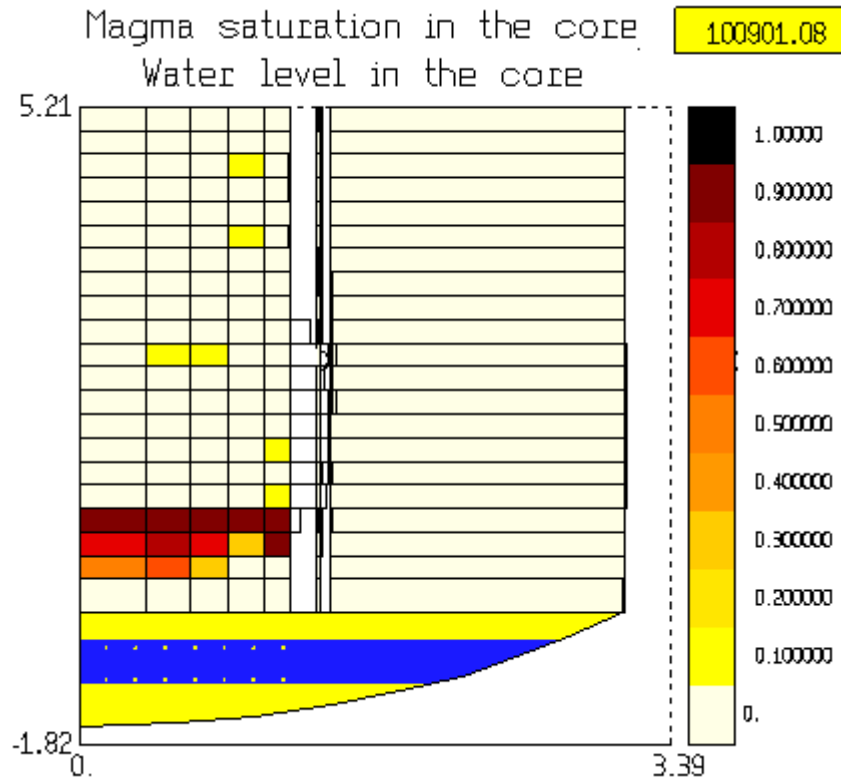
Figure 7-13: Core state after the corium slump into the lower head
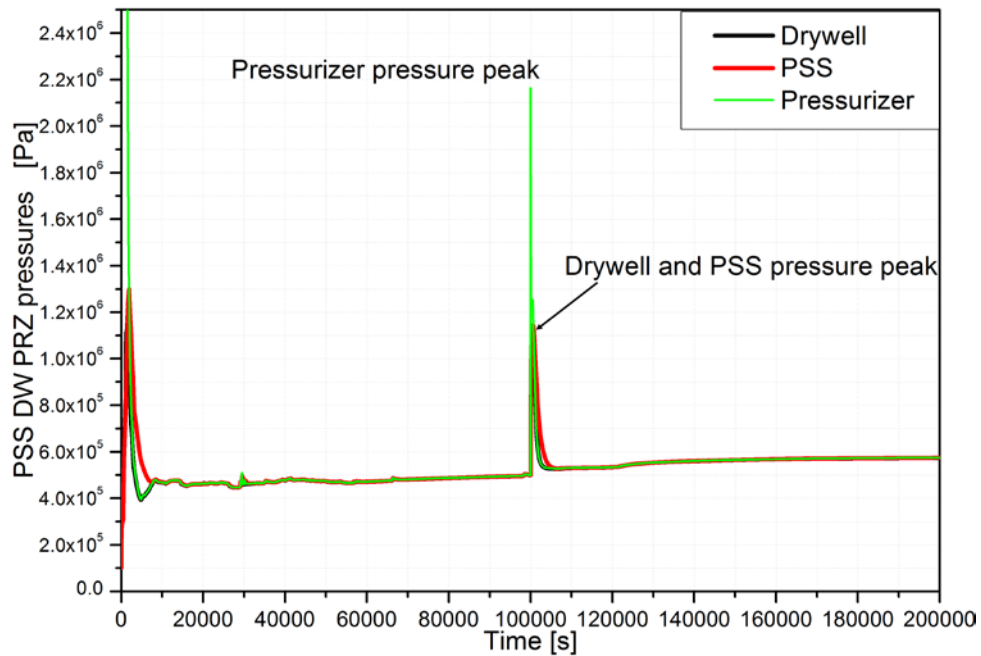
Figure 7-14: PRZ, DW, PSS pressure

Chapter 7. ASTEC severe accident analysis
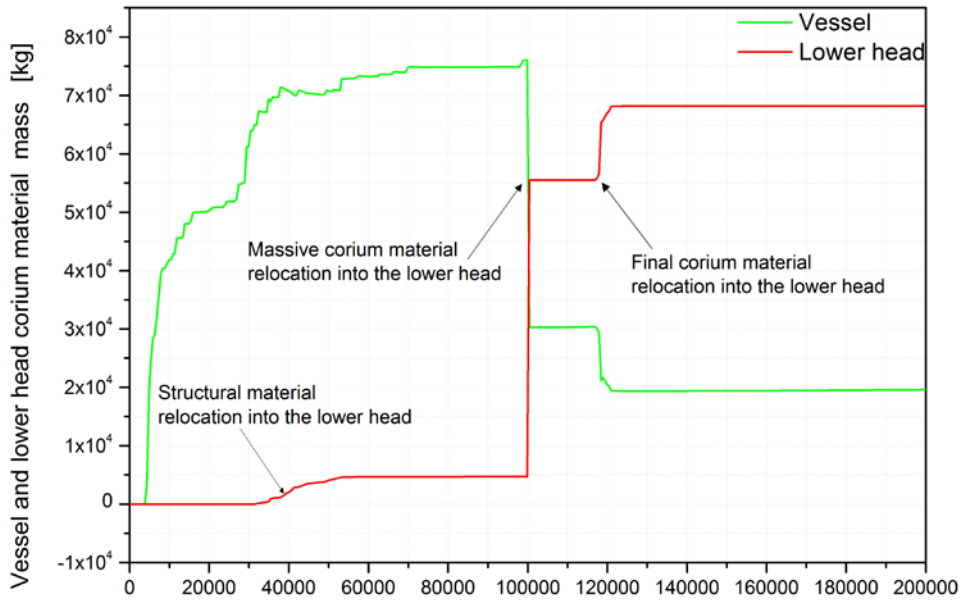
Figure 7-15: Corium material mass evolution
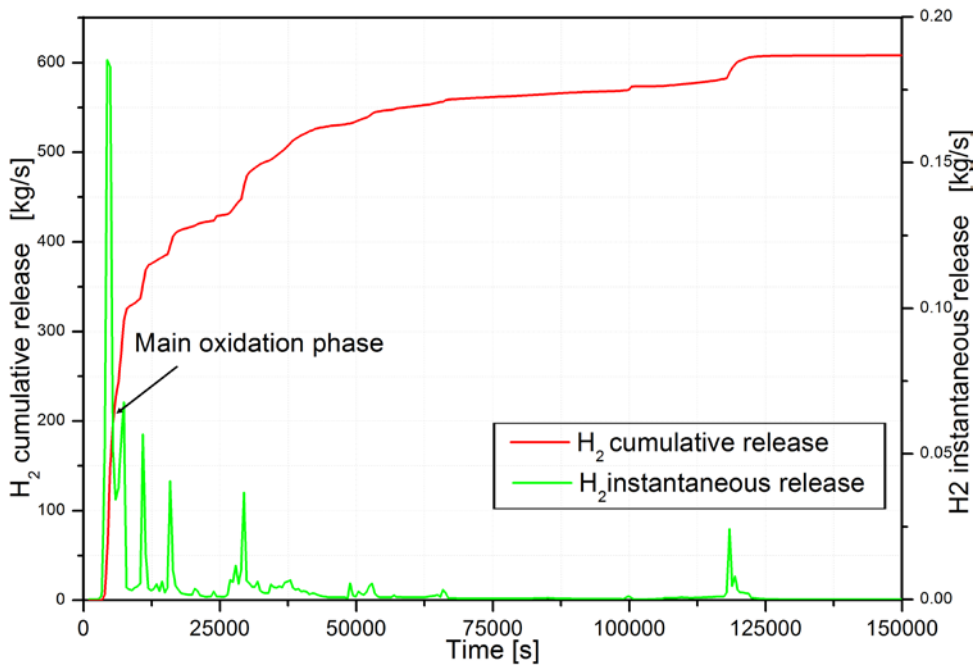
Figure 7-16: H2 cumulative and instantaneous release

Chapter 7. ASTEC severe accident analysis
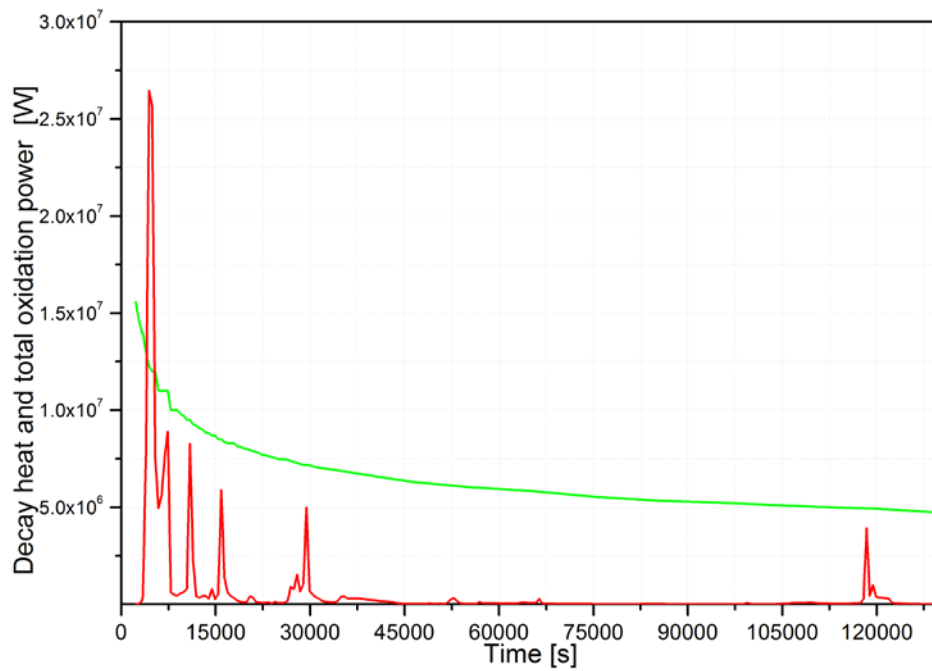
Figure 7-17: Decay heat and total oxidation power
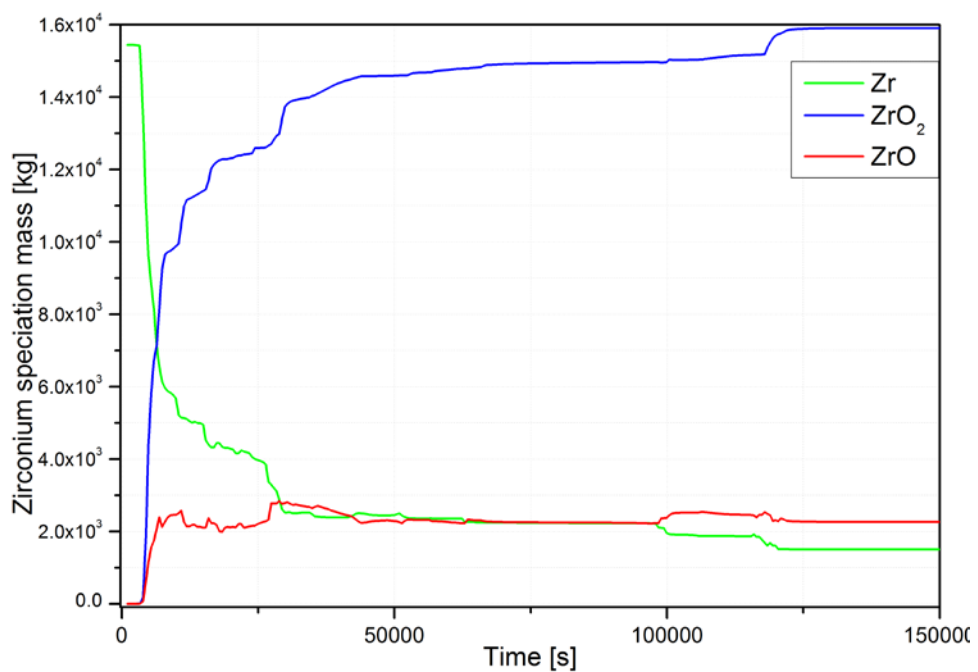
Figure 7-18: Zr speciation mass

Chapter 7. ASTEC severe accident analysis
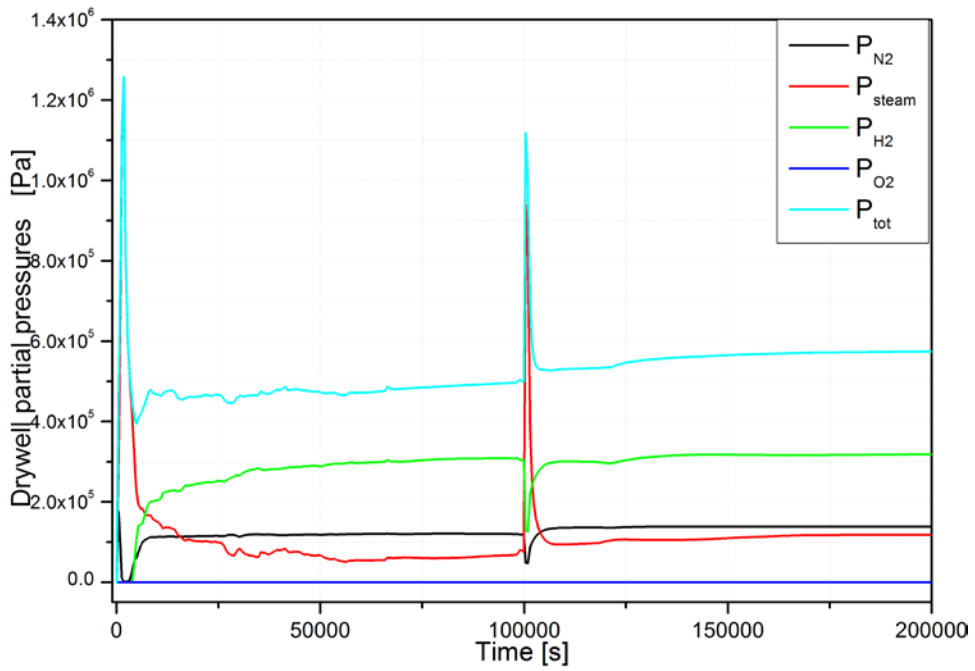
Figure 7-19: Drywell partial pressures
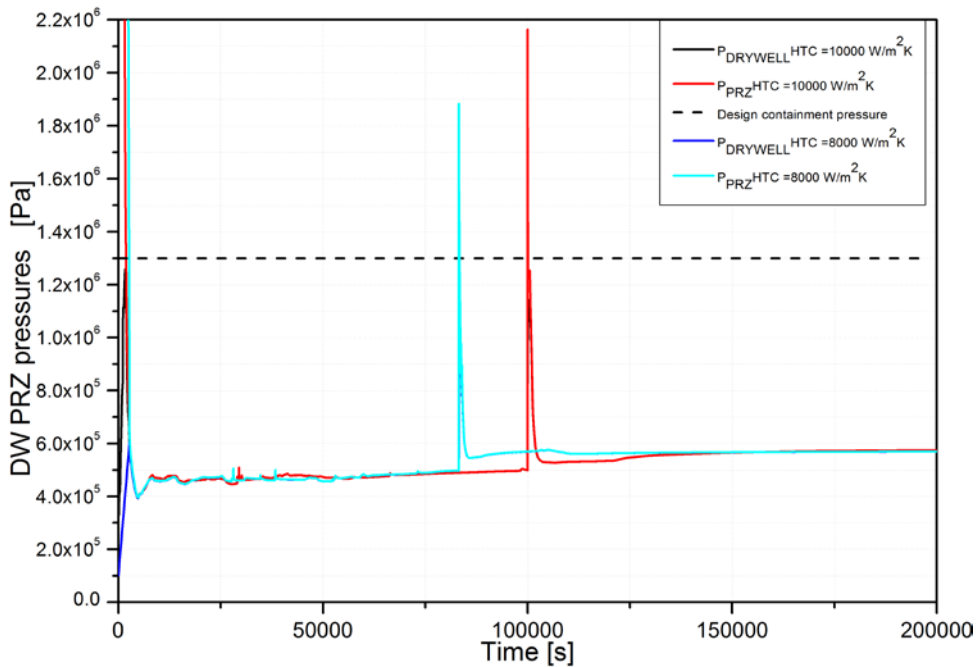
Figure 7-20: Pressure evolution comparison with different IVR HTC values

Chapter 7. ASTEC severe accident analysis
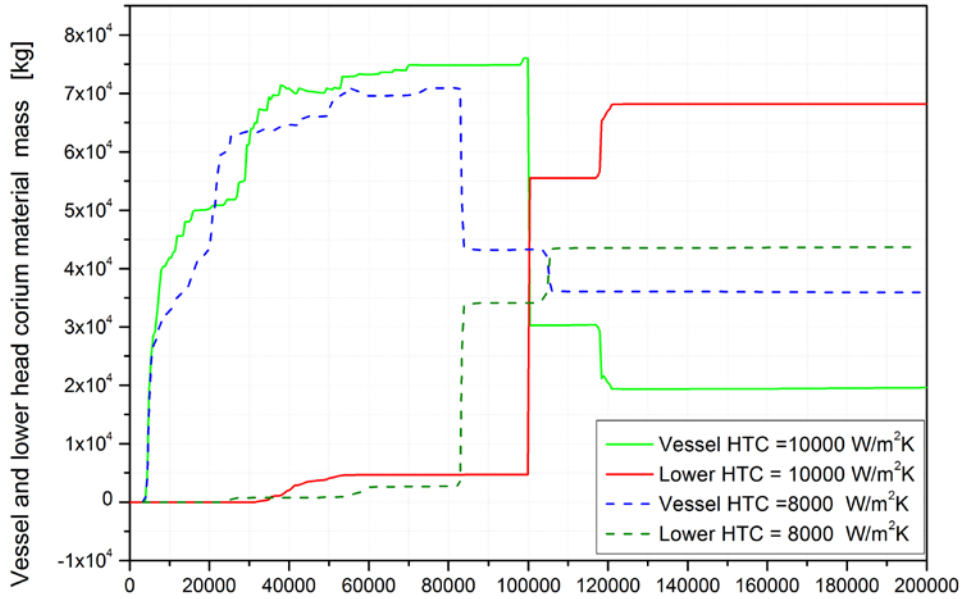
Figure 7-21: Corium material relocation comparison
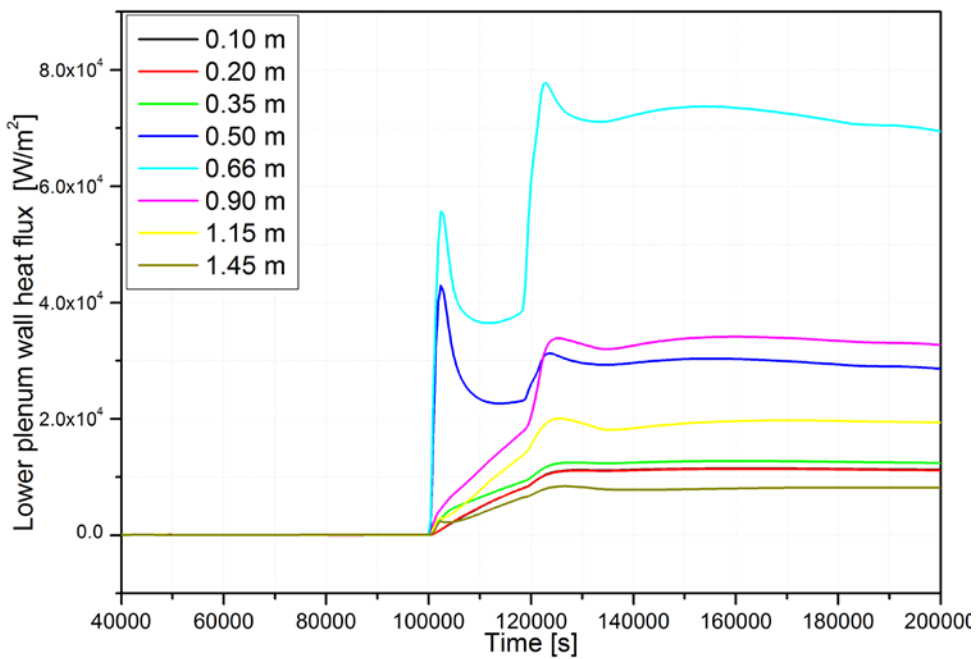
Figure 7-22: Heat flux on the lower head external surface at different levels
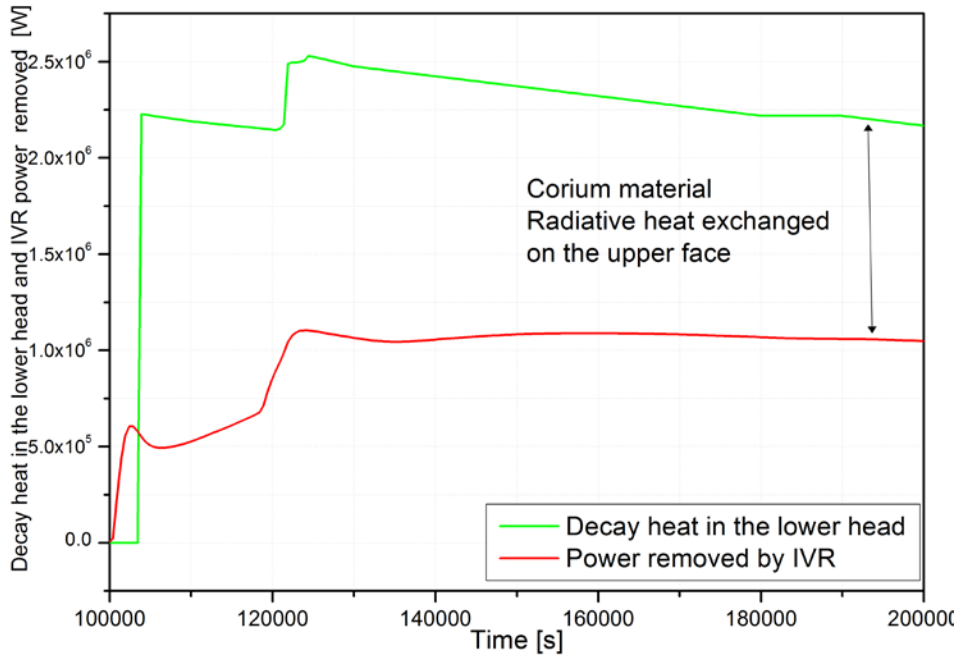
Chapter 7. ASTEC severe accident analysis

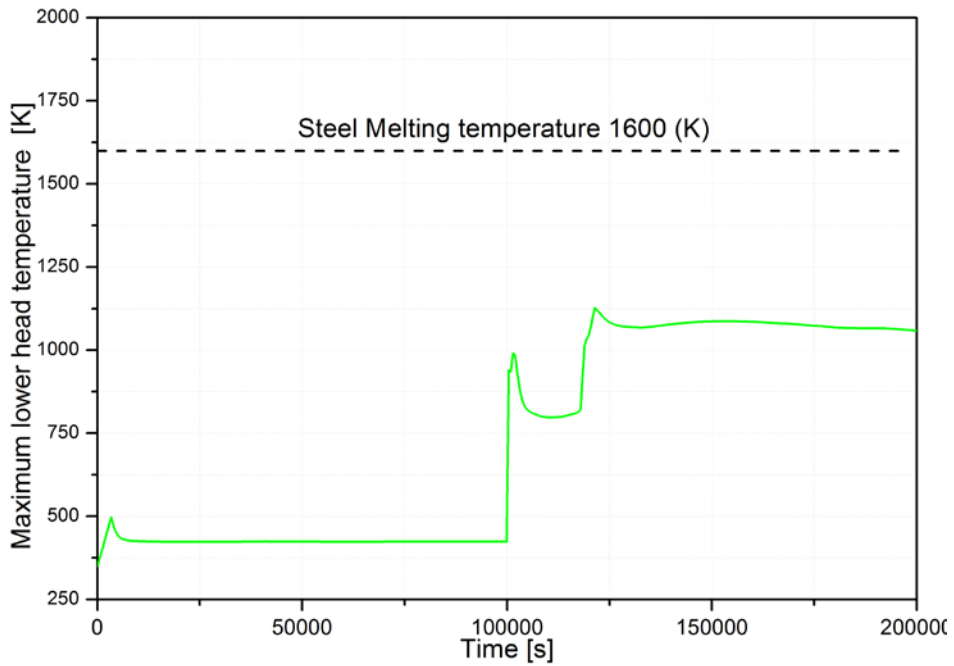Figure 7-23: Decay heat into the lower head and heat removed by IVR strategies

Figure 7-24: Maximum lower head temperature
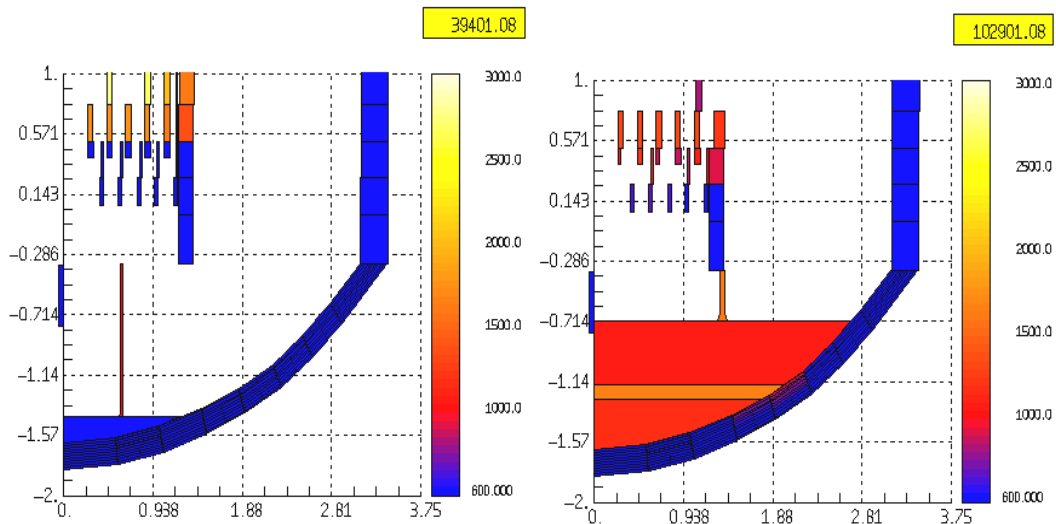
Chapter 7. ASTEC severe accident analysis

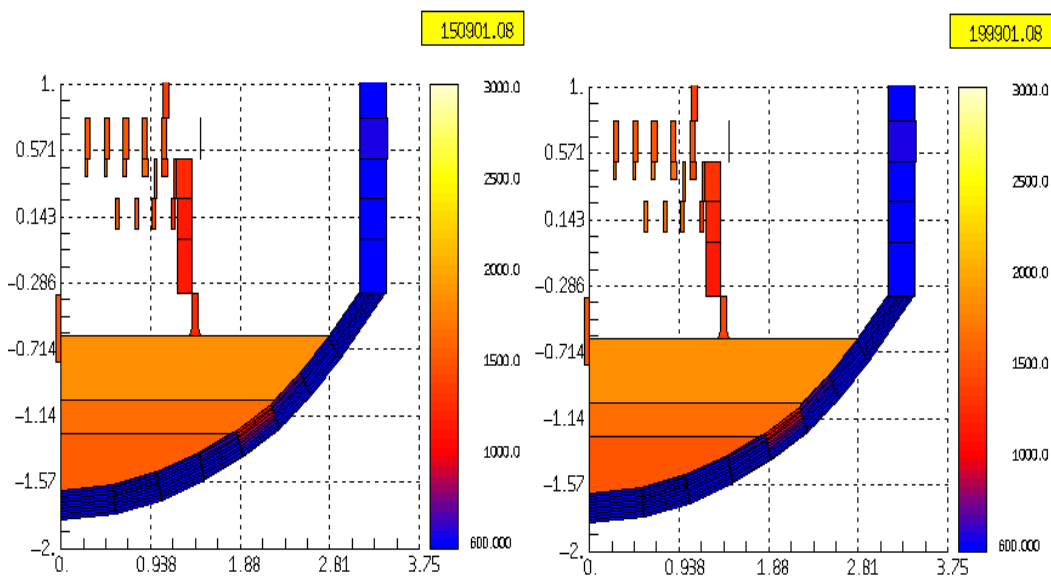Figure 7-25: Structural material relocation and corium material massive relocation

Figure 7-26: Evolution of the corium material inside the lower head

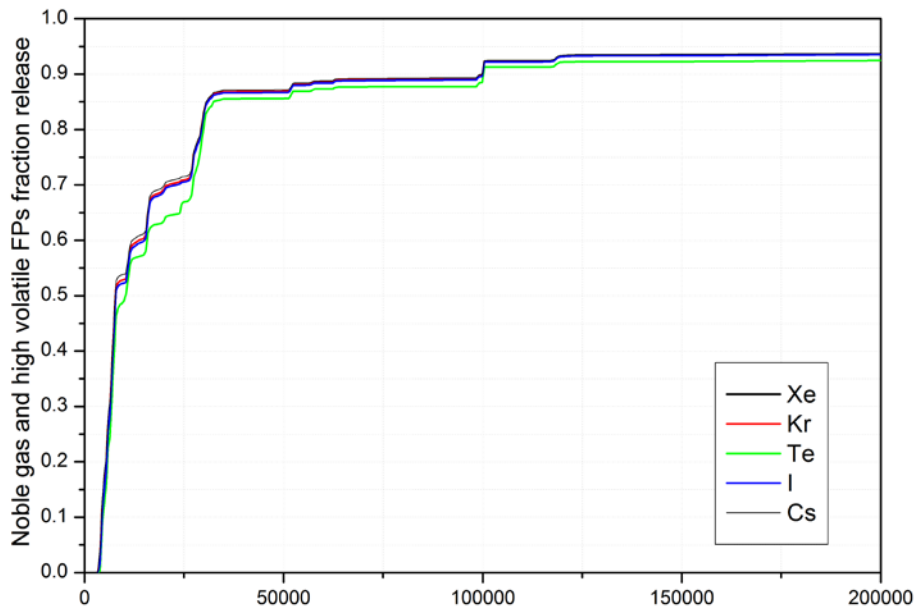**Chapter 7. ASTEC severe accident analysis**

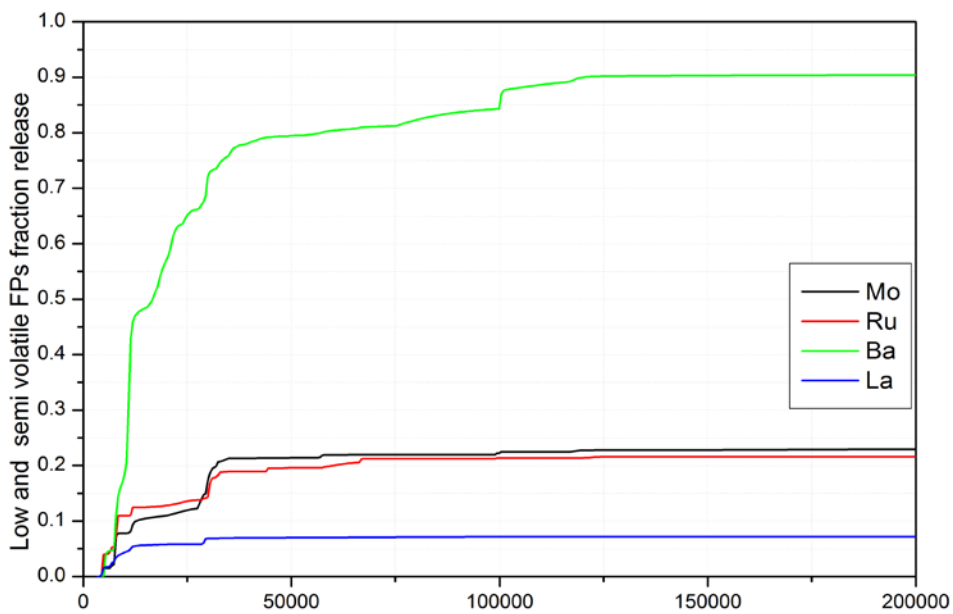Figure 7-27: Noble gases and high volatile FPs fraction release

Figure 7-28: Semi and low volatile FPs fraction release

Chapter 7. ASTEC severe accident analysis
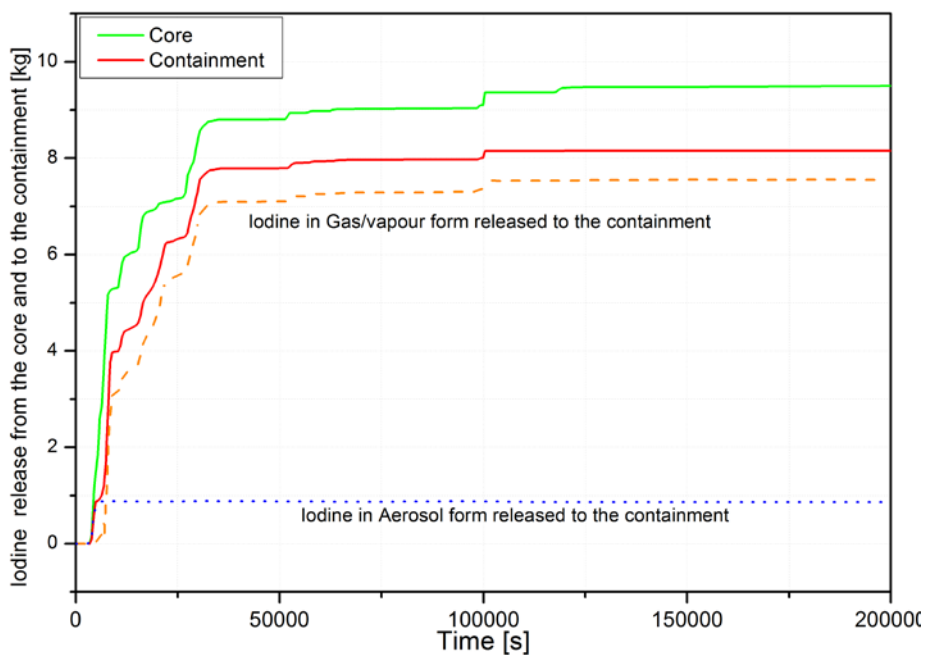

Figure 7-29: Iodine release from the core and to the containment

Figure 7-30: Caesium release to the vessel and to the containment

Figure 7-31: Tellurium release to the vessel and to the containment
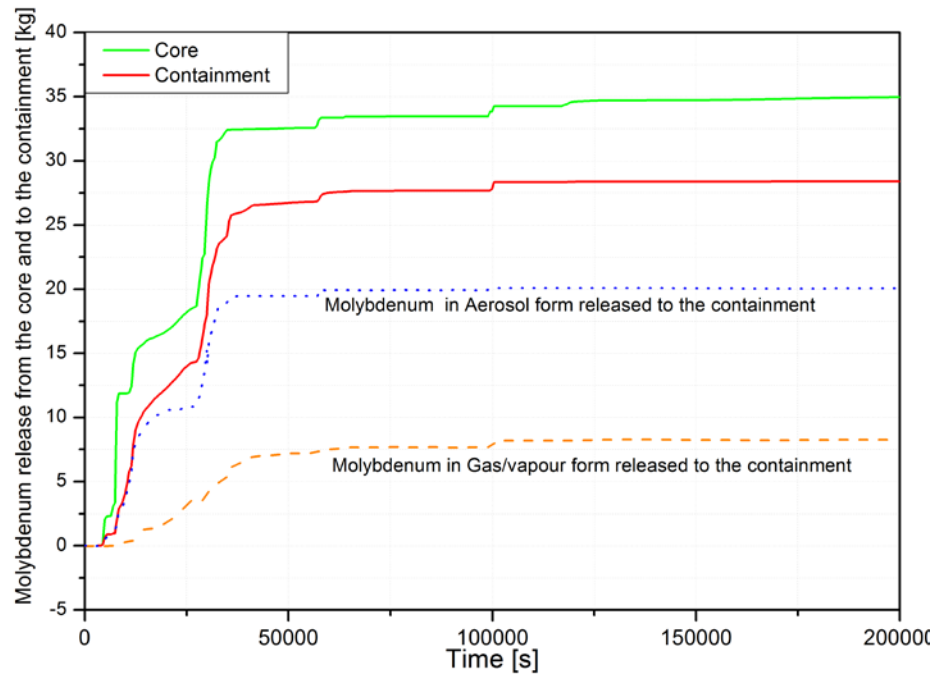
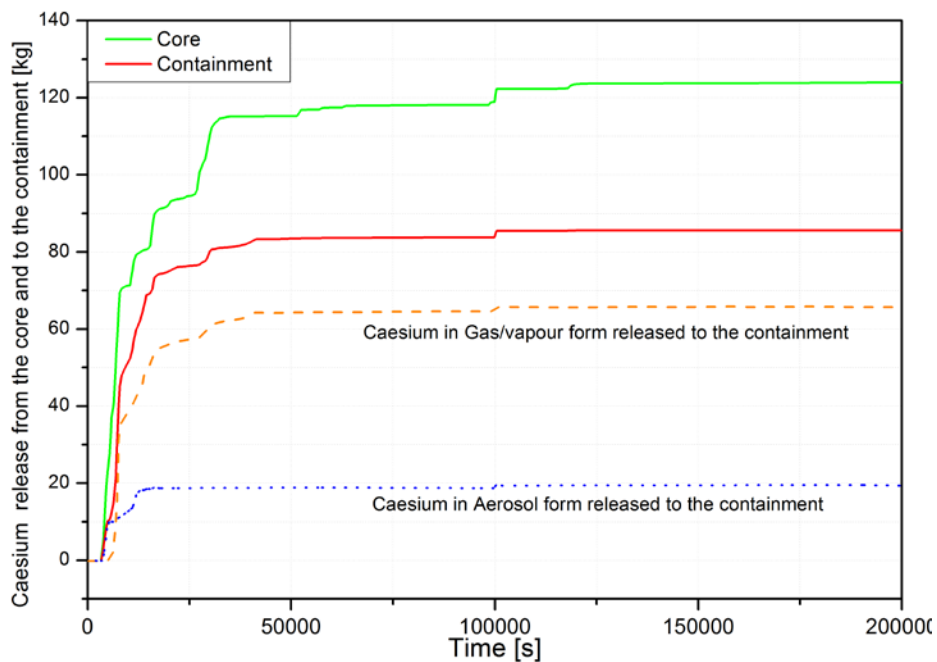Figure 7-32: Molybdenum release to the vessel and to the containment

Chapter 7. ASTEC severe accident analysis

Figure 7-33: Ruthenium release to the vessel and to the containment

Figure 7-34: Barium release to the vessel and to the containment

143

Chapter 7. ASTEC severe accident analysis
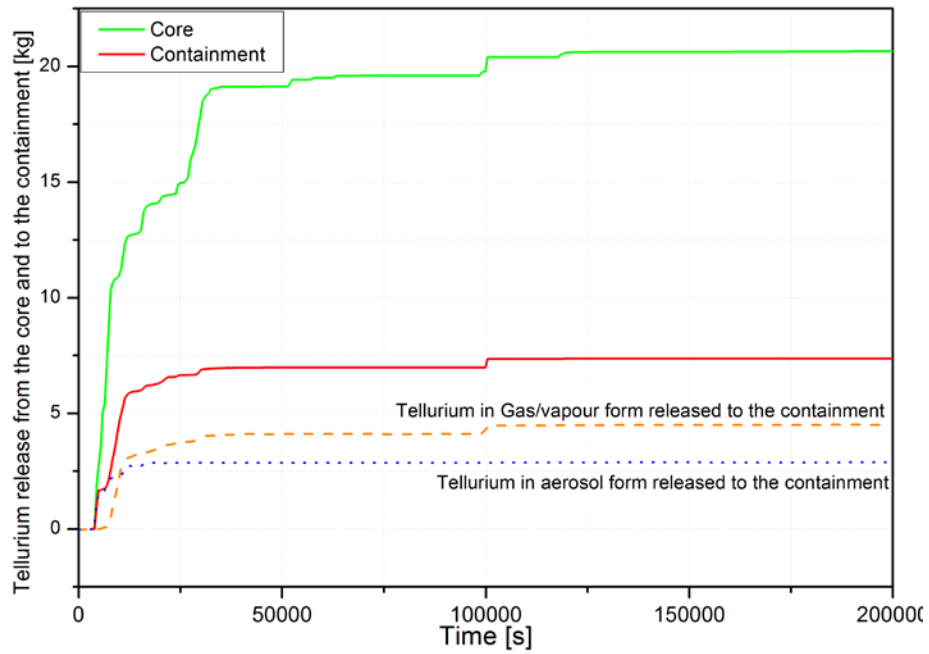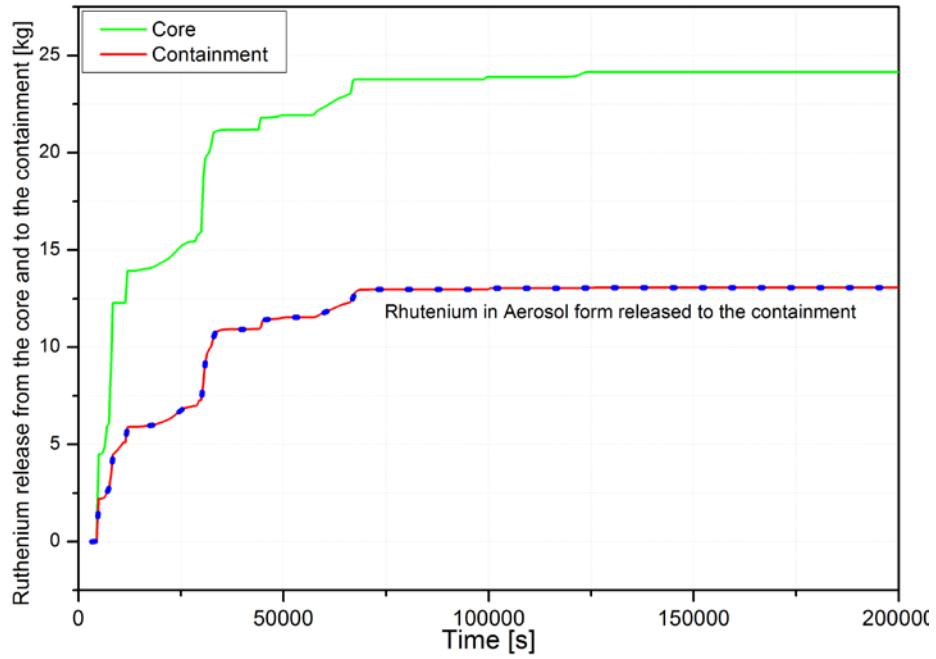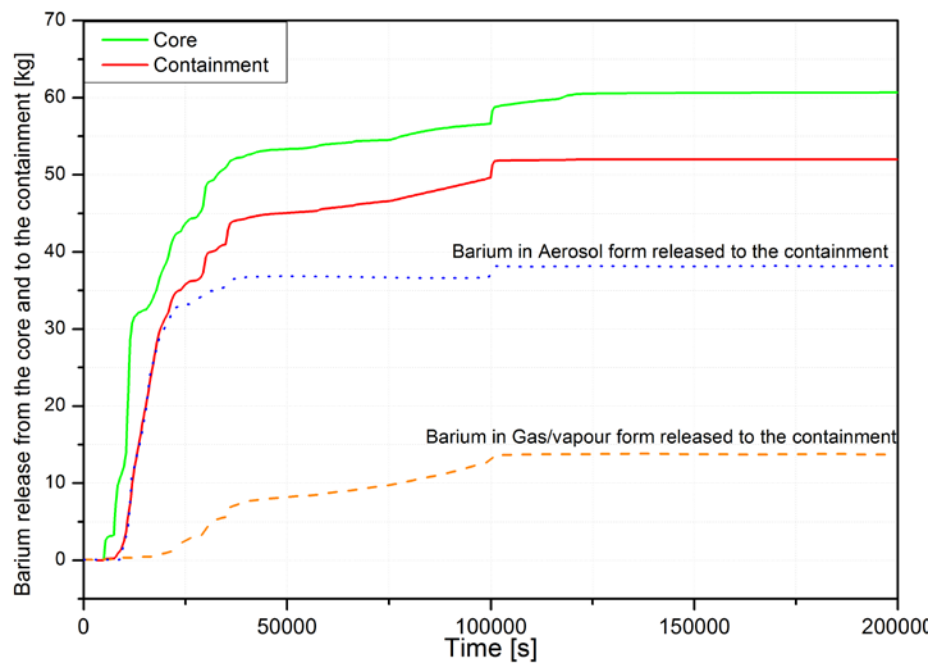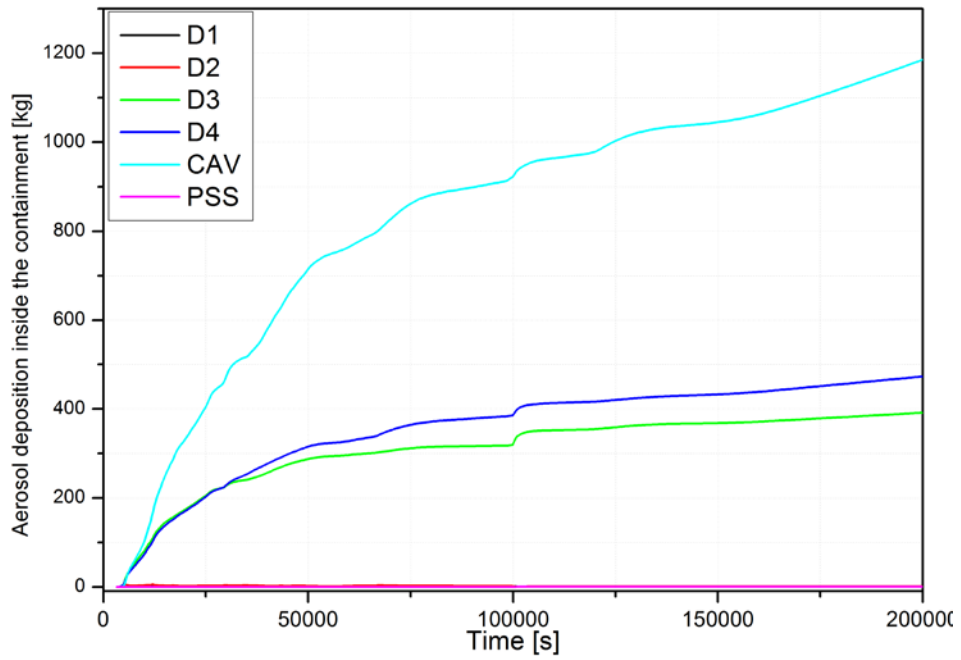

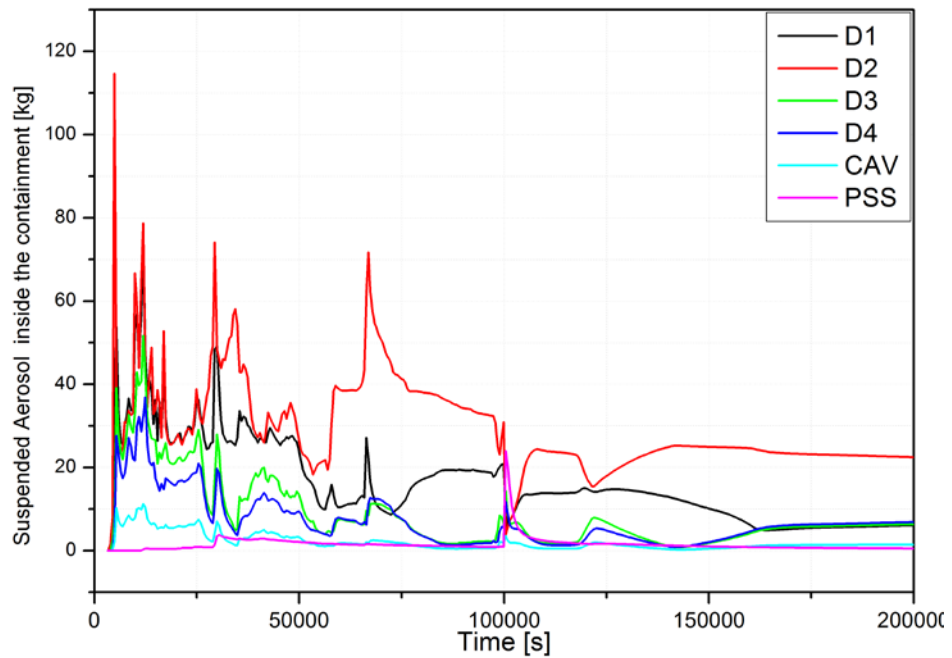Figure 7-35: Aerosol deposition inside the containment

Figure 7-36: Suspended aerosol inside the containment

Chapter 7. ASTEC severe accident analysis
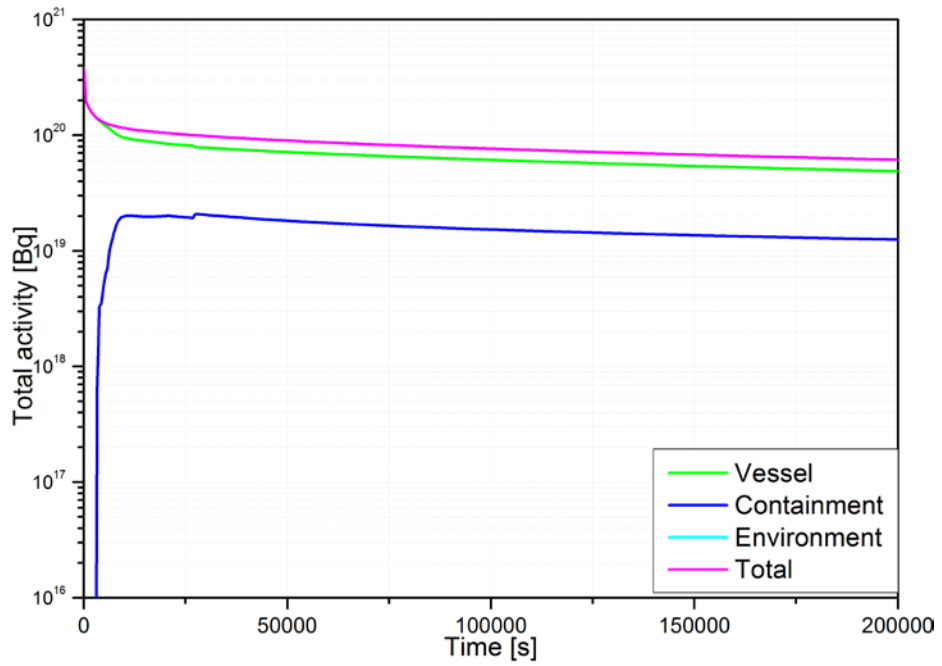
Figure 7-37: Total activity in the different zone of the plant

Chapter 7. ASTEC severe accident analysis

Refences chapter 7

[1] T.G. Theofanous, C. Liu, S. Additon, S. Angelini, O. Kymäläinen, T. Salmassi (1996): "*In-vessel Coolability and Retention of a Core Melt*", DOE/ID-10460, Vols. I and II

[2] M. Fischer (2004), "*The severe accident mitigation concept and the design measures for core melt retention of the European Pressurized Reactor (EPR)*", Nuclear Engineering and Design **230** (2004) 169-180.

[3] P. Matejovic, et al., "*ASTEC applications to VVER-440/V213 reactors*", Nuclear Engineering and Design **272** (2014) 245-260.

[4] Yu.A. Zvonarev, et al.," *ASTEC application for in-vessel melt retention modelling in VVER plants*", Nuclear Engineering and Design **272** (2014) 224-236.

[5] NUREG/CR-6849-ERI/NRC " *Analysis of In-Vessel Retention and Ex-Vessel Fuel Coolant Interaction for AP1000*"

[6] INTERNATIONAL ATOMIC ENERGY AGENCY, IAEA Mitigation of Hydrogen Hazards in Severe Accidents in Nuclear Power Plants, IAEA-TECDOC-1661, Vienna (2011).

[7] Karl-Heinz Neeb "The Radiochemistry of Nuclear Power Plants With Light Water Reactors" Part.1 Walter De Gruyter Inc, ISBN-10: 3110132427 1997

[8] M. Di Giuli, M. Sumini, G. Bandini, L. Chailan, "Exploratory Studies of Small Modular Reactors Using the ASTEC Code", Proc. of ICAAP 2015, 3-6 May Nice 2015.

Conclusion

The continued reduction in the potential for, and the consequences of, severe accidents will play an important role in the operation and development of NPPs and the associated improvements in standards of living worldwide. Improved training, effective accident management strategies and, ultimately, the development of more advanced reactor designs as the SMRs will continue to be the cornerstone of such a reduction. Fortunately, these activities can benefit from more than two decades of severe accident research and, in particular, the extensive suite of severe accident codes that embody the lessons learned from that research. However, the successful application of these codes requires that the end-user have a firm understanding of the important trends and phenomena associated with severe accidents. As illustrated in the last chapter the behaviour of a plant during a severe accident is affected by a complex range of thermal, mechanical and physical processes. The integral code calculation results obtained concerning the SA scenario more than the DBA scenario are affected by approximations that are unpredictable without the use of computational tools that account for the various sources of uncertainty. The uncertainties in predicting the early phases of a severe accident are relatively small, in comparison with the uncertainties for the later stages, which are still relatively large. In addition, the uncertainties associated, to prototypical systems are also still relatively large. Sensitivities and uncertainties analyses are compulsory in this kind of calculation and not only to evaluate the likelihood of all the possible results, which can provided, but also to search the weakness in the reactor model developed. For example, the consequences of reflooding the reactor cavity and implementation of the IVR management strategies, depends on the boundary conditions imposed. The heat transfer coefficient selected, affects the behaviour of the corium material inside the vessel. The actual heat exchanged depends on the collapsed corium material configuration inside the lower head. The design of the reactor core is also obviously important in determining the impact of different severe accident phenomena. For example, in IRIS the mass of the reflector is very high in comparison a standard PWR. The presence of this heavy reflector could affect the lateral movement of the melting material inside the core; the corium material will find more easy to collapse towards the core centre. The IRIS design of the reactor cooling system can also hidden critical aspects in the overall performances of the plant during a severe accident, that could not be foreseen a priori. The ability in accurately predict the response of a new type of reactor as the SMRs during a severe accident using a severe accident code depends on the

Conclusion

type of computer code used, the accuracy of the modelling options used. In general, integrated codes allow the user to model both the reactor coolant system and the containment but have more parametric models that must be tuned by the user. Because these codes were intended to be fast running, modelling accuracy was of less concern than speed. In addition, the users of integrated codes can have much more impact on the overall predicted response of the plant, because of the large number of modelling parameters that must be set. Overall, the SMR accident analyses carried out have provided interesting information about the capability of the ASTEC integral code to simulate the DBA transient and the phenomena associated. The strong interaction between the containment and the integral vessel has been adequately reproduced and furthermore, .the results comparison between the ASTEC code and the RELAP-GOTHIC coupled code has shown a good agreement for the most of parameters analysed. The few discrepancies observed are mainly due to the coarse mesh and simplified model adopted by the ASTEC code. Regarding the SA scenario, the results seem to provide a credible sequence of events quite similar to that seen in currents commercial water reactor designs, taking into account the strong coupling between integral vessel and containment. Obviously only one SA event simulated, using only one code, cannot provide a high level of certainty on the quality of the results. However, the calculated results can permit us, to understand, which could be a possible response of these not prototypical systems to a SA event, and what might be the best counter-measures to be taken to limit the accident consequences. Certainly, further code benchmarking, on reference scenarios and reference SMR, could be useful, to estimate properly the impact of some assumptions, and to point out some phenomenon, which could not been captured in this simulation. Overall, the creation of this new input deck has requested the application of all the potential of the integral ASTEC code, and the support of the ASTEC development team, also in order to use new tools combination, never used before
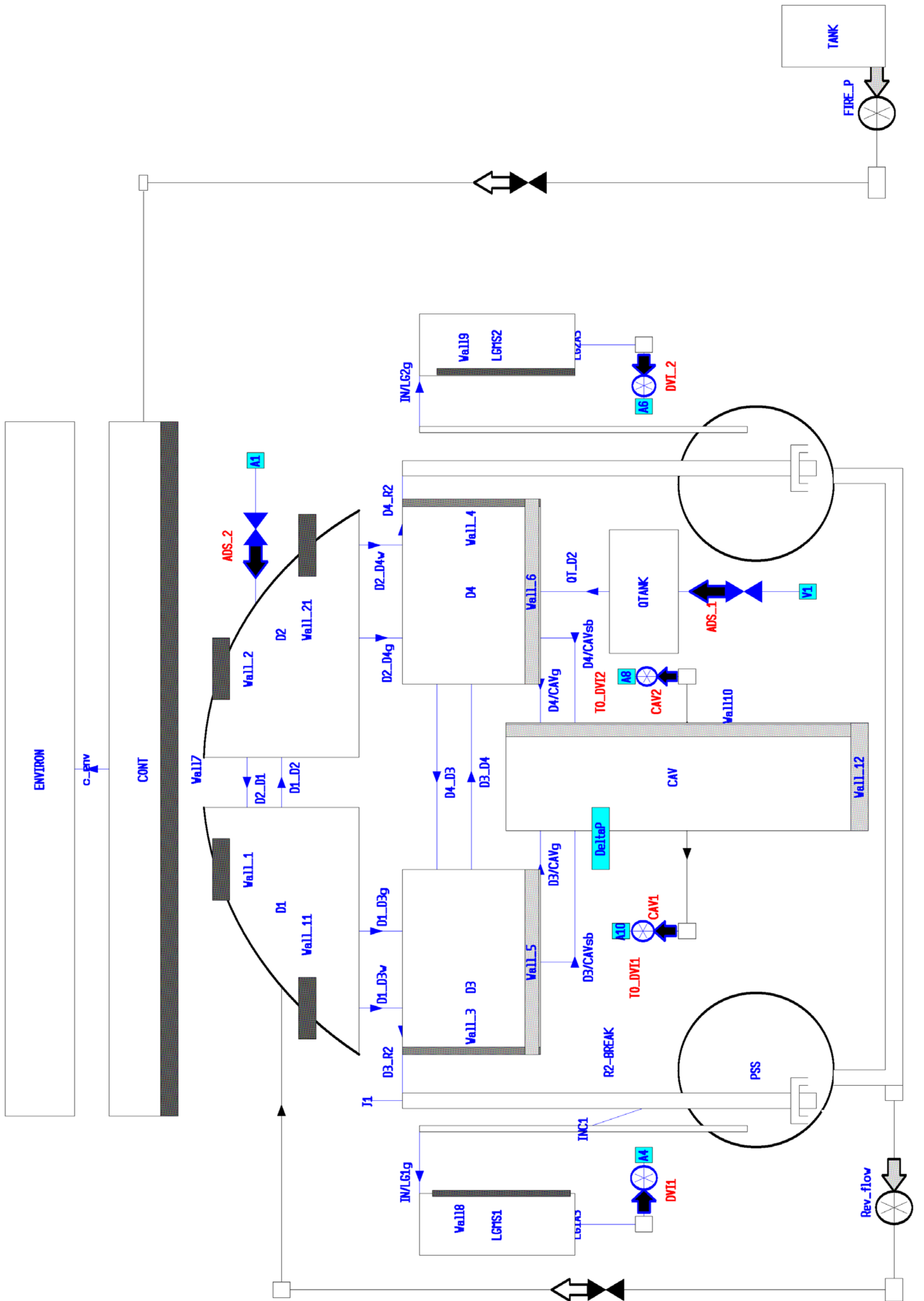
.
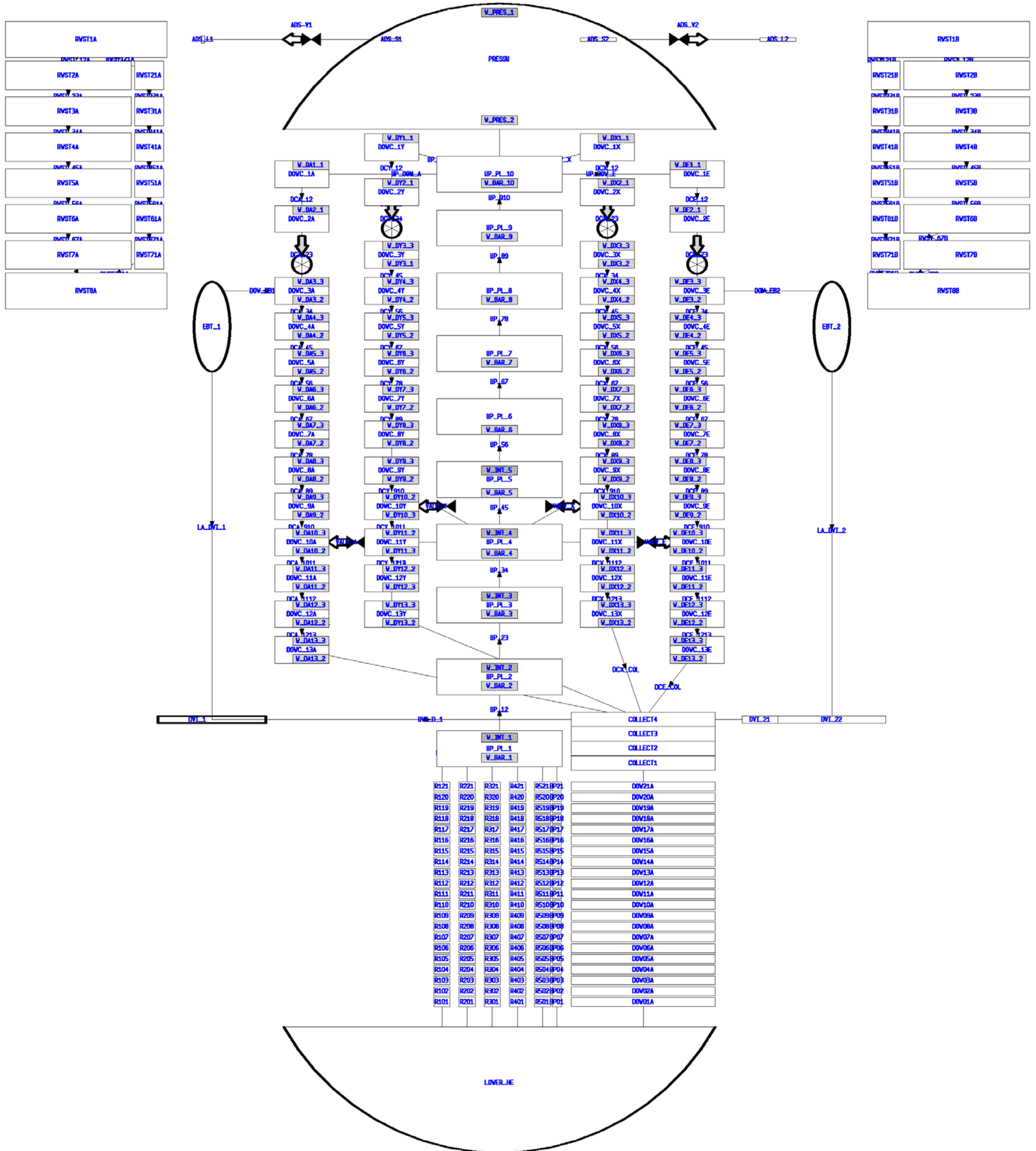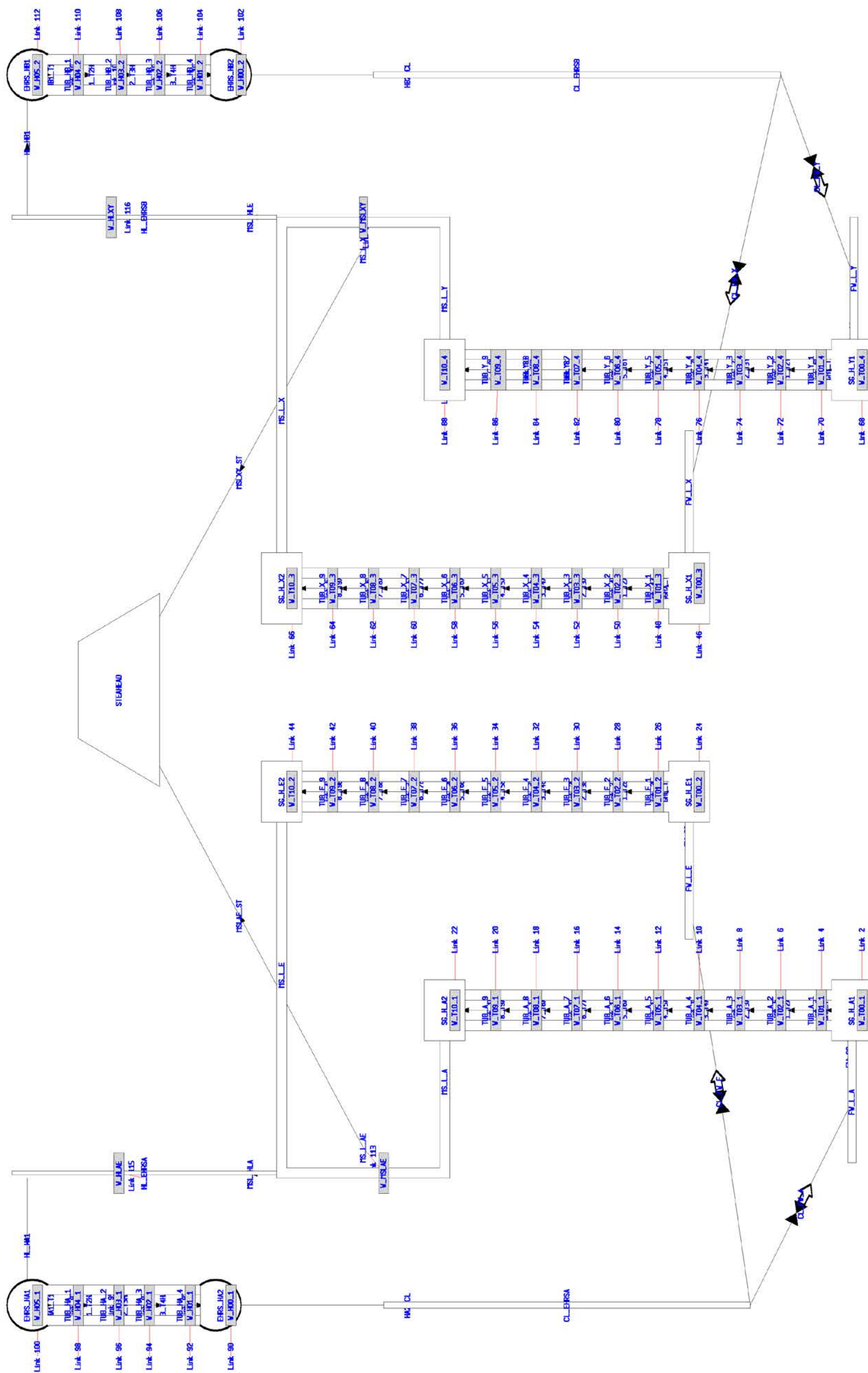
APPENDIX A

A.1   Lower head

In this appendix will be compared the behavior of the two different lower head configurations developed for the IRIS reactor with ICARE module. The reason why two different lower plenum configurations have been developed is that, in ICARE module is not possible arrange the lower support plate or any macro-component inside the elliptical part of the vessel, but only in the cylindrical part of the vessel. This is a strong limitation because some kind of reactor in order to enhance the natural convection regime placed the lower support plate inside the lower plenum as in the AP 1000 reactor. This lack of the code affects also the core degradation. For example, if during the core degradation the corium material relocated inside the lower head reach the lower support plate level the ICARE module does not take into account the possible contact between the two. On the contrary, to avoid this situation when the corium material volume exceed the lower head volume, the ICARE module reduces automatically the corium material volume maintaining the same decay power. This means that the power density of the corium material increase and consequently, the flux on the lower plenum surfaces is not correctly computed. In the IRIS case there is not this issue because it is impossible that the corium material can fill up the lower plenum, given its dimension, but anyway it is no possible reproduce the correct geometry of the IRIS lower plenum.

A.2   The lower head configuration

The actual lower head IRIS configuration along with the two different configurations are illustrated in Figure A-1 .The configuration 1 reproduce the exact geometry of the IRIS lower head but not the lower support plate position. The vessel configuration 1 volume is 25% greater than the IRIS one. The configuration 2 underestimates the lower head volume and surface but arranges the support plate at the exact elevation, and overestimate the IRIS vessel volume of 10%.

Appendix 1 Lower plenum comparison

Figure A-1: IRIS lower head vessel and the two lower part vessel configuration

The Table A.1 reports the IRIS vessel geometrical data and the volume of the two different ICARE vessel configuration. The data are referred to the vessel part that houses the core.

Table A.1: Vessel parameters

GEOMETRICAL DATA	IRIS	MODEL 1	MODEL 2
Low. Plenum height [m]	3.105	3.105	1.27
Cylindrical part Vessel height [m]	3.727	5.562	5.562
Total height [m]	6.832	8.667	6.832
Vessel ID [m]	6.223	6.223	6.223
Cylindrical part Vessel Vol. [m³]	113.357	169.168	169.168
Lower plenum volume [m³]	62.959	62.959	25.751
Total volume [m³]	176.31	232.128	194.920
Δ volume [m³]	0	55.811	18.6039
EXT Surf. lower plenum [m²]	60.830	60.830	39.057

Table A. 2: Lower head model 1 axial meshes

LOWER PLENUM CONFIGURATION 1 : EMISPHERICAL FORM		
material	Steel SA533B	
minimum thickness [m] 0.19	maximum thickness [m] 0.28	
Number of radial mesh (mesr.)		10
Number of axial mesh (mesas)		10
axial mesh positions		
degree	level [m]	radius [m]
0	-0.355	3.115
9.1	-0.8429	3.0463
16.8	-1.2505	2.966
24.7	-1.6439	2.8023
33.5	-2.0508	2.5722
42	-2.4138	2.2923
50.8	-2.7408	1.9474
59.5	-3.0283	1.5747
69.5	-3.2407	1.0789
79.2	-3.3849	0.578
90	-3.46	0

Appendix 1 Lower plenum comparison
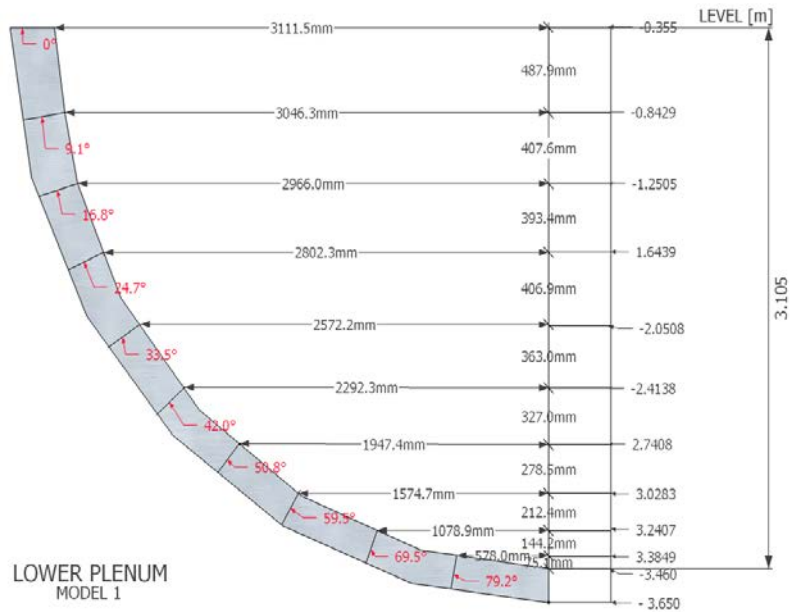
Figure A-2: Lower head configuration 1 radial meshes

Table A.3: Lower plenum configuration 2 meshing

LOWER PLENUM CONFIGURATION 2		
material	Steel SA533B	
minimum thickness [m] 0.19	maximum thickness [m] 0.28	
Number of radial mesh (mesr.)		10
Number of axial mesh (mesas)		8
axial mesh positions		
degree	level [m]	radius [m]
0	-0.355	3.115
5.7	-0.6315	2.7987
11.5	-0.8605	2.5006
18	-1.0687	2.1944
25.7	-1.2374	1.8351
35.3	-1.3761	1.4421
48.8	-1.5041	1.004
66.2	-1.59	0.5452
90	-1.625	0

In the Table A. 2 and Table A.3 and Figure A-2 Figure A-3are illustrated the lower head meshing of the model 1 and model 2.

Figure A-3: Lower head type 2 meshes

A.3 The ICARE stand-alone test

The tests included a series of ICARE stand-alone calculations of the same transient. For each transient has been adopted different failure model for both the configurations and the results were compared. The transient starts at 0 s with the core at full power and the vessel full of water, the shut-down occurs after 1 s. After that, no water makeup occurs until the lower plenum failure. The boundary condition imposed on the lower head external surface are HTC 25 kW/m^2 and 50 °C. The failure model applied are:
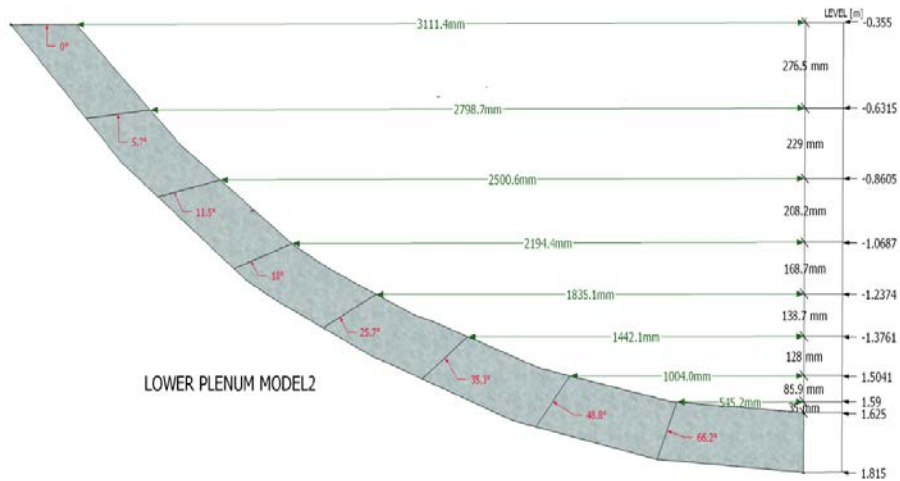
- ŒUF using the first four criteria. At each criteria is associated a type of rupture for the criteria 1 the type of rupture is fragile failure, for the criteria 2 is ductile failure, for the criteria 3 is too small thickness and for criteria 4 is excessive displacement. The default values were used for each criteria. The Oeuf model is applicable to a perfect half spherical lower head, thus only to the configuration 1.
- COMBESCURE model: In this model at each axial level of the vessel lower head, the applied stress σ is compared to the ultimate steel stress. It is applicable to half-spherical or half-ellipsoidal lower heads. It is possible chosen two criteria: Criteria 1 plastic rupture, Criteria 2 creep rupture.
- USER PARAMETER: The user can impose a condition on temperature, mechanical stress or molten fraction. The model can be used for both the configurations.
- LOHEY : Two failure criteria are included in the considered model. According to the first criterion the layer fails if the plastic strain intensity exceeds the ultimate failure strain Ɛ (T). The second criterion is based on the analysis of material damage induced by creep strains. Using the correlation for time to rupture at the given stress and temperature, provided by the user the current damage of each layer is determined.

In the Table A. 4 and Table A. 5 are presented the ICARE stand-alone calculated results for the configurations 1 and 2, for each

failure model adopted, each criteria chosen, the related type of rupture and the ICARE default values.

Table A. 4: Model 1 ICARE stand-alone result

MODEL 1	Type of rupture	Criteria	Time [s]	position	
		Default value		°	[m]
ŒUF model					
CRIT 0	All criteria				
CRIT 1	Fragile failure	Damage = 1	18824	50°-60°	-2.96647
CRIT 2	Ductile failure	Ultimate stress of the material	17683	50°-60°	-2.96647
CRIT 3	Too small thickness	0.001 m (total fusion)	19304	50°-60°	-2.96647
CRIT 4	Excessive displacement	10^{20} m (total fusion)	19304	50°-60°	-2.96647
COMBESCURE model					
CRIT 'ALL'		Ultimate stress of the material	16489	50°-60°	-2.96647
CRIT 'PLASTIC'		Ultimate stress of the material	16489	50°-60°	-2.96647
CRIT 'CREEP'		Creep velocity	18049	50°-60°	-2.96647
LOHEY model					
		melting failure	14840	60°-70°	-3.2239
USER parameter					
Maximum Temperature		1473 K	15332	60°-70°	-3.2239

Table A. 5: Model 1 ICARE stand-alone result

MODEL 2		Criteria	Time [s]	Location	
		Default value		°	[m]
COMBESCURE model					
CRIT 'ALL'		Ultimate stress of the material	10303	48°-66°	-1.5324
CRIT 'PLASTIC'		Ultimate stress of the material	10303	48°-66°	-1.5324
CRIT 'CREEP'		Creep velocity	12600	35°-48°	-1.3971
LOHEY model					
		melting failure	7791	90°	-1.6413
USER parameter					
Maximum Temperature		1473 K	8469	90°	-1.6413

The observed discrepancies between the two models concerning the failure time are mainly due to the different water inventory inside the lower head at the beginning of the transient : 44585 kg for configuration 1 and 18252 kg for configuration 2. In the configuration 1 the ŒUF and the COMBESCURE model for each criteria chosen, predict, the lower head failure at the same point, while in the LOHEY and the USER model the failure occurs at a lower level. The maximum failure time not taking into account the ŒUF model is 18049 s for COMBESCURE CREEP criteria whilst the minimum is 15332 s for USER parameter (maximum temperature 1473 K). In the Figure A-4 Figure A-5 are illustrated the initial and the final state of the configuration 1 using the model COMBESCURE CREEP, and the lower head external walls heat flux.
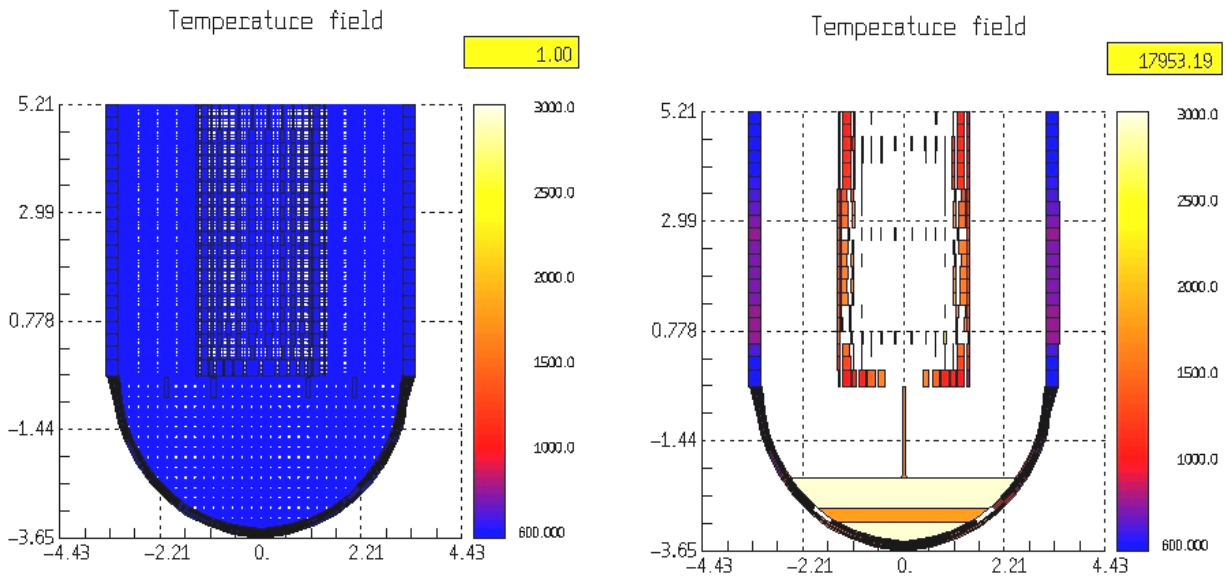

Figure A-4: Configuration 1 initial and final state COMBESCURE+CREEP
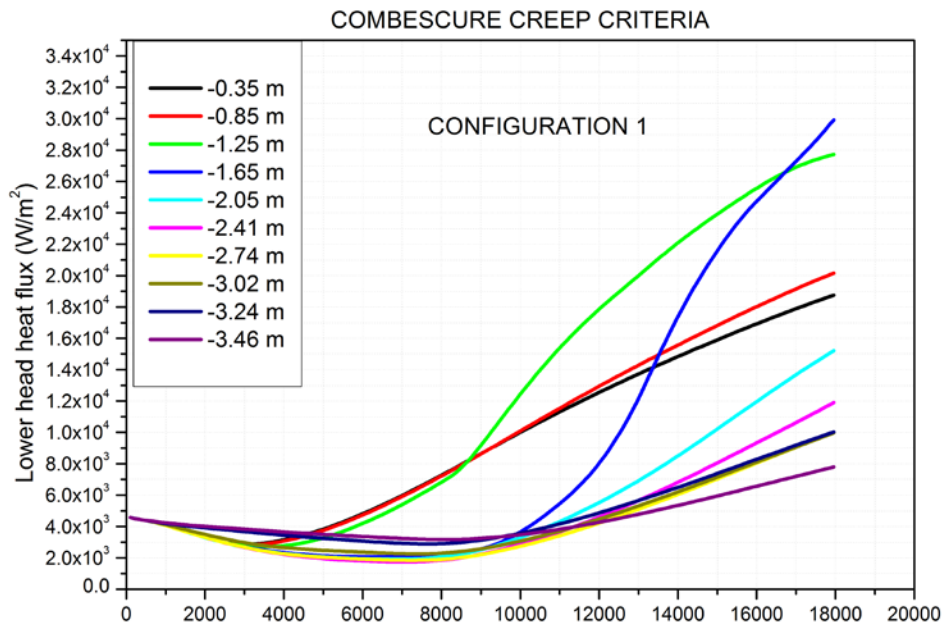

Figure A-5: Lower head external surface heat flux (configuration 1)

Regarding the configuration 2, the maximum failure time is 12600 s for COMBESCURE CREEP criteria and 8469 for USER parameter (maximum temperature 1473 K). The different failure position computed by the LOHEY and PARAMETER USER model is due only to the more restrict failure criteria imposed. These conditions are achieved earlier than the other ones in the bottom part of the lower head. In the Figure A-4 Figure A-5 are illustrated the initial and the final state of the configuration 1 using the model COMBESCURE CREEP, and the lower head external walls heat flux.
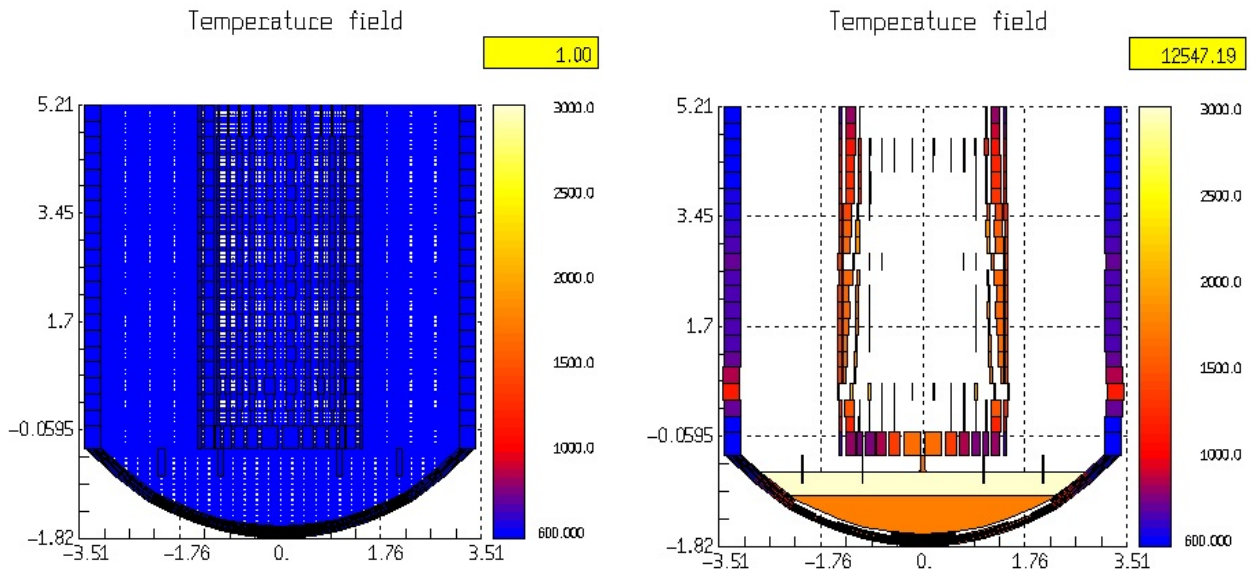
Figure A-6: Configuration 1 initial and final state COMBESCURE+CREEP
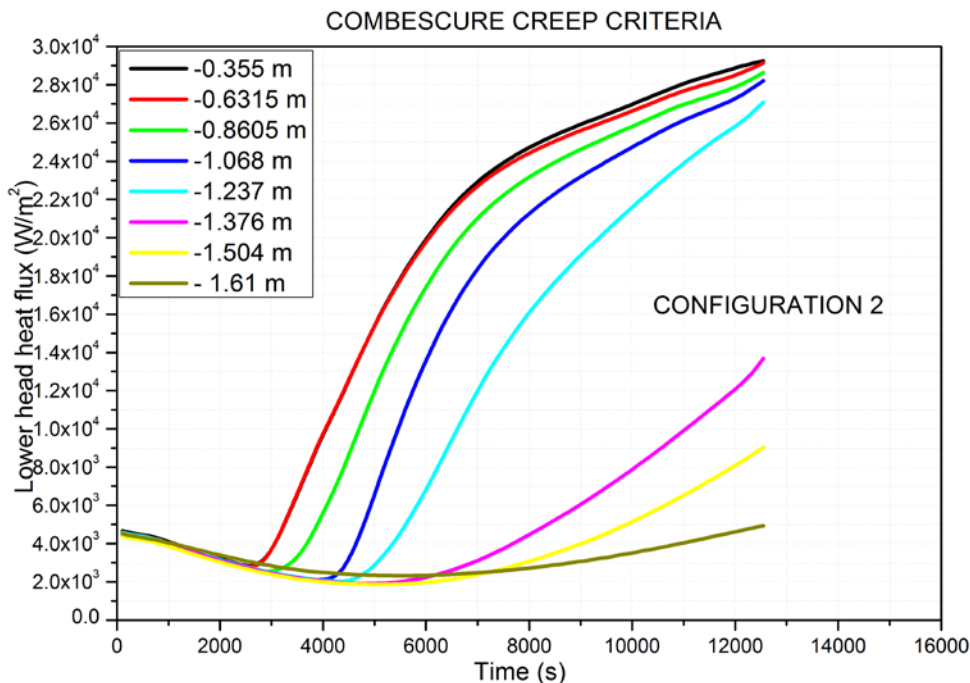
Figure A-7: Lower head external surface heat flux (configuration 2)

Both the configurations fail when the heat flux reaches the value of 30 kW/m². In the configuration 2 are involved more meshes in the

heat exchange with the corium material; indeed as illustrated in Figure A-7 at least 5 meshes reaches the higher heat flux value, while in the configuration 1 only two meshes reach the higher heat flux value.

Figure A-8: Lower head external surface heat flux (configuration 1)

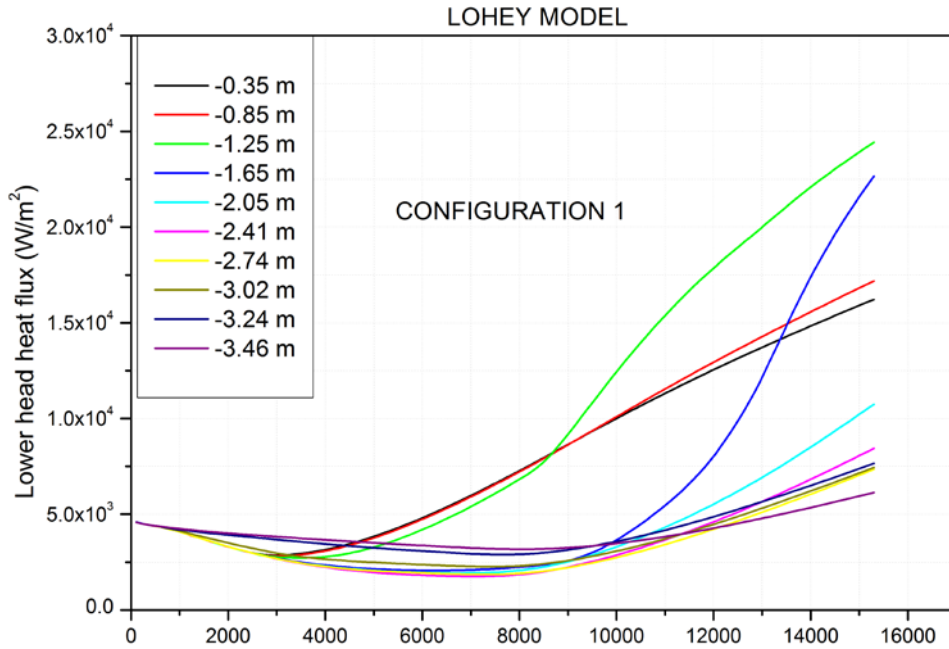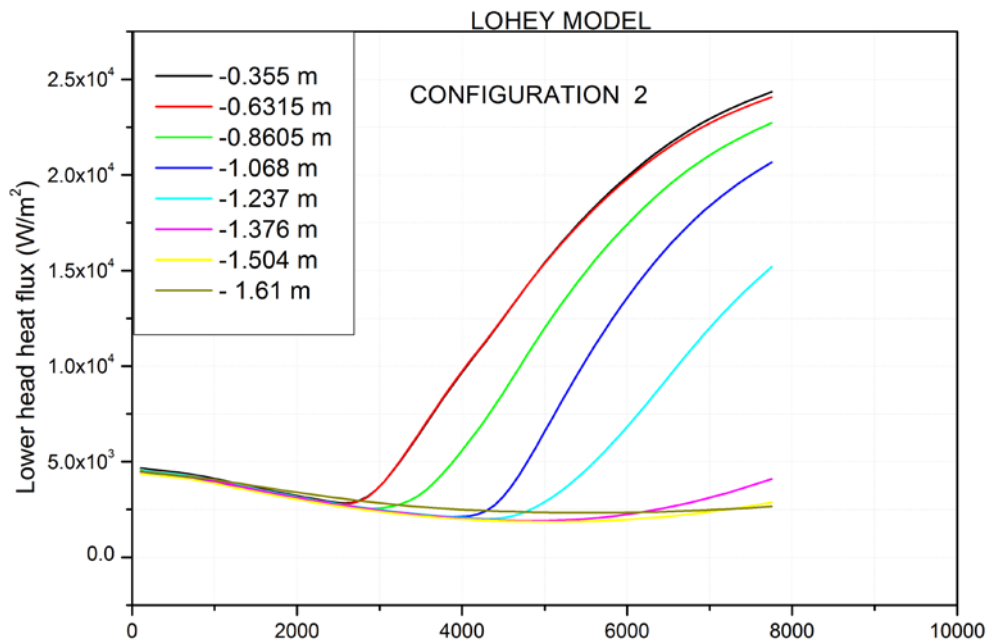Figure A-9: Lower head external surface heat flux (configuration 2)

The Figure A-8 and Figure A-9 illustrate the heat flux calculated using the LOHEY model, the lower head fails when the heat flux reaches the value of 25 kW/m^2 in both the configurations. Imposing more restrictive failure conditions, the ratio between the failure time increases, as illustrated in Table A. 6.

Table A. 6: Failure time ratio

MODEL	Failure time configuration 1/ Failure time configuration 2
COMBESCURE-CREEP	1.63
COMBESCURE PLASTIC	1.43
LOHEY	1.90
USER PARAMETER T_{max} = 1473 K	1.81

Table A. 7: Mesh data (in blue the failed mesh with COMBESCURE model in yellow that ones with the LOHEY model)

	Configuration 1		Configuration 2	
	Elevation (m)	Surface (m^2)	Elevation (m)	Surface (m^2)
Mesh 1	-0.355	1.20	-0.355	1.01
Mesh2	-0.8429	3.00	-0.6315	2.47
Mesh 3	-1.2505	5.08	-0.8605	3.77
Mesh 4	-1.6439	5.93	-1.0687	4.61
Mesh 5	-2.0508	7.07	-1.2374	5.55
Mesh 6	-2.4138	7.89	-1.3761	6.01
Mesh 7	-2.7408	8.82	-1.5041	6.74
Mesh 8	-3.0283	8.77	-1.59	12.56
Mesh 9	-3.2407	8.82		
Mesh 10	-3.3849	11.28		

The Table A.7 reports the mesh geometrical data of the two configurations. Analysing all the available data is possible to deduce that the failure time depends on (in order of importance):

162

- The initial lower head water inventory;
- The failure model selected;
- The shape of the lower head;
- The mesh surface;

In the IRIS reactor model, it has been chosen the more conservative assumption, selecting the configuration 2 and the LOHEY model
.

APPENDIX B

B.1 Summary

In this appendix will be presented the work performed for the paper on the development of the AP1000 ASTEC model [1].

B.2 Introduction

A new trend in reactor technology is the implementation of passive safety features for enhancing the safety of nuclear power plants. The AP1000 reactor includes passive safety systems to provide emergency core cooling following postulated design basis events [2]. These kind of safety systems are significantly simpler than typical PWR safety systems [3] eliminating many safety-related components including pumps, valves, pipes and their associated buildings. The AP1000 PCCS require no operator actions to mitigate design-basis accidents. Once actuated, they rely only on the natural forces of gravity, compressed gas, natural circulation and evaporation to perform their safety-related functions. The only exception is a few simple valves that automatically align and actuate the passive safety systems [4]. In support of the AP1000 design, a series of thermal-hydraulic analysis codes were developed by Westinghouse, including LOFTRAN/LOFTTR2 for non-LOCA transients, NOTRUMP for small-break LOCAs, WCOBRA/TRAC for large-break LOCAs and long-term cooling analysis and WGOTHIC for containment systems performance analysis [5]. However, all the codes mentioned above are proprietary and the thermal-hydraulic characteristics of AP1000 under steady state and transient accident conditions have not been

described in detail in open literature and further studies are still required. In the present work, modeling of the primary circuit, the secondary circuit and the PCCS of AP1000 was developed, and a reactor transient in accident conditions was simulated using the CESAR code. The accident scenario analysed was a 10-in. cold leg break, the break size approaching the upper limit size for small break LOCAs; this was chosen because for the safety analyses of AP1000, a small break LOCA is defined as a rupture of the reactor coolant pressure boundary with a total cross-sectional area less than 1.0 ft^2. This is considered a Condition III event (infrequent fault) that may occur during the life of the plant [6]. The main transient parameters obtained by the CESAR simulation, (RCS pressure, break flow, passive safety injection flow, cladding temperature, etc.), have been compared with the reference results calculated by Westinghouse using the NOTRUMP code and a detailed comparison will be discussed in the following sections.

Nomenclature

ACC	accumulator	PRHR HX	passive residual heat removal heat-exchanger
ADS	automatic depressurisation system	PCCS	passive core cooling system
CMT	core makeup tank	PWR	pressurised water reactor
DVI	direct vessel injection	RCP	reactor coolant pump
IRWST	in-containment refueling water storage tank	RCS	reactor coolant system
LOCA	loss of coolant accident	RPV	reactor pressure vessel
PMS	protection and safety monitoring system	SGFP	steam generator feed water pump
PRHRS	passive residual heat removal system		

B.3   AP1000 safety design

The AP1000 passive safety design approach is to depressurize the RCS if the leak or the break is greater than the makeup capability of the charging system. By depressurizing, a lot of borated water in the accumulator and in the containment refueling water storage tank becomes available for cooling the core [7]. The AP1000 PCCS

includes two core makeup tanks (CMTs), two accumulators (ACCs), a passive residual heat removal heat exchanger (PRHR-HX), an In-containment Refueling Water Storage Tank (IRWST), a sump and the Automatic Depressurization System (ADS). The CMTs are filled with borated water at room temperature, and located above the Reactor Coolant System (RCS); both are connected with two different cold legs by an open 'pressure balance' line. During normal operation, the outlet valves are closed and the system is static. This system operates at RCS pressure, and provides high pressure safety injection by gravity of the colder water in the CMTs. The pressurized ACCs are filled for 15% with nitrogen at a pressure of 48.7 bar and for 85% with borated water, providing additional borated water to the RCS. The IRWST provides a further source of borated water for long term cooling. To attain injection from IRWST, the RCS pressure must be lowered until the head of water in the tank overcomes the low RCS pressure and the pressure loss in the injection lines. One containment sump injects recirculation water to the primary system after the primary system is fully depressurized and the gravity head becomes great enough. All these systems share the same discharge line, called Direct Vessel Injection (DVI) lines. The PRHR-HX is a C-tube heat exchanger located inside the IRWST above the core promoting natural circulation heat removal between the RCS and the tank [8]. The ADS system consist of a series of valves, subdivided in four different stages, every stage including two lines and four valves. The first three-stage are connected to the pressurizer and discharge into the IRWST, the two four stage (4A,4B) are connected to the two hot legs and discharge inside the containment atmosphere. The aim of ADS system is to depressurize the RCS in order to permit the IRWST to discharge into the RCS.

B.4   AP 1000 RCS and secondary circuit model

A preliminary ASTEC model for the AP1000 reactor has been developed which represents all of the major primary, secondary and passive safety system components. Different type of components including volumes, junctions, accumulators, walls, valves and pumps were adopted to simulate the fluid systems of AP1000. Figure B-1 shows a view of the arrangement of different control volumes representing the RCS and the reactor pressure vessel (RPV).
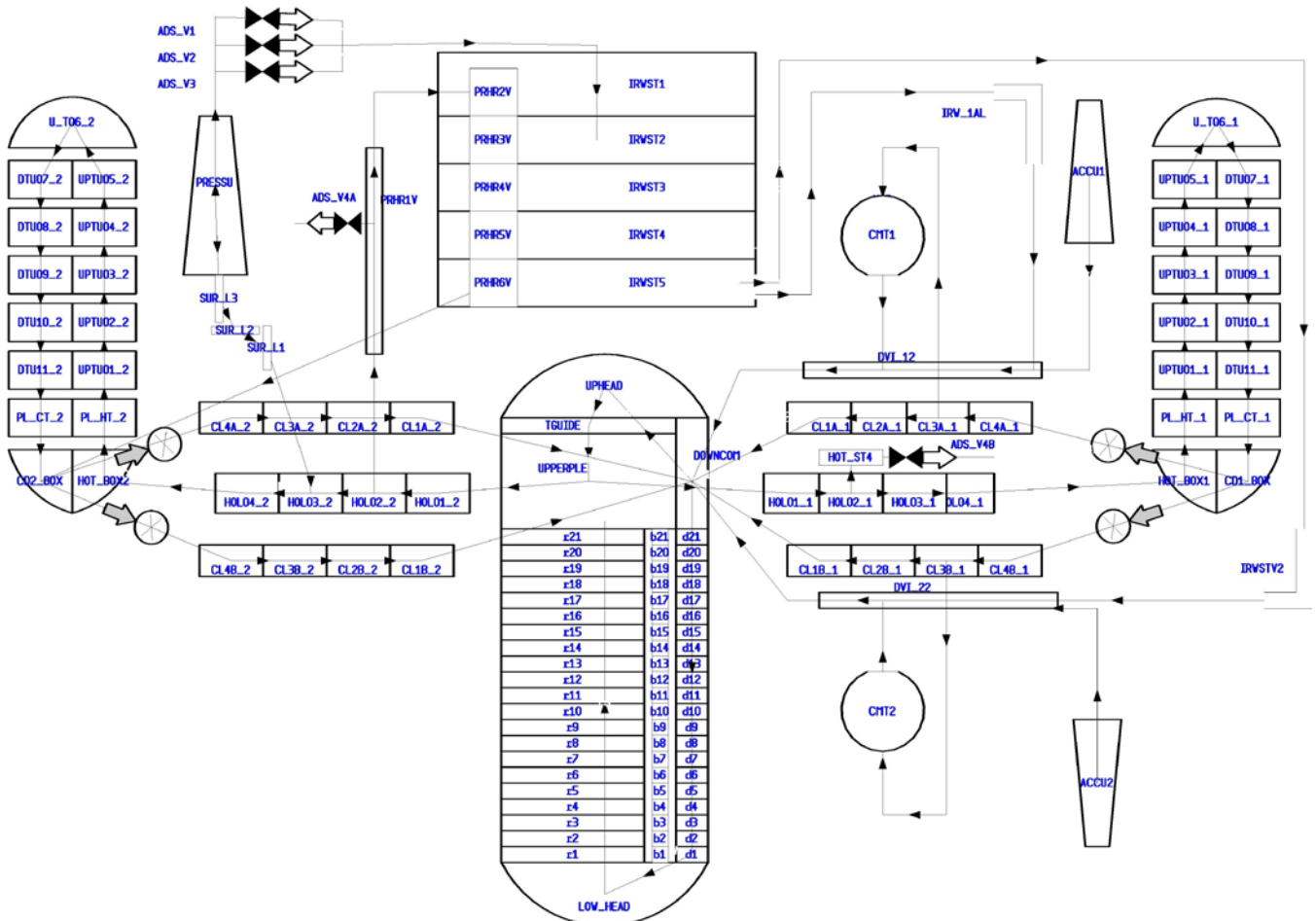
Figure B-1: AP1000 RCS nodalization scheme

The RPV model was represented in detail using the ICARE module (the ASTEC module in charge of the in-vessel core degradation simulation) [9]. The ICARE model contains representation of nearly all internal components [10]. However during the normal operating conditions (steady state) up to the front end sequence (i.e. from the initiation of the accident up to the core uncovery), the ASTEC code builds automatically a simplified description of the RPV for CESAR from the complete ICARE description [11]. When some parameters inside the RPV exceed determinate safety values (void fraction at the top of the core, cladding temperature, etc.) ASTEC code switches the RPV thermal-hydraulic computation from the CESAR model to the ICARE model. Since throughout the analysed scenario, all the parameters respected the safety criteria, the RPV thermal-hydraulic was simulated using the simplified model generated by ASTEC. The ICARE core detailed model will be used in the further work for the severe accident analyses. The RPV model generated by ASTEC consisted of four main volumes: core, by-pass, downcomer and lower plenum. The first three ones were further divided in 21 axial meshes, whilst for the lower plenum it was used only one mesh. The nodes that describe the core were simulated

using a heat source that generates the residual power. The core decay power was accurately calculated by mean of a dedicated code, taking into account a fuel with an average enrichment of 4% and a burnup equal to 32 GWd/tU. The upper part of the RPV was subdivided in 4 standard volumes where the higher part of downcomer has been connected to the four cold legs (CLs), and the two DVI lines, while the upper-plenum volume is connected to the two hot legs (HLs). Both CLs and HLs were represented by 4 homogenous volumes. The tube side of the steam generators (SGs) were subdivided in 13 nodes. To simulate the energy transfer between the RCS and secondary circuit the volumes that represent the SGs tube side, share the same wall structure along with the 6 nodes that model the shell side of the SGs in the secondary circuit. The same approach has been used to simulate the heat exchange between the PRHR-HX and the IRWST. A swollen type volume modeled the Pressurizer (PZR). The four reactor coolant pumps (RCPs) was represented using system pump following the correct technical characteristics. Concerning the PCCS, the IRWST was subdivided in 5 volumes; the higher volume is swollen type, and the lower volume has been connected to both the DVI lines nodes. The ADS valves were represented using the structures systems valve,'SEBIM' [12], the first three-stage discharging directly inside the second node of the IRWST; the spargers were not taken into account. Both CMTs are simulated by a single swollen type volume, and connected directly to CL and to the DVI. The ACCs are modeled by the structure systems 'ACCUMULATOR'. The PRHR-HX is represented by mean of 5 homogenous volume. Figure B-2 shows a view of the secondary circuit nodalisation used in the simulation. The secondary circuit includes the shell side of the two SGs, each of which was represented by 7 standard volumes, the high part of the SGs was modeled by one volume type swollen (the dome) and by one standard volume. The SGs downcomers as well as the two main steam lines (MSLs) were subdivided in 4 standard volumes, while the steam-head volume represents a sort of condenser. The safety valves on the MSLs are simulated using the structure systems valve type 'SAFETY VALVE'. The Steam Generators Feedwater Pumps (SGFPs) were connected to the higher nodes of the downcomer and were modeled by using system pumps. In this study, a 10-in. cold leg small break LOCA is simulated by adding a structure "CONNECTI" type 'BREAK' to the third node of the cold leg, which was connected to the CMT1 volume in the non-pressurizer side. The break location was specified on the bottom of the broken cold leg imposing the relative elevation of the break.
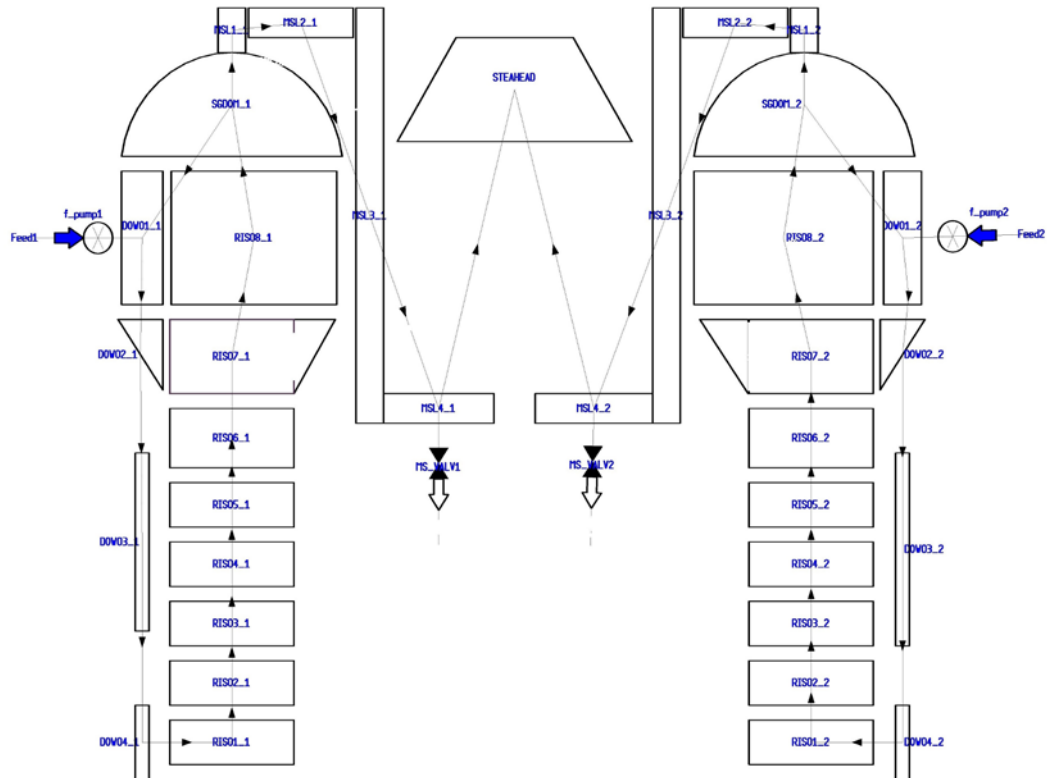
Figure B-2: AP1000 secondary circuit nodalization

B.5 Steady state calculation

To simulate the accident scenario a stationary input deck for the CESAR code was built to establish the initial conditions of the transient. This input deck was constrained by introducing different controllers by mean of structures 'REGU'. The task of the structures 'REGU' is to adjust the different parameters in order to fit the computed response with the expected one. In this way, they were set to the desired physical values for PZR level and pressure, SG recirculation flow rate, steam produced, water flow across the core, just to name a few. All the selected thermal-hydraulic parameters values were found in [13]. This stationary transient was run for 30000 s to verify that the calculated conditions were steady and the actual initial conditions of the simulation were achieved. After the desired steady-state conditions were achieved, some structures 'REGU' were removed to verify the stability of the modeling. Table B.1 shows the comparison between the CESAR thermal-hydraulic parameters values obtained in stationary simulation and the nominal AP1000 thermal-hydraulic parameters. It can be seen from the table that the calculated values were in good agreement with the rated values. The restart file generated by this run has been used as initial condition for the transient simulation.

Table B.1: Main thermal-hydraulic parameters steady state

Thermal hydraulic parameters	CESAR	AP1000 nominal operating parameters
Average core inlet temperature (K)	553.882	553.81
Average core outlet temperature (K)	597.878	596.48
Pressurizer pressure (bar)	155.1	155.1
Reactor coolant flow per loop (kg/s)	6879	6728
Pressurized water volume (m^3)	27.96	28.31
Steam flow from NSSS (kg/s)	948	943.7
Exit steam pressure (bar)	58.9	57.6

B.6 10 inch LOCA simulation

B.6.1 Accident evolution

A typical small break LOCA transient in the AP1000 reactor can be divided into four different phases [14] namely: the blow-down phase, the natural circulation phase, the ADS blow-down phase and the IRWST injection phase. When a small break occurs, the RCS system undergoes to depressurization. During the RCS depressurisation, when the pressure begin to fall up to the reactor trip set point (124.1 bar), a SCRAM signal is generated and the core power drops rapidly to the decay heat level. When the pressuriser pressure further drops below 117 bar, a safety system actuation signal ('S' signal) is generated. After the 'S' signal, both the CMTs isolation valves, and the PRHR isolation valves located on their RCS delivery lines, open with 5 seconds delay. The SGs are isolated 6 seconds after the reactor trip signal, due to closure of the turbine stop valves, and after another 2 seconds the reactor coolant pumps (RCPs) trip. Following actuation of the CMTs and PRHR-HX, two natural circulation flow paths are established through which the core decay heat is removed effectively. This phase is called blow-down phase and its duration is strictly dependent on the size of the break. After the RCPs trip, the decay heat is removed by mean of the break,

the SGs, the CMT recirculation flow and the PRHR-HX. The magnitude of each of these RCS cooling down mechanisms depends on the water system inventory. Indeed, once the steam generator primary side tubes had drained, because of the RCS inventory decrease, the heat exchange between primary and secondary circuit is drastically reduced. When this occurs the IRWST by mean of the PRHR-HX, becomes the primary heat sink for the RCS. The position of PRHR HX above the RCS ensures a sufficient inlet and outlet pressure difference which drives the RCS coolant to flow from one hot leg, through the C shape heat-exchanger, and back into its associated steam generator lower plenum. Heat transfer from the PRHR-HX tubes to the IRWST occurs either by free convection or by boiling, depending on the tube outer wall temperature, tank water temperature and pressure in the vicinity [15]. The CMTs inject cold borated water into the RCS through the DVI lines because of gravity-driven natural circulation and hot liquid from the cold legs collects gradually at the top of the CMTs, in this way the water level inside the tanks remains almost constant. This phenomenon is referred to as the CMTs recirculation mode. Until the water in the cold leg does not begin to flash or drain, the CMTs system remain in recirculation mode, afterwards the system switches to draining mode, and the tanks level, begin to decrease. When the pressuriser pressure reaches 48.3 bar another natural circulation system starts to inject water into the RCS, the ACCs. This system is able to discharge a high flow rate of borated water in a short time. Throughout this phase, called natural circulation phase the RCS depressurization slows down as coolant flashes and tends to be in saturated condition in the primary system [16]. When the CMT level drops to 67.5 percent, an ADS actuation signal is generated, and ADS stage 1 valves open with a 32 seconds delay. This is the beginning of the ADS-blow-down phase. The ADS Stage 2 and Stage 3 valves open in a timed sequence thereafter, to accelerate the RCS depressurization rate. The flows from the first ADS three-stage valves are discharged into the IRWST. In case of small break LOCA this first three-stage, usually are not able to depressurize the RCS system until the IRWST delivery pressure. For this reason when the CMT level reaches 20-percent other two stage called ADS stage 4A and ADS stage 4B are activated, with 60 seconds delay each other. These stages have greater vent capability with respect to the other three, and are able to depressurize the RCS up to atmospheric pressure also if the other three-stage do not work. After the primary system pressure drops to values near the containment pressure, injection from the IRWST initiates, marking the end of the Small Break LOCA transient and the beginning of the long term cooling. This phase is called IRWST injection phase. In Table B.2 are listed the protection and safety monitoring system (PMS) setpoints and time delay assumed in the

small break LOCA analysis for AP1000.

Table B.2: Safety system setpoints and time delay assumed in accident analysis

Function	Setpoint safety system	Time delay (s)
Reactor SCRAM on low pressuriser pressure	124.1 bar	0.2
'S' signal	11.72 bar	2
PRHR signal	'S' signal	5
CMTs signal	'S' signal	5
RCPs trip	'S' signal	8
ADS stage 1 actuation on CMT low level	67.5% tank level (ADS 1 stage signal)	32
ADS stage 2	48 s after ADS 1 stage signal (ADS 2 stage signal)	22
ADS stage 3	90 s after ADS 2 stage signal (ADS 3 stage signal)	0
ADS stage 4A actuation on CMT low-low level	20 % tank level and 128 s after (ADS 4 stage signal)	20
ADS stage 4B actuation on CMT low-low level	60 s after ADS 2 stage signal (ADS 3 stage signal)	2
IRWST signal	p(RCS) < p(IRWST) + Head -losses	0

B.6.2 Accident analysis

The 10-inch Small Break LOCA is thought to occur in the bottom of a cold leg connected to the CMT-1. The event chronology is shown in Table B.3

Table B.3: Safety events comparison 10-inch LOCA

EVENT	ASTEC Time (s)	NOTRUMP Time(s)
Break open	0	0
Reactor trip signal	4.3	5.2
'S' signal	5.4	6.4
Steam turbine isolation	12.5	11.2
RCP coastdown	10.5	12.4
Accumulators injection starts	102.2	85
Accumulator 1 empties	477.8	418.2
Accumulator 2 empties	478.3	425.5
ADS 1 Stage	817	750
ADS 2 Stage	877	820
ADS 3 Stage	997	940
ADS 4 Stage	1535	1491
CMT1 empties	~2000	1900
CMT2 empties	1830	1800
IRWST injection starts	1650	~1800

The predicted results obtained by CESAR are compared with the reference values calculated by NOTRUMP performed by Westinghouse. NOTRUMP is a specific small-break LOCA thermal-hydraulic code, which incorporates passive safety features that were developed for the AP600 safety analysis, and it was verified against integral system test data in the design certification process [16]. The table reveals a reasonable agreement between the two codes regarding the time sequence of events. Figure B-3 shows the RCS pressure history, the duration of the above-mentioned phase and the timing of intervention of the PCCS during the transient analysed. Once the cold leg break occurs, the RCS pressure drops rapidly from the initial operating pressure to the steam generator secondary side pressure due to mass and energy loss through the break. The

CESAR results, show that the pressure reaches quickly 60 bar, while NOTRUMP about 77 bar. The PRHR and CMTs are actuated 5 seconds after on receipt of the 'S' signal at 6.9 s during the blow-down phase. In Figure B-4 the heat rejection rate by the PRHR-HX and the break water and vapour mass flow rate calculated by the two codes are displayed. As it can be observed, the behavior of the PRHR are quite similar in both the simulations. The higher values of the PRHR-HX heat exchanged, computed by CESAR module, in the initial phase operation, are mainly due to the greater water mass flow, which goes throw the HX, driven by the high RCS pressure. The results comparison also shows that at the beginning of the natural circulation phase, the CESAR code calculates a lower and delayed break vapour discharge than NOTRUMP. This discrepancy is due mainly to the different models and parameters adopted by the two code for the computation of the critical flow and liquid entrainment through the break. Since the quality and the quantity of the break discharge flow has a great impact on the system depressurization rate; the CESAR simulation predicts a slower RCS depressurization process with respect to NOTRUMP during the natural circulation phase. Another reason could be due to the coarse mesh approach used to simulate the lower plenum. The model represents the lower plenum with a single volume. The entrance core head losses are reproduced as concentrated head losses at the junction, and calculated during the stationary transient to set the core mass flow. This nodalization scheme does not take into account, possible recirculation flow inside the lower plenum; this lack could have a not negligible effect on the slow initial RCS depressurization. Figure B-5 and Figure B-6 show the injected mass flow rate of the two CMTs throughout the transient, and, as it possible to see on the figures, the calculated results are in good agreement. An interesting aspect well captured by CESAR, is the reduction of the injection flow associated to CMTs, during operation of the ACCs. This is due to the pressurization of CMTs injection line by the ACCs, through the direct vessel injection (DVI) lines. Once the two ACCs are empty at about 477 s, the CMTs injection flow begins to resume. The slower RCS depressurization rate, predicted by CESAR, affects the ACCs discharge flow rate, given that, it is strongly depended on the pressure difference between the ACCs and the RCS. Indeed, as confirmed in Figure B-7 and Figure B-8, the ACCs discharge mass flows computed by CESAR, are lower and start in delay in comparison with those calculated by NOTRUMP code. In both the simulation, it was assumed that when the accumulators are emptied, the PRHR-HX, stops to work. This assumption is due to the fact that PRHR is designed only to exchange heat effectively with the liquid phase. The CMT-2 is the first one where the tank level drops to 67.5%, (this is because the break is located on the cold leg where the CMT-1 volume is

connected) and with a 32 seconds delay the ADS first stage valves open, sequentially the other two stages open in a controlled manner. These six motor operated valves (2 for each stage) are located in the high part of the pressurizer and when they open, a more rapid depressurization is calculated. After 1000s, the depressurisation effect of ADS-1/2/3 is reduced, and the RCS pressure tends to assume a constant value in both the simulations, throughout the ADS blow-down phase. The RCS pressure begins again to decrease, only after the opening of ADS4-A, and ADS4-B stages valves. The CESAR simulation computes a time delay of 115 seconds between the activation of the ADS4-A stage valves and the beginning of water injection from the IRWST into the RCS in comparison with about 300 s predicted by NOTRUMP code. The IRWST injection flows are illustrated in Figure B-9 and Figure B-10respectively. As it can see, the calculated results show a reasonable agreement, nevertheless CESAR code compute an early injection. In Figure B-11 it is possible to observed the strictly correlation between ADS 4 stage discharge flow rate and IRWST injection mass flow rate. The remarkable differences concerning the ADS4 discharge flows predicted by the two codes, are due mainly to the different models used to simulate the liquid entrainment in the hot legs, which influences the flow quality and critical flow rate out of the ADS4 stages, and it can determine the depressurization rate and the system inventory that occurs. In the RCS CESAR model, the void fraction in the node located above the core and connected to both hot legs was assumed homogeneous in whole volume. As shown by the results, this assumption tends, at least initially to overestimate the quantity of liquid that enter the hot leg and is released by ADS4 stage valves. Figure B-12 shows the comparison of void fraction at the top of the core. The trends of the two simulations are very similar, but the calculated results by CESAR do not capture the initial peak during the blow-down phase and predict a greater void fraction value than NOTRUMP, throughout the ADS blow-down phase. Figure B-13 presents the RCS water mass inventory along with the transient response of the cladding temperature, during the 10–in. small break LOCA process. As it can be observed the CESAR code computes a lower water mass inside the RCS during ADS blow-down phase than NOTRUMP, the result is in agreement with the high void fraction at the top of the core predicted by CESAR, during the same phase. Concerning the cladding temperature illustrated, it is the maximal cladding temperature calculated by CESAR, and as it is possible to check their values continually decrease during the transient, confirming that the PCCS are able to remove the decay heat and mitigate the consequence of this accident.

B.6.3 Discussion and conclusion

In the present study, the AP1000 reactor model was developed using CESAR, the thermal-hydraulic module of the ASTEC code, with the main aim to evaluate its capability to simulate the reactor passive systems. A 10 inch small break LOCA accident scenario was analyzed and compared with that of NOTRUMP code developed by Westinghouse Electric Company. The comparisons showed a reasonable agreement in terms of the changing trends. The different models adopted in the two codes, mainly cause the existing differences in some parameters. CESAR is a module of ASTEC integral code and uses simpler thermal-hydraulic models in comparison than NOTRUMP, which has been validated against applicable passive plant test data [16]. Overall, the results comparison between these two simulations confirms that CESAR module is able to reproduce the behavior of the passive systems during a 10-inch LOCA scenario.
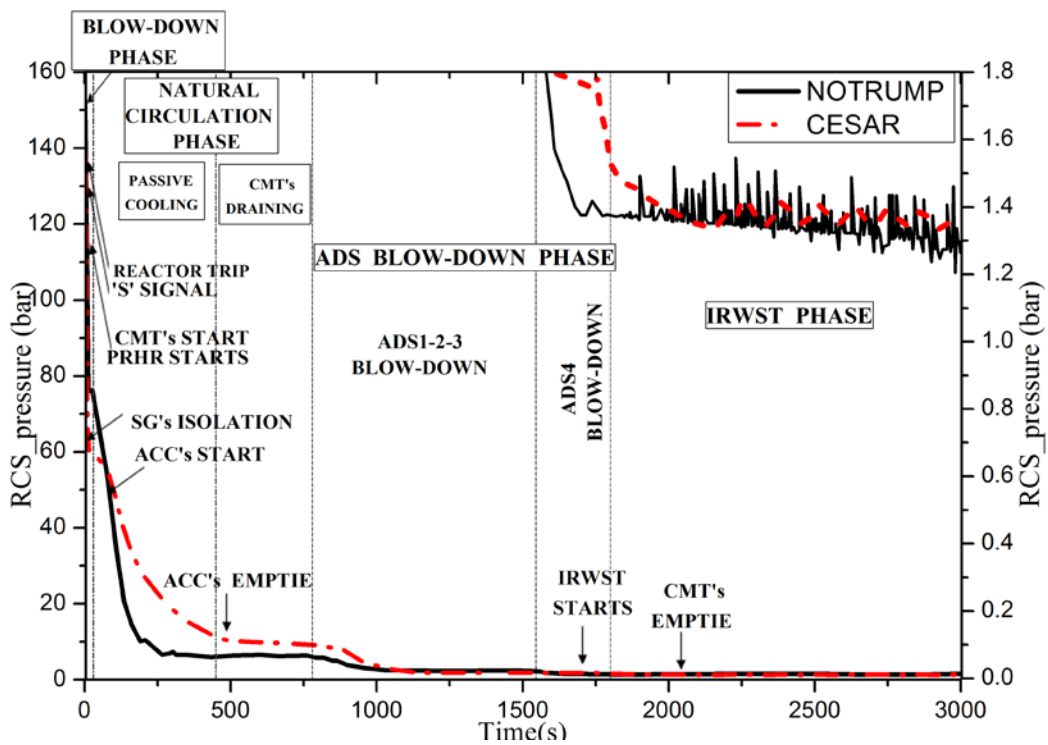
Figure B-3: RCS pressure
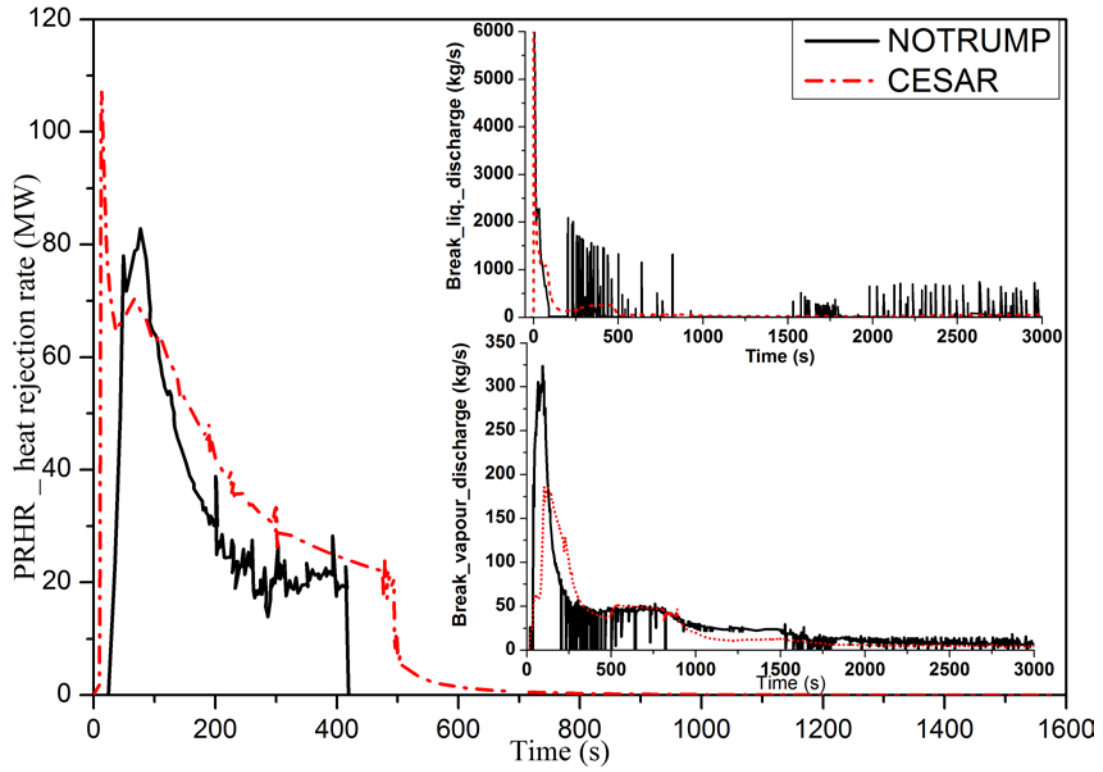
Figure B-4: PRHR heat rejection and Break water and steam mass flow
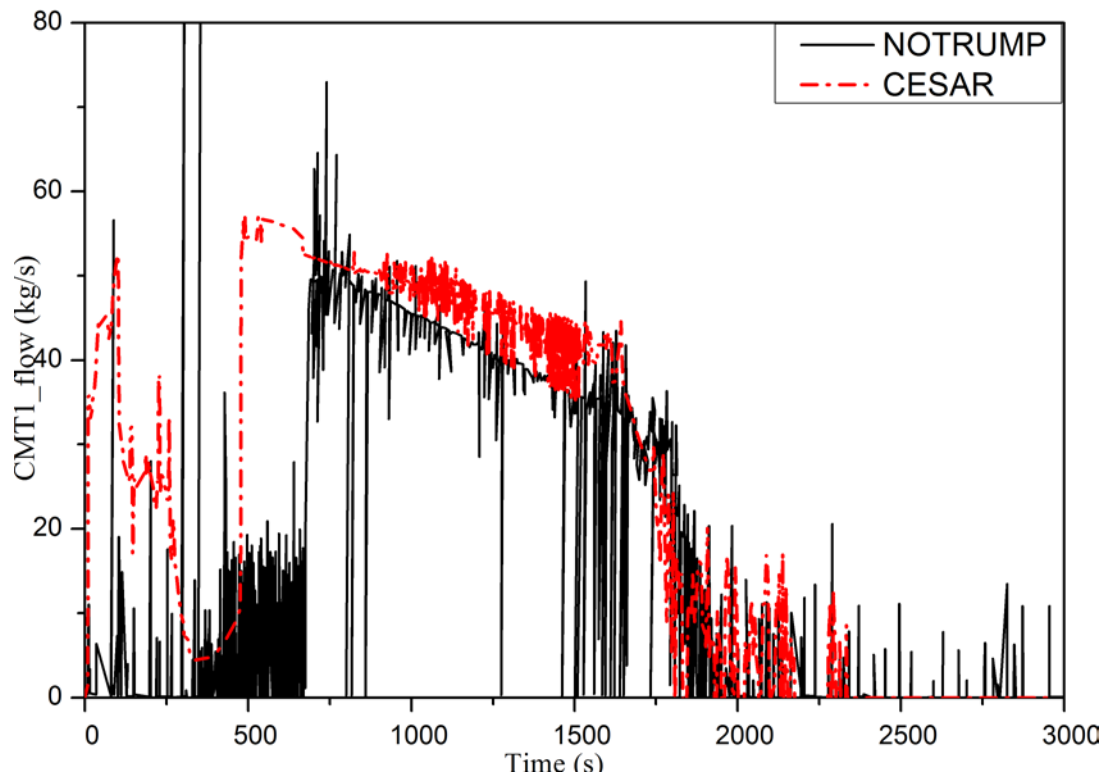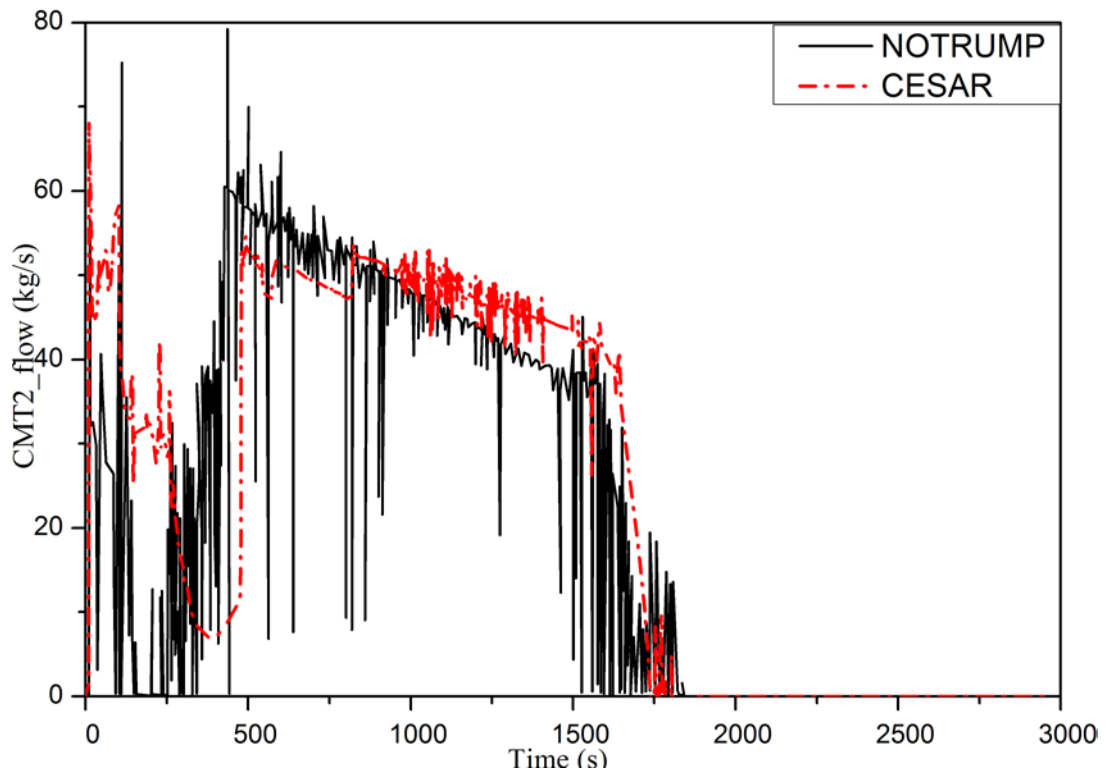

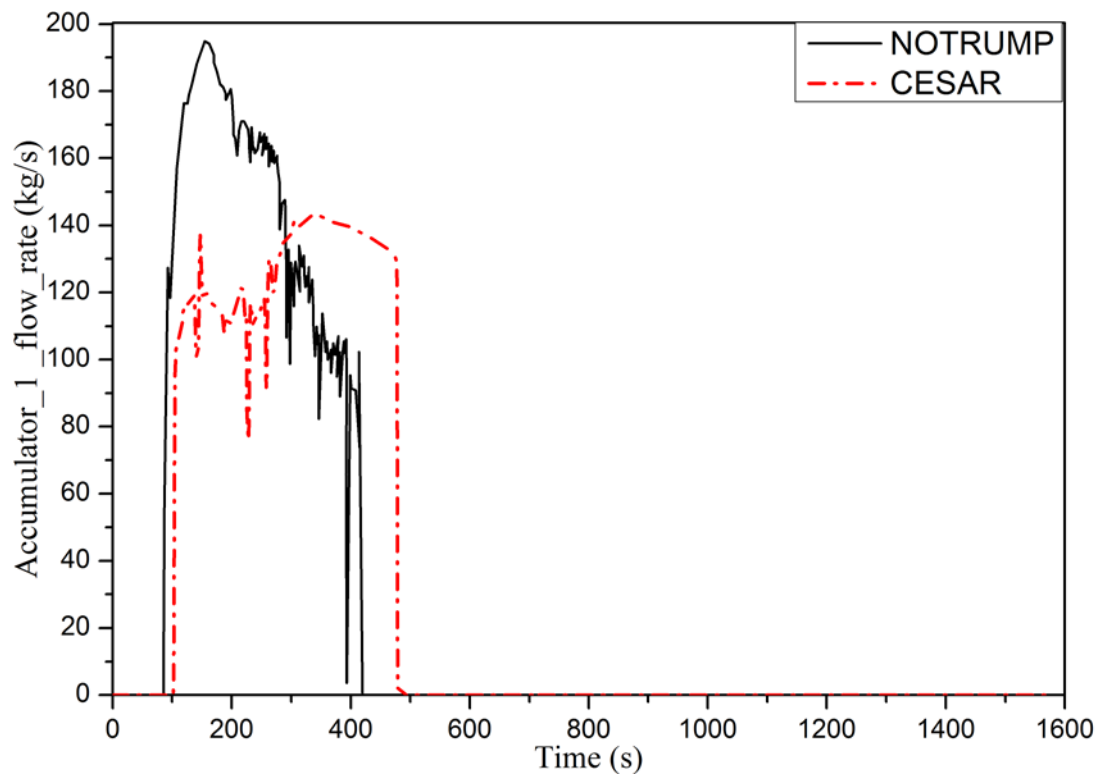Figure B-5: CMT-1 Mass flow

Figure B-6: CMT-2 Mass flow

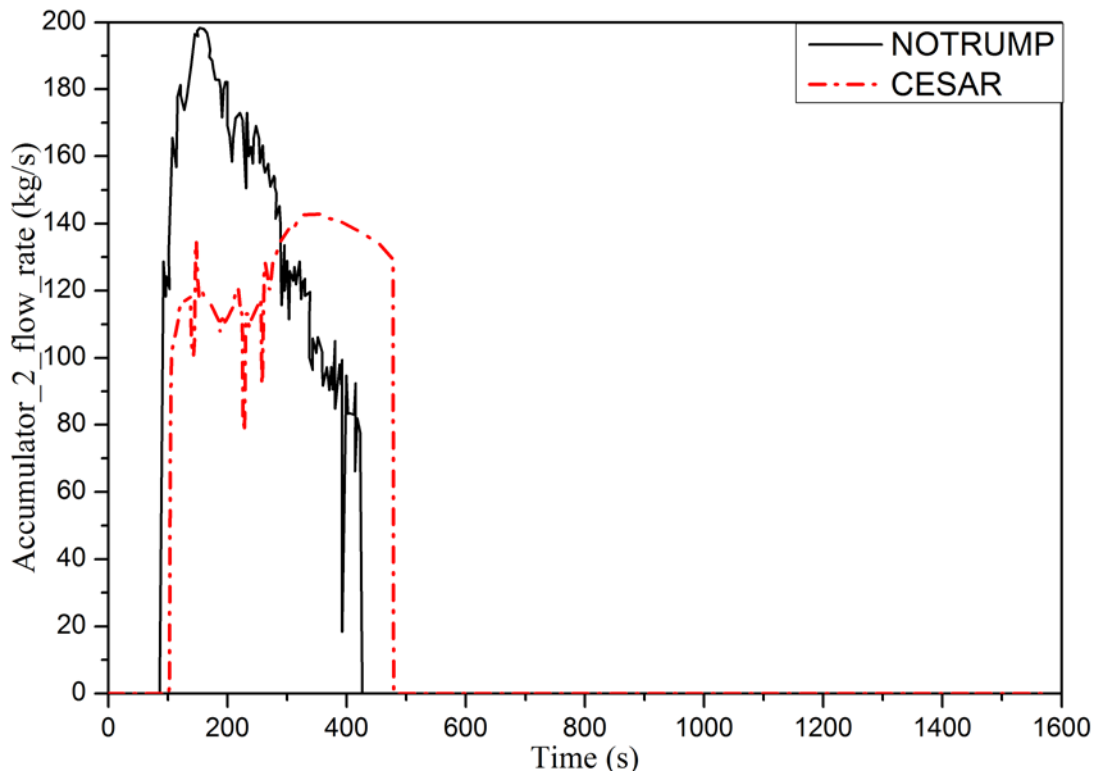Figure B-7: Accumulator 1 discharge flow
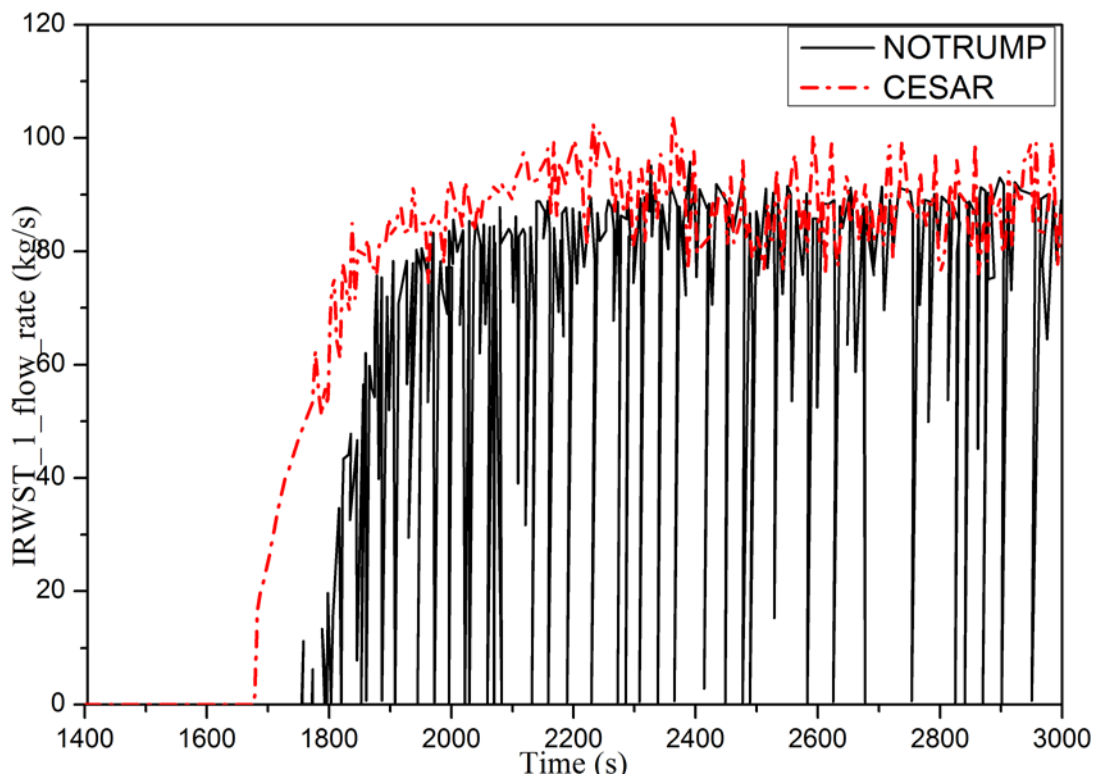
Figure B-8: Accumulator 2 discharge flow
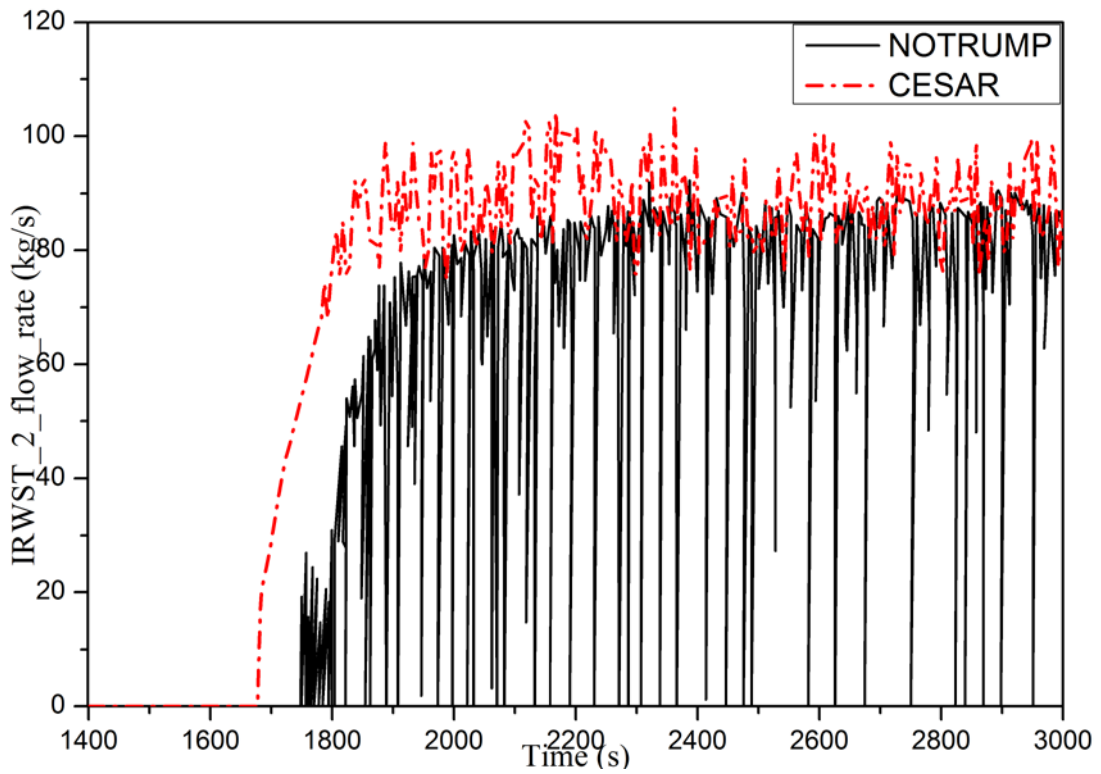

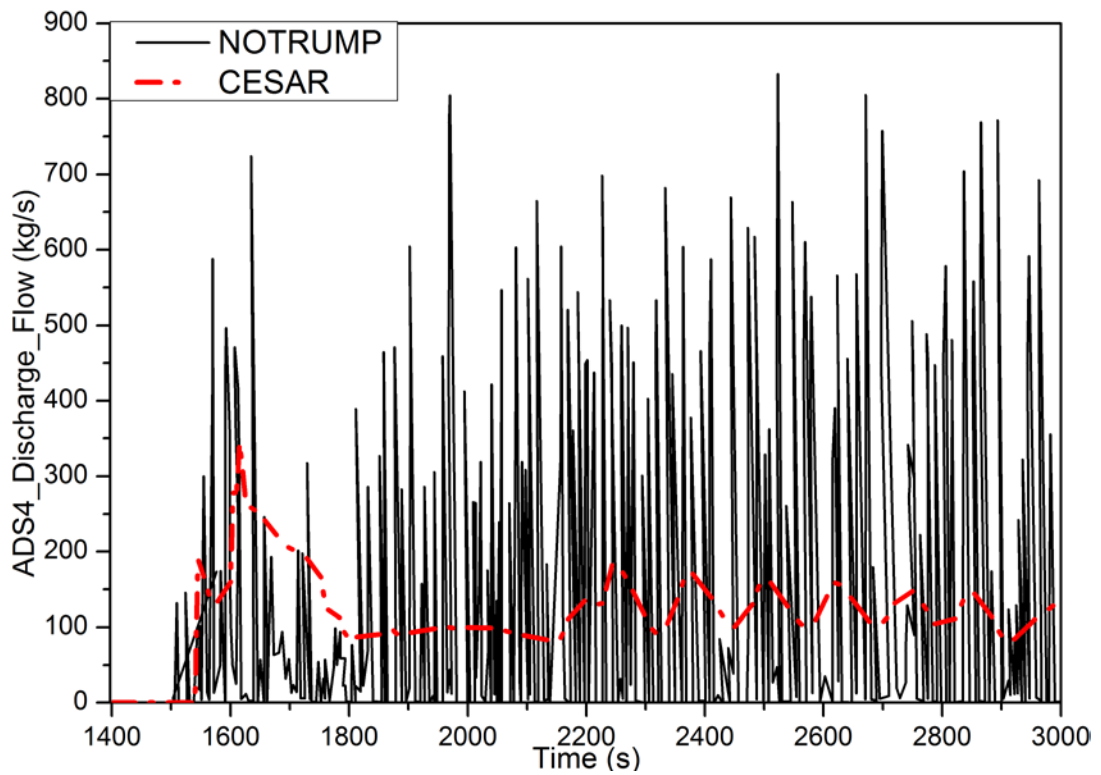Figure B-9: IRWST1 flow rate

Figure B-10: IRWST1 flow rate

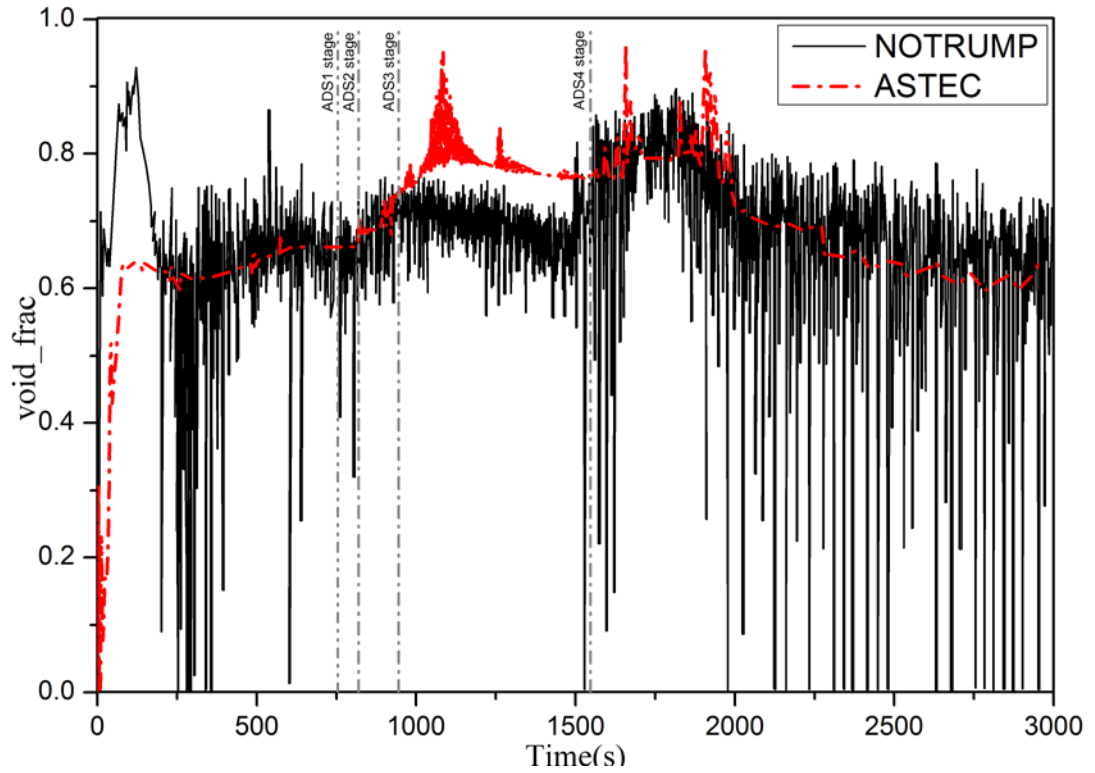Figure B-11: ADS stage-4 discharge flow
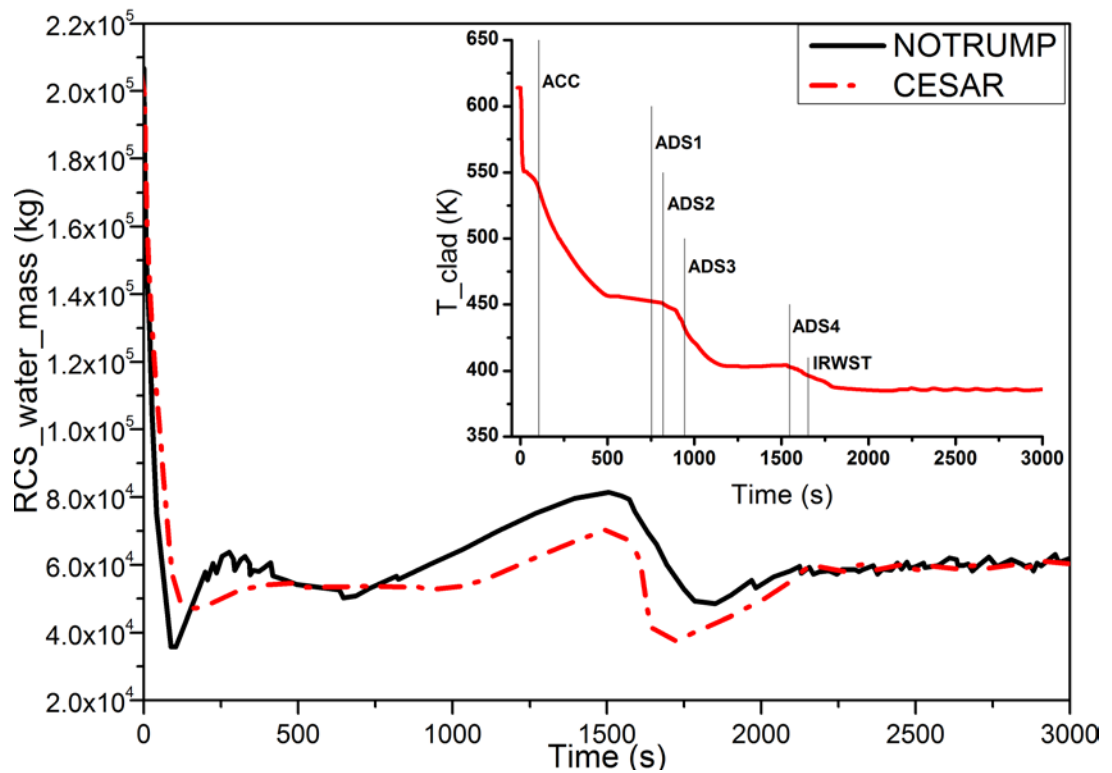
Figure B-12: Void fraction at the core exit

Figure B-13: RCS water inventory and peak clad temperature

References Appendix B

[1]   M. Di Giuli, M. Sumini, F. De Rosa., *"Modelling of AP1000 and simulation of 10-in. cold leg small break LOCA using the CESAR thermal-hydraulic module of ASTEC"* in press on Progress of Nuclear Energy 2015 .

[2]   Westinghouse, Westinghouse AP1000 Design Control Document Rev.19, Chapter 6, Section 6.0 (2011) Page.6.0-1

[3]   T.L. Schulz, "*Westinghouse AP1000 advanced passive plant*", Nuclear Engineering and Design 236 (2006)- pp. 1547–1557

[4]   Sh. Kamyab, M. Nematollahi, et al."Evaluting the Reliability of AP1000 Passive Core Cooling System with Risk Assessment Tool", IMECS 2010, Honk Kong, China, 17-19 March.

[5]   Westinghouse, Westinghouse AP1000 Design Control Document Rev.19, Chapter 15, Section 15.6, (2011) pp 15.6-1 – 15.6-263.

[6]   Westinghouse, Westinghouse AP1000 Design Control Document Rev.19, Chapter 15, Section 15.0, (2011) Page 15.0-4.

[7]   Westinghouse, Westinghouse AP1000 Design Control Document Rev.19 2011d, Chapter 6, Section 6.3, (2011) pp 6.3-1 - 6.3-73

[8]   R.F: Wright, J.R. Schwall,C, et al., AP1000 Passive residual heat removal heat exchanger confirmatory analysis, International Conference on Nuclear Engineering. Miami, 2006 USA, 17–20 July.

[9]   M. Di Giuli, M. Sumini, F. Rossi, F. De Rosa, "In-vessel-retention analysis with ASTEC code", ENC 2012, Manchester, UK, 9-12 December.

[10]   P. Chatelard, N. Reinke, Overview of the integral code ASTEC V2.0, Report ASTEC-V2 DPAM/SEMCA-2009-149.

[11]   G. Guillard, ASTEC V1 code Thermal-hydraulics coupling of CESAR and DIVA-Rev. 2, Report ASTEC-V2 DPAM/SEMCA/LESAG -2007-315.

[12]   G. Guillard, F. Jacq, C. Seropian, W. Plumecocq, ASTEC V1 code SYSINT module Management of events and safety systems interactions Rev. 1, Report ASTEC-V1/DOC/07-21, 2007

[13]   Westinghouse, Westinghouse AP1000 Design Control Document Rev.19, Chapter 5, Section 5.1, (2011) pp 5.1-10 – 5.1-11

[14]   M.T. Friend, R.F. Wright, et al., "*Simulated AP600 response to small-break loss-of-coolant-accident and non-loss-of-coolant accident events: analysis of SPES-2 integral test results*", Nuclear Technologies. 122, 1998, pp 19-42

[15]   W.E. Burchill, "*Physical phenomena of small-break loss-of-coolant accident in PWR*", Nuclear. Safety. 23, 1982, pp 525–536.

[16]   A.F. Gagnon, NOTRUMP Final Validation Report for AP600, WCAP 14807.

APPENDIX C

C.1 Summary

In this appendix will be presented a summary of the Phébus FPT3 benchmark results collected as leader author in the "Final Comparison Report on the Phébus FPT3 Benchmark" [1-2]. This work has been done at the IRSN SAG/LETR laboratory in the Cadarache research center. In the first part of this appendix will be briefly introduced the Phébus facility , the Phébus FPT3 test. In the second part will be presented the main results of the Phébus FPT3 benchmark.

C.2 Introduction

In the frame of the EU network of Excellence the SARNET2 work package WP8.3 "Bringing Research Results into Reactor Application" task "Benchmarking of available codes against integral experiments" the PHÈBUS FPT3 experiment, has been chosen as the basis for this benchmark. The aim was to assess the capability of computer codes to model in an integral way the physical processes taking place during a severe accident in a pressurised water reactor, from the initial stages of core degradation, the fission product transport through the primary circuit and the behaviour of the released fission products in the containment [3]. The FPT3 test studied especially the impact of the boron carbide control rod on the fuel degradation and FP speciation and transport in steam poor condition [3]. Overall, the four areas covered by the experiment, and therefore by the FPT3 benchmark, were the following:

- Fuel degradation, hydrogen and carbon production, release of fission products, fuel, and structural materials ('bundle' part of the FPT3 benchmark) from 0 to 17370 s;
- Fission product and aerosol transport in the circuit ('circuit' part of the FPT3 benchmark) from 0 to 17370 s ;
- Thermal hydraulics and aerosol physics in the containment ('containment' part of the FPT3 benchmark) from 22500 s for 37 h ;
- Iodine chemistry in the containment ('chemistry' part of the FPT3

benchmark) from 186960 to 386340 s.

The subdivision of the test in four different areas has permitted to the participants to perform integral calculations covering all four aspects of the exercise or to calculate any of the above areas in a stand-alone mode for example one or two of them. The FPT3 Benchmark was supported, with participation from 16 organisations in 11 countries, using 8 different codes.

C.3   The Phébus facility

The test train was located in a loop crossing the central part of the PHEBUS driver core, which supplied the nuclear power. In tests FPT0, FPT1, FPT2 and FPT3 the fuel rods were 1.12 m long with a 1 m long fissile zone (total mass of UO2 about 11kg). Two Zircaloy spacer grids held in place and arranged in a 5x5 square lattice the 21 fuel pin on a pitch of 12.6 mm, without the four corner rods, for a total of 21 fuel pins as shown schematically in Figure C-1.
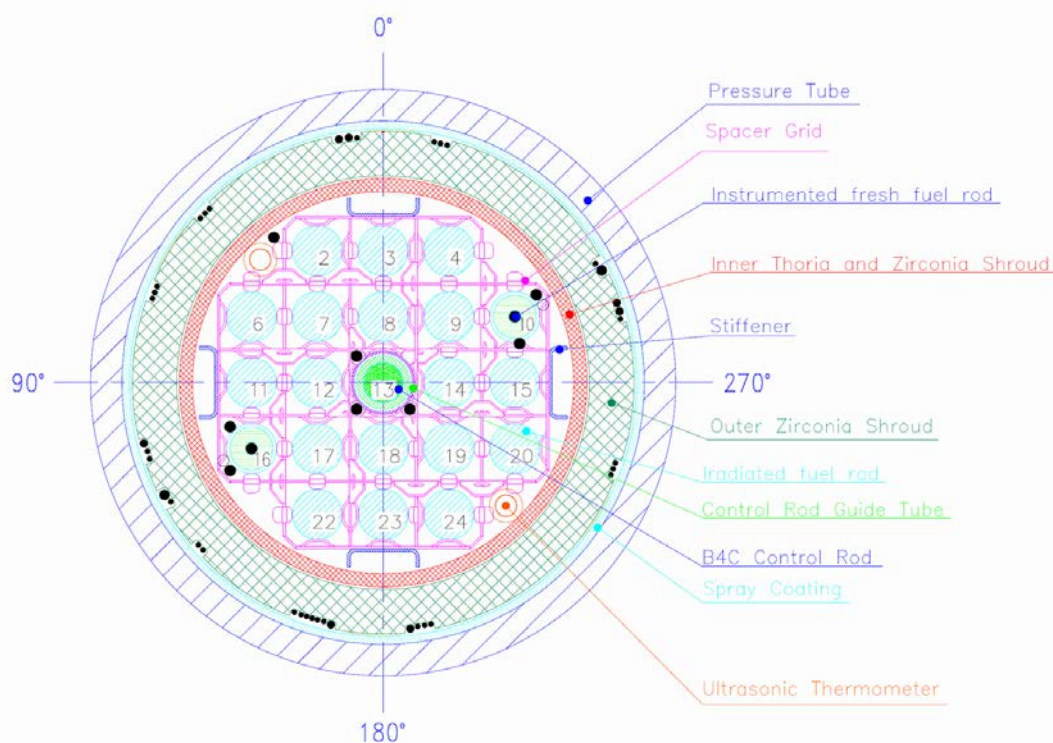

Figure C-1: FPT3 fuel bundle radial configuration

The absorber rod in the centre of the bundle contained Ag-In-Cd in the first three of these tests and B_4C in FPT3. Only the first test FPT0 was performed using trace-irradiated fuel. For the rest of the matrix, irradiated fuel rods (~ 23 GWd/tU for FPT1, ~ 32 GWd/tU for FPT2 and ~ 24.5 GWd/tU for FPT3) were used. The Figure C-2 provides a schematic layout of the Phébus FP. As it is possible to see in the figure the facility, aims to reproduce a 900 MW_e pressurised water

reactor in scaling 1: 5000. Further details including exact dimensions can be found in the FPT3 Final Report [4] and in the FPT3 Data Book [5].
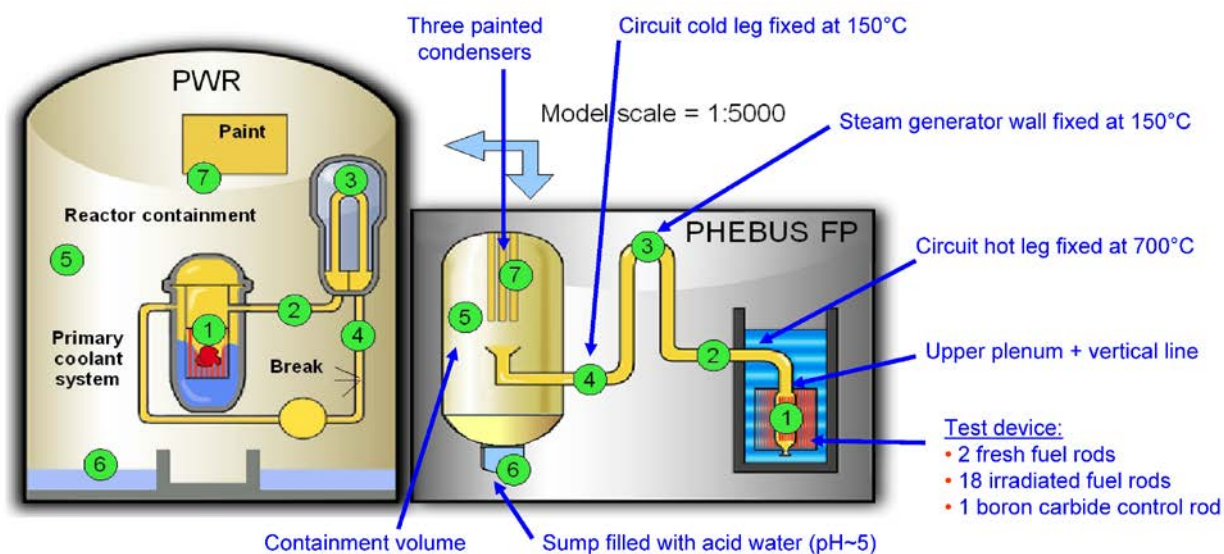

Figure C-2: Schematic layou of Phébus FP facility

The Bundle

An insulating zirconia shroud with an inner circular ThO2 layer (ZrO2 in FPT0), an external ZrO2 layer and a pressure tube of Inconel coated on the internal face by flame-sprayed dense ZrO2 surrounded the test bundle. These three annular structures were separated by two gaps under cold conditions. The outer pressure tube was cooled by an independent pressurised cooling circuit, with a high mass flow of water at a temperature of 438K. The rods were cooled by a measured gaseous flow of steam imposed at the entrance. Measurements in the bundle involved mainly temperatures: fuel centreline and cladding (for fresh fuel rods), control rod, stiffeners, shroud and coolant. After failure of the rod thermocouples (TCs), the bundle temperature was controlled by shroud TCs located inside and on the outer surface of the external ZrO2 insulating layer. Two ultrasonic thermometers enabled improved control of bundle temperatures at different levels. The tests involving irradiated fuel rods (FPT1, FPT2, and FPT3) included 18 rods with intermediate burn-up (no TCs) and 2 fresh fuel rods to enable the implementing of some rod TCs allowing a direct measurement of fuel temperature. Coolant flow rates, hydrogen production and FP were measured in the circuit. In particular, an On Line Aerosol Monitor (OLAM) device enabled the detection of major events of the core degradation. The measurement systems for the power of the driver core and fission chambers located around the bundle were also able to detect significant core material relocation events. Gamma-scanning examinations of some FPs and activation products of bundle structures enabled the mean axial profiles of fuel and control rod mixtures to be measured. In addition, a large set of

tomographies were performed enabling a rapid and precise overview of the bundle degradation and of the final axial distribution of bundle materials on the basis of their densities. Final destructive examinations included cross and axial cuts for more detailed quantification of the bundle degradation, but for PHEBUS FPT3 it was not carried out [6].

The circuit

The pipework between the upper end of the fuel bundle and the entrance into the containment tank consisted, for the PHEBUS FP tests, of the following components:
* the upper part of the test section (vertical line, ~3m high, internal diameter 0.073m reducing in stages until 0.03m), where the gas temperature drops to 970 K ;
* an isothermal (970 K) horizontal line (~9m long with an internal diameter of 0.03m), with sampling devices inside a furnace (point C);
* the vertical steam generator U-tube (~4m high with an internal diameter of 0.02m), with pipe walls maintained at 420 K;
* another isothermal (420 K) horizontal line (~4m long with an internal diameter of 0.03m), with sampling devices inside a furnace (point G), and the connection to the containment vessel;

The vertical and first horizontal line together simulated the hot leg of a PWR primary circuit, while the second horizontal line simulated the cold leg.

The containment

The containment consist of a 10m³ vessel (5m in height with an inner diameter of 1.8m). As for the circuit, representative fission products concentrations were preserved. Three vertical condensers simulated heat transfer and steam condensation phenomena in reactor containment. Their cooled surfaces were covered with epoxy paint as a possible source for molecular iodine trapping and organic iodine formation. Non-condensing painted structures were attached to the three condensers. The outer walls of the vessel were slightly superheated in order to prevent any steam condensation and to minimise aerosol deposition. The lower vessel part was closed by a curved bottom structure including a 0.1m³ sump. The sump had a diameter of only 0.584m in order to reproduce a representative atmosphere-water exchange surface. It contained a painted coupon. The sump water was recirculated by an auxiliary loop. During the washing phase another circuit injected water onto the vessel elliptic floor, thus washing settled aerosols into the sump.

C.4   The Phébus FPT3 test

The FPT3 test sequence [5| involved heating of the bundle through a succession of power ramps and plateaux, leading to an oxidation runaway, further ramps and plateaux leading to fuel melting and relocation, with the degradation phase being terminated by reactor shutdown at 17370 s (Bundle phase + Circuit phase). The transported material was injected into 10 m^3 vessel, simulating the nuclear building of a nuclear power plant. The 37 h aerosol phase started at 22500 s when the containment is being isolated. Airborne aerosols were deposited mainly by gravitational settling on the lower surface of the vessel (Containment phase). After about 51 h from the beginning of the transient, the aerosols deposited on the containment floor were washed out into the sump water. The 2 day chemistry phase starts at the end of the washing phase; it was devoted to the analysis of iodine chemistry under conditions representative of severe LWR accident, emphasizing iodine speciation. An important objective of the experiment was to study the iodine behaviour in the containment vessel, in particular the amount and speciation: inorganic versus organic of volatile iodine in the atmosphere (Chemistry phase).

C.5   The FPT3 benchmark

The Phébus FPT3 benchmark resulted in many conclusions for each of the four phases, and for integral code assessment. The most important points are given below; a full account is given in [1,6].The "user effect" (different results being obtained by different users of the same code) is minimised by choosing the most representative results for each code, thus excluding the outliers, in an attempt to assess the capabilities of the codes themselves, .

Bundle Phase

At the end of the bundle phase the total amount of hydrogen released was 120±6 g, whilst the gas release coming from the B$_4$C oxidation corresponds to 16 g of carbon dioxide and 17 g of carbon monoxide. The release fraction of the main volatile FPs ranges between 64% for Cs to around 80% of the initial inventory (i.i.) for I and Te, whilst the semi and low volatile FPs release show a wider spreading, see Table 1. The physical processes occurred in this phase are strongly related on the bundle thermal behaviour. So it was necessary correctly reproduce the thermal behaviour of the fuel rods during the calibration and preoxidation phase to obtain a correct analysis of control rod behaviour, gas release, and bundle degradation.

Table C.1 : FPT3 test FP and structural material release experimental data

Release element	Bundle release (% initial inventory)	Deposition in the bundle upper part (% initial inventory)	Fuel release (% initial inventory)
Noble gases			
Kr	72	0	72
Xe	84	0	84
Volatiles			
Cs	64	9	73
I	79	1	80
Te	80	1	81
Sb	40	n.d	40
Ag	70	27	70
Rb	35	n.d	35
Cd	>40	n.d	>40
Semi/low volatiles			
Mo	23	30	53
Ba	6	5	11
Ru	1	7	8
Sr	0.05	n.d.	0.05
La	>0.059	n.d.	>0.059
Ce	0.28	n.d.	0.28
Actinides			
U	>0.011	n.d.	>0.011
Pu	>0.0009	n.d.	>0.0009
Control rods and structural materials			
B	78	n.d.	
Sn	>29	n.d.	

Most of the participants have assumed a reduction of the input nuclear power of about 10% and an increased of the thermal conductivity of the shroud within the experimental uncertainties, with these assumptions, the thermal behaviour of the fuel rods is rather well reproduced by the codes. Comparison between measured fresh fuel temperatures and results are illustrated in Figure C-3 for 0.5 m elevation. The discrepancies during the preoxidation phase are due to the lower input power selected for the simulation. In general a good overall agreement is observed in the bundle and in the shroud up to the end of the first phase; despite this, there are stills some difficulties to reproduce the final degradation of the bundle. The nearly total destruction of the control rod is reproduced in the calculations, but the suspected effects of spreading molten materials of the control rods towards fuel rods of the bundle and the B_4C-SS

eutectics formation and liquid B_4C-SS-Zr relocation, are not accounted for in the codes (Figure C-4).
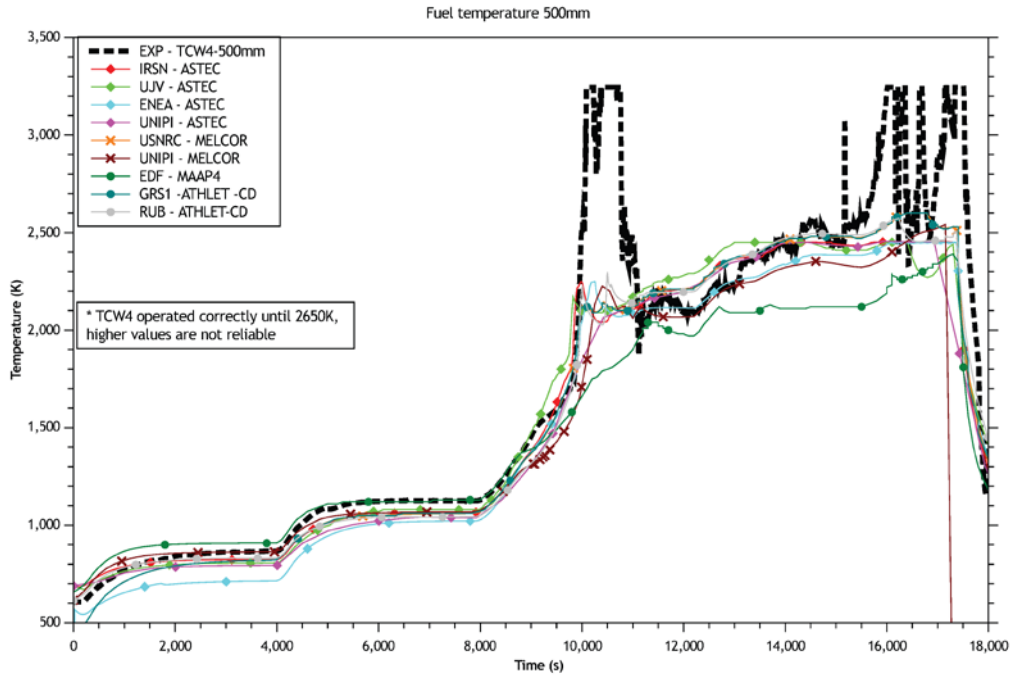

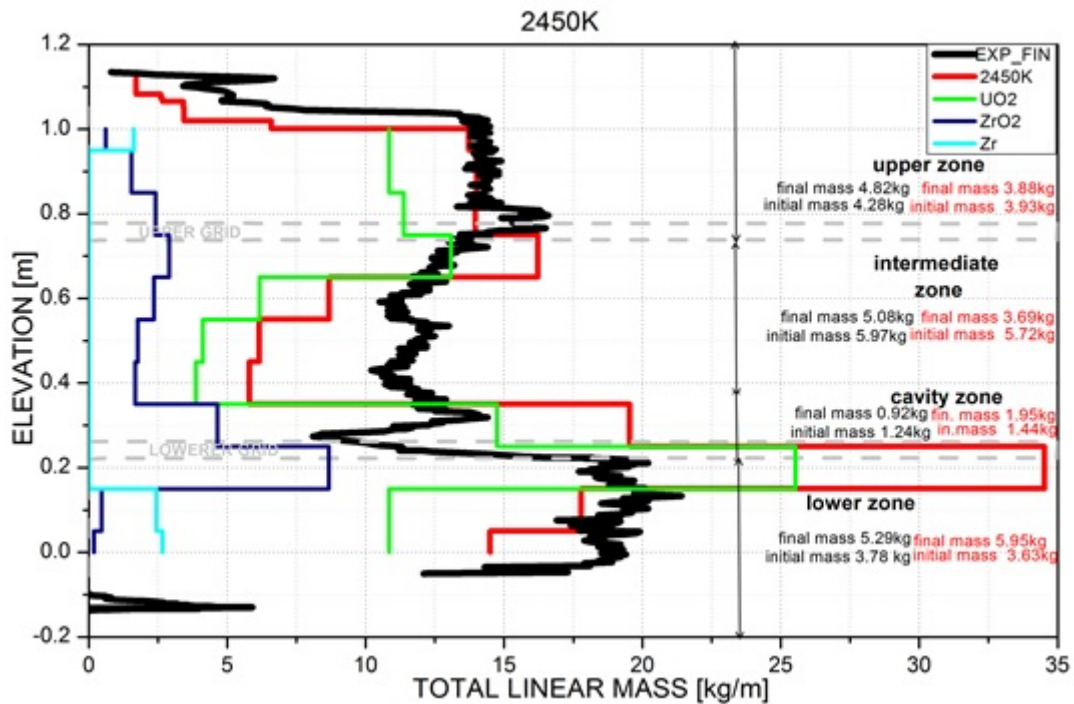Figure C-3: Fresh fuel temperature at 500 mm

Figure C-4: FPT3 final linear mass distribution

The need for further code developments of the early phase of core degradation is recognized for the absorber rod material behaviour. Therefore extensive programmes of separate-effect experiment have been performed, such as BECARRE (IRSN) and BOX, LAVA, QUENCH-SR (KIT), to enable a better understanding of B_4C oxidation and interactions with cladding materials. Regarding the total hydrogen generation, most of the results are consistent with experimental value, in the uncertainty range (~10%) and the kinetic of release is captured well enough as it is illustrated in Figure C-5.
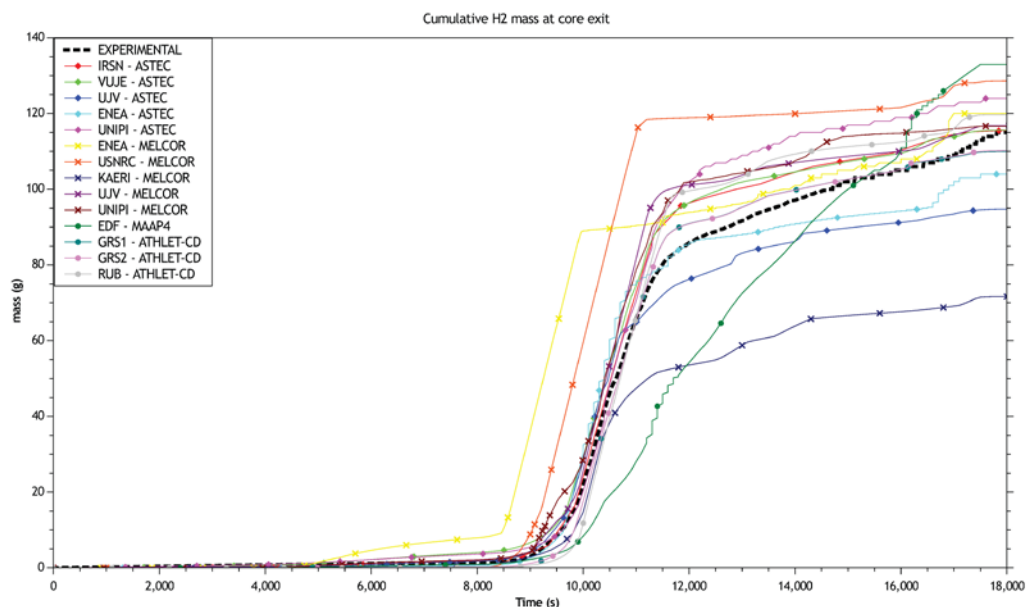
Figure C-5: H_2 mass cumulative release

A remarkable feature of the experiment was the substantial fraction of volatilised materials (Cs, Ag, Mo, Ru, and Ba) which has redeposited on the more intact upper part of the fuel rods [8]. The released material was swept by the steam flow through an experimental circuit; deposition of aerosol and vapour in some parts of the circuits were measured, as well the flow rates of the different elements in cold and hot leg. The deposition took place in the zones where thermal gradients are important, just above the fuel bundle and in the rising line of the steam generator. In this last zone, the mass deposited is enhanced by the formation of boron blockages. Another remarkable feature of the experiment was the very high iodine gas fraction (~90%) entering the containment during the transient, which determines the iodine behaviour in the short term in the containment atmosphere. The FPs release from intact fuel and control rods followed by the release from the in-core molten pool, depend mainly on temperature and oxygen potential but also on various physical and chemical processes that occur within the fuel matrix and in the surrounding gaseous atmosphere. In this test the

main fission products were basically classified according to the results of the VERCORS programme [9] in where the results of VERCORS and Phébus were consistent. The consequence classification is the following:

- Noble gases: Xe, Kr
- Highly volatile fission products: I, Cs, Rb, Te, Sb, Ag
- Semi-volatile/low fission products: Mo, Ba,/ Ru,

Concerning the bundle release, all of the experimental data were used for cross-checking, for statistical treatment, and for overall accuracy estimation. As a result the measured data fall within an estimated error band of ± 16% for gamma emitters (I, Te, Cs, Ag, Ru, Ba) and ±20% for Mo. An important feature of FPT3 was the significant deposition of several elements on the upper part of the fuel rods. The lower coolant flow in the test favoured this depositions, see Table C.1 and in order to take into account this phenomenon the reference value for Mo, Ba, Ru and Cs elements was the fuel release The results predicted for xenon and iodine are illustrated in Figure C-6 and Figure C-7and Figure 5. The total amounts released were in agreement with experimental data, but the kinetic was too quick, notably for the MELCOR 1.8 code versions. As regards caesium, all the results shown a general tendency to overestimate the total release, see Figure C-8. Most of prediction results for molybdenum release were in disagreement with the measured data. As stated before and as it is possible to see in Figure C-9 the bundle release and the fuel release show a large discrepancy 23% and 53% respectively, thus approximately 30% of Mo is deposited in the upper part of the bundle and revaporisation of such deposits is possible later. MELCOR is the only code, which can discriminate between the bundle and fuel release, but no participant has provided this parameter. In the case of Ru, ATHLET-CD and MAAP4 submissions tend overestimate, the final value. The other cases underestimate, experimental fuel release values, see Figure C-10. As regard the boron release as control rod material is illustrated in Figure C-11. The results show a wide spreading mainly due to the model adopted by the user, nevertheless the results predicted by ASTEC and ATHLET-CD codes are included in a range of ±10% and can be consider acceptable, taking into account the uncertainties related on the B experimental measures. The good predictions of hydrogen production as well as the total amount of high volatile FPs released are important safety relevant conclusion. The semi-volatile and low-volatile results are mainly consistent concerning the total amount released, but no code can predict correctly the release of all of these elements; the modelling need some improvement; because a correct prediction is of extreme importance, either due to their radio-toxicity and influence on the residual power, or by their propensity to react with other fission products. Same consideration are valid for structural materials, in spite of they have not radiological

significance, they potentially react with fission products, and their source terms are therefore necessary for accurate calculation of chemistry and transport in the circuit. Furthermore, the structural materials also form the bulk of the aerosol mass, affecting the aerosol concentration and the agglomeration processes.
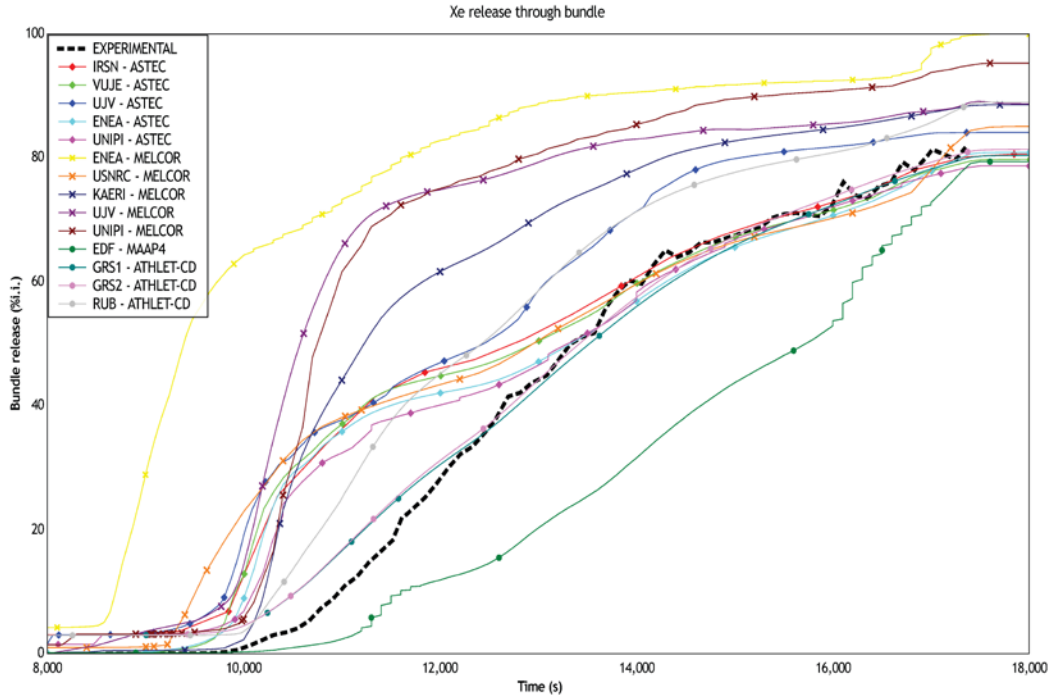

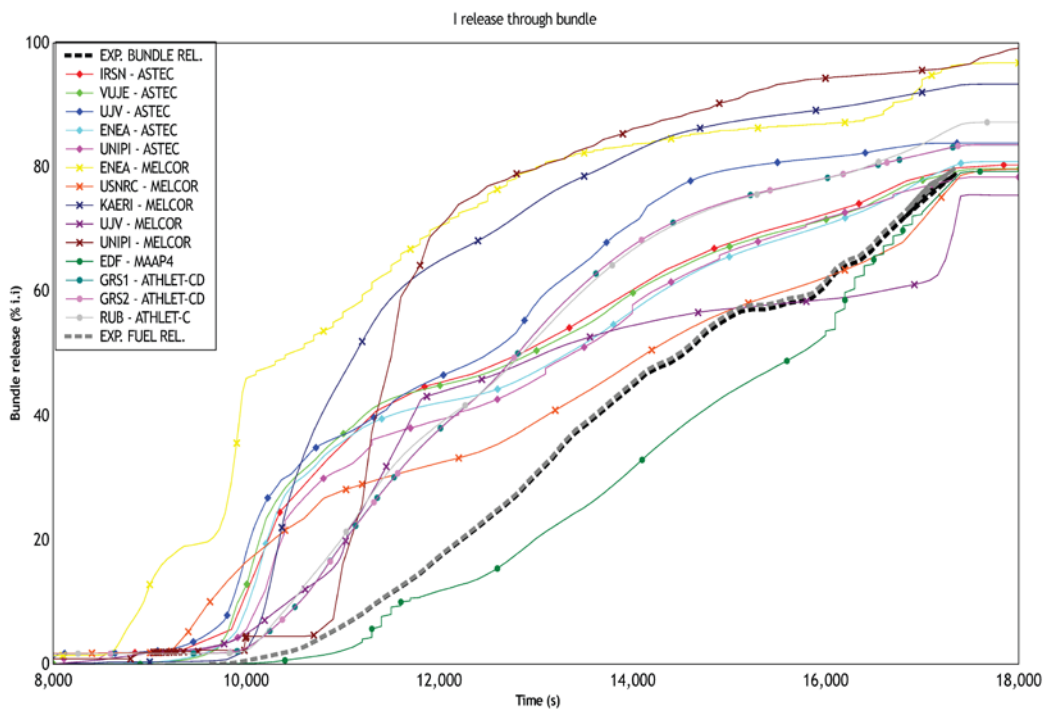Figure C-6: Xe cumulative fraction release
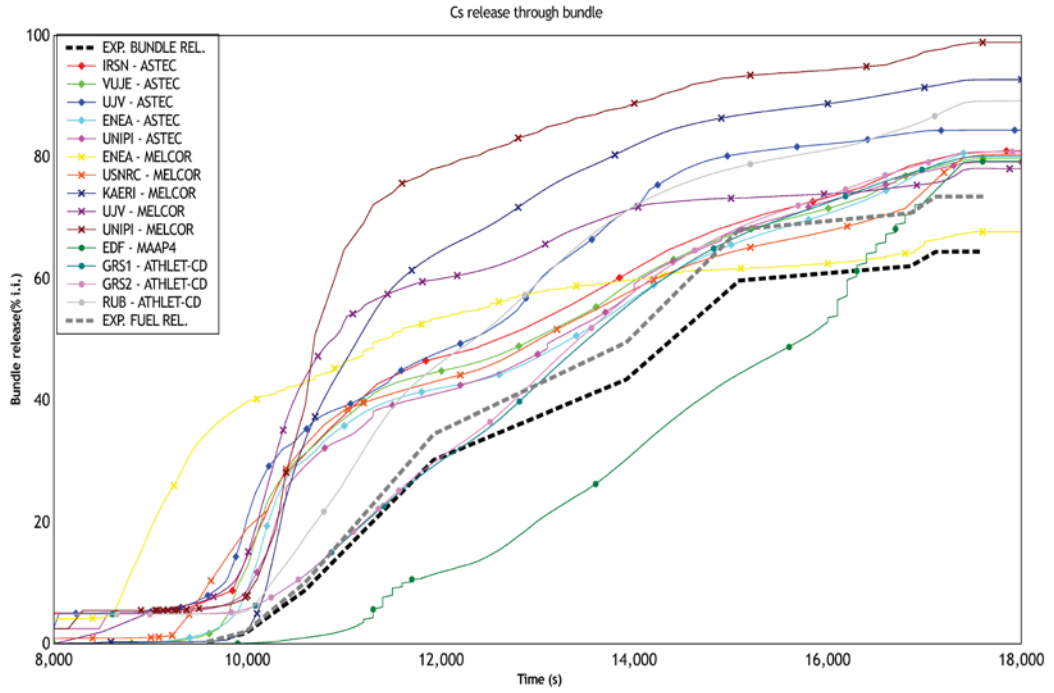

Figure C-7: I cumulative fraction release
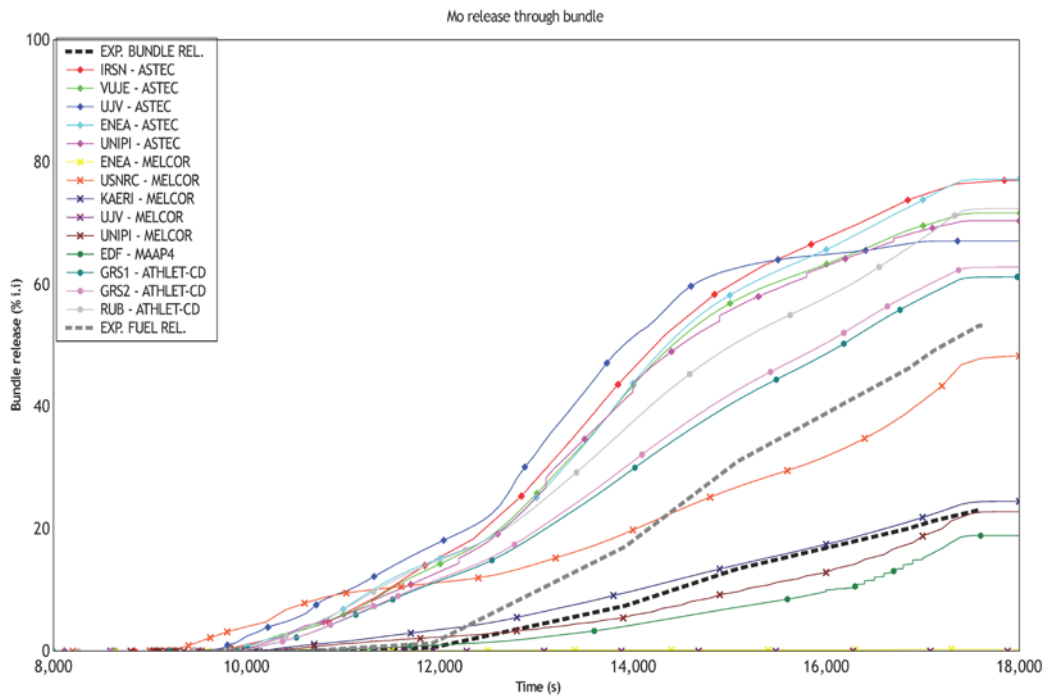
Figure C-8: Cs cumulative fraction release

Figure C-9: Mo cumulative fraction release
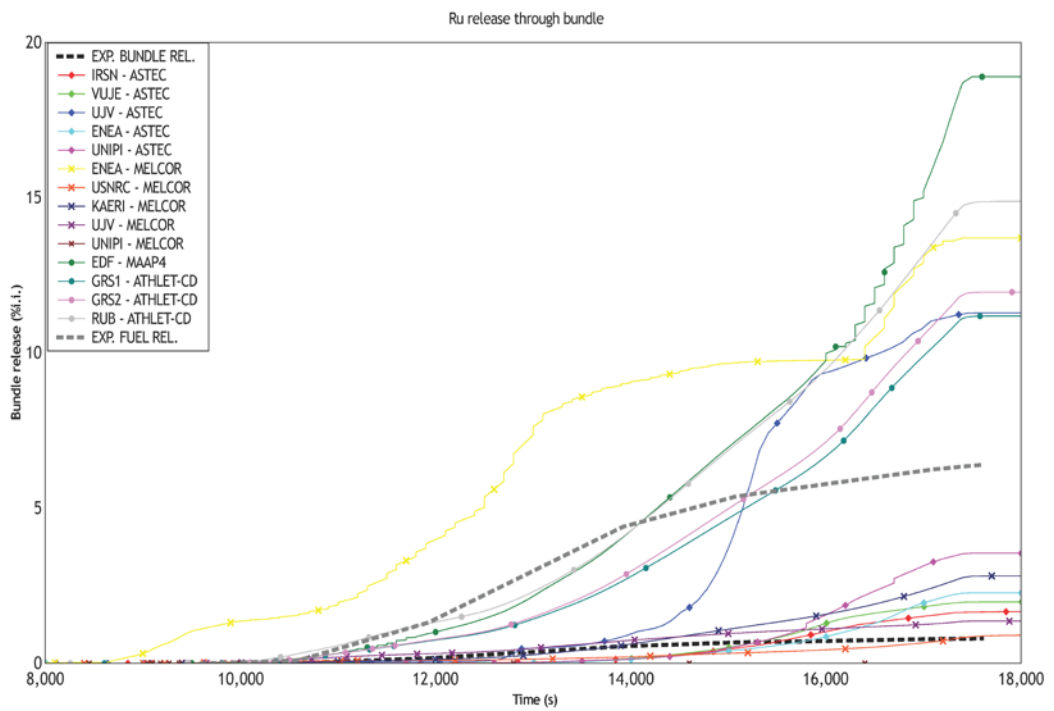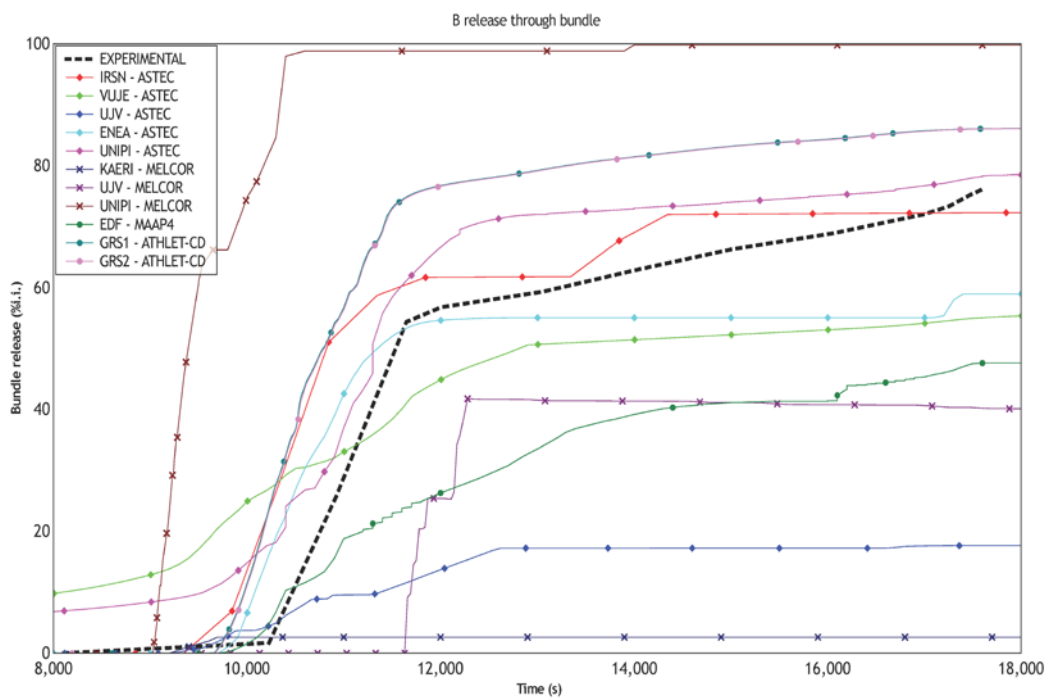
Figure C-10: Mo cumulative fraction release

Figure C-11: B cumulative fraction release

Circuit Phase

The injected steam flow swept FPs and structural materials (SMs) from the degrading fuel bundle through the circuit into the containment vessel. They were quantified by online instruments and by post-test analyses of the samples collected during the test. The experimental results tests shown, that all condensable FPs are transported through the simulated primary circuit in aerosol form, except iodine and cadmium which were detected mainly in gaseous form [8]. On their way through the primary circuit, the aerosols tend to deposit mainly where the temperature of the wall and fluid decrease strongly or where the flow is diverted: above the bundle, in the so-called upper plenum and vertical line and in the upstream part of the SG tube. The analyses of FP and SM transport in the Phébus FPT3 tests for the entire circuit with the integral codes showed that the total deposited mass is underestimated on average by a factor 1.5. Remarkable features of FPT3 test was the large deposition of boron-containing material between the hot leg and cold legs, with the potential of forming a partial blockage in the circuit [10-11]. The main effect of this phenomenon was the reduction of the tube section, and the increase of the deposition surfaces, both effects enhance the FPs retention in the involved circuit zones, notably in SG upstream. No code could have reproduced these conditions and thus, the submitted results tend to underestimate the overall mass retention in the circuit. The boron deposition in the primary circuit is not considered so important regarding plant safety assessment; taking into account that, the number of tubes in a PWR steam generator is around 5000 or more, and it is very unlikely that the boron contained in the water and in the control rods would form blockages in all the tubes at once. In FPT3 with only a single tube, the effect is more important and for a correct analysis of the results, considering this effect is necessary, maybe reducing the section of the tube. Nevertheless, it was also observed difficulties to capture the thermophoresis deposition in the upper plenum for elements as Cs and Te (Figure C-12), despite that, the steam temperatures along the circuit were well predicted by most of the contributions. These discrepancies are mainly due to the wrong prediction or assumption of the FPs chemical form, and therefore their volatility. However, this is also not enough to explain the differences in the upper plenum. As regard molybdenum, the general overestimation of its bundle release entailed that, the calculated total depositions along the system were in agreement with the measured one. It is worth noting that work is already in progress to improve circuit modelling in various codes. Regarding speciation, account is taken of the importance of caesium molybdates, while borates are also being considered. Similarly, in MELCOR2.1, caesium molybdate has been introduced as a default fission product class.
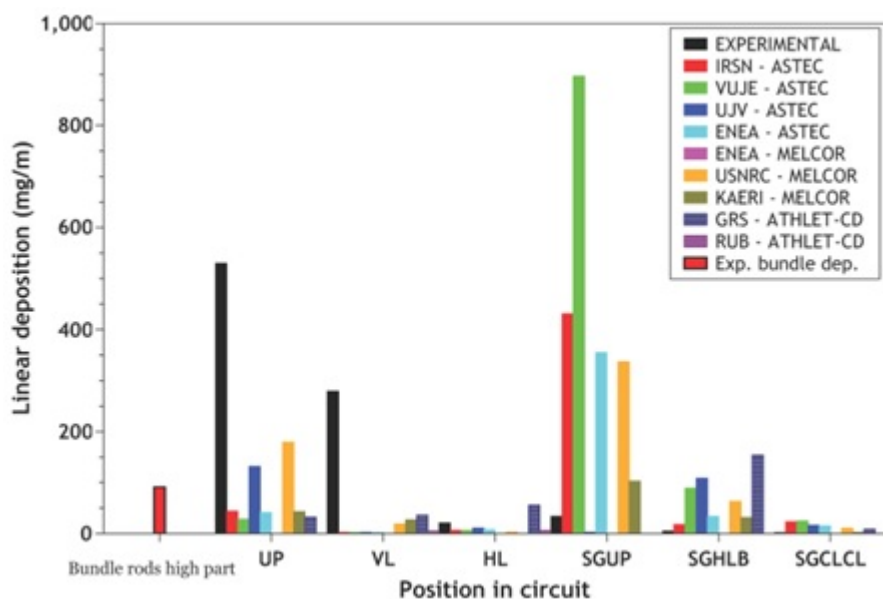
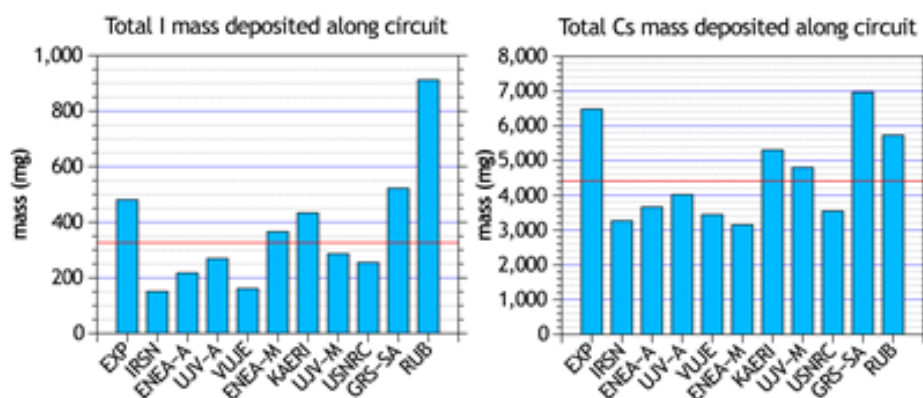Figure C-12: Te linear mass deposition along the circuit

Figure C-13: Total iodine and Caesium deposited along the circuit

Aerosol phase and containment thermal-hydraulic

The containment analysis is focused on parameters that may have an impact on fission product behaviour in the containment, especially for aerosol physics. The prediction of the thermal hydraulic parameters in the containment as temperature, pressure, condensation rate, humidity, etc. was in generally satisfactory and, the little differences observed had probably only a weak influence on aerosol physics calculations. The evolution of the aerosol airborne mass, largely depends on the quality of structural material and FP (Cs, Mo) releases calculation, for integral submissions. Most of the calculations overestimated the caesium and molybdenum release, and underestimated the total deposition along the circuit leads to overcalculated total airborne mass in the containment, Figure C-14.

Overestimation of the depletion rate seems to be correlated with overestimation of the aerosol aerodynamic median mass diameter (AMMD), likely due to higher aerosol concentration and agglomeration in the containment. The overall aerosol depletion rate evolution is generally well enough calculated in the stand-alone cases (where the input comes from the test data), Figure C-15 indicating that aerosol deposition processes are modelled properly.
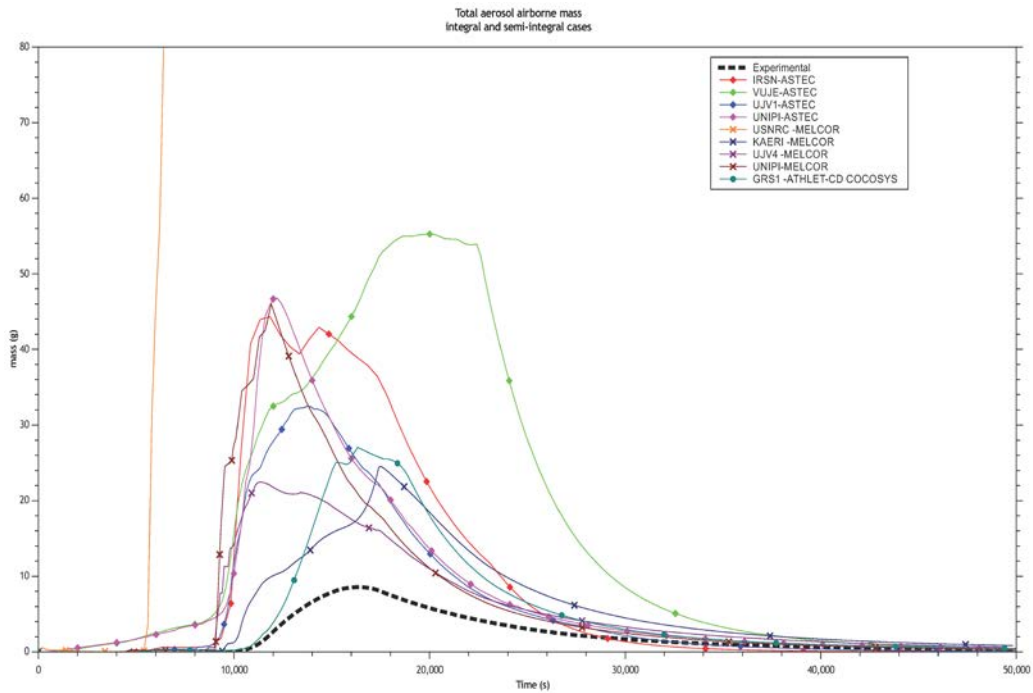

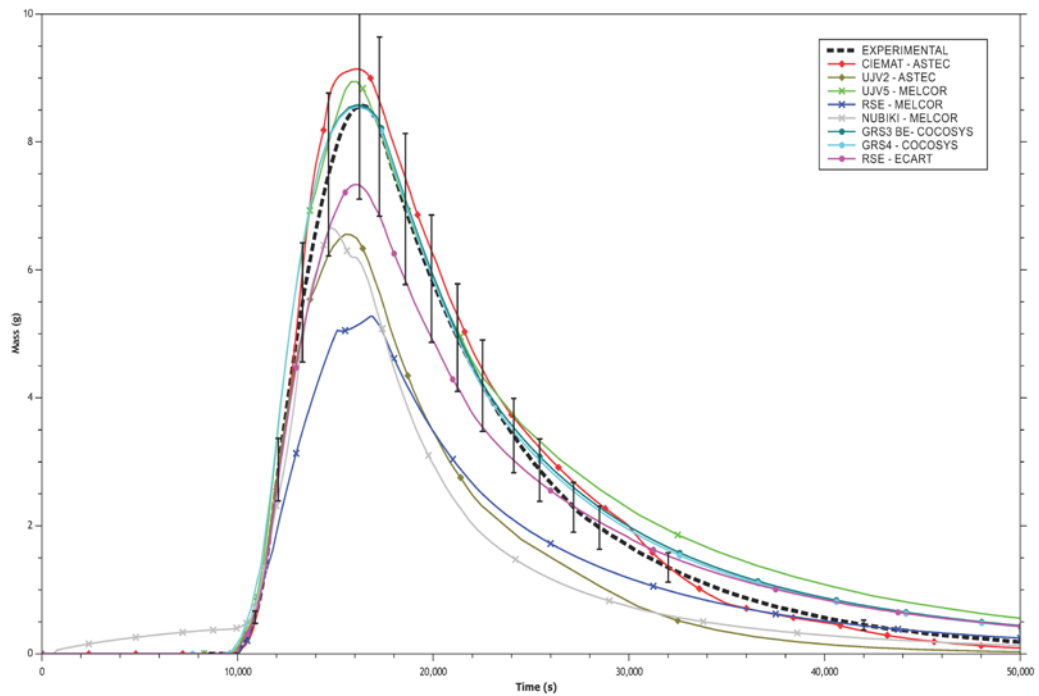Figure C-14: Aerosol depletion rate inside the containment (integral cases)

Figure C-15: Aerosol depletion rate inside the containment (stand-alone cases)

Chemistry phase

Given the difficulty in predicting the iodine source to the containment in the integral cases, more reliable assessment of the iodine models is obtained using stand-alone calculations with iodine source input based on the test data. In these stand-alone calculations, iodine deposition on painted surfaces, 54% containment inventory (c.i.), was well predicted, Figure C-16; while there were greater discrepancies with the organic iodine (RI) fraction in the gas phase, Figure C-17 (from iodine interactions with paint in the long term) with a tendency to over-calculation. The RI has a high safety significance as it is more difficult to remove by containment sprays or filtration than I_2 inorganic iodine which was rather better predicted than organic iodine, Figure C-18 [12].
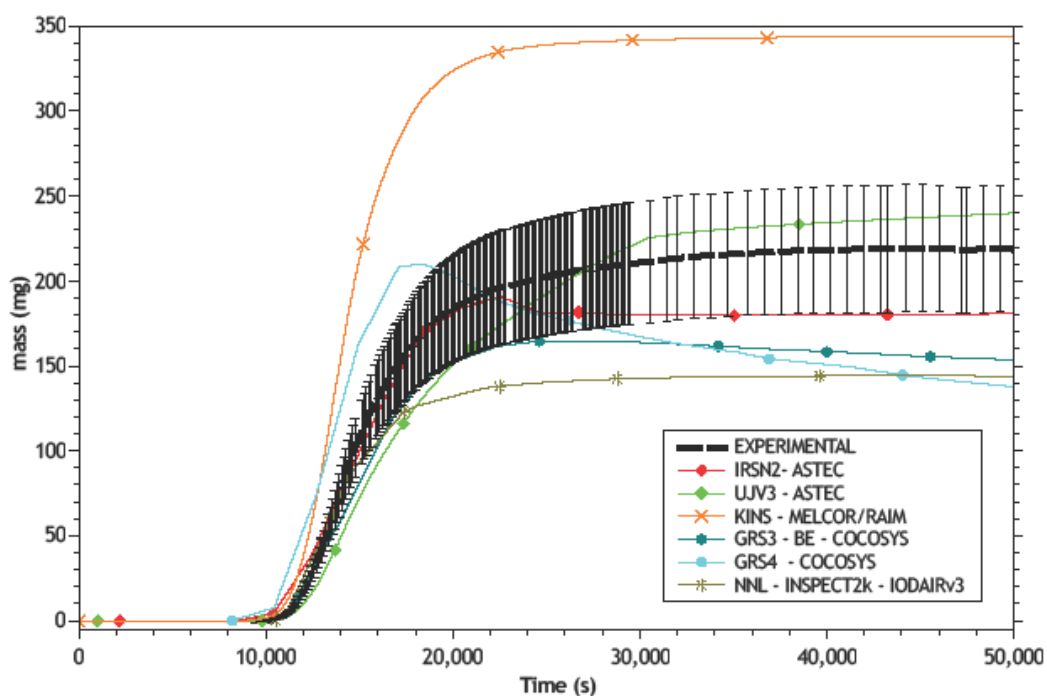

Figure C-16: Iodine deposition on painted surfaces
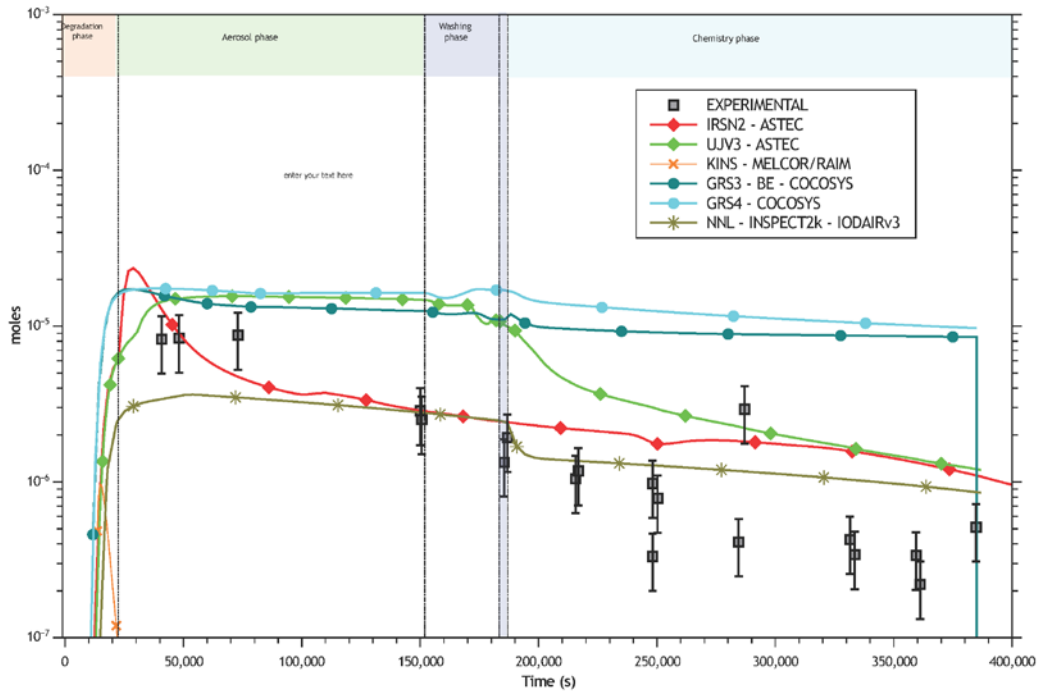
Figure C-17: Organic iodine gas concentration inside the containment
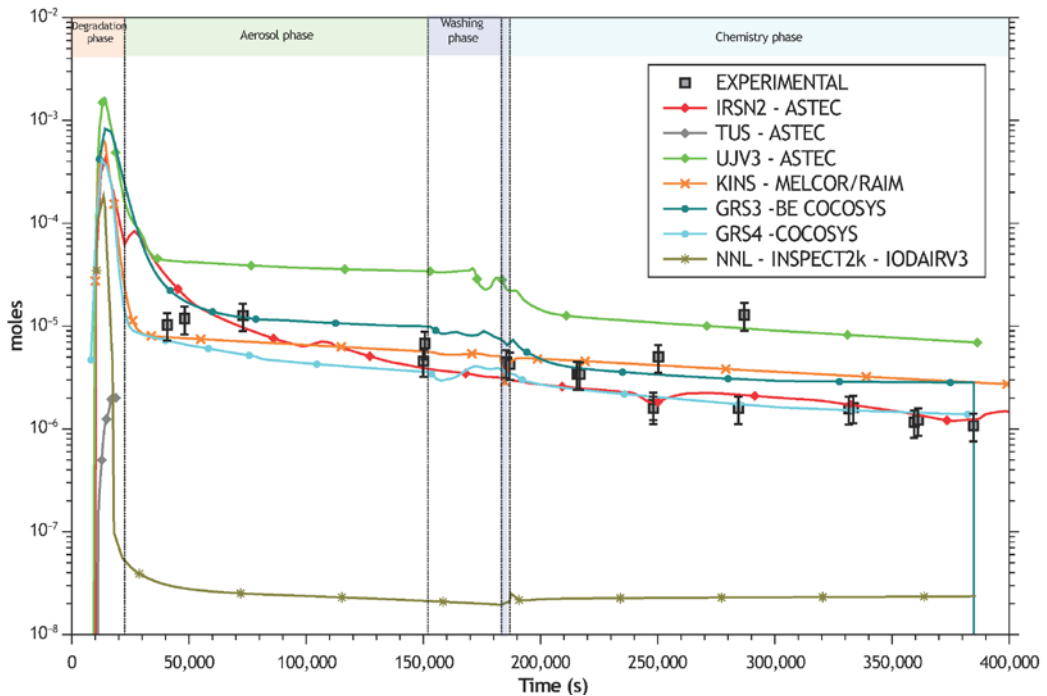

Figure C-18: Inorganic iodine gas concentration inside the containment

C.6   **The Phébus FPT3 test**

In this paragragh will be resumed the main conclusion of the FPT3 benchmark:

- The accuracy of containment calculations in integral cases is sensitive to results of calculations for previous stages (propagation of uncertainties);

- Uncertainties on calculation of FPs and SMs (Sn and especially B) released from the bundle, along with underestimation of deposits in the partial boron-rich blockage (not calculated), affect transport in all the subsequent stages, for both the kinetics and for the total transported amount;

- For those codes which calculate the chemistry, the speciation is influenced by the calculated release, both regarding the time dependence and the total;

- The deposition of SMs is underestimated, and comparison with the data is not easy, given the difficulty of having accurate information on B and Sn deposition;

- Iodine speciation and physical form in the circuit are poorly predicted; no code calculated the gaseous iodine fractions in the reactor coolant system (RCS). The chemistry models need to be improved to tackle properly the involved chemical systems both for thermodynamic equilibrium and for reaction kinetics;

- Given these limitations, it is hard for existing integral codes to predict well the containment iodine behaviour, whatever the level of detail of the corresponding modelling; uncertainties on iodine release from fuel and deposition in the RCS are overwhelmed by uncertainties in iodine chemistry both in the RCS and the containment, as exemplified by the high iodine gas fraction observed entering the containment;

- The results emphasise that stand-alone evaluations have to be performed considering uncertainties on the main processes affecting iodine speciation in the circuit and containment, using detailed containment iodine codes stand-alone as required to determine bounding cases and sensitivities.

C.7   **Conclusion**

The SARNET benchmark on Phébus FPT3 has provided many insights on the ability of severe accident codes to calculate the different phases of an accident sequence in an integral manner. Several areas where code improvements are recommended, where

data are available from Phébus FP tests, have been identified, considering the conclusions of a range of studies, particularly for iodine chemistry. These are being addressed by several separate-effects experimental programs, and code improvements have been/will be made as a result. When these will be completed, further benchmarks have been planned to assess their capability.

Aknowledgment

Reference Appendix C

[1] M. Di Giuli, T. Haste, R. Biehler, Final comparison report on the Phébus FPT3 benchmark, IRSN/SARNET internal document (2012).

[2] M. Di Giuli, T. Haste, R. Biehler, "*SARNET Benchmark On The Phébus Fpt3 Integral Experimenton Core Degradation And Fission Product Behaviour*", Proc. of NENE 2014, Portoroz 8-11 September 2014.

[3] Schwartz, M., Hache, G., von der Hardt, P., "*Phébus FP: a severe accident research programme for current and advanced light water reactors*", Nuclear Engineering and Design (**187**), 47-69, 1999.

[4] Payot F, Haste T, et al., "FPT3 Final Report", DPAM/DIR-2010-148, Document PHEBUS FP IP/10/587, Issue 1, December 2010.

[5] IRSN, 'PHEBUS Data Book FPT3', Document PF IP/07/575, Note Technique DPAM/CPEX NT/2007/253, August 2007.

[6] Bieliausks, A., 2011a. Specification of SARNET2 FPT3 benchmark, IRSN Note technique DPAM-SEMIC-2011-057

[7] Haste, T., Clément, B., et al., "*Main outcomes of fission product behavior in the Phébus FPT3 test*". In: 4th European Review Meeting on Severe Accident Research (ERMSAR-2010) Bologna Italy, 11-12 May

[8] Grégoire, A.-C., Haste, T., "*Material release from the bundle in Phébus FP*", Annals of Nuclear Energy (61), 63-74,2013.

[9] Ducros, G., et al., "*Synthesis of the VERCORS experimental programme: Separate-effect experiments on Fission Product release, in support of the PHEBUS-FP programme*", Annals of Nuclear Energy 61 75–87 2013

[10] Haste T, Payot F, Bottomley PDW, "*Transport and deposition in the Phébus FP circuit*", Annals of Nuclear. Energy 61, pp. 102-121, 2013.

[11] Haste T, Payot F, et al., M., "*Study of boron behavior in the primary circuit of water reactors under severe accident conditions: A comparison of Phébus FPT3 results with other recent integral separate-effects data*", Nuclear engineering and Design 246, pp. 147-156, 2012

[12] T. Haste, M. Di Giuli, G. Weber, S. Weber, "Iodine benchmark in the *SARNET 2 Network of Excellence"* Proc. of NENE 2014, Portoroz 8-11 September 2014.